

TEMPH 76-09514

File with

N77-11030

ASI-TR-75-26

NASA CR-145026

REPRODUCIBLE COPY (FACILITY CASEFILE COPY)

DISPLAY/CONTROL REQUIREMENTS

FOR VTOL AIRCRAFT

INTERIM TECHNICAL REPORT

by

William C. Hoffman
Renwick E. Curry
David L. Kleinman
Walter M. Hollister
Laurence R. Young

AEROSPACE SYSTEMS, INC.
Burlington, Massachusetts 01803

Approved

John Zvara

John Zvara
Technical Director

Prepared under
Contract No. NAS 1-13653

for

Langley Research Center
National Aeronautics and Space Administration
Hampton, Virginia 23665



August 1975

Page Intentionally Left Blank

FOREWORD

This report was prepared by Aerospace Systems, Inc. (ASI), Burlington, Massachusetts, for the National Aeronautics and Space Administration (NASA) under Contract No. NAS1-13653. The report documents the results of research performed during the period October 1974 to August 1975. The study was sponsored by the Flight Instrumentation Division, Navigation and Guidance Research Branch, the NASA Langley Research Center (LaRC), Hampton, Virginia. Dr. J. F. Creedon served as Technical Monitor on the contract.

The effort was directed by Mr. John Zvara, President and Technical Director of ASI. Mr. William C. Hoffman served as Project Engineer. Dr. Renwick E. Curry of the MIT Department of Aeronautics and Astronautics and the MIT Man-Vehicle Laboratory, Dr. David L. Kleinman of the University of Connecticut Department of Electrical Engineering and Computer Science, Dr. Walter M. Hollister of the MIT Department of Aeronautics and Astronautics, and Dr. Laurence R. Young, Director of the MIT Man-Vehicle Laboratory, contributed to the study as technical consultants and principal investigators.

Others who contributed to the study as technical consultants and/or co-investigators included Dr. Norman D. Ham, Director of the MIT V/STOL Technology Laboratory, Mr. Jack D. Howell, Pilot, Eastern Airlines, and the ASI engineering and programming support staff.

Page Intentionally Left Blank

TABLE OF CONTENTS

<u>Section</u>		<u>Page</u>
1	INTRODUCTION	1-1
2	VTOL DISPLAY/CONTROL DESIGN METHODOLOGY	2-1
	2.1 A Model for Simultaneous Monitoring and Control	2-1
	2.2 The Optimal Control Model of the Pilot at Three Levels	2-4
	2.2.1 Information Level	2-4
	2.2.2 Display Element Level	2-5
	2.2.3 Display Format Level	2-5
	2.3 VTOL Display/Control Design Procedure	2-5
3	DESIGN OF CANDIDATE CONTROL AND DISPLAY SYSTEMS	3-1
	3.1 Levels of Control Automation	3-1
	3.2 Uncoupled Control System Models	3-5
	3.2.1 Pitch and Roll Channel Models	3-5
	3.2.2 Yaw Channel Models	3-8
	3.2.3 Vertical Channel Models	3-11
	3.2.4 Bandwidth Summary	3-12
	3.3 Control System Design Using Quadratic Synthesis	3-13
	3.3.1 Quadratic Synthesis Summary	3-13
	3.3.2 Uncoupled Examples	3-15
	3.3.3 Coupled Longitudinal Control	3-19
	3.3.4 Coupled Lateral Control	3-22
	3.4 Flight Director Design Using Quadratic Synthesis	3-25
	3.4.1 Design Objectives	3-25

TABLE OF CONTENTS (Continued)

<u>Section</u>	<u>Page</u>
3.4.2	Signal Generation 3-26
3.4.3	Validation of Design Model 3-27
3.4.4	Modeling the Flight Director Effects 3-29
4	CONTROL THEORETIC MODELS FOR PREDICTING PILOT MONITORING PERFORMANCE 4-1
4.1	Characteristics of Monitoring Models 4-1
4.2	Monitoring Models 4-2
4.2.1	Non-Metric Based Models 4-3
4.2.2	Monitoring Metrics 4-6
4.2.3	Metric Based Monitoring Models 4-12
4.3	Simultaneous Monitoring and Control Within a Single Axis 4-20
5	MODEL VALIDATION 5-1
5.1	CH-46C Dynamic Equations of Motion 5-1
5.1.1	Basic Vehicle Dynamics 5-1
5.1.2	Augmentation Schemes 5-4
5.1.3	Wind Gust Disturbances 5-7
5.2	CH-46 Hover Display/Control Parameters 5-11
5.2.1	Primary Display Inputs - Hover Mode 5-11
5.2.2	Flight Director Inputs - Hover Mode 5-12
5.3	Model Predictions for CH-46 Hover 5-14
5.3.1	Model Predictions - No Flight Director Case 5-15
5.3.2	Single Axis Model Results - With Flight Director 5-16
5.3.3	Dual Axis Model Results - With Flight Director 5-18

TABLE OF CONTENTS (Continued)

<u>Section</u>		<u>Page</u>
6	CH-47 RESULTS	6-1
	6.1 Control Automation Levels	6-1
	6.2 Display Levels	6-4
	6.3 Program PIREP	6-14
	6.4 Control Model Results	6-22
	6.4.1 Attention Allocation vs Workload	6-23
	6.4.2 System Performance vs Workload	6-39
	6.4.3 Predicted rms Performance	6-39
	6.4.4 Attention Allocation vs Control Automation	6-50
	6.4.5 Attention Allocation vs Display Sophistication	6-50
	6.4.6 Control/Display Configuration Evaluation	6-50
	6.4.7 Fixed-Gain Flight Director	6-64
	6.5 Monitoring Model Results	6-67
7	DISPLAY CONCEPT AND FORMAT	7-1
	7.1 Straw-Man Display Concept - Panel Layout	7-2
	7.2 Attitude Director Indicator (ADI)	7-4
	7.3 Horizontal Situation Indicator (HSI)	7-4
	7.4 Altimeter	7-8
8	SUMMARY AND CONCLUSIONS	8-1
9	RECOMMENDATIONS	9-1
	9.1 Combined Lateral and Longitudinal Analysis	9-1
	9.2 Monitoring Model Investigation	9-1
	9.3 Effects of System Failures on the Piloting Task	9-2

TABLE OF CONTENTS (Continued)

<u>Section</u>	<u>Page</u>
9.4 Fixed-Base Simulation Experiments	9-2
9.5 Pilot Interaction With Automatic Systems	9-3
REFERENCES	R-1
BIBLIOGRAPHY	b-1
Appendices	
A EQUATIONS FOR THE OPTIMAL CONTROL MODEL FOR THE HUMAN OPERATOR	A-1
B ATTENTIONAL ALLOCATION USING THE OPTIMAL CONTROL MODEL	B-1
C LINEARIZED ROTORCRAFT EQUATIONS OF MOTION	C-1
D CH-46 DYNAMICS WITH MODEL-FOLLOWING AUGMENTATION	D-1
E STABILITY DERIVATIVES CH-47 HELICOPTER	E-1

LIST OF ILLUSTRATIONS

<u>Figure No.</u>		<u>Page</u>
2-1	System Control Performance Versus Workload	2-9
2-2	Monitoring Performance in the Control-Display Plane	2-11
2-3	Monitoring Performance for Candidate Systems Display/ Control	2-11
2-4	System Control Performance Versus Control Task Workload	2-16
3-1	Levels of Control Automation for Pitch or Roll Channel	3-2
3-2	Pitch or Roll Attitude Rate Model	3-6
3-3	Pitch or Roll Attitude Model	3-6
3-4	Horizontal Velocity Model - Hover Mode	3-7
3-5	Horizontal Position Model - Hover Mode	3-9
3-6	Airspeed Control Model - High Speed Mode	3-9
3-7	Heading Hold Model - Hover Mode	3-9
3-8	Turn Following Model - High Speed Mode	3-10
3-9	Heading Rate Model - High Speed Mode	3-10
3-10	Altitude Rate Model	3-11
3-11	Altitude Hold Model	3-12
3-12	Pitch Rate Controller	3-15
3-13	Pitch Controller	3-16
3-14	Horizontal Velocity Controller	3-18
4-1	Flow Diagram for Dual Axis Monitoring Allocations	4-22
5-1	System Matrices for Basic CH-46 Helicopter at Hover	5-3
5-2	System Matrices for Augmented CH-46 Helicopter at Hover	5-8
5-3	Scores Versus Attention, CH-46 Hover, Longitudinal Axis	5-19
5-4	Scores Versus Attention, CH-46 Hover, Lateral Axis	5-20

LIST OF ILLUSTRATIONS (Continued)

<u>Figure No.</u>		<u>Page</u>
5-5	Predicted Performance, CH-46 Hover, Flight Director Used	5-22
6-1	System Dynamics Matrices, System A	6-5
6-2	System Dynamics Matrices, System B	6-6
6-3	System Dynamics Matrices, System C	6-7
6-4	System Dynamics Matrices, System D	6-8
6-5	System Dynamics Matrices, System F	6-9
6-6	System Dynamics Matrices, System G	6-10
6-7	System Dynamics Matrices, System H	6-11
6-8	Display Vector for Basic Information	6-13
6-9	Flight Director Algorithms, System A	6-15
6-10	Flight Director Algorithms, System B	6-16
6-11	Flight Director Algorithms, System C	6-17
6-12	Flight Director Algorithms, System D	6-18
6-13	Flight Director Algorithms, System F	6-19
6-14	Flight Director Algorithms, System G	6-20
6-15	Flight Director Algorithms, System H	6-21
6-16	Principal Inputs and Outputs of Program PIREP	6-22
6-17	Attention Allocation Versus Total Control Attention (System A - No Flight Director)	6-24
6-18	Attention Allocation Versus Total Control Attention (System A - Full Flight Director)	6-25
6-19	RMS Performance Versus Total Control Attention (System A - No Flight Director)	6-26
6-20	Attention Allocation Versus Total Control Attention (System B - No Flight Director)	6-27

LIST OF ILLUSTRATIONS (Continued)

<u>Figure No.</u>		<u>Page</u>
6-21	Attention Allocation Versus Total Control Attention (System B - Full Flight Director)	6-28
6-22	Attention Allocation Versus Total Control Attention (System C - No Flight Director)	6-29
6-23	Attention Allocation Versus Total Control Attention (System C - Full Flight Director)	6-30
6-24	Attention Allocation Versus Total Control Attention (System D, E - No Flight Director)	6-31
6-25	Attention Allocation Versus Total Control Attention (System D, E - Full Flight Director)	6-32
6-26	Attention Allocation Versus Total Control Attention (System F - No Flight Director)	6-33
6-27	Attention Allocation Versus Total Control Attention (System F - Full Flight Director)	6-34
6-28	Attention Allocation Versus Total Control Attention (System G - No Flight Director)	6-35
6-29	Attention Allocation Versus Total Control Attention (System G - Full Flight Director)	6-36
6-30	Attention Allocation Versus Total Control Attention (System H - No Flight Director)	6-37
6-31	Attention Allocation Versus Total Control Attention (System H - Full Flight Director)	6-38
6-32	Control Performance Cost Versus Total Control Attention (Hover - No Flight Director)	6-40
6-33	Control Performance Cost Versus Total Control Attention (Hover - z Flight Director)	6-41
6-34	Control Performance Cost Versus Total Control Attention (Hover - x Flight Director)	6-42
6-35	Control Performance Cost Versus Total Control Attention (Hover - Full Flight Director)	6-43

LIST OF ILLUSTRATIONS (Continued)

<u>Figure No.</u>		<u>Page</u>
6-36	Control Performance Cost Versus Total Control Attention (Approach - No Flight Director)	6-44
6-37	Control Performance Cost Versus Total Control Attention (Approach - z Flight Director)	6-45
6-38	Control Performance Cost Versus Total Control Attention (Approach - x Flight Director)	6-46
6-39	Control Performance Cost Versus Total Control Attention (Approach - Full Flight Director)	6-47
6-40	RMS Performance Versus System Automation (No Flight Director)	6-48
6-41	RMS Performance Versus System Automation (Full Flight Director)	6-49
6-42	Control Attention Allocation Versus System Automation (No Flight Director)	6-51
6-43	Control Attention Allocation Versus System Automation (Full Flight Director)	6-52
6-44	Control Attention Allocation Versus Display Sophistication (System A)	6-53
6-45	Control Attention Allocation Versus Display Sophistication (System B)	6-54
6-46	Control Attention Allocation Versus Display Sophistication (System C)	6-55
6-47	Control Attention Allocation Versus Display Sophistication (System D)	6-56
6-48	Control Attention Allocation Versus Display Sophistication (System F)	6-57
6-49	Control Attention Allocation Versus Display Sophistication (System G)	6-58
6-50	Control Attention Allocation Versus Display Sophistication (System H)	6-59
6-51	Normalization of Performance and Workload Metrics	6-61

LIST OF ILLUSTRATIONS (Continued)

<u>Figure No.</u>		<u>Page</u>
6-52	Normalized Control Display Configuration Evaluation for CH-47	6-62
6-53	Average Gain Flight Director Algorithms	6-63
6-54	Fixed-Gain Flight Director Performance (System C)	6-65
6-55	Fixed-Gain Flight Director Performance (System G)	6-66
6-56	Monitoring Performance Cost Summary	6-68
6-57	Total Performance Cost Summary	6-69
7-1	Straw-Man Display Concept - Panel Layout	7-3
7-2	Straw-Man Display Concept - ADI Layout for System C	7-5
7-3	Straw-Man Display Concept - HSI Layout	7-7
7-4	Straw-Man Display Concept - Altimeter Layout	7-9

**Page
Intentionally
Left Blank**

LIST OF TABLES

<u>Table No.</u>		<u>Page</u>
2-1	VTOL Display/Control Design Procedure	2-6
3-1	Levels of Control Automation	3-4
3-2	CH-47 Automation Levels	3-4
3-3	Approximate Bandwidth of Uncoupled Control Model Responses	3-12
5-1	CH-46C Primary Display Inputs (Hover Mode)	5-12
5-2	Model Results. Longitudinal Axis, $f_l = 0.3$	5-15
5-3	Model Results. Lateral Axis, $f_c = 0.3$	5-16
5-4	Model Predictions Using Flight Director, $f_c = 0.3$	5-17
5-5	Attentional Allocations for Longitudinal Task	5-17
5-6	Model Results. Lateral Axis with Flight Director, $f_c = 0.3$	5-18
6-1	Levels of Control Channel Automation	6-1
6-2	Selected CH-47 Automation Levels	6-2
6-3	Weighting Functions for Longitudinal CH-47 Automation Levels	6-3
6-4	Control Cost Weighting Functions and Indifference Thresholds for CH-47	6-12

SECTION 1 INTRODUCTION

Vertical takeoff and landing (VTOL) aircraft have considerable potential for use in a viable short-haul air transportation system. The VTOL aircraft used in this context would provide convenient, safe and reliable access to long-haul air transportation by providing air service from major and smaller cities to regional airports. They would also contribute to the achievement of a more balanced total transportation system by providing direct links between smaller cities and major cities and between nearby major cities.

In order for such a VTOL short-haul system to be economically feasible, the aircraft must provide schedule reliability in all-weather conditions, must provide acceptable levels of ride quality, and must be operated directly into the city centers to provide the requisite convenience to passengers. Before a viable VTOL system can become a reality, technology developments are needed in a number of areas. During the past several years many advanced VTOL aircraft design programs have been carried out by NASA, DOD and the aircraft industry to develop economical vehicles with improved ride qualities and controllability which would be suitable for a commercial VTOL transportation system. However, to effectively utilize these vehicles and to exploit their unique characteristics for minimizing noise and both air and ground space requirements, corresponding advances must be made in handling qualities, operating procedures, and all-weather avionics.

The NASA Langley Research Center (LaRC) has undertaken a research program to develop the navigation, guidance, control, display and flight management technology base needed by Government and industry in establishing systems design concepts and operating procedures for VTOL short-haul transportation systems in the 1980s

time period and beyond. The VALT (VTOL Automatic Landing Technology) Program encompasses the investigation of operating systems and piloting techniques associated with VTOL operations under all-weather conditions from downtown vertiports; the investigation of terminal air traffic and airspace requirements; and the development of avionics including navigation, guidance, controls, and displays for automated takeoff, cruise, and landing operations.

In support of the VALT Program, Aerospace Systems, Inc. (ASI) has conducted a number of research studies for LaRC which provide a technology base for the present study. In the initial effort (Reference 1), ASI analyzed the navigation and guidance requirements for commercial VTOL operations in the takeoff, cruise, terminal area, and landing phases of flight in weather conditions up to and including Category III. A digital computer simulation (Program VALT) was developed to provide a means for evaluating the performance of candidate VTOL guidance and control systems. This program was used to conduct a sensitivity study of several VTOL guidance and control system concepts (Reference 2).

One conclusion in Reference 1 was that curved decelerating approaches will be required for safe, efficient, and independent VTOL operations. To facilitate these maneuvers, a spiral descent technique was formulated as a possible standard VTOL approach procedure. The spiral descent investigated by ASI in Reference 3 uses minimal airspace, accommodates arrivals from any direction, and can service multipad landings. The spiral approach also provides the benefits of a vertical descent, but avoids the vortex ring state, maintains a stable airspeed, and uses less fuel.

The guidance of a VTOL along this type of spiral descent trajectory is complicated by many control problems which are unique to this class of aircraft. To reduce the workload for the guidance and control tasks to a tolerable level for multiple daily landings, the aircraft controls will be partially or completely automated. As the level of

automation increases, the pilot's role shifts from primarily that of a controller towards that of a system monitor and manager. The purpose of the present study was to examine which tasks should be allocated to the pilot of an automated VTOL aircraft utilized as part of a short-haul air transportation system and to determine what displayed information will be required in performing these tasks.

While the study was intended to provide insight into problems associated with VTOL pilot tasks in an automated VTOL aircraft in general, several guidelines were specified by NASA to provide a frame of reference and to ensure that the results could be readily used and evaluated in VALT and other existing Langley Research Center programs. These guidelines included the following:

- **Flight Profile** - The emphasis of the study was to be on the approach and landing phase of flight; however, sufficient general consideration to the takeoff and enroute phases of flight was to be included to ensure that the study results would be compatible with the overall task of operating the vehicle as a commercial transport.
- **Vehicle Dynamics** - The study was to utilize the CH-46C and CH-47 helicopters used in the LaRC flight research programs.
- **Crew** - Crew tasks were to be configured to permit operation by one pilot. Routine calls, communication channel selection, or other tasks which might be handled by a second crew member in an operational context were not included in the scope of work.
- **Pilot Involvement** - The levels of automation considered were to be varied over a range extending from a fully automatic system with the pilot in a passive mode with respect to control activity to a system with full manual control.
- **Technology Date** - In defining a level of system automation, allocating tasks to automatic systems, and in conceiving displays for the control/display concept, decisions were to be based on the relevant technology projected as being available in the mid 1980s.
- **Pilot/Hardware Experiments** - Hardware tests, flight tests, and pilot/hardware interaction experiments were to be specifically excluded from the scope of the work.

Some preliminary results obtained during the present study were included in a paper presented by the principal investigators in Reference 4. This report includes a complete description of the work performed and the results obtained during the investigation. Section 2 discusses the VTOL display/control methodology used, including a description of the model developed for simultaneous monitoring and control. Section 3 includes a discussion of the logic used for the choice of control systems, a description of the different levels of automation investigated, and the models that were formulated. The different approaches for pilot monitoring performance prediction and choices of monitoring workload performance metrics are examined in Section 4. Section 5 presents the model validation analysis results which utilize data obtained by NASA during CH-46C helicopter flight tests. Results obtained for eight CH-47 levels of control automation are presented in Section 6. In Section 7 a CH-47 display concept and format is presented. Conclusions and recommendations are given in Sections 8 and 9 respectively, followed by a List of References and a Bibliography. The Appendices contain detailed technical information concerning the equations for the optimal control model for the human operator, attentional allocation using the optimal control model, and CH-46C and CH-47 aircraft characteristics used in the study.

SECTION 2

VTOL DISPLAY/CONTROL DESIGN METHODOLOGY

The pilot's functions throughout the entire flight of a VTOL aircraft can be broadly classified in the two areas of (1) control and (2) monitoring; both of these functions are necessary for safe and efficient operations. This study has addressed itself to the development of a pilot/vehicle model for simultaneous monitoring and control in order to explore the display/control tradeoffs inherent in the selection of a display and control system for an automated VTOL aircraft. The advantage of using the model in the preliminary stages is that a wide variety of candidate systems can be explored with a minimal amount of effort and cost. The detailed man-in-the-loop simulations can and should be reserved to resolve the minor details between competing display/control systems and to confirm the predictions of the model.

Regardless of the form of the model used to carry out the display/control design, it is imperative that this model have realistic and quantitative metrics for the following:

- System control performance
- Workload for control
- Monitoring performance
- Workload for monitoring

Without measures for these four quantities, one would be unable to explore the many and varied tradeoffs between control, monitoring, augmentation systems and displays.

2.1 A MODEL FOR SIMULTANEOUS MONITORING AND CONTROL

This section briefly outlines a model for simultaneous monitoring and control which is used in the design methodology outlined in Subsection 2.2. This model is based

on the optimal control model of the human operator (References 5 and 6), which is described in more detail in Appendix A.

The performance metric for the control task is given by

$$J_c = \sum_{i=1}^n \sigma_{x_i}^2 / x_i^2 \max \quad (2-1)$$

where J_c = performance metric for control

σ_{x_i} = standard deviation for x_i

x_i = i^{th} component of state vector x

Equation (2-1) is a relative weighting of the variances of the individual components of the state vector normalized by their maximum allowable excursions. When evaluating competing systems, one may use a subset of the state vector components; this is equivalent to assuming that some components have infinite allowable deviations.

The workload metric for control is based on the task-interference model of Reference 7. This metric states that for a single display element, the covariance of the observation noise at the input to the pilot model (see Appendix A) is given by

$$V_{y_i} = \rho_i \sigma_{y_i}^2 \quad (2-2)$$

where the noise-to-signal ratio ρ_i is approximately 0.01, and y_i is the i^{th} displayed variable. When the pilot devotes only a part of his attention to any one display element, then the observation noise can be modelled as

$$V_{y_i} = \frac{\rho_i \sigma_{y_i}^2}{f_{c_i}} \quad (2-3)$$

where f_{c_i} is the fraction of attention allocated to the i^{th} display. This observation noise has the appropriate limiting values: if $f_{c_i} = 1$, then Equation (2-3) reduces to the full-attention results, Equation (2-2); when the controller is not using the i^{th} display, then $f_{c_i} = 0$, and the observation noise is infinite, corresponding to no observations at all. The fractions of attention f_{c_i} must all be positive and sum to the total fraction of attention being used for control. Thus the control workload metric is given by

$$f_c = \sum_i f_{c_i}, \quad f_{c_i} \geq 0. \quad (2-4)$$

The pilot allocates his attention between the displays, spending the larger fractions of attentions on displays which are most useful for control. This behavior is formulated in the model by the assumption that the pilot minimizes a quadratic performance index with respect to the f_{c_i} subject to the constraints of Equation (2-4), i.e.,

$$\min_{(f_{c_i})} J = \min_{(f_{c_i})} E \left\{ \lim_{T \rightarrow \infty} \frac{1}{T} \int_0^T [x^T Q_x x + \dot{u}^T Q_r \dot{u}] dt \right\} \quad (2-5)$$

where Q_x and Q_r are positive semidefinite weighting matrices. Since the performance index in Equation (2-5) can be evaluated for any specific values of f_{c_i} in Equation (2-3), it is conceptually a simple problem to further minimize this cost function subject to the constraints of Equation (2-4). Appendix B contains details of the associated equations and the techniques for performing this minimization.

The basic form of the model for simultaneous monitoring and control can now be described. For a given level of control task workload, f_c , the pilot will allocate his attention as described by Equation (2-5) to minimize the performance index. This is first in the hierarchy of control and monitoring, i.e., the pilot will first attend to

the control task, and with any available attention remaining, will then attend to the monitoring task. Thus the control task workload metric of Equation (2-4) and the control task performance metric of Equation (2-1) can be used to draw the control performance/workload tradeoff curve. At any given level of system performance (or workload), the pilot will have some residual capacity or fraction of attention after attending to the control task. We assume a total fraction of attention of 0.8 should be allocated to both the control and monitoring tasks: e.g., if the control task requires a fraction of attention of 0.3, a fraction of attention of 0.5 is available for monitoring; similarly, if the control task requires $f = 0.7$, then only 0.1 fraction of attention is available for monitoring. Thus the control task workload metric and the monitoring task workload metric obey the constraint given in Equation (2-6).

$$f_c + f_m = f_{TOT} \sim 0.8 \quad (2-6)$$

2.2 THE OPTIMAL CONTROL MODEL OF THE PILOT AT THREE LEVELS

This section includes a description of the development and use of the optimal control model of the pilot which was refined during the course of this study. The model can be exercised at three levels of detail. These levels have been termed the "information level," the "display element level," and the "display format level." Each of these levels and the use of the model in these levels will now be briefly described.

2.2.1 INFORMATION LEVEL

At this level of operation, each of the elements of the state vector is assumed to be observable by the pilot. Each of these "observations" is assigned its own fraction of attention for control, and the optimization of the performance index, Equation (2-5), is carried out for various levels of control task workload f_c . This

procedure leads to a very simple way of determining the information requirements for the task, since those state variables of greater importance will receive the greater amount of attention.

2.2.2 DISPLAY ELEMENT LEVEL

The display element level is perhaps the most common level of operation for the optimal control model; each of the displayed quantities is assumed to be indicated by a display "element." The inputs to the model in this configuration are the position of the display element and its rate of change. Each of the display elements is assigned a given level of attention, so that the observation noise for both the display element position and display element rate are assigned the same fraction of attention for control, f_{c_i} . Attention allocation is found by minimizing Equation (2-5).

2.2.3 DISPLAY FORMAT LEVEL

This level of use of the pilot model is very similar to the display element level described above. However, in this case specific characteristics of the display format such as indifference thresholds, lack of a zero reference, saturation limits, smoothing filters for display augmentation, etc., are incorporated into the model.

The details of the use of the model at these three levels are explained in the next section on display/control system design methodology.

2.3 VTOL DISPLAY/CONTROL DESIGN PROCEDURE

The VTOL display/control design procedure developed and utilized in the study is a ten-step process. These ten steps can be broken down into four main categories: information requirements, control/monitor performance, pilot/automatic task allocation, and display format design. The ten steps, outlined in Table 2-1, are discussed in detail below.

Table 2-1. VTOL Display/Control Design Procedure.

CATEGORY	STEP
Information Requirements	<ol style="list-style-type: none"> 1. Determine max x_i and max J_c from mission requirements. 2. Select candidate control systems. 3. Calculate J_c vs. f_c at the information level for each control system (include steering commands). 4. Choose display elements.
Control/Monitor Performance	<ol style="list-style-type: none"> 5. Calculate J_c vs. f_c at the display element level for each display/control system. 6. Determine $f_m = f_{TOT} - f_c$ and J_m from monitoring model.
Pilot/Automatic Task Allocation	<ol style="list-style-type: none"> 7. Select display/control system configuration.
Display Format Design	<ol style="list-style-type: none"> 8. Select display format candidates. 9. Determine J_c, J_m vs. f_c for each display format. 10. Select display format.

Step 1. Determine max x_i and max J_c from mission requirements.

The maximum deviations of state vector components are selected from the mission requirements, pilot acceptance criteria, and passenger acceptance criteria. These maximum values of x_i are used to determine the coefficients in the quadratic cost functional. The maximum of the overall figure of merit of the system control performance, max J_c , is a function of the upper limit of the maximum acceptable

error variances which are determined by the mission requirements; i.e., for a given trajectory and attitude tolerance, there is a value of J_c which must not be exceeded for any system to be considered viable. For example, if the $|x_{i, \max}|$ values are exceeded with probability of 0.05, then $|x_{i, \max}|$ may be interpreted as twice the maximum standard deviation under the Gaussian assumption. If each of the variances is at its maximum (a worst case design), then $J_{c, \max}$ is $n/4$, where n is the number of terms in Equation (2-1).

Step 2: Select candidate control systems.

The candidate control systems which utilize different levels of augmentation are selected and designed. The output of this step of the procedure is a set of controlled-element dynamics which interact with the pilot. These levels of automation may cover the complete spectrum from the raw unaugmented vehicle through complete position feedback, i.e., a fully automatic system. The details of the control system design procedures used for this study are described in Section 3.

Step 3: Calculate J_c vs. f_c at the information level for each control system.

This is the key step in determining information requirements for the candidate control systems. Each element of the state vector of the system is considered as a measurement, with its own fraction of attention for control, i.e., the display element and its rate are treated independently. For a given level of control attention f_c , the performance index is minimized subject to the constraint of Equation (2-4),

$$\sum_i f_{c_i} = f_c, \quad f_{c_i} \geq 0.$$

Included in the displayed information should be director/steering commands designed for each particular level of automation. (See Section 3 for the description of the

flight director design used in this study.) The specified level of control fraction of attention, f_c , does not carry the same meaning as it does when operating at the display element level of the model. However, when i is varied from 0 to the number of states, f_i provides the relative importance of each of the states. These in turn are used as input to the next step of the design procedure.

Step 4: Choose display elements.

At this stage of the design procedure, the information requirements derived in the previous step are used to choose display elements. The most difficult part of this step is determining whether or not a separate display of rate is required for use by the pilot. For the pitch attitude display element, pitch and pitch rate are used as inputs to the optimal control model of the pilot; the same is true for altitude and altitude rate. However, it is empirically known that separate displays of pitch attitude and rate are not required, while a separate display of altitude rate is required. These differences are due to the accuracy with which the rate may be inferred from a position display; for pitch attitude, pitch rate may be discerned to sufficient accuracy from the indicator, whereas this is not true for the altitude indicator. This is due to the inherent delay in the barometric altitude indication and the dynamic range of the displayed signal. New types of altimeter systems and displays mediate this somewhat, but explicit vertical speed information is still used in the majority of conventional instrument panels.

The decision of whether or not to include a separate rate display can be inferred from the information level results of the previous step by examining the required accuracy of display.

Step 5: Calculate J_c vs f_c at the display element level for each display/control system.

This step is similar to Step 3, where the control performance metric, J_c , is computed for different values of workload metric f_c . This leads to curves of control performance vs. workload having the general shape shown in Figure 2-1. This curve is plotted for two systems, but in general there will be as many systems as there are levels of automation times the number of flight director options, i.e., if there were five levels of automation and two flight director options (with and without flight director), then there would be curves for ten competing display/control systems shown in Figure 2-1. It should be noted that Figure 2-1 is the plot of the minimum value of J_c for a given f_c , i.e., the attention has been allocated to minimize the performance index. Thus additional outputs of the model at this stage are the fractions of attention being spent on each of the display elements. To prevent overly optimistic predictions of performance at this stage, indifference thresholds should be incorporated in the model calculations (see Appendix A), since this is a well-known facet of pilot behavior. (In the present study, $x_{i, \max}/4$ was used as a representative value.)

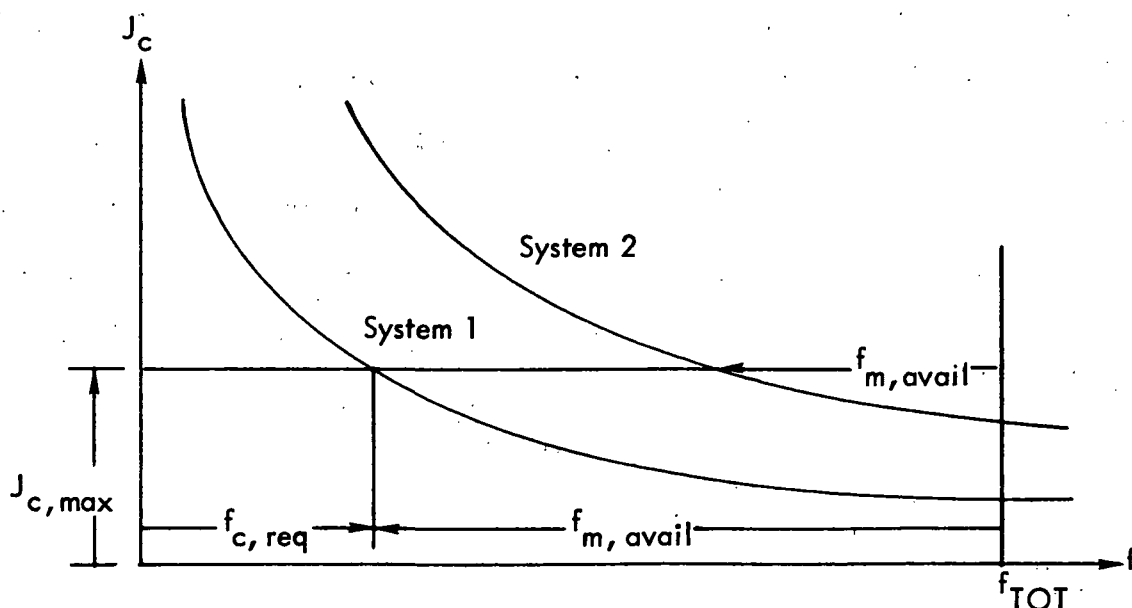


Figure 2-1. System Control Performance Versus Workload.

Step 6: Determine $f_m = f_{TOT} - f_c$ and J_m from monitoring model.

This step is also shown in Figure 2-1, where the value of total attention for the control and monitoring task (f_{TOT}) is specified. Since the curves will be monotonically decreasing (the more attention for control, the better the job of control one can do), a line has been drawn at the maximum value of control performance, $J_{c, max}$, consistent with the mission requirements. The intersection of this line of constant control performance and the J_c vs. f_c curve for each of the candidate systems determines the minimum amount of control attention required, $f_{c, req}$. The difference between this amount of attention, and the total available for the entire task is the residual fraction of attention available for monitoring $f_{m, avail}$.

Thus of the four important metrics required for the display/control design process, three have been determined at this stage: f_c , J_c , and f_m . The fraction of attention available for monitoring is then applied to the monitoring model (see Section 4 for a discussion of the monitoring models). Since the monitoring performance will be monotonic with monitoring attention, one simple monitoring strategy is equal allocation of attention to the monitoring instruments.

Results of applying the monitoring model may be plotted as shown in Figure 2-2. This shows the contours of constant monitoring performance in the control complexity-display complexity plane often used in discussions of the VTOL display/control design problem. Although curves of pilot workload are normally plotted in this plane, monitoring performance is an equivalent measure for our discussion. It should be noted that competing systems, which appear as points in this plane, are being compared on the basis of the same total workload and the same level of system performance.

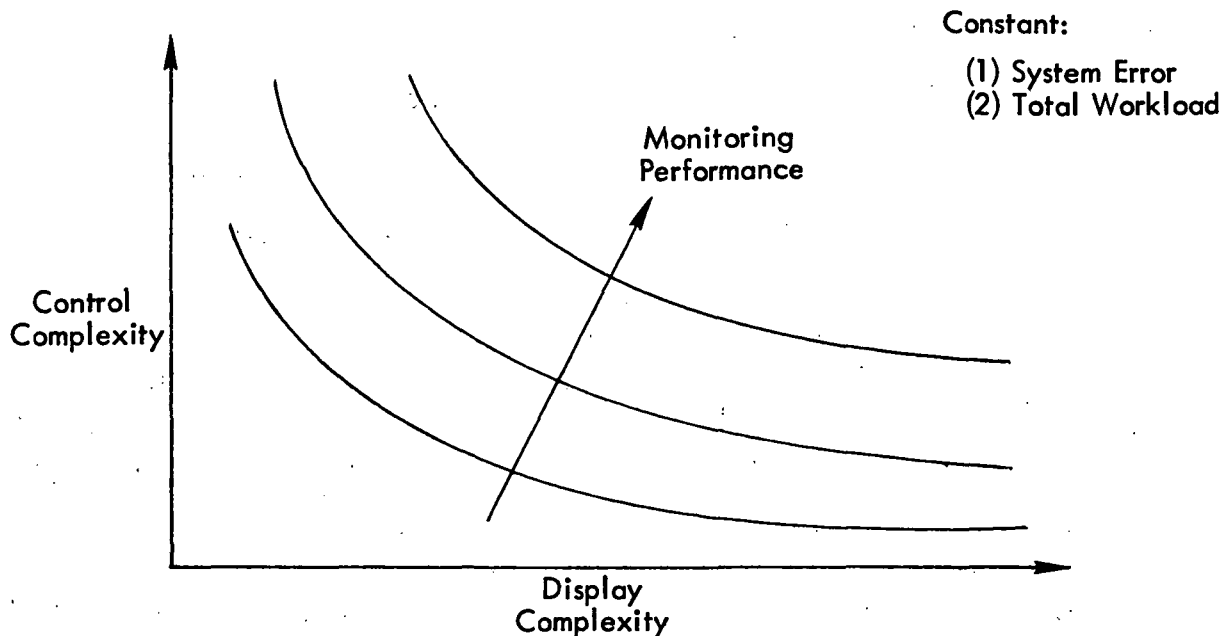


Figure 2-2. Monitoring Performance in the Control-Display Plane.

Perhaps a more meaningful presentation of the monitoring performance data is shown in Figure 2-3. This form of the data is easier to interpret when many tradeoffs are necessary during the system selection as described in the next step.

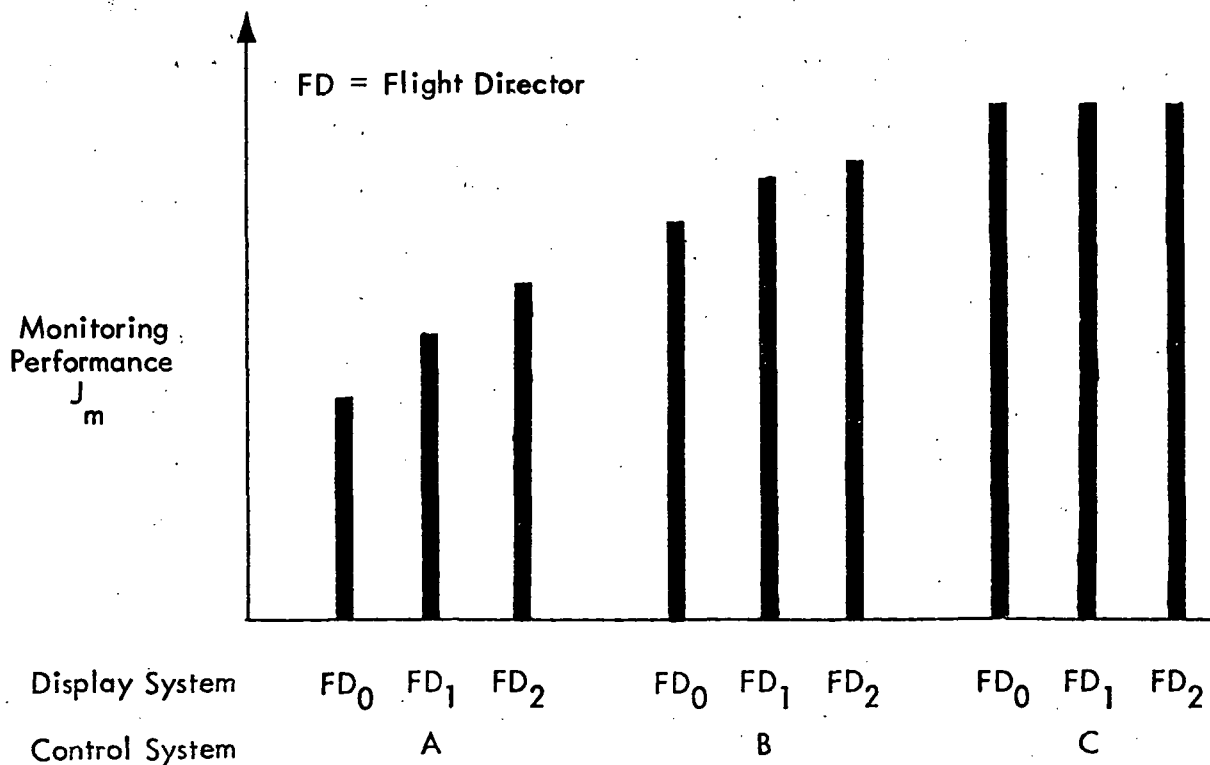


Figure 2-3. Monitoring Performance for Candidate Systems Display/Control.

Step 7: Select display/control system configuration.

Criteria for allocating the tasks between the pilot and the automatic system should be based on the following considerations ranked in order of importance.

- Required workload level less than or equal to approximately 0.8
- Sensitivity of workload level to changes in display control configuration system failure modes
- Sensitivity of performance to changes in control and monitoring workload
- Cost

An approximate level of 80% workload on which to base the next phase of design provides an adequate although not excessive margin for the more detailed design and analysis of the display format. The sensitivity of workload level to changes in display and control configurations is important because it minimizes the impact of modeling errors on the final decision and minor display or control mode changes will not place excessive workload on the pilot. A brief examination of systems failure modes is important during this part of the analysis because it provides an indication of whether or not the system can be controlled when either the display or the control system fails. However, Figures 2-2 and 2-3 are calculated for accuracy requirements that may be too stringent during the failed condition.

The first of the allocation criteria is satisfied by the conditions under which the calculations were made, i.e., Figures 2-2 and 2-3 have been obtained for a total workload level of 0.8. The sensitivity to changes in display/control configurations can be determined by examining Figure 2-3. For example, should System A be chosen with the flight director 2 display option (FD_2), then under flight director failure a change of monitoring performance (while maintaining the control performance) is given by the difference in the values of J_m for FD_2 and FD_0 conditions. Control system failures (while maintaining the same level of control performance) can be assessed by

examining the change from one configuration to another. For example, if the nominal system operates with the display of FD_2 and control system C, then a failure in the control system will revert the control task back to that of control system A with no flight director. (It is assumed that the flight director mode must be turned off if there is a change in control systems because of the difference in flight director gains for different control systems. That is, a flight director designed for control system C may not be adequate, and may even lead to deleterious performance, when used with control system A.)

Step 8: Select display format candidates.

The display formats, which may be one of three types (separated displays, perspective displays, or combined displays) should be selected according to the following guidelines discussed in Section 7:

- Operator centered and oriented
- Geometric "real world" compatibility
- Naturalness (for high stress situations)
- "Status at a glance" for situation displays
- Predictive capability for situation displays
- Compactness
- Lack of clutter

In addition to these interpretability considerations, operational guidelines should be used which include failure mode consideration (the ability to make missed approaches with a minimum of control and display augmentation), display options (such as change in scale), and flexibility and versatility in trajectory selection. Details of this procedure are described in Section 7.

Step 9: Determine J_c , J_m vs f_c for each display format.

The basic approach in evaluating the display format candidates is to perform the computations of Step 3 with a more detailed model and description to account for specific display formats and mechanizations. In general, one should expect the performance to degrade somewhat due to the practical aspects of implementing the information display. For a given display candidate, one should include the effect of scaling, thresholds, and a zero reference (or lack of one) by a detailed noise-variance model. Note that if each of the format candidates is chosen to be consistent with the indifference thresholds used in the calculations of Step 5, there should be only minor changes in performance due to this effect.

The specification of the observation noise variance model will take the form

$$V_{y_i}(t) = \frac{V_{y_i}^0}{f_{c_i}} \left[K^2 (\sigma_{y_i}) + \sigma_{0_i}^2 \right] \quad (2-7)$$

where V_{y_i} is the observation noise covariance for the i^{th} input to the Kalman filter portion of the pilot model. $V_{y_i}^0$ is the nominal sole-task noise variance, and f_{c_i} is the control-task fraction of attention allocated to this display variable. The quantity in the brackets is a detailed noise model that is a function of the particular display format being evaluated. Typically there are two effects as shown in Equation (2-7).

- K^2 represents the describing function which predicts and accounts for noise variances due to thresholds, saturations, and other nonlinearities of the display;
- $\sigma_{0_i}^2$ is a variance representing the effect of (or lack of) a zero reference for the display. In other words if there is no zero reference for the display and the pilot has to judge the value of the displayed variable relative to the position in its total range of travel, then the observation noise of this variable will be greater than if he is provided a zero, or commanded reference.

A further change in the model should be the incorporation of realistic flight director computers; since these signals must be generated from noisy information, which often involves high-pass or differentiation of such data, requiring that the navigation data be filtered before presentation to the pilot to avoid his rejection on the basis of noisy signals. Thus, one must specify the dynamics of the actual flight director to be used in the computations at this stage.

Using the more detailed model of the display format, one may again determine system control performance J_c vs control task workload f_c for the different display formats as shown in Figure 2-4. These curves are generated for several different formats of the display/control system selected in Step 7 and form the basis for making the final display format selection in the next step. In a manner similar to that of calculating the control performance J_c , one should recalculate the monitoring performance metric J_m for every value of f_m , which is the residual of the fraction of attention after attending to the control task.

Step 10: Select display format.

The specific selection of the individual candidate displays should be based on the following criteria:

- Workload level
- System performance
- Monitoring performance
- Sensitivity considerations
- Adherence to display design principles
- Operational considerations

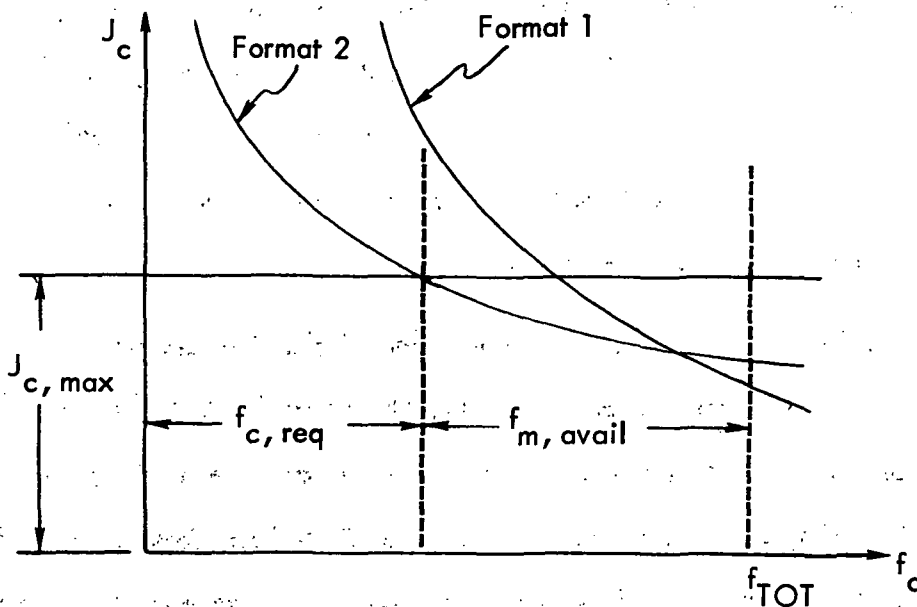


Figure 2-4. System Control Performance Versus Control Task Workload.

Primary consideration should be given to system performance and control task workload, since these two quantities are the ones for which the most empirical data exist. Furthermore, the pilot will attend to his control tasks in a hierarchal ordering of flight control (flight director) tasks and he will then attend to the monitoring tasks if there is available time.

The specification of the system performance level will have an impact on whether or not an automatic performance assessment and failure monitor needs to be included in the system for a given set of trajectory and wind conditions. If the system performance is fixed at a low enough level, then the amount of attention required to perform the control task f_c , will be close to the pilot's ultimate capacity, hence little, if any, margin is allowed for unexpected distractions or for monitoring. If these conditions prevail then an automatic failure monitor and performance assessment system must be considered to accomplish these approaches with the desired degree of pilot acceptance.

SECTION 3

DESIGN OF CANDIDATE CONTROL AND DISPLAY SYSTEMS

Realistic helicopter control system models are required in conjunction with the analytic representations of the human pilot and the aircraft displays. In accordance with the study guidelines the control system models which were developed represented levels of automation that varied over a wide range extending from 1) a fully automatic system with the pilot in a passive mode with respect to control activity to 2) a system with full manual control. This section includes a description of the different levels of control automation investigated and the models that were formulated, and a discussion of the flight director design process that was followed.

3.1 LEVELS OF CONTROL AUTOMATION

The potential control system configurations can be classified in terms of 1) the aircraft's three dynamic axes and 2) the outermost feedback loop closure. This can be seen in Figure 3-1 which shows the level of control automation for the pitch or roll channel. With the position feedback loop closed in a particular axis, the system is fully automatic and the pilot becomes simply a monitor for that axis. Completely automatic control would involve position feedback in all axes. For normal operation, the aircraft would have a stability augmentation system (SAS) with attitude rate feedback. However in the event of an SAS failure, the unaugmented configuration would exist.

The output of the control system in each case consists of the four actuator displacements that are used to control the unaugmented vehicle. These consist of

δ_e = pitch control (elevator or differential collective)

δ_a = roll control (aileron or roll cyclic)

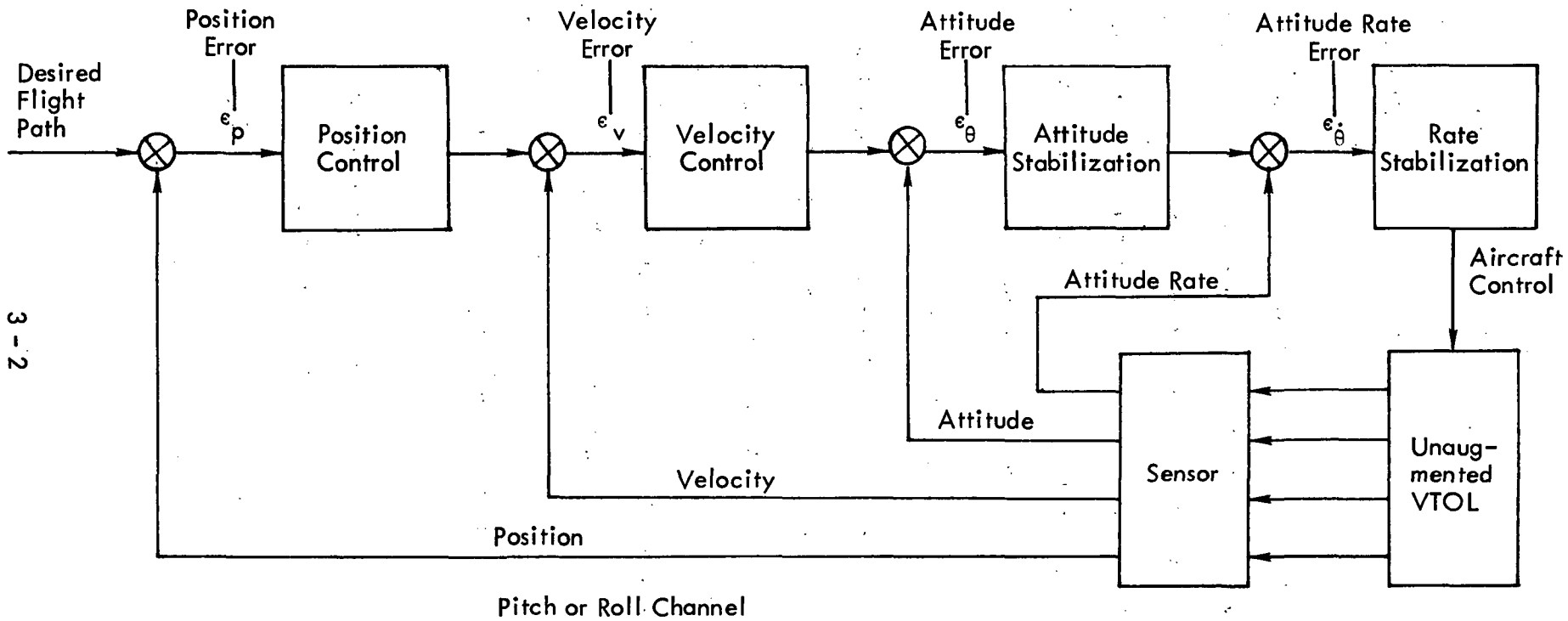


Figure 3-1. Levels of Control Automation for Pitch or Roll Channel.

δ_r = yaw control (rudder or yaw cyclic)

δ_c = vertical control (collective)

The input commands to the control system are to be selected. Since it may be desirable to design different levels of automation for each control channel, they were considered separately.

For the pitch and roll channels there are four possible input levels for each as indicated in Figure 3-1. These are termed horizontal position commands, horizontal velocity commands, attitude commands and attitude rate commands, respectively.

For the vertical channel there are only two input levels to be considered, since vertical translation acceleration is related directly to collective. For the yaw channel there are also only two input levels to be considered because yaw motion is not directly coupled to translation as are pitch and roll. Yaw control at the attitude rate command level is usually implemented such that yaw rate is proportional to yaw control displacement. Yaw control at the attitude level is usually implemented in either a "Heading Hold" or a "Turn Following" mode. The former is used during low speed and hover. The latter is used at higher speed to give coordinated turns. The "Heading Hold" mode is implemented by commanding present heading so long as the rudders are neutral. When the rudders are out of neutral, the commanded heading is changed at a rate proportional to yaw control displacement. The "Turn Following" mode is usually implemented by nulling either the sideslip angle, β , or y-axis specific force as measured by a body-mounted accelerometer.

Considering the unaugmented actuator as an additional mode in each channel, there are three or five levels of automation possible in each of the control channels of the the helicopter (see Table 3-1). Thus the number of possible combinations is $5 \times 5 \times 3 \times 3 = 225$. However, many of these combinations are not practical systems

Table 3-1. Levels of Control Automation.

Forward	Vertical	Lateral	Directional
δ_{e_c}	δ_{c_c}	δ_{a_c}	δ_{r_c}
q_c	V_{z_c}	p_c	r_c
θ_c	h_c	ϕ_c	ψ_c
V_{x_c}		V_{y_c}	
x_c		y_c	

for normal operations. A series of eight systems were selected to represent the full range of automation for the CH-47 helicopter ranging from purely manual with direct actuator commands to full position control. These are shown in Table 3-2.

Table 3-2. CH-47 Automation Levels.

System	Control Channel Command			
	Pitch or Forward	Vertical	Roll or Lateral	Yaw or Directional
A	δ_e	δ_c	δ_a	δ_r
B	q	δ_c	p	r
C	θ	δ_c	ϕ	r
D	θ	V_z	ϕ	r
E	θ	V_z	ϕ	ψ
F	θ	h	ϕ	ψ
G	V_x	h	V_y	ψ
H	x	h	y	ψ

3.2 UNCOUPLED CONTROL SYSTEM MODELS

This subsection discusses the approximate closed-loop dynamic response of the control system for each control channel. The intent is to provide an understanding of the design objectives for each level of automation and their overall hierarchy. Subsection 3.3 will present the unified design approach for the coupled systems using the vehicle dynamics models.

3.2.1 PITCH AND ROLL CHANNEL MODELS

The pitch and roll channels can be made to respond similarly in the low speed or hover mode. In the high speed mode air speed is substituted for forward ground velocity at the velocity command level and heading rate is substituted for lateral ground velocity. The switch from hover mode to high speed mode presents several complex design choices. For simplicity it will be assumed that those switches are accomplished manually by the pilot at an airspeed between 40 and 80 knots.

The pitch or roll attitude rate model is shown in Figure 3-2. The vehicle response to a pitch or roll rate command (q_c or $\dot{\phi}_c$) is approximately that of a first-order system:

$$\frac{q}{q_c} \approx \frac{1}{\tau_q s + 1} \quad (3-1)$$

where the time constant τ_q is typically about 0.5 second. The maximum pitch or roll rate for the CH-47 has been specified by NASA at 25 deg/sec; treating this as a step input to Equation (3-1), the maximum pitch or roll acceleration is

$$\dot{q}_{\max} = 50 \text{ deg/sec}^2 = 0.87 \text{ rad/sec}^2.$$

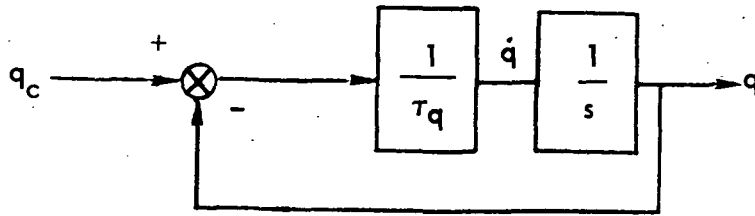


Figure 3-2. Pitch or Roll Attitude Rate Model.

Figure 3-3 shows the approximate model for pitch or roll attitude control. This system merely involves the addition of a pitch or roll attitude feedback loop around the attitude rate model. The closed-loop model response is second-order:

$$\frac{\theta}{\theta_c} \cong \frac{\omega_n^2}{s^2 + 2\zeta\omega_n s + \omega_n^2} \quad (3-2)$$

with a natural frequency $\omega_n^2 = K_\theta/\tau_q$ and damping ratio $\zeta = 1/2\sqrt{K_\theta\tau_q}$. For a typical system gain $K_\theta \sim 0.5 - 1.0 \text{ sec}^{-1}$, the response has nearly critical damping ($\zeta = 0.7 - 1.0$) with a natural frequency $\omega_n = 1.0 - 1.4 \text{ rad/sec}$.

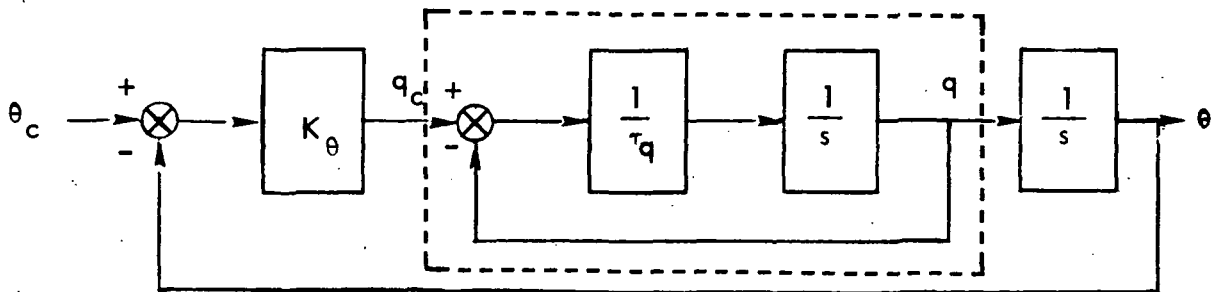


Figure 3-3. Pitch or Roll Attitude Model.

The next level in low speed pitch and roll automation is the horizontal velocity control model shown in Figure 3-4. Again, this system essentially involves an outer feedback loop around the pitch or roll attitude control system of Figure 3-3. The pilot input V_c is compared with the measured velocity V to generate a commanded pitch or roll attitude; V_{c_ref} provides a trim capability. The closed-loop transfer function, using Equation (3-2) for the inner attitude loop, is third order:

$$\frac{V}{V_c} = \frac{gK_V\omega_n^2}{s^3 + 2\zeta\omega_n s^2 + \omega_n^2 s + gK_V\omega_n^2} \quad (3-3)$$

This can be simplified at frequencies below ω_n by approximating $\theta/\theta_c \sim 1$, which results in the closed-loop response

$$\frac{V}{V_c} \sim \frac{1}{\tau_V s + 1} \quad (3-4)$$

where $\tau_V = 1/g K_V$. If we select a gain of $K_V \sim 0.9$ deg/ft/sec, the time constant becomes $\tau_V \sim 2$ sec.

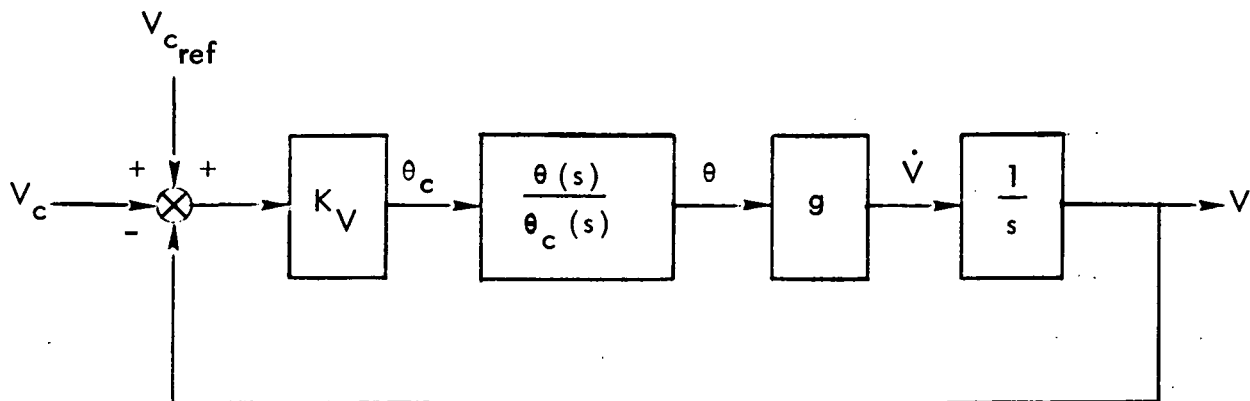


Figure 3-4. Horizontal Velocity Model - Hover Mode.

The highest level of automation in the horizontal channels at low speed is the hover position model, shown in Figure 3-5. The position feedback loop is closed around the velocity control model of Figure 3-4; changes to the reference hover position x_c are fed forward through a differentiating network to generate the reference velocity signal. The closed-loop response of this system is

$$\frac{x}{x_c} = \frac{s/K_V + 1}{\tau s^2/K_V + s/K_V + 1} \quad (3-5)$$

Selecting the position gain at $K_x \sim 0.25$ ft/sec/ft, gives a critically damped system ($\zeta \sim 0.7$) with a natural frequency of $\omega_n \sim 0.35$ rad/sec.

In the higher speed flight regime, the only change in the pitch channel models is that forward ground speed V is replaced by airspeed as shown in Figure 3-6. The roll channel in the high speed mode is used to control heading rate, as discussed in the next subsection.

3.2.2 YAW CHANNEL MODELS

At low speed, the yaw channel is in a heading hold mode, as shown in Figure 3-7. The closed-loop response is given by

$$\frac{\psi}{\psi_c} = \frac{K_\psi}{s^2 + s/\tau_\psi + K_\psi \tau_\psi} \quad (3-6)$$

Typical values are $K_\psi \sim 2$ sec and $\tau_\psi \sim 0.5$ sec, which result in a critically damped system ($\zeta = 0.7$) with a natural frequency $\omega_n \sim 1.4$ rad/sec. The maximum yaw rate command is about $\dot{\psi}_{c \max} \sim \pm 25$ deg/sec.

At high speed, the yaw and roll channels operate in a turn following mode with heading rate control, as shown in Figures 3-8 and 3-9. Normally, there is no

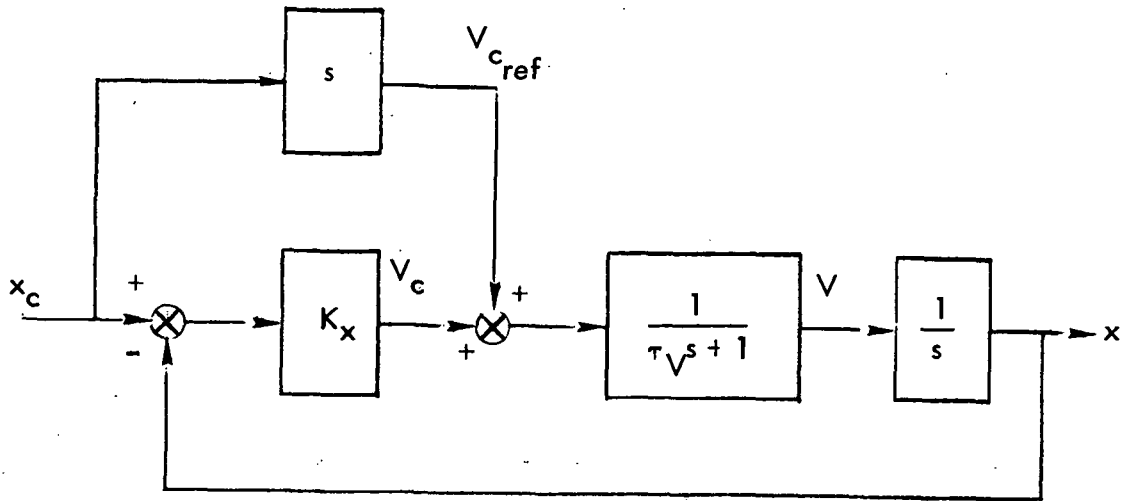


Figure 3-5. Horizontal Position Model - Hover Mode.

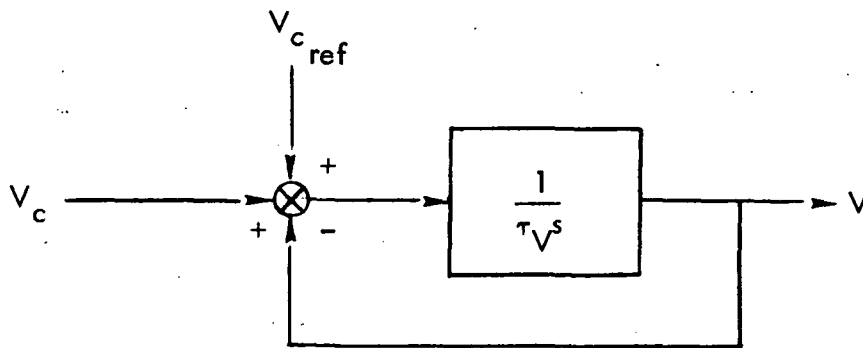


Figure 3-6. Airspeed Control Model - High Speed Mode.

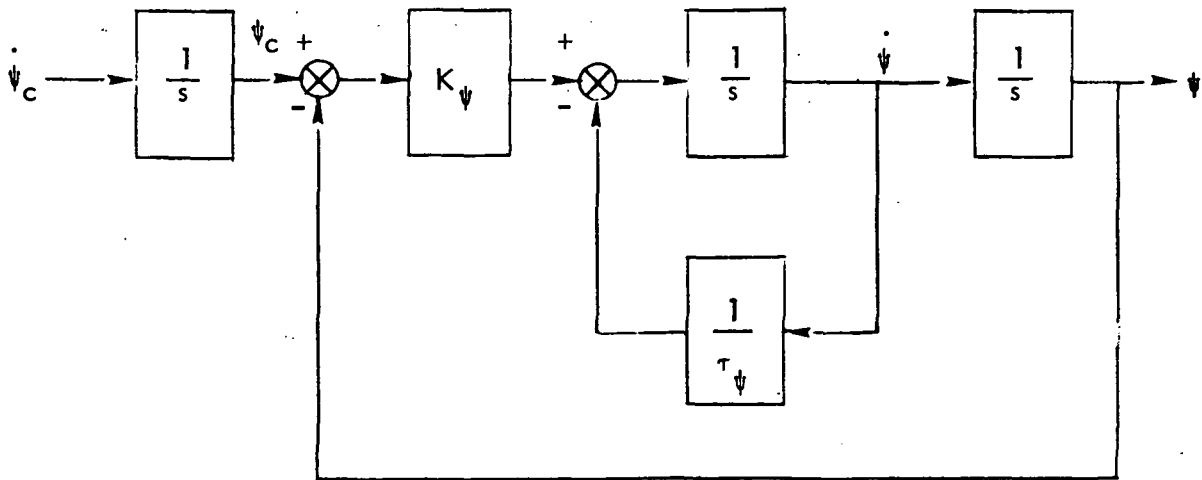


Figure 3-7. Heading Hold Model - Hover Mode.

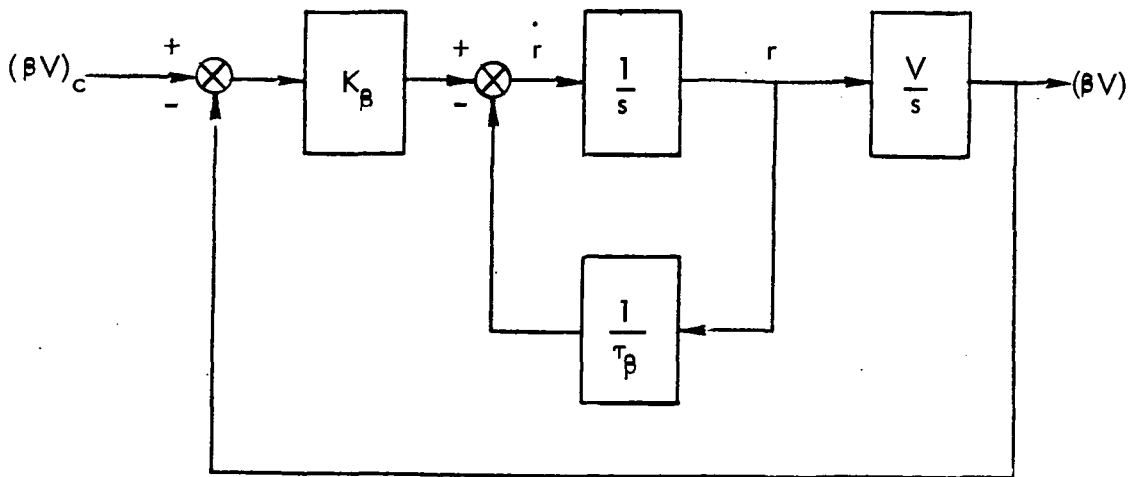


Figure 3-8. Turn Following Model - High Speed Mode.

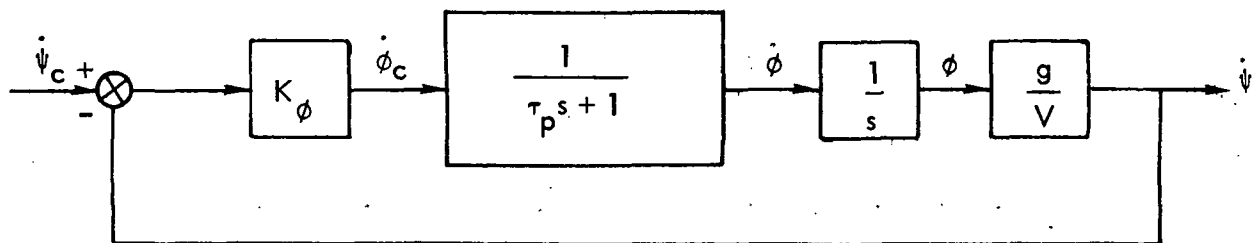


Figure 3-9. Heading Rate Model - High Speed Mode.

command input to Figure 3-8, and the system maintains zero sideslip. If the pilot wants to slip the vehicle, the input is proportional to sideslip velocity, βV , with a maximum value of approximately 60 ft/sec. The closed-loop sideslip response is

$$\frac{(\beta V)}{(\beta V)_c} = \frac{K_\beta V}{s^2 + s/\tau_\beta + K_\beta V} \quad (3-7)$$

Typical parameter values are $K_\beta \sim 0.004$ rad/sec/ft, and $\tau_\beta \sim 1.4$ sec. The resulting dynamics depend on airspeed, as shown by the following:

\underline{V}	$\underline{\omega}_n$	$\underline{\zeta}$
60 kt	0.6 rad/sec	0.6
120 kt	0.9 rad/sec	0.4

The heading rate loop in Figure 3-9 is nearly identical to the roll attitude model in Figure 3-3, since yaw rate is proportional to roll attitude at a given airspeed. The closed-loop dynamics are the same as Equation (3-2), except the natural frequency $\omega_n^2 = gK_\phi/V\tau_p$ and damping of $\zeta = 1/(2\tau_p\omega_n)$. For $\tau_p \sim 0.5$ sec and $K_\phi \sim 5 \text{ sec}^{-1}$, the resulting dynamics are also functions of airspeed:

\underline{V}	$\underline{\omega}_n$	$\underline{\zeta}$
60 kt	1.8 rad/sec	0.6
120 kt	1.3 rad/sec	0.8

3.2.3 VERTICAL CHANNEL MODELS

The vertical speed model is a simple first-order response, as shown in Figure 3-10, with a time constant of $\tau_h \sim 2.5$ sec. The maximum input is of the order of $\dot{h}_{c \text{ max}} \sim 16$ ft/sec, which limits the vertical acceleration response to about 0.1 g (3 ft/sec).

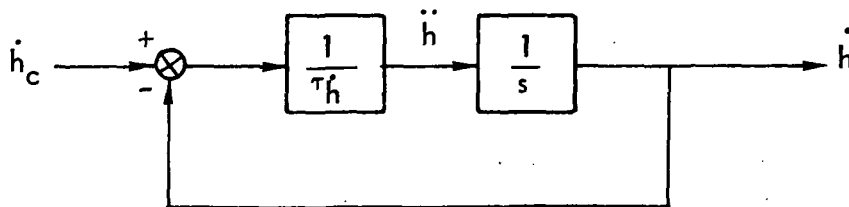


Figure 3-10. Altitude Rate Model.

The altitude hold model merely adds an outer loop around the altitude rate model, as shown in Figure 3-11. The closed-loop response is second-order:

$$\frac{h}{h_c} = \frac{K_h/\tau_h}{s^2 + s/\tau_h + K_h/\tau_h} \quad (3-8)$$

Selecting the gain $K_h \sim 0.2 \text{ sec}^{-1}$ gives a damping of $\zeta \sim 0.7$ with a natural frequency of $\omega_n \sim 0.25 \text{ rad/sec}$.

3.2.4 BANDWIDTH SUMMARY

The bandwidths of the uncoupled models in the various modes discussed previously are summarized in Table 3-3.

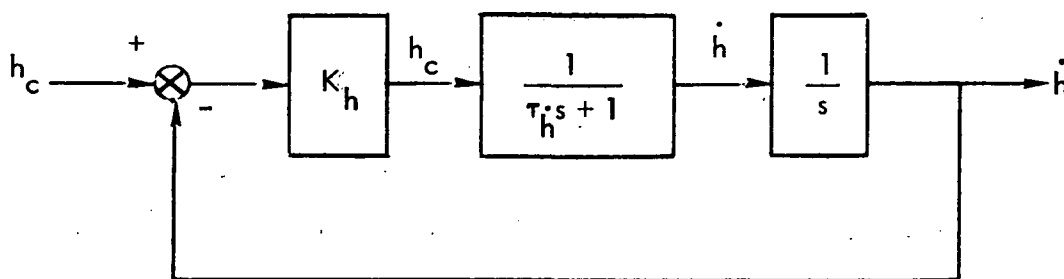


Figure 3-11. Altitude Hold Model.

Table 3-3. Approximate Bandwidth of Uncoupled Control Model Responses.

Channel	Mode	Rad/Sec
Horizontal	Attitude Rate	2.0
	Attitude	1.0 - 1.4
	Velocity	0.5
	Position	0.35
Yaw	Turn Following	0.6 @ 60 kt
		0.9 @ 120 kt
	Heading Rate	1.8 @ 60 kt
		1.3 @ 120 kt
Vertical	Heading Hold	1.4
	Velocity	0.4
	Position	0.25

3.3 CONTROL SYSTEM DESIGN USING QUADRATIC SYNTHESIS

This section discusses the design of control systems for the CH-47 which minimizes cross coupling between controlled axes. From a theoretical viewpoint it can be shown that there are insufficient degrees of freedom available to completely eliminate all cross coupling. The problem then is to use the available degrees of freedom in some optimum manner while constraining the direct control to respond with dynamics previously determined to be desirable.

In this analysis the control was found using quadratic synthesis. The cost function was established by using those weightings on the state variables that would produce the model response in each channel if it were uncoupled. The control determined will automatically suppress the cross coupling in the optimum manner for the cost function selected. Using quadratic synthesis the cost function was determined by the maximum acceptable magnitudes of the control and state variables. The maximum values of available control are known for the vehicle, while the maximum values for the state disturbances are determined indirectly. The ratio of the maximum value of control and state in a direct channel is directly related to the bandwidth that results for that channel. Since the desired bandwidth has been determined for all the direct channels, these numbers can be used to generate the maximum values for each state variable. The philosophy used was that every control system is optimum for some cost function. The cost function for which the optimum control is the same control desired in each direct channel assuming no cross coupling is first obtained; then the same cost function is used to optimize the coupled system.

3.3.1 QUADRATIC SYNTHESIS SUMMARY

The steady-state quadratic synthesis design procedure provides a convenient method for determining the feedback law to minimize the control performance index

$$J = \int_0^{\infty} (x'Ax + u'Bu) dt \quad (3-9)$$

where x is the plant state vector and u is the input vector. The diagonal weighting matrices A and B are determined from the maximum desirable variations in the states and controls, i.e.,

$$A_{ii} = 1/(x_{i \max})^2 \quad (3-10)$$

$$B_{ii} = 1/(u_{i \max})^2 \quad (3-11)$$

The linear system dynamics are given by the standard form

$$\dot{x} = Fx + G(u + u_p) \quad (3-12)$$

where u_p is the additional input from the pilot. The feedback control law is

$$u = -Kx \quad (3-13)$$

where the feedback gain matrix is given by

$$K = B^{-1}G'S \quad (3-14)$$

The symmetric matrix S is the steady-state solution to the Ricatti equation

$$S = -SF - F'S + SGB^{-1}G'S - A = 0 \quad (3-15)$$

The closed-loop system dynamics are found from substituting Equation (3-13) into Equation (3-12):

$$\dot{x} = (F - GK)x + G u_p \quad (3-16)$$

$$= F^*x + G u_p \quad (3-16a)$$

where $F^* = (F - GK)$ is the closed-loop system matrix.

Occasionally, it will be useful to consider one or more of the pilot inputs as a commanded value for an element of the state vector. For example, if it is desired that pilot input u_{p_i} correspond to direct control of state variable x_i , we can use Equation (3-13) to obtain the transformation

$$u_{p_i} = -K_{ij} x_j \quad (3-17)$$

3.3.2 UNCOUPLED EXAMPLES

Several simple uncoupled examples are presented briefly to illustrate the design procedure and the relationship of the desired system bandwidth.

3.3.2.1 PITCH RATE CONTROLLER

Consider the quadratic synthesis design of the pitch rate controller shown in Figure 3-12.

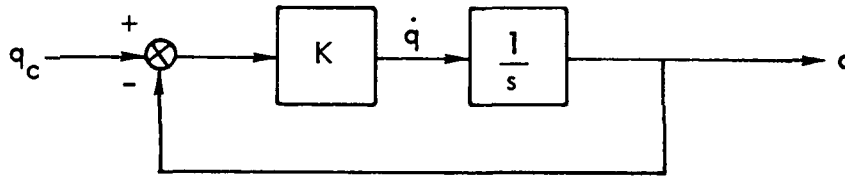


Figure 3-12. Pitch Rate Controller.

The open-loop system is defined by

$$x = q, u = \dot{q}, F = 0, G = 1$$

The performance index weightings are scalars:

$$A = \frac{1}{q_m^2} \quad B = \frac{1}{\dot{q}_m^2}$$

The feedback control gain is

$$K = B^{-1}G^T S = \dot{q}_m^2 S$$

where S , the Ricatti solution is easily found.

$$S = \frac{1}{\dot{q}_m q_m}$$

Hence,

$$K = \frac{\dot{q}_m}{q_m} \quad \text{or} \quad \tau = \frac{q_m}{\dot{q}_m}$$

In this first-order system the system bandwidth is directly related to the ratio \dot{q}_m/q_m . Thus, if \dot{q}_m is known from physical constraints, the desired bandwidth can be achieved by properly selecting q_m in the design process.

3.3.2.2 PITCH ATTITUDE CONTROLLER

The same technique is applied to the pitch attitude controller shown in Figure 3-13.

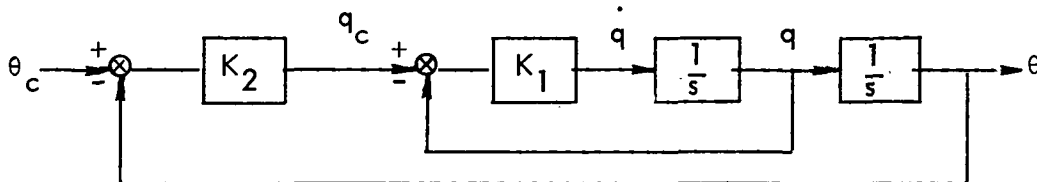


Figure 3-13. Pitch Controller.

The natural frequency and damping of this system are

$$\omega_n = \sqrt{K_1 K_2}$$

$$\zeta = 1/2 \sqrt{K_1/K_2}$$

The state vector and the open loop control are

$$x = \begin{bmatrix} q \\ \theta \end{bmatrix}, \quad u = \dot{q}$$

and the system matrices are

$$F = \begin{bmatrix} 0 & 0 \\ 1 & 0 \end{bmatrix} \quad G = \begin{bmatrix} 1 \\ 0 \end{bmatrix}$$

The performance index weightings are

$$A = \begin{bmatrix} 0 & 0 \\ 0 & 1/\theta_m^2 \end{bmatrix} \quad B = 1/\dot{q}_m^2$$

where \dot{q}_m , q_m , θ_m are the maximum permissible values of pitch acceleration, rate, and attitude, respectively.

The quadratic synthesis feedback controller is

$$u = -K \begin{bmatrix} q \\ \theta \end{bmatrix}$$

where $K = [K_q \ K_\theta] = [K_1 \ K_1 K_2]$.

The Ricatti equation for this system can be solved explicitly to find the feedback gains

$$K = \left[\sqrt{\frac{2\dot{q}_m}{\theta_m}}, \quad \dot{q}_m/\theta_m \right]$$

Thus the quadratic synthesis design leads to the following dynamic response

$$\zeta = \sqrt{2}/2 = 0.7$$

$$\omega_n^2 = \dot{q}_m / \theta_m$$

Therefore, the only parameter needed to design the system using quadratic synthesis is the ratio $\dot{q}_m / \theta_m = \omega_n^2$. If a cost had been specified on q as well as θ , only the damping in the system would have changed; the bandwidth would still be determined by \dot{q}_m / θ_m .

3.3.2.3 HORIZONTAL VELOCITY CONTROLLER

As a final example, consider the horizontal velocity controller designed using quadratic synthesis (Figure 3-14).

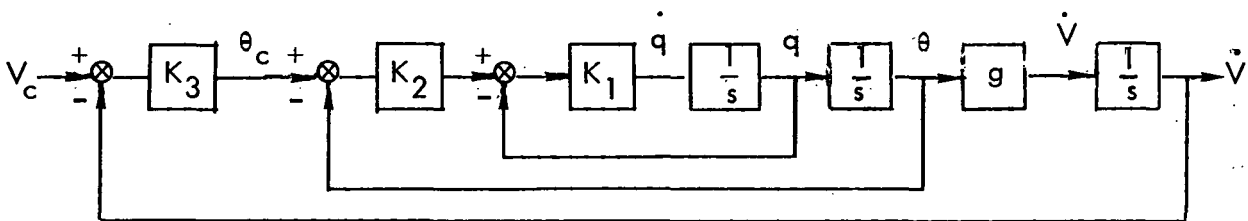


Figure 3-14. Horizontal Velocity Controller.

The open-loop system is defined by

$$\mathbf{x} = \begin{bmatrix} V \\ q \\ \theta \end{bmatrix}, \quad \mathbf{u} = \dot{q}, \quad \mathbf{F} = \begin{bmatrix} 0 & 0 & g \\ 0 & 0 & 0 \\ 0 & 1 & 0 \end{bmatrix}, \quad \mathbf{G} = \begin{bmatrix} 0 \\ 1 \\ 0 \end{bmatrix}$$

The performance index weights are

$$\mathbf{A} = \begin{bmatrix} 1/\sqrt{V_m^2} & 0 & 0 \\ 0 & 0 & 0 \\ 0 & 0 & 0 \end{bmatrix} \quad \mathbf{B} = 1/\dot{q}_m^2$$

The feedback controller is

$$\dot{u} = -K \begin{bmatrix} V \\ q \\ \theta \end{bmatrix}$$

where $K = [K_V, K_q, K_\theta] = [K_1 K_2 K_3, K_1, K_1 K_2]$.

Solving the Riccati equation to obtain K_V , gives

$$K_V = K_1 K_2 K_3 = \dot{q}_m / V_m$$

which could have been deduced intuitively. It is not necessary to solve for the other terms since we have sufficient information to determine the \dot{q}_m / V_m ratio.

There is now sufficient information to use the quadratic synthesis technique to determine the feedback control for the coupled equations.

3.3.3 COUPLED LONGITUDINAL CONTROL

For the coupled longitudinal helicopter control system design, the state and control vectors are defined by

$$x = \begin{bmatrix} x \\ z \\ \theta \\ V_x \\ V_z \\ q \end{bmatrix} \quad \begin{array}{l} \text{forward position} \\ \text{vertical position} \\ \text{pitch angle} \\ \text{forward velocity} \\ \text{vertical velocity} \\ \text{pitch rate} \end{array} \quad (3-18)$$

$$u = \begin{bmatrix} \delta_e \\ \delta_c \end{bmatrix} \quad \begin{array}{l} \text{differential collective input} \\ \text{gang collective input} \end{array} \quad (3-19)$$

The system matrices F and G describing the kinematic and aerodynamic response of the rotorcraft are developed in Appendix B. Numerical values of the CH-47 stability derivatives for various flight conditions are presented in Appendix E.

The control weighting matrix in the performance index is

$$B = \begin{bmatrix} (\delta_{e_{\max}})^{-2} & 0 \\ 0 & (\delta_{c_{\max}})^{-2} \end{bmatrix} \quad (3-20)$$

The control input limits $\delta_{e_{\max}}$ and $\delta_{c_{\max}}$ can be determined approximately for each flight condition from the constraints on vehicle angular and vertical accelerations

$$\delta_{e_{\max}} \sim \frac{\dot{q}_{\max}}{M_{\delta_e} / I_{yy}} \quad (3-21)$$

$$\delta_{c_{\max}} \sim \frac{\dot{w}_{\max}}{Z_{\delta_c} / m} \quad (3-22)$$

where M_{δ_e} / I_{yy} and Z_{δ_c} / m are the stability derivatives explaining pitching acceleration due to δ_e and vertical acceleration due to δ_c , respectively. From the models in Subsection 3.2, typical limits on the accelerations were found to be

$$\dot{q}_{\max} \sim 0.87 \text{ rad/sec}^2$$

$$\dot{w}_{\max} \sim 3 \text{ ft/sec}^2$$

The state weighting matrix A takes on different forms depending on the level of automation, as shown by the following examples.

- Pitch Rate and Vertical Velocity Command

$$A = \begin{bmatrix} 0 & 0 & 0 & 0 & 0 & 0 \\ 0 & 0 & 0 & 0 & 0 & 0 \\ 0 & 0 & 0 & 0 & 0 & 0 \\ 0 & 0 & 0 & 0 & 0 & 0 \\ 0 & 0 & 0 & 0 & V_{z_{\max}}^{-2} & 0 \\ 0 & 0 & 0 & 0 & 0 & q_{\max}^{-2} \end{bmatrix}$$

- Pitch Attitude and Vertical Velocity Command

$$A = \begin{bmatrix} 0 & 0 & 0 & 0 & 0 & 0 \\ 0 & 0 & 0 & 0 & 0 & 0 \\ 0 & 0 & \theta_{\max}^{-2} & 0 & 0 & 0 \\ 0 & 0 & 0 & 0 & 0 & 0 \\ 0 & 0 & 0 & 0 & V_{z_{\max}}^{-2} & 0 \\ 0 & 0 & 0 & 0 & 0 & 0 \end{bmatrix}$$

- Forward Velocity and Vertical Position Command

$$A = \begin{bmatrix} 0 & 0 & 0 & 0 & 0 & 0 \\ 0 & h_{\max}^{-2} & 0 & 0 & 0 & 0 \\ 0 & 0 & 0 & 0 & 0 & 0 \\ 0 & 0 & 0 & V_{x_{\max}}^{-2} & 0 & 0 \\ 0 & 0 & 0 & 0 & 0 & 0 \\ 0 & 0 & 0 & 0 & 0 & 0 \end{bmatrix}$$

The maximum values of the states to be used in the "A" weighting matrix can be determined from the uncoupled model bandwidths in Table 3-3, and the acceleration limits described above: For the horizontal channel of the CH-47:

$$q_{\max}/\dot{q}_{\max} \sim 0.5 \text{ sec} \rightarrow q_{\max} = 0.435 \text{ rad/sec}$$

$$\theta_{\max}/q_{\max} \sim 1.0 \text{ sec} \rightarrow \theta_{\max} = 0.435 \text{ rad}$$

$$u_{\max}/g\theta_{\max} \sim 2.0 \text{ sec} \rightarrow u_{\max} = 28.0 \text{ ft/sec}$$

$$x_{\max}/u_{\max} \sim 3.0 \text{ sec} \rightarrow x_{\max} = 84.0 \text{ ft}$$

For the vertical channel of the CH-47:

$$w_{\max}/\dot{w}_{\max} \sim 2.5 \text{ sec} \rightarrow V_{z_{\max}} \sim \dot{w}_{\max} = 7.5 \text{ ft/sec}$$

$$z_{\max}/w_{\max} \sim 4.0 \text{ sec} \rightarrow z_{\max} = 30.0 \text{ ft}$$

These design parameters and the quadratic synthesis technique were used to generate the closed-loop system dynamics for the seven different levels of longitudinal control automation presented in Section 6.

3.3.4 COUPLED LATERAL CONTROL

The state and control vectors for the coupled lateral helicopter control system design are defined below:

$$x = \begin{bmatrix} y \\ \phi \\ \psi \\ V_y \\ p \\ r \end{bmatrix} \begin{array}{l} \text{lateral position} \\ \text{roll angle} \\ \text{yaw angle} \\ \text{lateral velocity} \\ \text{roll rate} \\ \text{yaw rate} \end{array} \quad (3-23)$$

$$u = \begin{bmatrix} \delta_a \\ \delta_r \end{bmatrix} \begin{array}{l} \text{roll cyclic input} \\ \text{yaw cyclic input} \end{array} \quad (3-24)$$

The system matrices F and G for the lateral modes are also developed in Appendix B, and the stability derivatives for the CH-47 are given in Appendix E.

The control weighting matrix is

$$B = \begin{bmatrix} (\delta_{a_{\max}})^{-2} & 0 \\ 0 & (\delta_{r_{\max}})^{-2} \end{bmatrix} \quad (3-25)$$

In this case the maximum control inputs are again related to the angular acceleration limits:

$$\delta_{a_{\max}} = \frac{\dot{p}_{\max}}{L_{\delta_a}/I_{xx}} \quad (3-26)$$

$$\delta_{r_{\max}} = \frac{\dot{r}_{\max}}{N_{\delta_r}/I_{zz}} \quad (3-27)$$

From the uncoupled models in Subsection 3.2, the values of the lateral accelerations are

$$\dot{p}_{\max} = 0.87 \text{ rad/sec}^2$$

$$\dot{r}_{\max} = 0.87 \text{ rad/sec}^2$$

As before, the A weighting matrix takes on different forms depending on the level of control automation. Examples are

- Roll Rate and Yaw Rate Command

$$A = \begin{bmatrix} 0 & 0 & 0 & 0 & 0 & 0 \\ 0 & 0 & 0 & 0 & 0 & 0 \\ 0 & 0 & 0 & 0 & 0 & 0 \\ 0 & 0 & 0 & 0 & 0 & 0 \\ 0 & 0 & 0 & 0 & p_{\max}^{-2} & 0 \\ 0 & 0 & 0 & 0 & 0 & r_{\max}^{-2} \end{bmatrix}$$

- Roll Angle and Yaw Rate Command

$$A = \begin{bmatrix} 0 & 0 & 0 & 0 & 0 & 0 \\ 0 & \phi_{\max}^{-2} & 0 & 0 & 0 & 0 \\ 0 & 0 & 0 & 0 & 0 & 0 \\ 0 & 0 & 0 & 0 & 0 & 0 \\ 0 & 0 & 0 & 0 & 0 & 0 \\ 0 & 0 & 0 & 0 & 0 & r_{\max}^{-2} \end{bmatrix}$$

- Lateral Velocity and Yaw Angle Command

$$A = \begin{bmatrix} 0 & 0 & 0 & 0 & 0 & 0 \\ 0 & 0 & 0 & 0 & 0 & 0 \\ 0 & 0 & \psi_{\max}^{-2} & 0 & 0 & 0 \\ 0 & 0 & 0 & v_{y_{\max}}^{-2} & 0 & 0 \\ 0 & 0 & 0 & 0 & 0 & 0 \\ 0 & 0 & 0 & 0 & 0 & 0 \end{bmatrix}$$

Maximum values for the state weightings again can be determined from the uncoupled models and the acceleration limits above. For the CH-47, these are

$$r_{\max} / \dot{r}_{\max} \sim 0.5 \text{ sec} \rightarrow r_{\max} = 0.435 \text{ rad/sec}$$

$$\psi_{\max} / \dot{\psi}_{\max} \sim 0.7 \text{ sec} \rightarrow \psi_{\max} = 0.30 \text{ rad}$$

$$p_{\max} / \dot{p}_{\max} \sim 0.5 \text{ sec} \rightarrow p_{\max} = 0.435 \text{ rad/sec}$$

$$\phi_{\max} / \dot{\phi}_{\max} \sim 1.0 \text{ sec} \rightarrow \phi_{\max} = 0.435 \text{ rad}$$

$$v_{\max} / g\phi_{\max} \sim 2.0 \text{ sec} \rightarrow v_{y_{\max}} \sim v_{\max} = 28.0 \text{ ft/sec}$$

$$y_{\max} / v_{\max} \sim 3.0 \text{ sec} \rightarrow y_{\max} = 84.0 \text{ ft}$$

3.4 FLIGHT DIRECTOR DESIGN USING QUADRATIC SYNTHESIS

This section describes a procedure for using the quadratic synthesis technique to design flight director signals for the optimal control pilot model.

3.4.1 DESIGN OBJECTIVES

The basic concept associated with the use of a flight director is to provide the pilot information that is useful for control, thus rendering the piloting task easier in some sense. The general form of the flight director signal is a linear combination of vehicle states

$$FD = h'x(t) \quad (3-28)$$

with possibly some filtering to remove high frequency components[†]. The flight director gains h are chosen so that if $FD(t)$ is kept "small" the resulting aircraft motion is desirable. Since the pilot is still in the loop, there are two issues that relate to the harmony between $FD(t)$ and pilot response. The first concerns the nature of the control task as viewed by the pilot. Thus, the task of keeping $FD(t)$ small should not conflict with the overall control task requirements. In the optimal control pilot model the latter is manifested in the choice of a control input, u , that minimizes the quadratic cost functional

$$J(u) = E \lim_{T \rightarrow \infty} \frac{1}{T} \int_0^T \{y'Q_y y + \dot{u}'Q_u \dot{u}\} dt \quad (3-29)$$

The second issue relates to the required form of the pilot compensation. It is well known from experimental results in manual control that one of the easiest control tasks is associated with K/s dynamics, wherein the pilot acts (approximately) like

$$H_o(s) = \frac{Ke^{-\tau s}}{\tau_N s + 1} = \frac{u(s)}{y(s)} \quad (3-30)$$

[†]Note that pilot control is not added directly into the flight director signal.

Thus, from a workload point of view, one should design a flight director signal $FD(t)$ where the resulting pilot response is

$$u(s) = H_o(s) \cdot FD(s) = H_o(s) \cdot h' x(s) \quad (3-31)$$

This is tantamount to picking h so that the open loop transfer function

$$V(s) = h' (sI - A)^{-1} B \quad (3-32)$$

is approximated by K/s .

3.4.2 SIGNAL GENERATION

The above concepts and objectives have been recognized in the literature (References 8-10). Within the framework of the optimal control model, Reference 9 has suggested constructing $FD(s)$ as

$$FD(s) = \sum_{i=1}^{n_y} h_i(s) y_i(s) \quad (3-33)$$

where $y_i(s)$ are the displayed outputs and $h_i(s)$ are the internal transfer functions generated by the optimal control model (Reference 11). This approach has $FD(s)$ compatible with pilot (subjective) control requirements, and has inherent filtering built into the generated signals via the $h_i(s)$. However, only the system outputs are included in FD , and the computation of the h_i require arbitrary choices for pilot observation noises, thresholds, etc.

The approach that we follow in selecting a flight director signal to be associated with a given control is to recognize that the "optimal" control generated by the pilot model is (see Appendix A),

$$\tau_{N_i} \dot{u}_i + u_i = -l_i' \hat{x}(t) = u_c(t) \quad (3-34)$$

Thus, associating the $\log (\tau N_i s + 1)^{-1}$ with the pilot, it is seen that a flight director signal

$$FD_i = -\ell_i^! \hat{x}(t) = u_c(t) \quad (3-35)$$

is precisely the control that the pilot model would apply under ideal conditions.[†] Summarizing, the design of a flight director associated with control i is as follows:

- Select the nominal cost functional weighting associated with the subjective task requirements,
- Compute the feedback gains ℓ_i ,
- Retain only the important elements in ℓ_i to simplify implementation.

The above approach is simple, is related to the pilot's interpretation of the task, and assures that the pilot's transfer function between FD_i and control u_i is approximately as given above.

3.4.3 VALIDATION OF DESIGN MODEL

To test the above technique, we perform a design for the pitch axis and the power (collective) axis, for the CH-46 in hover mode. The results are compared to the flight director described in Reference 12. The cost functional weightings for this task are selected as (see Section 4)

$$q_{y_i} = \left(\frac{1}{y_{i,max}} \right)^2 \quad (3-36)$$

where the corresponding maxima are

[†]This approach is valid if the pilot time-delay τ is negligible with respect to system time-constants.

$$\Delta x = 25 \quad V_x > 100 \text{ ft/sec}$$

$$\Delta z = 5 \quad V_z = 2 \text{ ft/sec}$$

$$\theta = 2^\circ \quad q = 1^\circ/\text{sec}$$

The control rate weightings are selected to give $\tau_{N_i} \sim 0.1$ with $q_{u_{i,\min}} = 0.25 \text{ (in/sec)}^{-2}$.

The important feedback gains in each of the flight director channels are

$$FD_x = C_x x(t) + C_{\dot{x}} V_x(t)$$

$$FD_z = C_z z(t) + C_{\dot{z}} V_z(t)$$

Since the overall scale factors of these signals are arbitrary (depending on display gain) we normalize the signals by the positional gain. This provides an intuitive feel for the ensuing time response as well, since if the flight director signal is zeroed, then the system response is exponential with time constant $C_{\dot{x}}/C_x$, or $C_{\dot{z}}/C_z$. The normalized values of gain ratios found via the optimal control model are

$$\frac{C_{\dot{x}}}{C_x} = 10.3, \quad \frac{C_{\dot{z}}}{C_z} = 2.51$$

For the flight director design given in Reference 12, which was obtained through extensive flight testing, the gain ratio $C_{\dot{x}}/C_x = 10.0$ which is in excellent agreement with the above result.

The results for the power flight director command are somewhat different though and require further analysis. The form of the flight director given in Reference 12

$$FD_z = \alpha z(t) + \beta \dot{z}(t) + \gamma \ddot{z}(t)$$

where α , β , and γ are weighting coefficients, and the velocity/displacement weightings are given by

$$\frac{\beta}{\alpha} = 10 \text{ sec}$$

If the values of the accelerometer signal are expressed in terms of the state variables through the state variable equation, we obtain

$$\ddot{z} = \gamma \dot{z}(t) + \nu \delta_c(t)$$

which becomes

$$FD_z = \alpha z(t) + (\beta + \gamma \nu) \dot{z}(t) + \gamma \nu \delta_c(t)$$

Using the numerical values for the stability derivatives at hover, we find that the ratio of actual velocity gain to position gain is given by

$$\frac{\beta + \gamma \nu}{\alpha} = 2.64 \text{ sec}$$

which is in very close agreement with the value obtained above. This gives further confidence to our flight director signal design technique.

3.4.4 MODELING THE FLIGHT DIRECTOR EFFECTS

In order to include the flight directors within the framework of the optimal control model it is necessary to select threshold values and cost functional weightings. If instruments have been specified (i.e. format level) then thresholds can be chosen based on eye physiological considerations. At the element or informational levels, thresholds and/or maximum excursions must be chosen via alternate means.

Before we select cost functional weightings it is appropriate to consider whether indeed the signals FD_i should even be included in the cost functional. This issue has been raised in Reference 9, in a somewhat broader context. Basically, one must decide on the nature of the pilot's control strategy. Excluding the FD_i from the cost functional implies that the pilot's control objectives are basically the same as before introducing these signals, i.e., in terms of the situation variables Δx , Δy , etc.,

and the flight directors provide only for enhanced state information. Including the FD_i within the cost functional, in addition to the other terms, implies that one of the pilot's direct control objectives is to keep the FD_i small.

In our work we will interpret the piloting task to be the latter. Our method for choosing the associated cost functional weightings on the FD_i is to pick

$$q_i = \left(\frac{1}{FD_{i,max}} \right)^2 \quad (3-37)$$

where we determine $FD_{i,max}$ by

$$FD_{i,max} = \left| \ell_i' \hat{x}(t) \right|_{x = x_{max}} \quad (3-38)$$

for displacement variables i.e. we substitute into the expression for FD_i the maximum subjective values for the positional variables, Δx , Δz , θ . The rate variable terms are set to zero when evaluating the $FD_{i,max}$. The threshold values on the flight director displacements are chosen as

$$a_{FD_i} = \frac{1}{4} (FD_{i,max}) \quad (3-39)$$

and the corresponding rate thresholds are picked as

$$a_{FD_i \dot{}} = \frac{1}{2} a_{FD_i} \quad (3-40)$$

SECTION 4

CONTROL THEORETIC MODELS FOR PREDICTING PILOT MONITORING PERFORMANCE

A very important aspect of evaluating different display/automatic systems is the ability to predict human monitoring behavior, and to give a metric for assessing monitoring performance. With the optimal control model, we have already obtained such predictive capabilities for human control response. This section examines different approaches for monitoring prediction and choices of monitoring workload performance metrics.

4.1 CHARACTERISTICS OF MONITORING MODELS

The approach for determining display requirements and for evaluating systems of differing automation levels is discussed in Section 2. Basically, the total workload level f_{TOT} is selected; then, for a given automation/display system configuration, the fraction of control attention $f_c \leq f_{TOT}$ that is required to achieve a desired performance level is determined. The excess capacity, $f_{TOT} - f_c = f_m$ is thus available to the pilot for monitoring the displays. This approach, in which control performance is established first, was followed since it a priori limits consideration to those systems that have realistic requirements at the initial stages of investigation. Thus, for systems in which $f_m > 0$, the objective is to determine how this monitoring workload is allocated among the n_y displays; i.e., to determine the f_{m_i} , $i = 1, \dots, n_y$.

The monitoring models that are considered have all been evaluated in the light of certain desirable characteristics. These are determined by the overall goals of the monitoring process as used by pilots:

1. Assess aircraft situation with respect to mission requirements, by minimizing the (relative) estimation errors associated with variables y_i .

2. Assess operation of aircraft displays and controls by cross-checking displays for redundancy and self-consistency to detect system failures.

The first goal is a statement of the well-known fact that pilots desire situation information in addition to the control information provided by the flight director and other tracking aids. The second goal indicates that the pilots will continue to scan every available instrument which is important to the approach, even though straightforward application of optimal estimation/control models of the pilot would indicate that some instruments may not be scanned because of the correlated information among displayed variables. The goal of this scanning process may be thought of as the detection of instrument and control system failures.

Thus, the important characteristics of the monitoring models are assumed to be:

1. The ability to assess the performance of the aircraft from situation displays. Implicitly derived variable rates are not monitored, but their information is used to obtain better estimates of the explicitly presented display variables.
2. No monitoring of flight directors, or other combined state information that is geared to aircraft control. Thus, for these instruments, $f_{m_i} = 0$ so that $f_{TOT_i} = f_{c_i}$.
3. Required monitoring of all primary status instruments. Thus, $f_{m_i} \geq \epsilon > 0$.

4.2 MONITORING MODELS

The two major components of a monitoring model are the monitoring performance metric (the method by which monitoring performance is evaluated), and the attentional allocation scheme (the manner in which the model allocates the attention among the various displays). Ideally, the two components can be combined by requiring that the attention allocations f_{m_i} be chosen to minimize the given metric subject to the constraint $\sum_i f_{m_i} = f_m$ and that each f_{m_i} be greater than some specified value. However, it is possible to choose the f_{m_i} according to criteria other than optimizing a performance

metric. Several methods for choosing the f_{m_i} are discussed below. In order to keep the presentation simple, these assume that the pilot is monitoring an automatically controlled system so that each $f_{c_i} = 0$ and thus $f_{TOT_i} = f_{m_i}$. Situations in which the aircraft is under manual control, i.e., $f_{c_i} > 0$ are considered in Subsection 4.3, wherein the f_{m_i} is added to f_{c_i} .

4.2.1 NON-METRIC BASED MODELS

4.2.1.1 EQUAL ATTENTION

Choosing the attentional allocation according to

$$f_{m_i} = f_m / n_y \quad , \quad (4-1)$$

while simple, does not take into account the relative importance of instruments, nor their correlations. However, it does assure that all instruments will be scanned for failure detection.

4.2.1.2 PEAK EXCURSION MONITORING

It is reasonable to expect that a pilot will monitor a signal when its value exceeds some multiple, β , of its standard deviation. Thus, usual signal levels are not of immediate concern, but signal values greater than usual are monitored. The choice of f_{m_i} becomes

$$f_{m_i} = f_{o_i} \Pr \left\{ |y_i| > \beta \sigma_{y_i} \right\} \quad (4-2)$$

This technique assumes that the pilot will look at variable y_i with probability f_{o_i} whenever $|y_i|$ exceeds $\beta \sigma_{y_i}$. β is a parameter chosen so that $\sum_i f_{m_i} = f_m$. However, the f_{o_i} remain to be chosen in some plausible manner. This scheme introduces the concept that monitoring is dependent on relative signal values (i.e., on the ratio of

$|y_i|/\sigma_{y_i}$ where σ_{y_i} is the standard deviation of y_i). Conceptually, the f_{o_i} should be related to the "importance", or information content of the display. However, a pilot may not necessarily look at a variable just because $|y_i| > \beta\sigma_{y_i}$ if

1. He can acquire this information from a second display highly correlated with y_i .
2. His estimation error in y_i is sufficiently small so that looking at y_i serves no purpose except instrument verification.
3. Both y_i and σ_{y_i} are less than the display visual or indifference thresholds (i.e., the display may be poor).

Nevertheless, this model with $\beta = 1.5-3$ means that the human will monitor the unusual occurrences. In fact, this model with $f_{o_i} = 1$ and $\beta = 3$ requires a minimal or residual attention be placed on each display of $f_{m_i} \sim .01$; if $\beta = 2$, each $f_{m_i} \geq .05$. By interpreting this to mean a monitoring of unusual or failed situations[†], this model handily provides a lower bound for each f_{m_i} .

4.2.1.3 NYQUIST CRITERIA MODELS AND THEIR EXTENSIONS

As first postulated in Reference 13, a human samples an instrument periodically in an attempt to reconstruct the associated time signal. Thus, information-theoretic ideas, particularly Shannon's sampling theorem, were used to obtain the expression

$$f_{m_i} = 2c_1 \omega_i \log_2 \frac{A_i}{E_i} + 2\omega_i c_2 \quad (4-3)$$

where ω_i = signal bandwidth, A_i = signal RMS amplitude and E_i = permissible rms error. c_1 and c_2 are constants, the latter used to account for minimum fixation time. For multiple instruments where the ratio of signal power to magnitude of significant deviations E_i are roughly constant, the f_{m_i} would be proportional to signal bandwidths.

[†]One might conjecture that $f_{m_i} > .05$ will enable the detection of system failures in short time.

Thus, since ω_i is proportional to σ_{y_i}/σ_y ,

$$f_{m_i} = k \frac{\sigma_{y_i}}{\sigma_y} y_i \quad (4-4)$$

with

$$k = \left(\sum_i \frac{\sigma_{y_i}}{\sigma_y} y_i \right)^{-1} \cdot f_m \quad (4-5)$$

This simple periodic sampling model would not adequately predict behavior in more complex situations with correlated signals and aperiodic sampling behavior. Noting that pilots are often concerned only with detection of extreme readings rather than with signal reconstruction, Reference 14 proposed a conditional sampling scheme that would result in aperiodic behavior. In this approach, the human is considered as a channel for the transmission of discrete messages in lieu of a complete time function. In this context it is possible to postulate several (somewhat related) sampling strategies. Thus, References 14 and 15 hypothesize a strategy in which a sample is taken when the probability that the signal exceeds a prescribed limit is greater than some subjective probability threshold[†]. Reference 15 assumes that a sample is taken when the probability of exceeding the limit is a maximum. On the other hand, Reference 15 suggests a sampling strategy based on a "Variable Nyquist Interval". Unfortunately, none of these conditional sampling models have been tested against experimental data nor have they achieved a high level of acceptance in the manual control field.

4.2.1.4 MONITORING FOR FAILURE ANTICIPATION

The assumption that a pilot monitors an automatic system in such a manner as to anticipate a manual takeover provides a basis for an alternate monitoring model. For a given failure, one can solve the control problem associated with the pilot control-

[†]The form of this model is somewhat similar to that of Subsection 4.2.1.2.

ling the failed dynamics subject to an attentional level of $f_c = f_m$. Optimizing the control cost for the f_{c_i} will provide the monitoring fractions f_{m_i} by equivalence.

Although this method has some intuitive appeal, it suffers drawbacks in that

1. A specific anticipated failure mode and dynamics must be assumed.
2. If there were a failure, the f_c would probably not equal f_m so that the f_{c_i} as found may have little relation to the f_{m_i} .

4.2.2 MONITORING METRICS

The monitoring models discussed above are not geared to a performance metric with which to evaluate sampling behavior. However, once a monitoring strategy f_{m_i} is determined, any number of metrics may be applied after-the-fact. This suggests an alternate, more appealing approach to the monitoring problem: to first specify a meaningful performance metric that embodies the goals of the monitoring function, and then to choose the f_{m_i} to minimize the selected metric. Consequently, the dual goals of monitoring as status determination and failure detection suggest the following two monitoring cost functionals.

4.2.2.1 ESTIMATION ERROR COST FUNCTIONAL

For status determination the pilot's monitoring strategy is to choose the f_{m_i} subject to

$$\sum_{i=1}^n f_{m_i} = f_m; f_{m_i} > 0 \quad (4-6)$$

to minimize the monitoring cost

$$J_m = \frac{1}{n_y} \sum_{i=1}^n \gamma_i \frac{\sigma^2 e_i}{\sigma^2 y_i} \quad (4-7)$$

where σ_{e_i} is the rms estimation error in monitoring signal y_i . The γ_i are scale factors that are either 0 or 1 to indicate whether an instrument is of monitoring concern. Observe that this cost functional has the properties

1. $J_m \leq 1$ since it is the relative estimation error that is weighted.
2. Only if $f_{m_i} = 0$ and no information concerning y_i is obtained from other instruments can $\sigma_{e_i}^2 = \sigma_{y_i}^2$, otherwise $\sigma_{e_i}^2 < \sigma_{y_i}^2$.

Another interpretation of J_m is obtained by defining

$$k_i = \frac{\sigma_{e_i}}{\sigma_{y_i}} = \text{error fraction for variable } y_i \quad (4-8)$$

so that

$$J_m^{1/2} = \text{rms monitoring "error fraction"}$$

The optimal choice of the f_{m_i} provides a prediction of the monitoring fraction for each displayed variable. Note that

1. All instrument correlations are considered in this formulation, so that key instruments have larger f_{m_i} .
2. If $\sigma_{y_i}^2 \ll \text{threshold value}$, the model will not try in vain to lower $\sigma_{e_i}^2$, but accept $\sigma_{e_i}^2 \sim \sigma_{y_i}^2$ by keeping $f_{m_i} \sim 0$.

The error fractions k_i are useful in relation to the probabilities associated with estimation error criteria. By defining

$$E(\beta) = \Pr \left\{ |e(t)| > \beta \sigma_y \right\} \quad (4-9)$$

as the probability that the estimation error at any time exceeds a fraction β of the signal rms, then (assuming Gaussian statistics)

$$E(\beta) = \frac{2}{\sqrt{2\pi} \sigma_e} \int_{\beta \sigma_y}^{\infty} e^{-y^2/2\sigma_e^2} dy \quad (4-10)$$

Making the change of variable $w = y/\sigma_e \sqrt{2}$ yields, noting $k = \sigma_e/\sigma_y$,

$$\begin{aligned} E(\beta) &= \frac{2}{\sqrt{\pi}} \int_{\beta/k\sqrt{2}}^{\infty} e^{-w^2} dw \\ &= \operatorname{erfc} \left(\frac{\beta}{k\sqrt{2}} \right) \end{aligned} \quad (4-11)$$

A reasonable performance level to expect in monitoring is $\beta = 1/2$, i.e., the estimation error should not exceed $\sigma/2$ of the monitored variable. The percent of time (or probability) that this criteria is exceeded is $E(1/2)$, and is monotonically related to the error fraction k . This gives another interpretation to the cost functional (Equation (4-7)).

4.2.2.2 FAILURE DETECTION COST FUNCTIONAL

A recent decision model based on Wald's sequential analysis (Reference 16) provides an excellent description of the human's ability to detect failures in random processes. A single-channel version of the model was successfully validated with experimental data. A more elaborate test of the model was made by applying it to the task of monitoring a fully automatic ILS approach, with equally encouraging results in describing the experimental data.

The model for monitoring a single instrument uses Wald's Sequential Probability Ratio Test to derive a decision function based on the log likelihood ratio of each observed residual from the Kalman filter. The decision function λ_m at time t_m is given by

$$\lambda_m = \begin{cases} \tilde{\lambda}_m & \tilde{\lambda}_m \geq 0 \\ 0 & \tilde{\lambda}_m < 0 \end{cases} \quad (4-12)$$

where

$$\tilde{\lambda}_m = \lambda_{m-1} + \left(\frac{r_m - \tilde{\theta}/2}{\sigma_r} \right) \quad (4-13)$$

and r_m is the Kalman filter residual at t_m , σ_r is its standard deviation, and $\tilde{\theta}$ is a bias parameter beyond which the process is considered to be "failed". Note that the decision function is reset to zero should it become negative.

The decision of "failure" or "no failure" is made from the current value of λ_m according to the rule

$$\begin{aligned} &\text{if } \lambda_m > \frac{\sigma_r}{\tilde{\theta}} \ln A, \text{ decide "failure"} \\ &\text{if } 0 \leq \lambda_m \leq \frac{\sigma_r}{\tilde{\theta}} \ln A, \text{ decide "no failure"} \end{aligned} \quad (4-14)$$

The constant A is related to the probabilities of the two types of errors: the probability of a missed alarm P_{MA} (deciding "no failure" when a failure is present); and the probability of a false alarm P_{FA} (deciding "failure" when no failure is present), (Reference 4).

There are two metrics proposed here: the mean time to detect a failure and the mean number of looks to detect a failure. These can be determined from the ensemble performance of the model of human monitoring and decision making as follows.

Assume that a constant (bias) failure of magnitude θ^* has occurred, i.e., the residual r_m has increased by θ^* , and that all residuals have the same variance σ_r^2 which will

be a function of all the fractions of attention for monitoring $\{f_{m_i}\}$. Then the decision function is given by

$$\lambda_m \sim \lambda_{m-1} + \left(\frac{r_m + \theta^* - \tilde{\theta}/2}{\sigma_r} \right) \quad (4-15)$$

$$\sim (m - m_f) \frac{(\theta^* - \tilde{\theta}/2)}{\sigma_r} + \sum_{i=m_f}^m \frac{r_i}{\sigma_r} \quad (4-16)$$

where r_i is the zero-mean component of the residual and λ_{m_f-1} is assumed zero. The index m in Equation (4-16) represents the "look number" since a decision cannot be made without glancing at the instrument, and $(m - m_f)$ is the number of looks that have elapsed since the failure occurred. The above approximation is valid when σ_r is much less than the level of the detection threshold, a reasonable assumption when the false alarm rate is not too high. This approximation is also useful in determining the mean number of looks to detect the failure since at the moment of detection

$$\lambda_m = m_D \left(\frac{\theta^* - \tilde{\theta}/2}{\sigma_r} \right) + \sum_{i=m_f}^{m_f+m_D} \frac{r_i}{\sigma_r} = \frac{\sigma_r}{\tilde{\theta}} \ln A \quad (4-17)$$

where m_D is the number of looks to detect the failure. The mean value of m_D is thus (approximately)

$$\bar{m}_D \sim \frac{\ln A}{\frac{\tilde{\theta}}{\sigma_y} \left(\frac{\theta^* - \tilde{\theta}/2}{\sigma_y} \right)} \frac{\sigma_r^2}{\sigma_y^2} = \gamma \frac{\sigma_r^2}{\sigma_y^2} \quad (4-18)$$

where σ_y^2 is the a priori variance of the displayed signal. For the case of multiple instruments the mean number of looks to detect failures is therefore

$$J_m = \frac{1}{n_y} \sum_{i=1}^{n_y} \gamma_i \frac{\sigma_r^2}{\sigma_y^2} \quad (4-19)$$

and is a reasonable metric to minimize by proper choice of the f_{m_i} .

Another important performance metric, is the mean time to detect a failure. This can be expressed in terms of the relevant parameters of the optimal estimation model as we now show by using a measure of "looks per second". If the i^{th} instrument has received n_i looks in T seconds, and each look requires Δ_t seconds ($\Delta_t \cong 0.3 - 0.4$ seconds according to experimental eye movement data), then the fraction of time spent looking at the i^{th} instrument (dwell fraction) is

$$\text{dwell fraction} = \frac{n_i \Delta_t}{T} \quad (4-20)$$

Under the assumption that this is close to the fraction of attention f_{m_i} , the scan period (seconds/look) can be determined

$$\frac{T}{n_i} = \frac{\Delta_t}{f_{m_i}} \quad (4-21)$$

Thus the mean time to detect a failure on the i^{th} instrument is

$$\bar{t}_{D_i} = \bar{m}_D \frac{\Delta_t}{f_{m_i}} = \frac{\Delta_t \ln A}{\frac{\tilde{\theta}_i}{\sigma_{y_i}} \left(\frac{\theta_i^* - \theta_i/2}{\sigma_{y_i}} \right)} \frac{1}{f_{m_i}} \frac{\sigma_r^2}{\sigma_y^2} \quad (4-22)$$

so that minimizing the functional

$$J_m = \frac{1}{n_y} \sum_{i=1}^{n_y} \frac{\gamma_i}{f_{m_i}} \frac{\sigma_r^2}{\sigma_y^2} \quad (4-23)$$

minimizes the average mean time to detect failures, as compared to minimizing Equation (4-18) which is the mean number of looks to detect failures. The disadvantage of using Equation (4-23) is that it does not reflect the differences in bandwidths among the displayed signals. If one postulates, as Senders does, that the look rate is proportional to the Nyquist sampling rate, then the number of "looks" required to detect a failure is proportional to the number of elapsed "cycles" of the displayed signal required to detect the failure. This has an obvious intuitive appeal. On the other hand, we suspect that pilots may sometimes monitor the lower frequency signals at a somewhat higher rate because of time considerations. One example of this is a relatively smooth, coupled ILS approach in which the ILS needles have very low frequency content (on the order of 2 to 10 cycles for the entire approach). Detection time would take precedence over detection looks in this case.

4.2.3 METRIC BASED MONITORING MODELS

Having postulated metrics for monitoring performance, one must next consider the mathematical problems of minimization with respect to the f_{m_i} . These are considered below.

4.2.3.1 RESIDUAL MONITORING FOR FAILURE DETECTION

In considering the cost functional (Equation (4-19)) within the context of an optimal control/estimation model, the Kalman filter residuals are (neglecting the humans time delay τ),

$$r_i(t) = y_i(t) - c_i^T \hat{x}_i(t) \quad (4-24)$$

where c_i^T is the i^{th} row of the C matrix: it is well known that for optimal filtering the residuals are white with covariance equal to the observation noise covariance. Thus,

$$\sigma_{r_i}^2 = \sigma_{v_i}^2 = \rho_i \hat{\sigma}_{y_i}^2 / f_{m_i} \quad (4-25)$$

where

$$\hat{\sigma}_{y_i} = \sigma_{y_i} / N_i (\sigma_{y_i}) \quad (4-26)$$

and N is the describing function gain for the display variable threshold.

Substituting into Equation (4-19) gives

$$J_m = \frac{1}{n_y} \sum_{i=1}^{n_y} \frac{Y_i \rho_i}{N_i} \cdot \frac{1}{f_{m_i}} \quad (4-27)$$

This expression is minimized (subject to constraints) at

$$f_{m_i}^* = \frac{Y_i \rho_i}{N_i} \cdot \left(\sum_{i=1}^{n_y} \frac{Y_i \rho_i}{N_i} \right)^{-1} \cdot f_m \quad (4-28)$$

Thus, for well-designed displays ($N_i \cong 1$, $\rho_i \cong .01\pi$), each subject to the same probability of failure ($Y_i = Y_i$),

$$f_{m_i}^* = f_m / n_y$$

This provides a new interpretation of the simple, equal attention allocation scheme, noted in Subsection 4.2.1.1.

The second failure-related cost functional given by Equation (4-23) can also be optimized in a straightforward manner. For the case $N_i = 1$, $\rho_i = \rho_i$, $Y_i = Y_i$, an equal division of attention is again obtained. This is to be expected, since the cost functionals in question have been motivated in terms of (uncorrelated) bias errors on instruments.

4.2.3.2 RELATIVE ERROR MINIMIZATION (ASSUMING UNCORRELATED INSTRUMENTS)

As an approach towards minimizing the metric (Equation (4-7)), inter-instrument correlations can be neglected, and each instrument can be considered to represent an un-

coupled second order system consisting of y_i and \dot{y}_i [†]. The human thus monitors these two variables to obtain an estimate of y_i with associated estimation error e_i . The problem is then: "given observations $y_1(t) = x(t) + v_1(t)$, $y_2(t) = \dot{x}(t) + v_2(t)$, determine the best estimate of $x(t)$."

This problem can be solved by designing a Kalman filter for the system

$$\dot{x}(t) = y_2(t) - v_2(t) \quad (4-29)$$

where

$$y_2(t) = \dot{x}(t) + v_2(t) = \text{velocity measurement}$$

$$y_1(t) = x(t) + v_1(t) = \text{position measurement}$$

$$V_i = \text{cov} [v_i(t)] \quad i = 1, 2$$

The optimal estimate is

$$\hat{\dot{x}}(t) = g[y_1(t) - x(t)] + y_2(t) \quad (4-30)$$

where

$$g = \sqrt{V_2/V_1}$$

Defining

$$\tau = \frac{1}{g} = \sqrt{V_1/V_2}$$

[†]Since relations between y_i and \dot{y}_i are neglected, information concerning y_i can only be obtained by viewing \dot{y}_i .

yields

$$\tau \dot{\hat{x}}(t) + \hat{x}(t) = y_1(t) + \tau y_2(t) \quad (4-32)$$

as the first-order filter that generates the position estimate $\hat{x}(t)$. The error covariance is

$$\text{cov}[x(t) - \hat{x}(t)] = \sigma_e^2 = \sqrt{V_1 V_2} \quad (4-33)$$

Note that if $V_1 \rightarrow 0$ or $V_2 \rightarrow \infty$, $\tau \rightarrow 0$ and $x(t)$ is obtained directly from $y_1(t)$. If $V_2 \rightarrow 0$ or $V_1 \rightarrow \infty$, $g \rightarrow 0$ and $x(t)$ is obtained by integrating $y_2(t)$.

For pilot monitoring,

$$V_i = \rho_i \sigma_i^2 / f_i N_i^2 \quad i = 1, 2 \quad (4-34)$$

Thus, for y_1 and y_2 obtained from a single display indicator

$$\frac{\sigma_e^2}{\sigma_x^2} = \left(\frac{\rho_i}{N_x N_{\dot{x}}} \right) \frac{\sigma_{\dot{x}}}{\sigma_x} \cdot \frac{1}{f_{m_i}} \quad (4-35)$$

For the case of multiple instruments, where it is assumed that only the position (and not the rate) variables are monitored, the monitoring cost functional becomes

$$\begin{aligned} J_m &= \frac{1}{n_y} \sum_{i=1}^{n_y} \frac{\sigma_{e_i}^2}{\sigma_{y_i}^2} \\ &= \frac{1}{n_y} \sum_{i=1}^{n_y} \frac{\rho_i}{N_{y_i} N_{\dot{y}_i}} \left(\frac{\sigma_{\dot{y}_i}^2}{\sigma_{y_i}^2} \cdot \frac{1}{f_{m_i}} \right) \end{aligned} \quad (4-36)$$

where the sum is taken over the position variables only. For well-designed displays,

$N_{y_i} \cong 1$, $N_{\dot{y}_i} \cong 1$ and $\rho_i \cong .01\pi$, and the optimum f_{m_i} are

$$f_{m_i}^* = \frac{\sigma_{\dot{y}_i}^2}{\sigma_{y_i}^2} \cdot \left(\sum_{i=1}^{n_y} \frac{\sigma_{\dot{y}_i}^2}{\sigma_{y_i}^2} \right)^{-1} \cdot f_m \quad (4-37)$$

This result, wherein f_{m_i} is proportional to signal bandwidth, is precisely the Senders' monitoring model arrived at via an entirely different process.

Despite its simplicity, there are drawbacks with the model as proposed,

1. Instrument correlations are not treated.
2. If $\sigma_{x_i} \gg \sigma_{x_i}$ the model would place a high percent of attention on instrument i . In this case $x(t) = y_1(t) + r_1(t)$ and the white estimation error has infinite MSE. This is impossible since we must have $\sigma_e^2 \leq \sigma_x^2$ and suggests that the first order model for $x(t)$, Equation (4-29) may need modification.
3. All of the attendant deficiencies of the original Senders' model resurface.

4.2.3.3 RELATIVE ERROR MINIMIZATION (ASSUMING CORRELATED INSTRUMENTS)

Given the deficiencies of the simple, uncorrelated model we consider the entire dynamics of the system being monitored. Thus, we assume that the pilot is monitoring an automatic (stable) system that is driven by white noise

$$\begin{aligned} \dot{x}(t) &= \bar{A} x(t) + E w(t) \\ y(t) &= Cx(t) = \text{displayed variables} \end{aligned} \quad (4-38)$$

The pilot observes

$$y_{p_i}(t) = y_i(t - \tau) + v_i(t - \tau) \quad i = 1, 2, \dots, n_y \quad (4-39)$$

The estimation error covariance for this monitoring task is

$$S = e^{\bar{A}\tau} \Sigma e^{\bar{A}'\tau} + \int_0^\tau e^{\bar{A}\xi} EWE'e^{\bar{A}'\xi} d\xi \quad (4-40)$$

where $W = \text{cov}[w(t)]$ and Σ satisfies the Ricatti equation

$$0 = \Sigma \bar{A}' + \bar{A} \Sigma + EWE' - \Sigma C' V_y C \Sigma \quad (4-41)$$

and the observation noise covariances are as given in Equations (4-25) and (4-26).

Substituting into Equation (4-7), and neglecting those terms that do not depend on V_y (or f_{m_i}) gives

$$J_m = \frac{1}{n_y} \text{tr} [C_e \Sigma C_e'] \quad (4-42)$$

where

$$C_e = \text{diag} \left(\frac{y_i}{\sigma_{y_i}} \right) C_e \bar{A}^T \quad (4-43)$$

The minimization of J_m with respect to the f_{m_i} is indeed a formidable task. Fortunately, the results of the optimal control allocation problem (see Appendix B) are applicable.

The similarity to the control cost functional used to determine the control fractional attention f_{c_i} (sampling cost) is readily evident where

$$J_o = \text{tr} [L_e \Sigma L_e'] \quad (4-44)$$

with

$$L_e = \text{diag} (Q_u) L_e \bar{A}^T \quad (4-45)$$

Thus, the same techniques used to find $\partial J_o / \partial f$ can be used (with some minor changes) to find $\partial J_m / \partial f$ and to do the subsequent optimizing of J_m subject to the various constraints on f_{m_i} . The computations are greatly simplified in the monitoring case since $\sigma_{y_i}^2$ is not affected by f_{m_i} . Thus, using the techniques of Appendix B,

$$\frac{\partial J_m}{\partial f_{m_i}} = \frac{V_{y_i}}{f_{m_i}} P_{ii} \quad (4-46)$$

where

$$P = G' \int_0^{\infty} e^{\hat{A}'\sigma} C_e' C_e \hat{A}^{\sigma} d\sigma \cdot G \quad (4-47)$$

$$G = \Sigma C' V_y^{-1} = \text{filter gains}$$

$$\hat{A} = A - \Sigma C' V_y^{-1} C = \text{filter matrix}$$

The same gradient projection scheme used to minimize J_0 is thus directly applicable to the monitoring situation. In order to avoid a situation where $f_{m_i}^* = 0$, a constraint $f_{m_i}^* \geq \epsilon > 0$ is imposed to assure each instrument is monitored for failure detection purposes.

4.2.3.4 SUMMARY OF MONITORING MODEL

The monitoring model that was chosen in this study is that of the previous subsection. The monitoring cost functional has various interpretations via the error ratios k_i , and in the case of uncorrelated instruments the model reduces to the Senders' model. There is intuitive appeal to the model, plus the ability to solve the optimization problem using techniques already developed for solving the optimal control allocation problem.

The one drawback to the model is that the constraint $f_{m_i} \geq \epsilon$ must be imposed artificially. As $f_{m_i} = 0$ could not happen in a failure detection oriented metric it might seem logical to consider a monitoring cost functional that was a sum of estimation and failure detection metrics. Thus, a reasonable modified cost metric might be (assuming equal weights to estimation and failure monitoring)

$$J_m = \frac{1}{n_y} \sum_{i=1}^{n_y} \frac{\sigma_{e_i}^2 + \rho_i \sigma_{y_i}^2 / f_{m_i}}{\sigma_{y_i}^2} \quad (4-48)$$

The noise ratio ρ_i is on the order of 0.01; thus for moderate attention levels, minimizing Equation (4-48) is equivalent to minimizing Equation (4-7). At low levels of attention, however, (say, $f_{m_i} \sim 0.01$) the second term in Equation (4-48) becomes important and prevents f_{m_i} from approaching zero as may happen when minimizing $\sigma_{e_i}^2$. Thus we see that the two following optimization problems will yield nearly identical results.

$$I: \min_{\{f_{m_i}\}} \frac{1}{n_y} \sum_{i=1}^{n_y} \left(\frac{\sigma_{e_i}^2}{\sigma_{y_i}^2} + \frac{\rho_i}{f_{m_i}} \right) \quad (4-49)$$

$$f_{m_i} > 0, \sum f_{m_i} = f_m$$

$$II: \min_{\{f_{m_i}\}} \frac{1}{n_y} \sum_{i=1}^{n_y} \frac{\sigma_{e_i}^2}{\sigma_{y_i}^2}$$

$$f_{m_i} > \epsilon_i, \sum f_{m_i} = f_m \quad (4-50)$$

In conclusion, after an examination of various schemes for predicting human monitoring performance, the scheme involving Kalman filter optimization on the full aircraft model seems to hold greatest potential. It is not simple mathematically, but fortunately the optimization of the f_{m_i} can be performed using existing human operator computer programs with only slight modification. A default option should be included to treat (singular) situations where the optimized filter produces $f_{m_i} \sim 0$ for some i .

4.3 SIMULTANEOUS MONITORING AND CONTROL WITHIN A SINGLE AXIS

The above discussion is relevant to the pilot monitoring assessment for a completely automatic system. However, if a pilot is actively controlling a vehicle (or axis) there are two reasons for looking at a display variable:

1. For control purposes, fraction f_{c_i} .
2. For monitoring purposes, fraction f_{m_i} .

Obviously there is an overlap that must be resolved. The following assumptions are made in this situation:

1. The pilot allocates his attention first to the control task requirements. Spare capacity is then available for monitoring. Thus, f_c and f_{c_i} are chosen (subject to $f_c < f_{TOT} \sim 0.8$) such that a desired level of performance is attained. The available monitoring fraction is then $f_{TOT} - f_c = f_m$.
2. The pilot next allocates f_m among all displayed variables — those being controlled manually and those being controlled automatically — to minimize the total monitoring cost.

$$J_m = J_{m1} + J_{m2} \quad (4-51)$$

where

$$J_{m1} = \sigma_e^2 / \sigma_y^2 \text{ for instruments associated with the manual control task.}$$

$$J_{m2} = \sigma_e^2 / \sigma_y^2 \text{ for instruments associated with the automatically controlled loops.}$$

3. The optimal f_{c_i} is not dependent on the optimal f_{m_i} (the reverse is not generally true). Thus, any additional monitoring of a display does not change control strategy.

For the manually controlled task, it is possible to optimize for f_{c_i} and compute the relative estimation error fraction σ_e^2 / σ_y^2 associated with each displayed variable. Thus, it remains to distribute the f_m by allocating an f_{m_i} to each display to minimize

$J_{m1} + J_{m2}$. It is quite likely that the optimal f_{m_i} will be non-zero even for displays for which f_{c_i} is a reasonable fraction. This is because the information required of a display for monitoring is generally different than that required for control (i.e., C_e vs L_e in J_m vs J_o).

Therefore the problem of determining f_{m_i} for only a manually controlled loop is solved by first finding f_{c_i} to minimize J_o . Next find f_{m_i} while $\sum_i f_{m_i} = f_m$ to minimize J_m , bearing in mind that the total attention to a display for purposes of observation is $f_{TOT_i} = f_{m_i} + f_{c_i}$ — i.e., monitoring proceeds over and above control allocation and is geared to J_m .

For the case of an aircraft with both a manual and an automatic control loop, the allocation of f_{m_i} is accomplished by considering two "independent" tasks. The following one-dimensional search technique for optimizing J_{m1} and J_{m2} is suggested, once the optimal f_{c_i} are found, (Figure 4-1).

In some situations it may not be necessary to allocate any additional monitoring attention to a display used for control purposes already. However it is difficult to ascertain this a priori since there may be displays needed only marginally for control purposes (e.g., pitch indicator for attitude stability system) but which will most likely be monitored to a higher percentage than the control-allocated f_{c_i} . Thus, the above technique makes no a priori assumptions as to whether instruments are used primarily for monitoring or for control purposes.

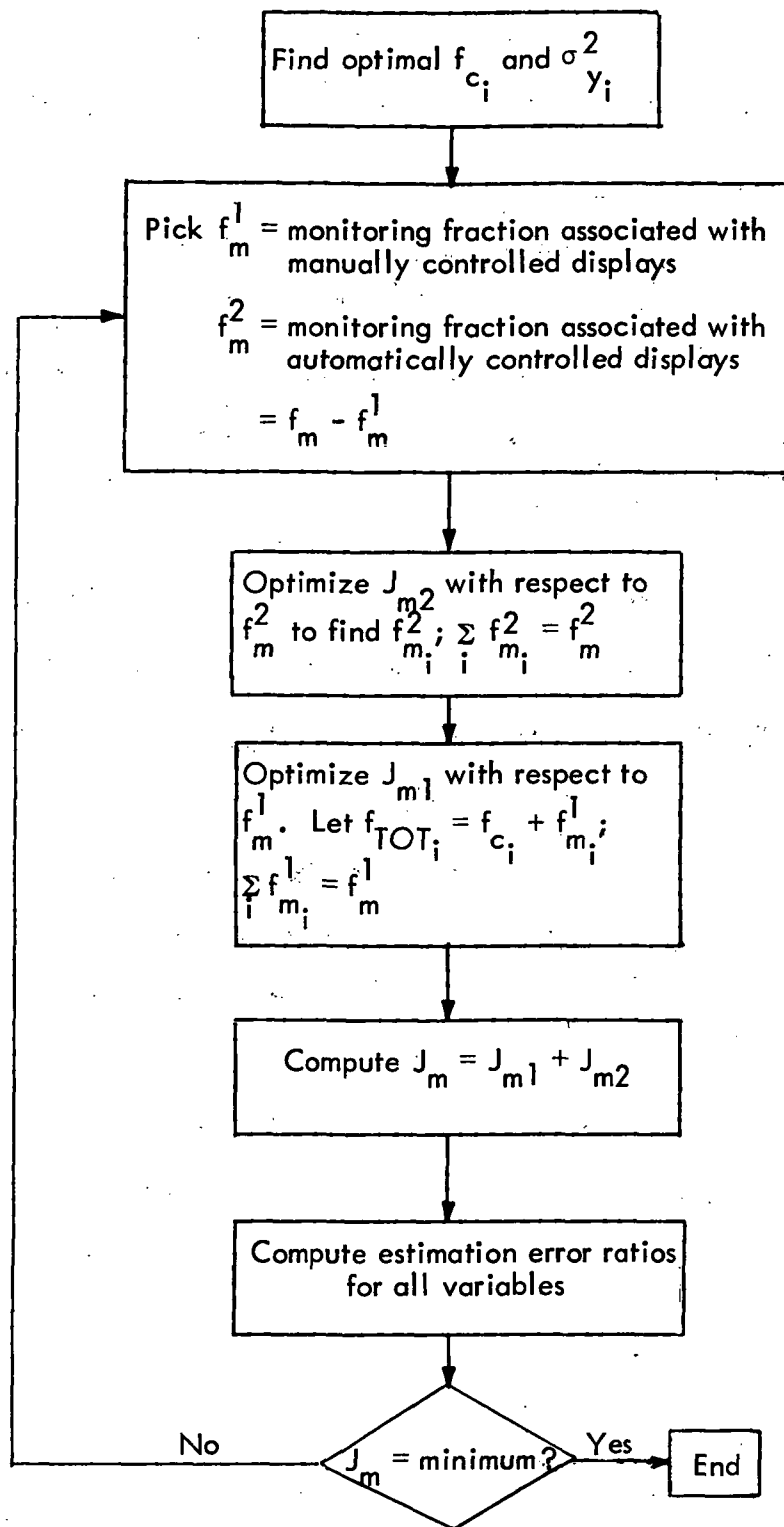


Figure 4-1. Flow Diagram for Dual Axis Monitoring Allocations.

SECTION 5

MODEL VALIDATION

In order to validate the pilot vehicle model, including the means by which workload metrics are established, the analysis procedure is applied to a CH-46C VTOL. As the CH-46C has been the subject of several studies at NASA Langley Research Center (References 12, 17 and 18), there exists a (flight test) data base against which model predictions may be compared. This analysis will consider the hover task only, as this represents one of the most difficult VTOL control requirements, and is amenable to steady-state analysis techniques. The analysis is further restricted to the display format level by considering only the display panel/instruments used in the actual CH-46C tests. The information and/or display element level analysis would be appropriate if new display systems were being proposed. The automation levels that we consider are the attitude command systems designed at NASA (Reference 17); the flight directors are also the NASA designs (References 12-17).

5.1 CH-46C DYNAMIC EQUATIONS OF MOTION

This section presents the basic equations of motion of the CH-46C, including a representation for the external wind-gusts. It also derives the equations for the control stick inputs, taking into account the attitude command system used on the CH-46C.

5.1.1 BASIC VEHICLE DYNAMICS

The analysis uses the perturbation equations derived in Appendix C, written about a hover equilibrium ($\theta_0 = 6.8^\circ$). The state variables are chosen as the Euler angles and body rates to be consistent with the control augmentation and guidance schemes employed. Thus, for the longitudinal equations, the state vector is

$$x = [\Delta x, \Delta z, \Delta \theta, \Delta V_x, \Delta V_z, q]^T \quad (5-1)$$

where

Δx = longitudinal (inertial) hover error

Δz = vertical (inertial) hover error

$\Delta \theta$ = pitch deviations (from θ_0)

ΔV_x = longitudinal (inertial) velocity

ΔV_z = vertical (inertial) velocity

q = body-axis pitch rate

The control inputs for the basic vehicle are the differential and gang collective deviations from trim, so that $u = [\Delta \delta_c, \Delta \delta_c]^T$. The longitudinal equations, in the form

$$\dot{x} = Ax + Bu \quad (5-2)$$

are given in Figure 5-1.

For the lateral direction dynamics we choose as state vector

$$x = [\Delta y, \phi, \Delta \Psi, \Delta V_y, p, r]^T \quad (5-3)$$

where

Δy = lateral (inertial) hovering error

ϕ = inertial roll angle

$\Delta \Psi$ = heading angle error

ΔV_y = lateral (inertial) velocity

p = body-axis roll rate

r = body-axis yaw rate

These states have been chosen to be compatible with subsequent model following augmentation schemes. The two lateral controls are $u = [\Delta \delta_a, \Delta \delta_r]^T$ where $\Delta \delta_a$ = roll cyclic input and $\Delta \delta_r$ = rudder or yaw cyclic input. The numerical values for the A and B matrices are included in Figure 5-1.

Longitudinal Direction:

$$A = \begin{bmatrix} 0 & 0 & 0 & 1 & 0 & 0 \\ 0 & 0 & 0 & 0 & 1 & 0 \\ 0 & 0 & 0 & 0 & 0 & 1 \\ 0 & 0 & -32.17 & -.01611 & -.003392 & .4783 \\ 0 & 0 & 0 & .002208 & -.3786 & -.8030 \\ \hline 0 & 0 & 0 & .006013 & .003786 & -.7317 \end{bmatrix}$$

$$B = \begin{bmatrix} 0 & 0 \\ 0 & 0 \\ 0 & 0 \\ .1740 & -.01257 \\ -.03263 & -7.527 \\ \hline .3545 & -.04765 \end{bmatrix}$$

Lateral Direction:

$$A = \begin{bmatrix} 0 & 0 & 0 & 1 & 0 & 0 \\ 0 & 0 & 0 & 0 & 1 & .1639 \\ 0 & 0 & 0 & 0 & 0 & 1.013 \\ 0 & 31.75 & 0 & -.02663 & -.7651 & -.1252 \\ \hline 0 & 0 & 0 & -.007889 & -.4919 & .02622 \\ 0 & 0 & 0 & .000970 & .03645 & -.05599 \end{bmatrix}$$

$$B = \begin{bmatrix} 0 & 0 \\ 0 & 0 \\ 0 & 0 \\ .9979 & .1465 \\ \hline .4401 & -.2739 \\ -.02022 & .1890 \end{bmatrix}$$

Figure 5-1. System Matrices for Basic CH-46 Helicopter at Hover.

5.1.2 AUGMENTATION SCHEMES

The basic CH-46 is unstable and virtually impossible for a pilot to control without some form of stability augmentation system or command following system. The automation schemes that will be investigated are the NASA designed pitch, roll and heading command systems using the differential collective, roll cyclic and rudder, respectively. The pitch command model is

$$\dot{q}_m = -2\zeta\omega q_m + \omega^2\theta_m + K_\theta\omega^2\delta_e \quad (5-4)$$

with $\zeta = 0.75$, $\omega = 2.0$ rad/sec, $K_\theta = 0.15$ rad/in. The roll model

$$\dot{p}_m = 2\zeta\omega p_m + \omega^2\phi_m + K_\phi\omega^2\delta_a \quad (5-5)$$

is identical to the pitch model with $K_\phi = K_\theta$. The heading hold model in yaw,

$$\dot{r}_m = 2\zeta_0\omega r_m + \omega^2\psi_m + K_\psi\omega^2\delta_r \quad (5-6)$$

has $\zeta_0 = 0.7$, $\omega = 2.0$ rad/sec and $K_\psi = 0.35$ rad/in.

Having formulated the desired model characteristics, the next step is to develop the compensation that will force the aircraft response to follow the model. In the NASA-LaRC design, the compensation used included lead, rate error and integrated rate error. The resulting frequency response characteristics showed that the aircraft response closely followed attitude commands over a wide frequency range, beyond that normally associated with pilot control bandwidth. If one wishes to precisely model pilot-vehicle response for the augmented systems it is necessary to include the model-following compensation in the system description. This adds additional states in the vehicle equations, needlessly complicating the analysis process since the pilot effectively "sees" a system that responds as the model. The simplified approach we follow in studying pilot response is to assume that the system exactly follows the model, and

solve for the feedbacks that are required to assure this condition. Additional vehicle states are not needed, but a difficulty arises because of cross-coupling between the control actuator dedicated to provide the model response and the effect of that actuator in other state variables. For example, a differential collective may be used to satisfy the pitch response of the helicopter, but by so doing, it will have an influence in the translational equations.

To show the means by which the augmented equations are developed, assume that the basic unaugmented vehicle equations can be written (Appendix D)

$$\begin{pmatrix} \dot{x}_1 \\ \dot{x}_2 \end{pmatrix} = \begin{pmatrix} A_{11} & A_{12} \\ A_{21} & A_{22} \end{pmatrix} \begin{pmatrix} x_1 \\ x_2 \end{pmatrix} + \begin{pmatrix} B_1 \\ B_2 \end{pmatrix} \delta. \quad (5-7)$$

We have divided the state vector into two parts with x_2 that portion of the state vector to be controlled according to some desired model response. The inputs to this system are the actuator inputs δ which are dedicated to satisfying the model response. Disturbance inputs and other actuators affecting the equations of motion, but not being used to satisfy the model response can be added to Equation (5-7) but are not shown here.

Assume that it is desired to have the partition of the state vector x_2 follow a model equation given by

$$\dot{x}_{2m} = A_{21}^* x_1 + A_{22}^* x_{2m} + B_2^* u \quad (5-8)$$

Note that the derivative of the model response is given by linear combinations of the model itself x_{2m} , feedback of the other partition of the state vector x_1 (e.g. position), and the control stick inputs u .

The actual response of x_2 is given in Equation (5-7) as

$$\dot{x}_2 = A_{21} x_1 + A_{22} x_2 + B_2 u \quad (5-9)$$

In order that the system response given by Equation (5-9) follow the model response of Equation (5-8), i.e., $x_2 = x_{2m}$, we subtract the two equations and solve for the actuator activity which is dedicated to satisfy this response:

$$\delta = B_2^{-1} [(A_{21}^* - A_{21}) x_1 + (A_{22}^* - A_{22}) x_2 + B_2^* u] \quad (5-10)$$

Substituting this value of the actuator activity into Equation (5-7) provides the following form for the state equations when the system follows the model.

$$\begin{pmatrix} \dot{x}_1 \\ \dot{x}_2 \end{pmatrix} = \begin{pmatrix} A_{11}^* & A_{12}^* \\ A_{21}^* & A_{22}^* \end{pmatrix} \begin{pmatrix} x_1 \\ x_2 \end{pmatrix} + \begin{pmatrix} B_1^* \\ B_2^* \end{pmatrix} u \quad (5-11)$$

where

$$A_{11}^* = A_{11} + B_1 B_2^{-1} (A_{21}^* - A_{21})$$

$$A_{12}^* = A_{12} + B_1 B_2^{-1} (A_{22}^* - A_{22}) \quad (5-12)$$

$$B_1^* = B_1 B_2^{-1} B_2^*$$

Note that the partition of the state vector x_2 has the desired response of the model, but also that the dynamics of the other partition of the state vector x_1 have been altered because of the effect of the actuator δ on these equations.

The above model-following process is easily applied to include the command systems of Equations (5-4) through (5-6). For example, in the pitch command model (Equation (5-4)), the differential collective is the dedicated actuator, and the partitions A_{21} , A_{22} , B_2 are shown in Figure 5-1; the model partitions are

$$A_{21}^* = [0 \ 0 \ -\omega^2 \ 0 \ 0]$$

$$A_{22}^* = -2\zeta\omega$$

$$B_2^* = K_\theta \omega^2$$

The resulting A^* , B^* matrices for the augmented system are shown in Figure 5-2. Note that the second column of the B matrix, associated with the power collective, is unmodified since this control is not used in the model matching scheme.

In the lateral case, both controls are used in the model matching process. The partitions A_{21}^* , A_{22}^* , B_2^* are shown in Figure 5-1; the model partitions follow from Equations (5-5) and (5-6) as

$$A_{21}^* = \begin{pmatrix} 0 & -\omega^2 & 0 & 0 \\ 0 & 0 & -\omega^2 & 0 \end{pmatrix}$$

$$A_{22}^* = \begin{pmatrix} -2\zeta\omega & 0 \\ 0 & -2\zeta_o\omega \end{pmatrix}$$

$$B_{22}^* = \begin{pmatrix} \omega^2 K_\phi & 0 \\ 0 & \omega^2 K_\psi \end{pmatrix}$$

and provide the lateral directional equations of motion for the aircraft with the roll and yaw augmentation systems engaged.

5.1.3 WIND GUST DISTURBANCES

The principal external disturbances acting on the helicopter are due to the wind turbulence or gusts. The representation of these effects in the linear system model involves two considerations: a model of the wind spectrum, and the way in which the wind affects the vehicle aerodynamic forces. The gust model that is used is the Dryden model with power spectral density

$$\Phi_{\xi}(w) = 2 \sigma_g^2 \frac{V_o}{L} \left(\frac{1}{(V_o/L)^2 + w^2} \right) \quad (5-13)$$

To obtain a random wind model with this PSD, a white noise $\eta(t)$ with variance

Longitudinal Direction:

$$A^* = \begin{bmatrix} 0 & 0 & 0 & 1 & 0 & 0 \\ 0 & 0 & 0 & 0 & 1 & 0 \\ 0 & 0 & 0 & 0 & 0 & 1 \\ 0 & 0 & -34.14 & -.01906 & -.005293 & .6350 \\ 0 & 0 & .3682 & .002762 & -.3783 & -.5942 \\ \hline 0 & 0 & -4.0 & 0 & 0 & -3.0 \end{bmatrix}$$

$$B^* = \begin{bmatrix} 0 & 0 \\ 0 & 0 \\ 0 & 0 \\ .2945 & .01082 \\ -.05524 & -7.532 \\ \hline 0.6 & 0 \end{bmatrix}$$

Lateral Direction:

$$A^* = \begin{bmatrix} 0 & 0 & 0 & 1 & 0 & 0 \\ 0 & 0 & 0 & 0 & 1 & .1639 \\ 0 & 0 & 0 & 0 & 0 & 1.013 \\ 0 & 21.88 & -17.41 & -.01138 & -7.112 & -12.13 \\ \hline 0 & -4 & 0 & 0 & -3 & 0 \\ 0 & 0 & -4 & 0 & 0 & -2.8 \end{bmatrix}$$

$$B^* = \begin{bmatrix} 0 & 0 \\ 0 & 0 \\ 0 & 0 \\ 1.480 & 6.092 \\ \hline .6 & 0 \\ 0 & 1.4 \end{bmatrix}$$

Figure 5-2. System Matrices for Augmented CH-46 Helicopter at Hover.

$$E \{ \eta(t) \eta(t-\tau) \} = 2\sigma_g^2 \frac{V_0}{L} \quad (5-14)$$

is passed through the linear system

$$\dot{\xi}(t) = -\frac{V_0}{L} \xi(t) + \eta(t) \quad (5-15)$$

In our modeling work we will assume moderate turbulence with representative parameters

$$\sigma_g = \text{rms gust velocity} = 3 \text{ ft/sec.}$$

$$V_0/L = \text{gust bandwidth} = 0.1 \text{ rad/sec}$$

We assume that independent gusts act along all three of the aircraft (body) axes. A normal component ξ_w induces primarily normal accelerations, or perturbations in angle-of-attack. An axial component ξ_u induces primarily forward speed perturbations, and a lateral component ξ_v perturbs lateral velocity. For simplicity we assume $\sigma_{gw} = \sigma_{gu} = \sigma_{gv} = 3 \text{ ft/sec.}$

The components $\xi_w(t)$, $\xi_u(t)$ and $\xi_v(t)$ are subtracted from the dynamical states $w(t)$, $u(t)$ and $v(t)$, respectively, in the equations of motion. The result is the modifications

$$\left. \begin{aligned} \dot{u} &= -\frac{X_w}{m} \xi_w - \frac{X_u}{m} \xi_u + \dots \\ \dot{v} &= -\frac{Y_v}{m} \xi_v + \dots \\ \dot{w} &= -\frac{Z_w}{m} \xi_w - \frac{Z_u}{m} \xi_u + \dots \\ \dot{p} &= -\frac{L_v}{I_{xx}} \xi_v + \dots \\ \dot{q} &= -\frac{M_w}{I_{yy}} \xi_w - \frac{M_u}{I_{yy}} \xi_u + \dots \\ \dot{r} &= -\frac{N_v}{I_{zz}} \xi_v + \dots \end{aligned} \right\} \quad (5-16)$$

When these terms are carried through the Euler transformations to the inertial frame state variables as defined in Equations (5-1) and (5-3), the end result is the addition of the terms

$$F_U \xi_U(t) + F_W \xi_W(t) \quad (5-17a)$$

to the longitudinal equations, and the term

$$F_V \xi_V(t) \quad (5-17b)$$

to the lateral equations†. For the CH-46C at hover, these terms are

$$F_U = \begin{bmatrix} 0 \\ 0 \\ 0 \\ 0.01535 \\ -0.0634 \\ -0.00656 \end{bmatrix}; \quad F_W = \begin{bmatrix} 0 \\ 0 \\ 0 \\ 0.00595 \\ 0.3733 \\ 0.00285 \end{bmatrix}; \quad F_V = \begin{bmatrix} 0 \\ 0 \\ 0 \\ 0.02663 \\ 0.00789 \\ -0.00097 \end{bmatrix}$$

Note that these terms are appropriate to both the basic and augmented vehicles as the wind gust states are not included in model following feedbacks. Thus, we arrive at the final model for the system/gust dynamics compatible with the pilot model formulation of Appendix A,

$$\dot{x}(t) = Ax(t) + Bu(t) + E\xi(t) \quad (5-18)$$

where, in the longitudinal case

$$x = [\xi_U, \xi_W, \Delta x, \Delta z, \theta, V_x, V_z, q] \quad (5-19a)$$

and, in the lateral case

$$x = [\xi_V, \Delta y, \phi, \psi, V_y, p, r] \quad (5-19b)$$

and where $\xi(t)$ is a white noise vector.

†Additional states must be added to the system dynamics to include the noise shaping dynamics Equation (5-15) for each ξ_i .

5.2 CH-46 HOVER DISPLAY/CONTROL PARAMETERS

In applying the optimal control model of the pilot, it is necessary to describe the display information in a form compatible with vehicle states and controls,

$$y(t) = Cx(t) + Du(t) \quad (5-20)$$

In addition, values must be chosen for the visual and/or indifference thresholds, i.e. those limits on displayed items within which the pilot is less likely to take corrective action. The values are estimates derived from the display gains, display resolution, display markings and pilot opinions.

5.2.1 PRIMARY DISPLAY INPUTS - HOVER MODE

The four primary instruments appropriate to the hover mode are the map (or HSI), radar altimeter, IVSI and ADI. Assuming that the pilot perceives both the position and rate of a display indicator, we have the model inputs listed in Table 5-1. Also given in Table 5-1 are the values chosen for the display thresholds, as well as subjective values for the maximum deviations that a pilot will tolerate in the observed quantities. These latter values are used to generate cost functional weightings in the optimal control model according to

$$q_{y_i} = \left(\frac{1}{y_{i, \max}} \right)^2 \quad (5-21)$$

The large thresholds associated with perceiving horizontal position and velocity errors at hover is a reflection of the small map scale (100 ft/in at hover) and the relatively large size of the aircraft symbol†. The associated maximum deviations for Δx , Δy reflect the 50-ft diameter of the landing pad. The small threshold on altitude deviations reflects the expanded scale of the radar altimeter below 100 ft, with an

† At a viewing distance of 28 in, a 20 ft error is less than 0.5° visual arc.

Table 5-1. CH-46C Primary Display Inputs (Hover Mode).

INSTRUMENT	VARIABLE	THRESHOLD	MAX. DEVIATION
MAP	Δx	20 ft	25 ft
	V_x	10 ft/sec	--
ALTIM	Δz	4 ft	5 ft
	V_z	2 ft/sec	2 ft/sec
ADI	θ	1°	2°
	q	0.5°/sec	1°/sec
IVSI	V_z	1 ft/sec	2 ft/sec
	\dot{V}_z	0.5 ft/sec	--
MAP	Δy	20 ft	25 ft
	V_y	10 ft/sec	--
ADI	ϕ	1°	5°
	$\dot{\phi}$	0.5°/sec	2°/sec
MAP/COMPASS	ψ	1°	2°
	$\dot{\psi}$	0.5°/sec	1°/sec

instrument scale marking at the nominal 50 ft hovering altitude. Finally, we have chosen thresholds on the rates of a display indicator equal to 1/2 the corresponding position threshold in accordance with previous work (Reference 21).

5.2.2 FLIGHT DIRECTOR INPUTS - HOVER MODE

The flight director has undergone many revisions throughout the course of the flight test of the CH-46C. Herein, the director form and values for the flight director gains at hover are taken from Reference 12; Table 11. There are three flight director signals corresponding to pitch, power and roll commands respectively. The form of these signals is (neglecting the effects of any additional filtering),

$$\left. \begin{aligned}
 FD_x &= .004 \Delta x + .04 V_x + .5 \delta_e \\
 FD_z &= .0057 \Delta z + .057 V_z + .115 \dot{V}_z \\
 FD_y &= .004 \Delta y + .04 V_y + .5 \delta_a
 \end{aligned} \right\} \quad (5-22)$$

In order to express the signal FD_z in the requisite form of Equation (5-20), we substitute for \dot{V}_z using the equations of motion. The result is (approximately)

$$FD_z \sim .04 \xi_v + .0057 \Delta z + .04 \theta + .0515 V_z - .068 q - .85 \delta_c \quad (5-23)$$

or, if we keep only the dominant terms,

$$FD_z \sim .0057 \Delta z + .015 V_z - .85 \delta_c \quad (5-24)$$

The rates of the flight director signals were not included as "observed" variables in our application of the pilot model. There were several reasons for this decision:

- The director rates would contain control rate ($\dot{\delta}$) and white noise terms, giving rise to a complex modeling problem that could only be solved by adding "pseudo" filters in the equations.
- The flight director signals are basically high frequency in nature so that the value of their rate information in a low bandwidth hover task is small.
- The flight directors have been designed so that the pilot acts essentially as a gain (especially at low frequencies) on the observed signal. This minimizes the pilot reliance on the rate information.

In order to include the flight directors within the modeling framework we require a selection of threshold values and cost functional weightings. The thresholds were chosen as 0.1 in for all three directors, corresponding to approximately 1/10 full scale.

As discussed in Subsection 3.2, including the FD_i within the cost functional, in addition to the other terms, implies that one of the pilot's direct control objectives is to keep the FD_i small. Based on an analysis of the flight director instruments, and piloting task, we choose as maximum deviations

$$(FD_x)_{MAX} = 0.2 \text{ in}$$

$$(FD_z)_{MAX} = 0.4 \text{ in}$$

$$(FD_y)_{MAX} = 0.2 \text{ in}$$

5.3 MODEL PREDICTIONS FOR CH-46 HOVER

Having obtained state-space equations for the vehicle and display dynamics, the ability of the pilot model to analyze the relationship between CH-46 hovering performance and pilot workload is investigated. We consider pilot control performance for the augmented (attitude command) system, both with and without use of the flight director signals. Various levels of total attention f_c from 0.3 to 0.8 are assumed so that we may obtain the performance vs. workload curves. The cost functional output weightings, q_{y_i} , are as given in the previous section. The control rate weightings q_{u_i} are adjusted to give resulting "neuro-motor" lags of $\tau_{Ni} \sim 0.1 \text{ sec}$, with a minimum value of $q_{u_i} = 0.25$ allowable. This corresponds to an assumed maximum pilot stick-rate deflection of 2 in/sec. The remaining basic parameters for the pilot model are selected at their nominal a priori values:

$$\tau = 0.2 \text{ sec}$$

$$\rho_{y_i} = 0.01 \text{ (i.e., -20 dB) for all displayed variables}$$

$$\rho_{u_i} \sim 0.01 \text{ (-20 dB) for all control variables.}$$

5.3.1 MODEL PREDICTIONS - NO FLIGHT DIRECTOR CASE

The pilot model is used to predict hovering performance with only primary instruments. In the flight tests, the pilots were unable to maintain the CH-46 in a hover under these conditions. Table 5-2 gives model results corresponding to an allocation of attention of 0.3 to the longitudinal axis. The results clearly show that accurate hover is virtually impossible longitudinally. One-sigma errors of 26 ft imply that about 40 percent of the time the helicopter is not over the pad. Instrument attentional allocations are equally divided between map and IVSI, with some attention to the altimeter†. Thus, height information is obtained primarily through integrating the IVSI with cross-checks from the altimeter.

Table 5-2. Model Results. Longitudinal Axis, $f_i = 0.3$.

Instrument	σ_i	f_{c_i}	f_{c_i} / f_c
MAP, x	25.5 ft	0.11	0.37
ALTIM, z	4.6 ft	0.05	0.17
ADI, θ	1°	< 0.01	< 0.03
IVSI, V_z	1.3 ft/sec	0.12	0.40

The following information relative to the longitudinal task has also been obtained from the model analysis:

- The total cost $J(u) = 3.01$ whereas the scanning cost (the part of J due to human observational processing noise) $I(u) = 2.86$. Thus, over 95 percent of the hovering errors are due to the human's own injected random errors, and only 5 percent are directly attributable to the wind gusts.
- The sensitivity of performance to higher attentional (workload) levels is fairly low. Thus, $f_{c, \text{long}} = 0.5$ results in only 12 percent improvement in hovering errors. Consequently, even very high workload levels will not result in satisfactory hover.

†The given f_{c_i} are accurate to ± 10 percent as in the vicinity of the optimal. The cost functional $J(u)$ is relatively flat with respect to f_{c_i} .

- Rate information obtained from the displays (i.e., the derivatives of displayed quantities) is not very useful for control. Running the model with only the four position variables (Δx , Δz , θ , V_z) gave attentional and performance results within 5 percent of Table 5-2.

The results for the lateral axis hover task, corresponding to an attention level of 0.3, are given in Table 5-3. As can be seen, hover performance is unacceptable. However, the attitude hold systems are performing as expected. As a result, little pilot attention is placed on the roll and course indicators.

Table 5-3. Model Results. Lateral Axis, $f_c = 0.3$.

Instrument	σ_i	f_{c_i}	f_{c_i}/f_c
MAP, y	19.4	0.27	0.90
ADI, ϕ	1.4°	0.02	0.06
DG, ψ	0.4°	<0.01	0.04
δ_a	0.17 in.	-	-
δ_r	0.05 in.	-	-

The results correspond with the pilot's inability to hover on the primary status instruments. Although the model predicts a hover rms of 25 feet, this result is under the assumption of a well-trained pilot. Thus, an experiment where only several runs are tried is likely to result in much larger errors. Finally, the model predicted hovering error rates (V_x , V_y) of about 2.5 ft/sec indicate the slow drifting/divergence observed experimentally.

5.3.2 SINGLE AXIS MODEL RESULTS - WITH FLIGHT DIRECTOR

The results using the flight director in the longitudinal task are given in Table 5-4 for a 0.3 level of attention. There is a substantial improvement in rms

hovering error from 25.5 to 17 feet, accompanied by only slight changes in the performance of other variables. What is interesting, of course, is the model's prediction of a dramatic shift of attention away from the status instruments onto the flight directors.

Table 5-4. Model Predictions Using Flight Director, $f_c = 0.3$.

Instrument	σ_i	f_{c_i}	f_{c_i}/f_c
MAP, x	16.7 ft	<0.01	<0.03
ALTIM, z	4.7 ft	0.025	0.1
ADI, θ	0.7°	<0.01	<0.03
IVSI, V_z	1.2 ft/sec	0.025	0.1
FD _x	0.13	0.10	0.3
FD _z	0.14	0.13	0.45

A sensitivity analysis was performed for the longitudinal axis by running the model at assumed workload levels of 0.3 to 0.7. The optimal attentional allocations to the flight directors are evident in all cases, as seen in Table 5-5.

Table 5-5. Attentional Allocations for Longitudinal Task.

Total	Map	Altim	ADI	IVSI	FD _x	FD _z
0.3	<0.01	0.025	<0.01	~0.02	0.10	0.13
0.4	<0.01	0.027	<0.01	~0.02	0.12	0.21
0.5	<0.01	0.037	<0.01	~0.02	0.17	0.25
0.6	<0.01	0.043	<0.01	~0.02	0.22	0.30
0.7	<0.01	0.045	<0.01	~0.02	0.27	0.36

Figure 5-3 shows the sensitivity of the performance measures (both scanning cost and x hover error) to workload level on the longitudinal task. The results show that a level of ~0.6 is required to keep the aircraft over the pad in the x-direction 95 percent of the time.

The results for the lateral axis are given in Table 5-6. RMS hovering error improves to 13 feet at 0.3 attention level with a total shift of attention to the flight director. A sensitivity analysis of lateral axis performance is shown in Figure 5-4. For attention levels greater than 0.15, scanning cost is reasonable insensitive. For each attention level, the allocations among instruments remain the same - full attention to the flight director!

Table 5-6. Model Results. Lateral Axis with Flight Director, $f_c = 0.3$.

Instrument	σ_i	f_i	f_{c_i}/f_c
MAP, y	13.0	< 0.01	< 0.03
ADI, ϕ	1.1°	< 0.01	< 0.03
DG, ψ	0.4°	< 0.01	< 0.03
FD _y	0.1 in	0.27+	0.9+

5.3.3 DUAL AXIS MODEL RESULTS - WITH FLIGHT DIRECTOR

The curves of lateral and longitudinal cost, $l(u)$, vs attentional allocation can be used to determine performance for the combined task given a level of total control workload $f_c = f_{c,lat} + f_{c,long}$. Thus for a given f_c the optimal $f_{c,lat}$ and $f_{c,long}$ are determined to minimize

$$l(u)_{TOTAL} = l(u)_{lat} + l(u)_{long} \quad (5-25)$$

This minimization is accomplished here using a simple one dimensional search procedure. It could also be done via computer by constructing a state space representation for the entire two axis task. In this example, the first approach is easier.

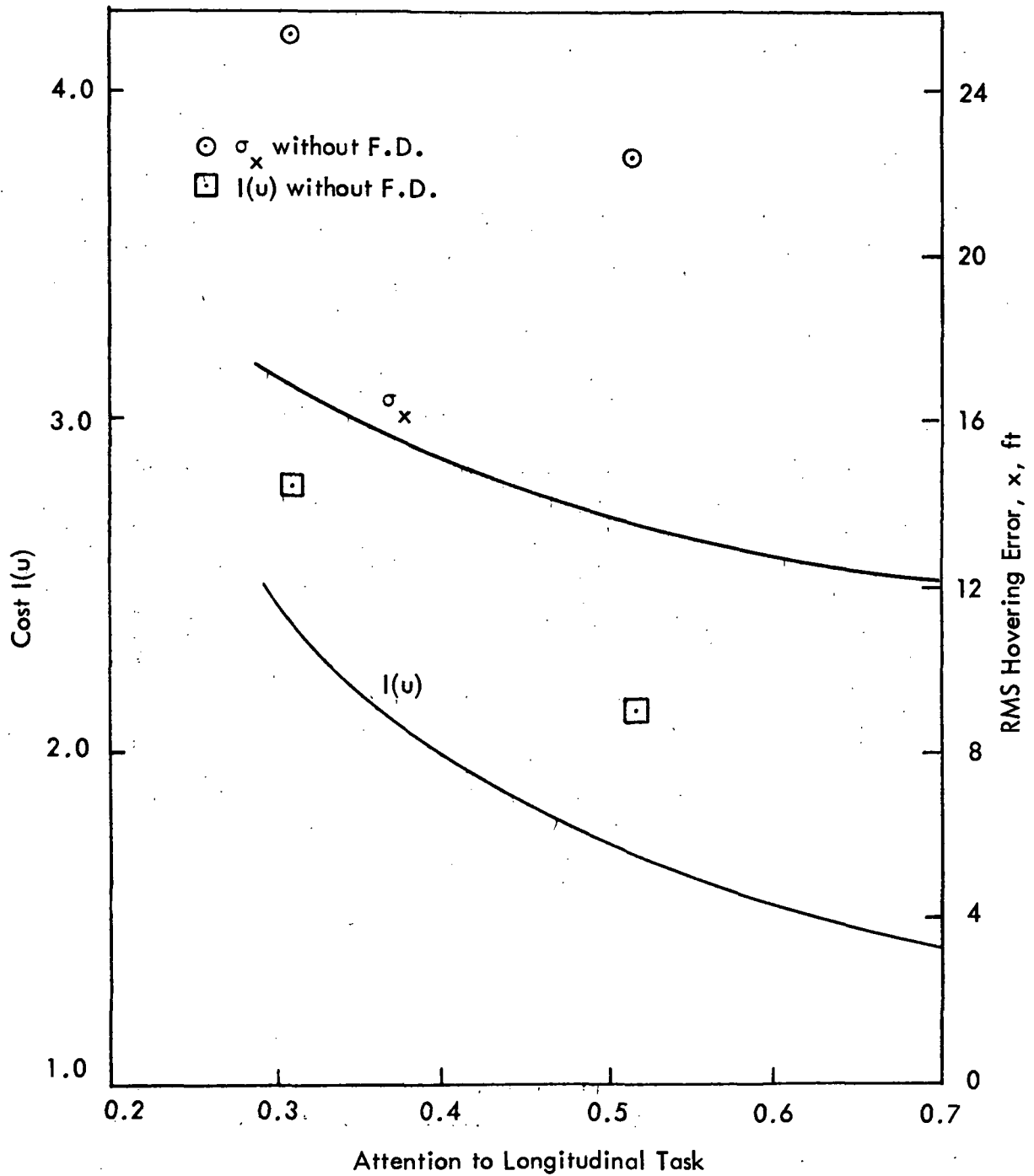


Figure 5-3. Scores vs Attention, CH-46 Hover, Longitudinal Axis.

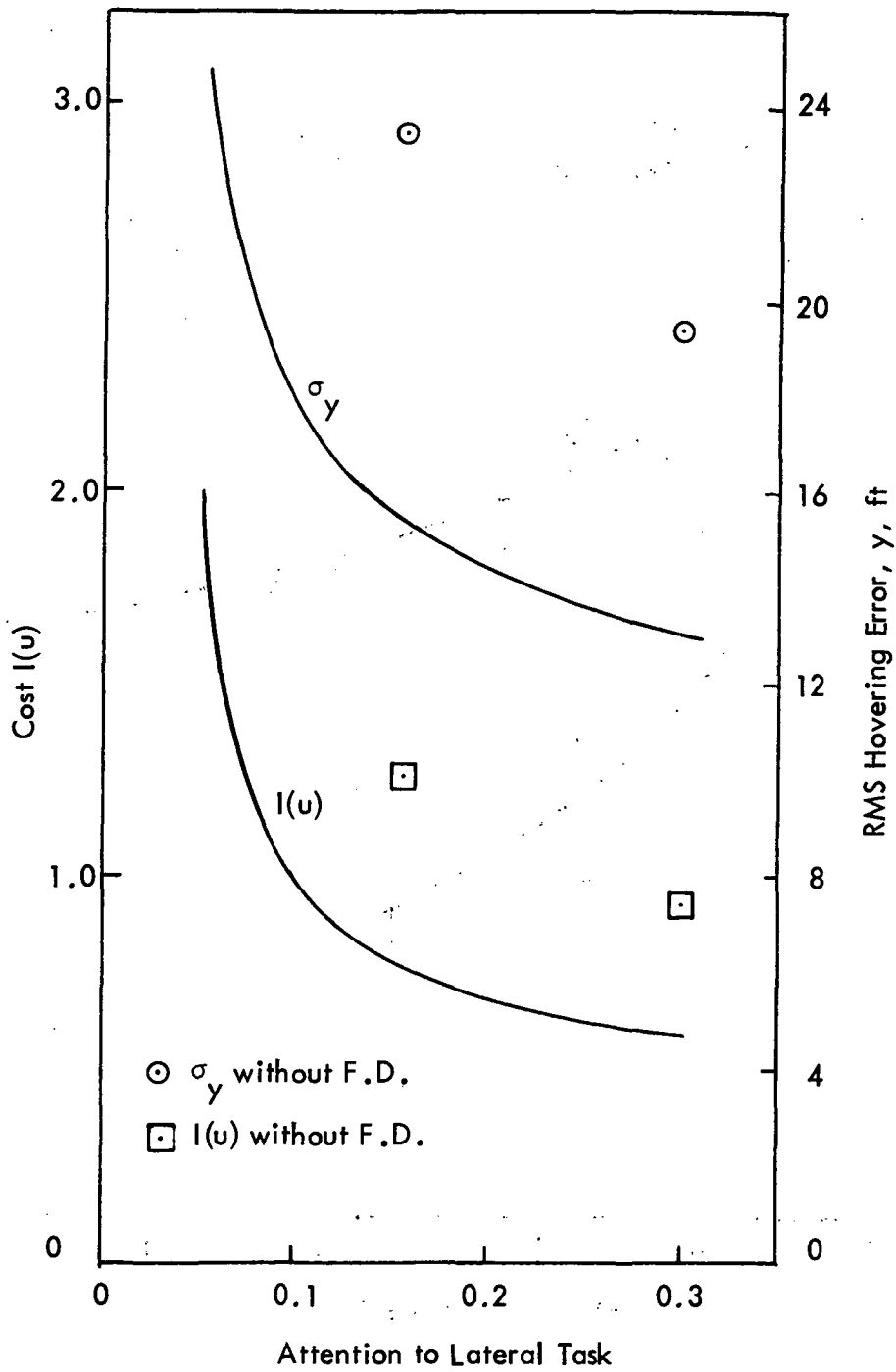


Figure 5-4. Scores vs Attention, CH-46 Hover, Lateral Axis.

The results are shown in Figure 5-5 which represents the overall predictions of the model for the hover task. The following comments are pertinent:

- The optimal attention to the lateral task $f_{c, lat}^*$ is 0.15 - 0.2 or in the vicinity of the "knee" in Figure 5-4 as might be expected.
- At the optimal point ($f_{c, lat}^*$, $f_{c, long}^*$) the RMS hover errors $\sigma_x \sim \sigma_y$ to within 5 percent.
- The sensitivity of total $I(u)$, in the vicinity of the optimum is extremely low. Thus lateral attention could be increased by 0.05, while longitudinal attention is decreased by 0.05, with little change in $I(u)$.

- The "average" hovering error

$$\sigma_{avg} = \left(\frac{\sigma_x^2 + \sigma_y^2}{2} \right)^{1/2} \quad (5-26)$$

shows the same relative insensitivity as does $I(u)$. However, there is a fairly sharp trade-off between σ_x and σ_y .

- Thus, it is quite likely that different pilots will adopt different operating points with respect to lateral vs. longitudinal trade-offs. Total performance $J(u)$ is insensitive here but different distribution of errors is to be expected.

It is possible to investigate the probability of hovering within a circle of radius R for different workload levels. Since we assume Gaussian statistics, the probability densities of x and y hover errors are, respectively,

$$p(x) = \frac{1}{\sigma_x \sqrt{2\pi}} e^{-x^2/2\sigma_x^2} \quad (5-27)$$

$$p(y) = \frac{1}{\sigma_y \sqrt{2\pi}} e^{-y^2/2\sigma_y^2} \quad (5-28)$$

Assuming $\sigma_x^2 \sim \sigma_y^2 = \sigma^2$, it is easy to show that the probability $x^2 + y^2 < R^2$ is

$$\Pr \{ \sqrt{x^2 + y^2} < R \} = 1 - e^{-R^2/2\sigma^2} \quad (5-29)$$

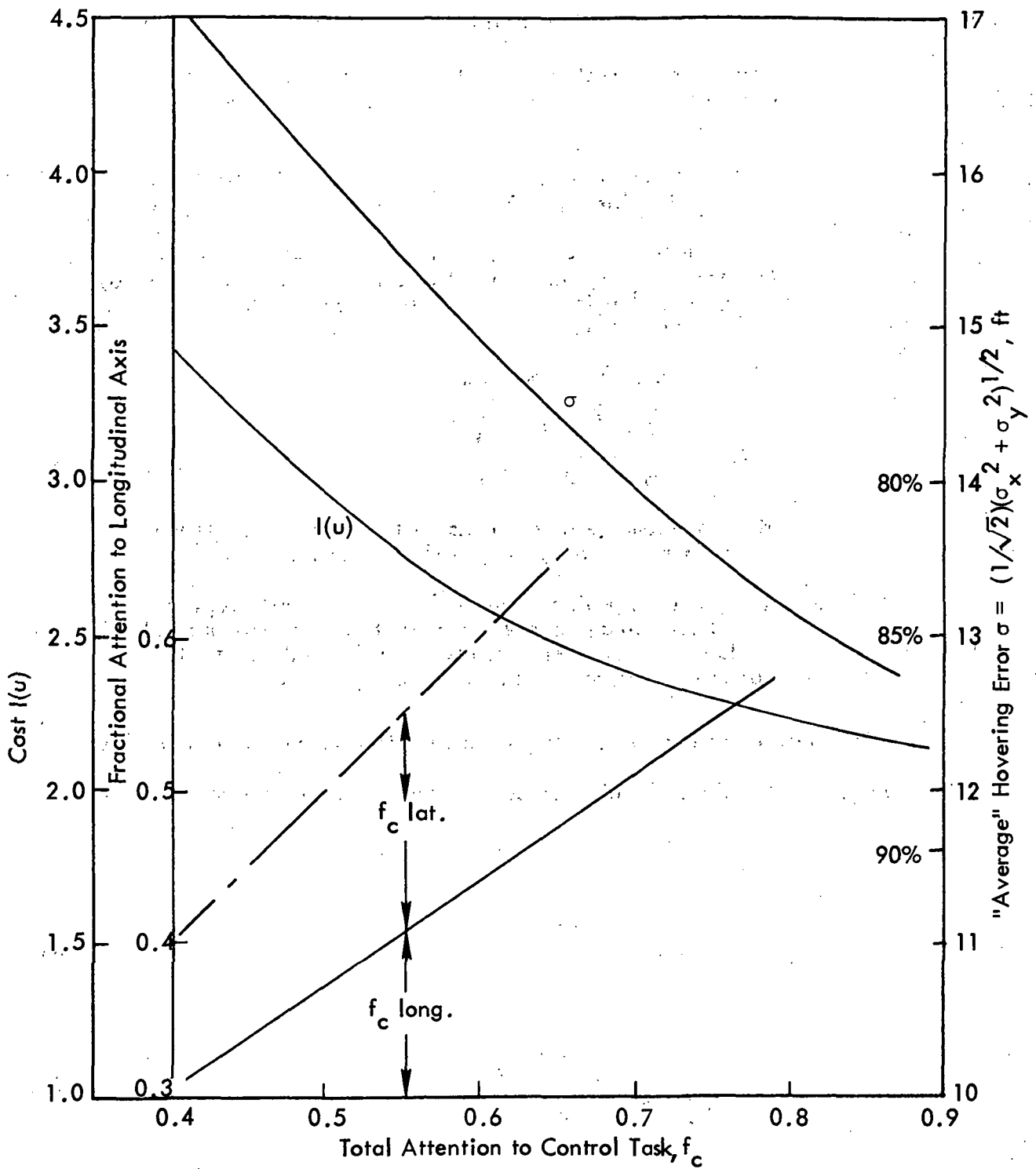


Figure 5-5. Predicted Performance, CH-46 Hover, Flight Director Used.

Thus, the probability of being within a 25 ft radius at any time is easily found for any given "average" hovering error. Several probabilities are noted in Figure 5-5.

We see that workload levels of 0.7 - 0.8 are required to maintain the aircraft over the pad 80 to 85 percent of the time. Thus at this criterion level on performance, we find that the workload level is barely acceptable.[†] The hover task can be accomplished, but no time is left for monitoring the status instruments. (Recall most attention goes to the flight-directors). If we require a tighter hovering performance, the model predicts that the pilot will be overworked. At lower workload levels (e.g., 0.6) the aircraft is over the pad only 75 percent of the time.

The conclusions of our modeling effort thus indicate that

- Hovering cannot be satisfactorily accomplished using the existing status display.
- The flight directors make hovering possible with high workload
- Virtually full control attention is given to the flight director needles
- There is little or no remaining pilot capacity to monitor the status instruments.

These conclusions are very much the same as those from the flight experiments.

[†]We consider $f_t \sim 0.8$ to be full capacity.

SECTION 6

CH-47 RESULTS

The synthesis and analysis techniques described in the preceding section were applied to the Langley CH-47 tandem rotor helicopter, which will be used as the flight research aircraft for the VALT program. The numerical results presented in this section are limited to the longitudinal axes due to time constraints and uncertainty in the lateral directional stability derivative data. Two flight conditions were analyzed to indicate the differences in performance over the expected flight environment:

- hover (sea level)
- approach (1000 ft/min descent at 60 knots)

6.1 CONTROL AUTOMATION LEVELS

As discussed previously in Section 4, each of the control channels of the helicopter has three or five possible levels of automation, shown in Table 6-1.

Table 6-1. Levels of Control Channel Automation.

Forward	Vertical	Lateral	Directional
δ_{e_c}	δ_{c_c}	δ_{a_c}	δ_{r_c}
q_c	v_{z_c}	p_c	r_c
θ_c	h_c	ϕ_c	ψ_c
v_{x_c}		v_{y_c}	
x_c		y_c	

The total number of automation levels from Table 6-1 is $5 \times 3 \times 5 \times 3 = 225$. Obviously it would be impractical to analyze all combinations of automation levels, and indeed many of the combinations in Table 6-1 would not be practical systems. Consequently, several levels of control augmentation were selected to perform the control/display analyses. Table 6-2 shows the control channel commands for each of the eight selected systems. These range from the completely manual, basic vehicle (System A) to a full position feedback system for automatic hover (System H). Note that for the longitudinal axes, Systems D and E are identical.

Table 6-2. Selected CH-47 Automation Levels.

System	Control Channel Command			
	Forward	Vertical	Lateral	Directional
A	δ_e	δ_c	δ_a	δ_r
B	q	δ_c	p	r
C	θ	δ_c	ϕ	r
D	θ	V_z	ϕ	r
E	θ	V_z	ϕ	ψ
F	θ	h	ϕ	ψ
G	V_x	h	V_y	ψ
H	x	h	y	ψ

The quadratic synthesis technique described in Section 4 was used to obtain the closed loop longitudinal system matrices for each of the systems in Table 6-2. As discussed in Section 4, the weighting functions used in the quadratic synthesis can all

be related to the specifications on the maximum allowable pitch acceleration and vertical acceleration. For the CH-47, the maximum state and control variable excursions which define the weighting functions are shown in Table 6-3.

Table 6-3. Weighting Functions for Longitudinal CH-47 Automation Levels.

State Variables - Hover and Approach						
System	x (ft)	z (ft)	θ (rad)	V_x (ft/sec)	V_z (ft/sec)	q (rad/sec)
A	-	-	-	-	-	-
B	-	-	-	-	-	0.435
C	-	-	0.435	-	-	-
D, E	-	-	0.435	-	7.5	-
F	-	30.0	0.435	-	-	-
G	-	30.0	-	28.0	-	-
H	84.0	30.0	-	-	-	-
Control Variables: Systems A-H						
Flight Condition				δ_e (in)	δ_c (in)	
Hover				2.19	0.336	
Approach				2.45	0.404	

Recall that the dynamics of the system to be controlled by the pilot are given by

$$\dot{x} = Ax + Bu + Ew \quad (6-1)$$

where the state vector x consists of the vehicle states shown in Table 6-3 augmented by shaping states for the disturbances. From the CH-46 results it was concluded that a first-order wind gust in both the forward and vertical directions provided a sufficient disturbance input to the system. Consequently, the system state x in Equation (6-1) is augmented by two wind gust velocities given by

$$\begin{aligned} \dot{w}_{gx} &= -w_{gx}/\tau_x + w_x \\ \dot{w}_{gz} &= -w_{gz}/\tau_z + w_z \end{aligned} \quad (6-2)$$

Again from the CH-46 results the time constants τ_x and τ_z were each selected as ten seconds, and the power of the white driving noises (w_x, w_z) were chosen to give an rms gust velocity of 3 ft/sec.

The quadratic synthesis technique was applied for the above weighting functions at hover and approach to generate the closed loop system matrices for Systems B through H (the wind disturbances were not included in this process). The resulting closed loop dynamics for each system are shown in Figures 6-1 through 6-7.

6.2 DISPLAY LEVELS

The optimum control pilot model was used to determine the attention allocations and system performance at the information level and at the display element level for each of the systems described previously. Without flight director signals, the control performance metric weights quadratic terms for each of the basic aircraft states

HOVER

$$A = \begin{bmatrix} -.1 & 0 & 0 & 0 & 0 & 0 & 0 & 0 \\ 0 & -.1 & 0 & 0 & 0 & 0 & 0 & 0 \\ 0 & 0 & 0 & 0 & 0 & 1 & 0 & 0 \\ 0 & 0 & 0 & 0 & 0 & 0 & 1 & 0 \\ 0 & 0 & 0 & 0 & 0 & 0 & 0 & 1 \\ .0014 & .0180 & 0 & 0 & -32.17 & -.0181 & .0007 & 2.671 \\ .2650 & -.0177 & 0 & 0 & 0 & -.0123 & -.2653 & -.0100 \\ -.0020 & -.0049 & 0 & 0 & 0 & .0051 & -.0014 & -1.155 \end{bmatrix}$$

$$B = \begin{bmatrix} 0 & 0 \\ 0 & 0 \\ 0 & 0 \\ 0 & 0 \\ 0 & 0 \\ .1217 & .0026 \\ .0222 & -8.424 \\ .3402 & .0222 \end{bmatrix}$$

$$E = \begin{bmatrix} 1 & 0 \\ 0 & 1 \\ 0 & 0 \\ 0 & 0 \\ 0 & 0 \\ 0 & 0 \\ 0 & 0 \\ 0 & 0 \end{bmatrix}$$

APPROACH

$$A = \begin{bmatrix} -.1 & 0 & 0 & 0 & 0 & 0 & 0 & 0 \\ 0 & -.1 & 0 & 0 & 0 & 0 & 0 & 0 \\ 0 & 0 & 0 & 0 & 0 & 1 & 0 & 0 \\ 0 & 0 & 0 & 0 & 0 & 0 & 1 & 0 \\ 0 & 0 & 0 & 0 & 0 & 0 & 0 & 1 \\ -.0076 & .0237 & 0 & 0 & -31.25 & -.0232 & .0091 & 2.174 \\ .5200 & .0888 & 0 & 0 & -51.99 & -.1214 & -.5134 & -1.850 \\ -.0204 & .0064 & 0 & 0 & -2.022 & -.0051 & -.0208 & -1.737 \end{bmatrix}$$

$$B = \begin{bmatrix} 0 & 0 \\ 0 & 0 \\ 0 & 0 \\ 0 & 0 \\ 0 & 0 \\ .1601 & -.0732 \\ .5813 & -8.946 \\ .3973 & .1868 \end{bmatrix}$$

$$E = \begin{bmatrix} 1 & 0 \\ 0 & 1 \\ 0 & 0 \\ 0 & 0 \\ 0 & 0 \\ 0 & 0 \\ 0 & 0 \\ 0 & 0 \end{bmatrix}$$

Figure 6-1. System Dynamics Matrices, System A.

HOVER

$$A = \begin{bmatrix} -0.1 & 0 & 0 & 0 & 0 & 0 & 0 & 0 \\ 0 & -0.1 & 0 & 0 & 0 & 0 & 0 & 0 \\ 0 & 0 & 0 & 0 & 0 & 1 & 0 & 0 \\ 0 & 0 & 0 & 0 & 0 & 0 & 1 & 0 \\ 0 & 0 & 0 & 0 & 0 & 0 & 0 & 1 \\ 0.0014 & 0.0180 & 0 & 0 & -32.40 & -0.0182 & 0.0009 & 2.188 \\ 0.2650 & -0.0177 & 0 & 0 & -0.0126 & -0.0121 & -0.2653 & -0.0265 \\ -0.0020 & -0.0049 & 0 & 0 & -0.6352 & 0.0047 & -0.0007 & -2.506 \end{bmatrix}$$

$$B = \begin{bmatrix} 0 & 0 \\ 0 & 0 \\ 0 & 0 \\ 0 & 0 \\ 0 & 0 \\ 0.4834 & 0.0026 \\ 0.0881 & -8.424 \\ 1.351 & 0.0222 \end{bmatrix}$$

$$E = \begin{bmatrix} 1 & 0 \\ 0 & 1 \\ 0 & 0 \\ 0 & 0 \\ 0 & 0 \\ 0 & 0 \\ 0 & 0 \\ 0 & 0 \end{bmatrix}$$

APPROACH

$$A = \begin{bmatrix} -0.1 & 0 & 0 & 0 & 0 & 0 & 0 & 0 \\ 0 & -0.1 & 0 & 0 & 0 & 0 & 0 & 0 \\ 0 & 0 & 0 & 0 & 0 & 1 & 0 & 0 \\ 0 & 0 & 0 & 0 & 0 & 0 & 1 & 0 \\ 0 & 0 & 0 & 0 & 0 & 0 & 0 & 1 \\ -0.0076 & 0.0237 & 0 & 0 & -31.26 & -0.0226 & 0.0116 & 1.806 \\ 0.5200 & 0.0888 & 0 & 0 & -52.01 & -0.1203 & -0.5085 & -2.885 \\ -0.0204 & 0.0064 & 0 & 0 & -2.053 & -0.0036 & -0.0144 & -2.663 \end{bmatrix}$$

$$B = \begin{bmatrix} 0 & 0 \\ 0 & 0 \\ 0 & 0 \\ 0 & 0 \\ 0 & 0 \\ 0.3705 & -0.0732 \\ 1.345 & -8.946 \\ 0.9194 & 0.1868 \end{bmatrix}$$

$$E = \begin{bmatrix} 1 & 0 \\ 0 & 1 \\ 0 & 0 \\ 0 & 0 \\ 0 & 0 \\ 0 & 0 \\ 0 & 0 \\ 0 & 0 \end{bmatrix}$$

Figure 6-2. System Dynamics Matrices, System B.

HOVER

$$\begin{matrix}
 A = & \begin{bmatrix}
 -.1 & 0 & 0 & 0 & 0 & 0 & 0 & 0 \\
 0 & -.1 & 0 & 0 & 0 & 0 & 0 & 0 \\
 0 & 0 & 0 & 0 & 0 & 1 & 0 & 0 \\
 0 & 0 & 0 & 0 & 0 & 0 & 1 & 0 \\
 0 & 0 & 0 & 0 & 0 & 0 & 0 & 1 \\
 .0014 & .0180 & 0 & 0 & -32.88 & -.0185 & .0010 & 2.260 \\
 .2650 & -.0177 & 0 & 0 & -.0272 & -.0120 & -.2653 & -.0177 \\
 -.0020 & -.0049 & 0 & 0 & -1.985 & .0040 & -.0004 & -2.305
 \end{bmatrix} &
 B = & \begin{bmatrix}
 0 & 0 \\
 0 & 0 \\
 0 & 0 \\
 0 & 0 \\
 0 & 0 \\
 .7099 & .0026 \\
 .1293 & -8.424 \\
 1.985 & .0222
 \end{bmatrix} &
 E = & \begin{bmatrix}
 1 & 0 \\
 0 & 1 \\
 0 & 0 \\
 0 & 0 \\
 0 & 0 \\
 0 & 0 \\
 0 & 0 \\
 0 & 0
 \end{bmatrix}
 \end{matrix}$$

APPROACH

$$\begin{matrix}
 A = & \begin{bmatrix}
 -.1 & 0 & 0 & 0 & 0 & 0 & 0 & 0 \\
 0 & -.1 & 0 & 0 & 0 & 0 & 0 & 0 \\
 0 & 0 & 0 & 0 & 0 & 1 & 0 & 0 \\
 0 & 0 & 0 & 0 & 0 & 0 & 1 & 0 \\
 0 & 0 & 0 & 0 & 0 & 0 & 0 & 1 \\
 -.0076 & .0237 & 0 & 0 & -31.72 & -.0222 & .0134 & 1.942 \\
 .5200 & .0888 & 0 & 0 & -53.17 & -.1193 & -.5046 & -2.418 \\
 -.0204 & .0064 & 0 & 0 & -3.202 & -.0025 & -.0099 & -2.324
 \end{bmatrix} &
 B = & \begin{bmatrix}
 0 & 0 \\
 0 & 0 \\
 0 & 0 \\
 0 & 0 \\
 0 & 0 \\
 .4710 & -.0732 \\
 1.710 & -8.946 \\
 1.169 & .1868
 \end{bmatrix} &
 E = & \begin{bmatrix}
 1 & 0 \\
 0 & 1 \\
 0 & 0 \\
 0 & 0 \\
 0 & 0 \\
 0 & 0 \\
 0 & 0 \\
 0 & 0
 \end{bmatrix}
 \end{matrix}$$

Figure 6-3. System Dynamics Matrices, System C.

HOVER

$$A = \begin{bmatrix} -.1 & 0 & 0 & 0 & 0 & 0 & 0 & 0 \\ 0 & -.1 & 0 & 0 & 0 & 0 & 0 & 0 \\ 0 & 0 & 0 & 0 & 0 & 1 & 0 & 0 \\ 0 & 0 & 0 & 0 & 0 & 0 & 1 & 0 \\ 0 & 0 & 0 & 0 & 0 & 0 & 0 & 1 \\ .0014 & .0180 & 0 & 0 & -32.89 & -.0183 & -.0002 & 2.257 \\ .2650 & -.0177 & 0 & 0 & -.1742 & -.0067 & -.5255 & -.0636 \\ -.0020 & -.0049 & 0 & 0 & -2.007 & .0046 & -.0034 & -2.314 \end{bmatrix}$$

$$B = \begin{bmatrix} 0 & 0 \\ 0 & 0 \\ 0 & 0 \\ 0 & 0 \\ 0 & 0 \\ .7179 & -.0001 \\ .1308 & .2601 \\ 2.007 & -.0007 \end{bmatrix}$$

$$E = \begin{bmatrix} 1 & 0 \\ 0 & 1 \\ 0 & 0 \\ 0 & 0 \\ 0 & 0 \\ 0 & 0 \\ 0 & 0 \\ 0 & 0 \end{bmatrix}$$

APPROACH

$$A = \begin{bmatrix} -.1 & 0 & 0 & 0 & 0 & 0 & 0 & 0 \\ 0 & -.1 & 0 & 0 & 0 & 0 & 0 & 0 \\ 0 & 0 & 0 & 0 & 0 & 1 & 0 & 0 \\ 0 & 0 & 0 & 0 & 0 & 0 & 1 & 0 \\ 0 & 0 & 0 & 0 & 0 & 0 & 0 & 1 \\ -.0076 & .0237 & 0 & 0 & -32.77 & -.0150 & .0332 & 1.542 \\ .5200 & .0888 & 0 & 0 & -53.84 & -.0676 & -.5674 & -2.834 \\ -.0204 & .0064 & 0 & 0 & -5.957 & .0143 & .0449 & -3.359 \end{bmatrix}$$

$$B = \begin{bmatrix} 0 & 0 \\ 0 & 0 \\ 0 & 0 \\ 0 & 0 \\ 0 & 0 \\ 1.554 & .0012 \\ 5.642 & .1457 \\ 3.856 & -.0030 \end{bmatrix}$$

$$E = \begin{bmatrix} 1 & 0 \\ 0 & 1 \\ 0 & 0 \\ 0 & 0 \\ 0 & 0 \\ 0 & 0 \\ 0 & 0 \\ 0 & 0 \end{bmatrix}$$

Figure 6-4. System Dynamics Matrices, System D.

HOVER

$$A = \begin{bmatrix} -.1 & 0 & 0 & 0 & 0 & 0 & 0 & 0 \\ 0 & -.1 & 0 & 0 & 0 & 0 & 0 & 0 \\ 0 & 0 & 0 & 0 & 0 & 1 & 0 & 0 \\ 0 & 0 & 0 & 0 & 0 & 0 & 1 & 0 \\ 0 & 0 & 0 & 0 & 0 & 0 & 0 & 1 \\ .0014 & .0180 & 0 & -.0007 & -32.89 & -.0182 & -.0017 & 2.256 \\ .2650 & -.0177 & 0 & -.1132 & -.3640 & -.0017 & -.5440 & -.1356 \\ -.0020 & -.0049 & 0 & -.0018 & -2.015 & .0048 & -.0076 & -2.317 \end{bmatrix}$$

$$B = \begin{bmatrix} 0 & 0 \\ 0 & 0 \\ 0 & 0 \\ 0 & 0 \\ 0 & 0 \\ .7207 & 0 \\ .1313 & .1131 \\ 2.015 & -.0003 \end{bmatrix}$$

$$E = \begin{bmatrix} 1 & 0 \\ 0 & 1 \\ 0 & 0 \\ 0 & 0 \\ 0 & 0 \\ 0 & 0 \\ 0 & 0 \\ 0 & 0 \end{bmatrix}$$

APPROACH

$$A = \begin{bmatrix} -.1 & 0 & 0 & 0 & 0 & 0 & 0 & 0 \\ 0 & -.1 & 0 & 0 & 0 & 0 & 0 & 0 \\ 0 & 0 & 0 & 0 & 0 & 1 & 0 & 0 \\ 0 & 0 & 0 & 0 & 0 & 0 & 1 & 0 \\ 0 & 0 & 0 & 0 & 0 & 0 & 0 & 1 \\ -.0076 & .0237 & 0 & .0069 & -32.33 & -.0133 & .0248 & 1.704 \\ .5200 & .0888 & 0 & -.0493 & -54.25 & .0440 & -.5837 & -2.645 \\ -.0204 & .0064 & 0 & .0203 & -4.767 & .0140 & .0238 & -2.942 \end{bmatrix}$$

$$B = \begin{bmatrix} 0 & 0 \\ 0 & 0 \\ 0 & 0 \\ 0 & 0 \\ 0 & 0 \\ 1.092 & .0006 \\ 3.964 & .0766 \\ 2.710 & -.0016 \end{bmatrix}$$

$$E = \begin{bmatrix} 1 & 0 \\ 0 & 1 \\ 0 & 0 \\ 0 & 0 \\ 0 & 0 \\ 0 & 0 \\ 0 & 0 \\ 0 & 0 \end{bmatrix}$$

Figure 6-5. System Dynamics Matrices, System F.

HOVER

$$\begin{matrix}
 A = & \begin{bmatrix}
 -.1 & 0 & 0 & 0 & 0 & 0 & 0 & 0 \\
 0 & -.1 & 0 & 0 & 0 & 0 & 0 & 0 \\
 0 & 0 & 0 & 0 & 0 & 1 & 0 & 0 \\
 0 & 0 & 0 & 0 & 0 & 0 & 1 & 0 \\
 0 & 0 & 0 & 0 & 0 & 0 & 0 & 1 \\
 .0014 & .0180 & 0 & -.0006 & -32.92 & -.0095 & -.0007 & 2.252 \\
 .2650 & -.0177 & 0 & -.1133 & -.2191 & -.0058 & -.5447 & -.0852 \\
 -.0020 & -.0049 & 0 & -.0014 & -2.093 & .0290 & -.0047 & -2.327
 \end{bmatrix} &
 B = & \begin{bmatrix}
 0 & 0 \\
 0 & 0 \\
 0 & 0 \\
 0 & 0 \\
 0 & 0 \\
 -.0086 & -.0003 \\
 -.0016 & -.1132 \\
 -.0240 & -.0003
 \end{bmatrix} &
 E = & \begin{bmatrix}
 1 & 0 \\
 0 & 1 \\
 0 & 0 \\
 0 & 0 \\
 0 & 0 \\
 0 & 0 \\
 0 & 0 \\
 0 & 0
 \end{bmatrix}
 \end{matrix}$$

APPROACH

$$\begin{matrix}
 A = & \begin{bmatrix}
 -.1 & 0 & 0 & 0 & 0 & 0 & 0 & 0 \\
 0 & -.1 & 0 & 0 & 0 & 0 & 0 & 0 \\
 0 & 0 & 0 & 0 & 0 & 1 & 0 & 0 \\
 0 & 0 & 0 & 0 & 0 & 0 & 1 & 0 \\
 0 & 0 & 0 & 0 & 0 & 0 & 0 & 1 \\
 -.0076 & .0237 & 0 & .0060 & -32.21 & -.0074 & .0231 & 1.751 \\
 .5200 & .0888 & 0 & -.0582 & -54.12 & .0887 & -.6031 & -2.543 \\
 -.0204 & .0064 & 0 & .0182 & -4.458 & .0276 & .0200 & -2.821
 \end{bmatrix} &
 B = & \begin{bmatrix}
 0 & 0 \\
 0 & 0 \\
 0 & 0 \\
 0 & 0 \\
 0 & 0 \\
 -.0145 & .0007 \\
 -.0527 & .0823 \\
 -.0360 & -.0017
 \end{bmatrix} &
 E = & \begin{bmatrix}
 1 & 0 \\
 0 & 1 \\
 0 & 0 \\
 0 & 0 \\
 0 & 0 \\
 0 & 0 \\
 0 & 0 \\
 0 & 0
 \end{bmatrix}
 \end{matrix}$$

Figure 6-6. System Dynamics Matrices, System G.

HOVER

$$A = \begin{bmatrix}
 -.1 & 0 & 0 & 0 & 0 & 0 & 0 & 0 \\
 0 & -.1 & 0 & 0 & 0 & 0 & 0 & 0 \\
 0 & 0 & 0 & 0 & 0 & 1 & 0 & 0 \\
 0 & 0 & 0 & 0 & 0 & 0 & 1 & 0 \\
 0 & 0 & 0 & 0 & 0 & 0 & 0 & 1 \\
 .0014 & .0180 & .0035 & -.0005 & -32.97 & -.0069 & 0 & 2.236 \\
 .2650 & -.0177 & -.0013 & -.1134 & -.1306 & -.0084 & -.5450 & -.0538 \\
 -.0020 & -.0049 & .0099 & -.0011 & -2.217 & .0364 & -.0028 & -2.372
 \end{bmatrix}$$

$$B = \begin{bmatrix}
 0 & 0 \\
 0 & 0 \\
 0 & 0 \\
 0 & 0 \\
 0 & 0 \\
 -.0035 & 0 \\
 -.0006 & .1133 \\
 -.0099 & -.0003
 \end{bmatrix}$$

$$E = \begin{bmatrix}
 1 & 0 \\
 0 & 1 \\
 0 & 0 \\
 0 & 0 \\
 0 & 0 \\
 0 & 0 \\
 0 & 0 \\
 0 & 0
 \end{bmatrix}$$

APPROACH

$$A = \begin{bmatrix}
 -.1 & 0 & 0 & 0 & 0 & 0 & 0 & 0 \\
 0 & -.1 & 0 & 0 & 0 & 0 & 0 & 0 \\
 0 & 0 & 0 & 0 & 0 & 1 & 0 & 0 \\
 0 & 0 & 0 & 0 & 0 & 0 & 1 & 0 \\
 0 & 0 & 0 & 0 & 0 & 0 & 0 & 1 \\
 -.0076 & .0237 & .0041 & .0021 & -32.35 & .0091 & .0167 & 1.717 \\
 .5200 & .0888 & .0234 & -.0868 & -55.22 & .2092 & -.6503 & -2.812 \\
 -.0204 & .0064 & .0099 & .0091 & -4.793 & .0660 & .0051 & -2.900
 \end{bmatrix}$$

$$B = \begin{bmatrix}
 0 & 0 \\
 0 & 0 \\
 0 & 0 \\
 0 & 0 \\
 0 & 0 \\
 -.0040 & .0008 \\
 -.0147 & .0972 \\
 -.0101 & -.0020
 \end{bmatrix}$$

$$E = \begin{bmatrix}
 1 & 0 \\
 0 & 1 \\
 0 & 0 \\
 0 & 0 \\
 0 & 0 \\
 0 & 0 \\
 0 & 0 \\
 0 & 0
 \end{bmatrix}$$

Figure 6-7. System Dynamics Matrices, System H.

(excluding gust states) and the pilot control input rates, as discussed in Section 2.

Recall that the displayed information vector presented to the pilot is

$$y = Cx + Du \tag{6-3}$$

For the information level and the display element level without flight director, the matrices C and D are shown in Figure 6-8. Desirable maximum allowable values (2σ) are presented in Table 6-4 for each of the basic vehicle states and for the control rates. Table 6-4 also shows the indifference thresholds for each of the displayed states. As discussed previously, these are taken to be 1/4 of their respective maximum allowable values in the cost functional.

Flight director algorithms were obtained for each automation level/flight condition as described in Section 4. The flight director commands were simplified by neglecting cross coupling terms to give the following general forms:

$$FD_x = K_x x + K_\theta \theta + K_{V_x} V_x + K_q q \tag{6-4}$$

$$FD_z = K_z z + K_{V_z} V_z$$

Table 6-4. Control Cost Weighting Functions and Indifference Thresholds for CH-47.

Variable	Units	Maximum Values for Cost Function		Indifference Thresholds	
		Hover	60 kt Descent	Hover	60 kt Descent
x	ft	5.	25.	1.25	6.25
z	ft	5.	25.	1.25	6.25
θ	deg	1.	1.	.25	.25
V_x	ft/sec	1.	2.5	.25	.625
V_z	ft/sec	1.	2.5	.25	.625
q	deg/sec	0.5	0.5	.125	.125
δ_e	in/sec	2.	2.	-----	-----
δ_c	in/sec	2.	2.	-----	-----

$$C = \begin{bmatrix} 0 & 0 & 1 & 0 & 0 & 0 & 0 & 0 \\ 0 & 0 & 0 & 0 & 0 & 1 & 0 & 0 \\ 0 & 0 & 0 & 1 & 0 & 0 & 0 & 0 \\ 0 & 0 & 0 & 0 & 0 & 0 & 1 & 0 \\ 0 & 0 & 0 & 0 & 57.3 & 0 & 0 & 0 \\ 0 & 0 & 0 & 0 & 0 & 0 & 0 & 57.3 \end{bmatrix}$$

$$D = \begin{bmatrix} 0 & 0 \\ 0 & 0 \\ 0 & 0 \\ 0 & 0 \\ 0 & 0 \\ 0 & 0 \end{bmatrix}$$

$$y = [x, V_x, z, V_z, \theta, q]^T$$

Figure 6-8. Display Vector for Basic Information.

The flight director signal rates were obtained by simply differentiating Equation (6-4) and substituting from Equation (6-1). The effect of the flight director signal presence on the pilot strategy is taken into account by including the flight director signals in the control cost functional. The maximum allowable values used to weight these signals in the cost functional are obtained from the maximum allowable excursions of the position states, e.g.,

$$\begin{aligned} (FD_x)_{\max} &= |K_x(x)_{\max}| + |K_\theta(\theta)_{\max}| \\ (FD_z)_{\max} &= |K_z(z)_{\max}| \end{aligned} \tag{6-5}$$

Finally, the indifference thresholds for the flight director signals are obtained in the standard 1/4 of the associated maximum value, i.e.

$$\begin{aligned} (FD_x)_{\min} &= (FD_x)_{\max}/4 \\ (FD_z)_{\min} &= (FD_z)_{\max}/4 \end{aligned} \tag{6-6}$$

The resulting flight director algorithms, indifference thresholds, and control cost weightings are shown in Figures 6-9 through 6-15 for the seven automation levels.

6.3 PROGRAM PIREP

Program PIREP is an interactive program that predicts human operator performance and response characteristics in complex control tasks involving varying levels of control automation and pilot monitoring. The human operator model is based on optimal control and estimation theory coupled with a mathematical description of the human's limitations. The basic underlying assumption is that the well-motivated, well-trained human operator behaves in a near optimal manner, subject to his inherent limitations and constraints and his control task. The program subroutines are written in Fortran IV and have been operated on PDP-10, IBM 360-65 and CDC 6600 computers.

FLIGHT DIRECTOR SIGNALS	(FD) _{max}	Indif. Threshold
<u>HOVER</u>		
$FD_x = .0321 x - 21.35 \theta + .2355 V_x - 18.33 q$	0.60	0.15
$\dot{FD}_x = -7.577 \theta - .0653 V_x + .4391 q - 6.207 \delta_e$		0.075
$FD_z = .0696 z + .3406 V_z$	0.40	0.10
$\dot{FD}_z = -.0208 V_z - 2.869 \delta_c$		0.05
<u>APPROACH</u>		
$FD_x = .0046 x - 5.617 \theta + .0892 V_x - 14.29 q$	0.21	0.055
$\dot{FD}_x = 26.02 \theta + .0753 V_x + 19.40 q - 5.663 \delta_e$		0.028
$FD_z = .0223 z + .1866 V_z$	0.56	0.14
$\dot{FD}_z = -.0735 V_z - 1.669 \delta_c$		0.07

Figure 6-9. Flight Director Algorithms, System A.

FLIGHT DIRECTOR SIGNALS	(FD) _{max}	Indif. Threshold
<u>HOVER</u>		
$FD_x = .0090 x - 5.487 \theta + .0663 V_x - 4.168 q$	0.16	0.04
$\dot{FD}_x = .4990 \theta - .0120 V_x + 5.103 q - 5.599 q_c$		0.02
$FD_z = .0696 z + .3406 V_z$	0.40	0.10
$\dot{FD}_z = -.0208 V_z - 2.869 \delta_c$		0.05
<u>APPROACH</u>		
$FD_x = .0022 x - 2.790 \theta + .0397 V_x - 5.762 q$	0.10	0.025
$\dot{FD}_x = 10.59 \theta + .0221 V_x + 12.63 q - 5.283 q_c$		0.013
$FD_z = .0221 z + .1842 V_z$	0.55	0.14
$\dot{FD}_z = -.0715 V_z - 1.648 \delta_c$		0.07

Figure 6-10. Flight Director Algorithms, System B.

FLIGHT DIRECTOR SIGNALS		(FD) _{max}	Indif. Threshold
<u>HOVER</u>			
$FD_x = .0061 x - 3.036 \theta + .0453 V_x - 2.854 q$		0.10	0.025
$\dot{FD}_x = 4.178 \theta - .0063 V_x + 3.644 q - 5.633 \theta_c$			0.013
$FD_z = .0696 z + .3406 V_z$		0.40	0.10
$\dot{FD}_z = -.0208 V_z - 2.869 \delta_c$			0.05
<u>APPROACH</u>			
$FD_x = .0017 x - 1.137 \theta + .0299 V_x - 4.579 q$		0.062	0.016
$\dot{FD}_x = 13.71 \theta + .0124 V_x + 9.563 q - 5.339 \theta_c$			0.008
$FD_z = .0220 z + .1825 V_z$		0.55	0.14
$\dot{FD}_z = -.0701 V_z - 1.633 \delta_c$			0.07

Figure 6-11. Flight Director Algorithms, System C.

FLIGHT DIRECTOR SIGNALS	(FD) _{max}	Indif. Threshold
<u>HOVER</u>		
$FD_x = .0060 x - 2.972 \theta + .0443 V_x - 2.978 q$	0.10	0.025
$\dot{FD}_x = 4.521 \dot{\theta} - .0085 \dot{V}_x + 4.019 \dot{q} - 5.945 \dot{\theta}_c$		0.013
$FD_z = -1.962 z - 12.51 V_z$	0.60	0.15
$\dot{FD}_z = -1.920 \dot{V}_z - .0244 \dot{V}_{z_c}$		0.075
<u>APPROACH</u>		
$FD_x = .0006 x + .2490 \theta + .0057 V_x - 1.220 q$	0.020	0.005
$\dot{FD}_x = 7.080 \dot{\theta} - .0169 \dot{V}_x + 4.356 \dot{q} - 4.695 \dot{\theta}_c$		0.0025
$FD_z = -1.261 z - 9.363 V_z$	32.	8.0
$\dot{FD}_z = 4.052 \dot{V}_z - 1.364 \dot{V}_{z_c}$		4.0

Figure 6-12. Flight Director Algorithms, System D.

FLIGHT DIRECTOR SIGNALS	(FD) _{max}	Indif. Threshold
<u>HOVER</u>		
$FD_x = .0058 x - 2.852 \theta + .0428 V_x - 2.684 q$	0.10	0.025
$FD_x = 4.002 \theta - .0078 V_x + 3.463 q - 5.378 \theta_c$		0.013
$FD_z = -4.280 z - 23.29 V_z$	22.	5.5
$FD_z = 2.636 z + 8.390 V_z - 2.634 z_c$		2.8
<u>APPROACH</u>		
$FD_x = .0008 x + .0193 \theta + .0067 V_x - 1.811 q$	0.020	0.0050
$FD_x = 8.415 \theta - .0246 V_x + 5.359 q - 4.900 \theta_c$		0.0025
$FD_z = -1.478 z - 18.96 V_z$	37.	9.5
$FD_z = .9349 z + 9.657 V_z - 1.453 z_c$		4.8

Figure 6-13. Flight Director Algorithms, System F.

FLIGHT DIRECTOR SIGNALS		(FD) _{max}	Indif. Threshold
<u>HOVER</u>			
$FD_x = -.5956 x + 238.0 \theta - 2.637 V_x + 229.6 q$		5.2	1.3
$FD_x = -393.8 \theta + 6.196 V_x - 302.2 q - 5.474 V_{x_c}$			0.65
$FD_z = -4.348 z - 23.62 V_z$		22.	5.5
$FD_z = 2.676 z + 8.518 V_z - 2.676 z_c$			2.8
<u>APPROACH</u>			
$FD_x = -.0588 x + 3.334 \theta - .0970 V_x + 137.8 q$		1.6	0.40
$FD_x = -611.2 \theta + 3.747 V_x - 385.6 q - 4.958 V_{x_c}$			0.20
$FD_z = -1.331 z - 17.73 V_z$		33.	8.5
$FD_z = 1.031 z + 9.362 V_z - 1.460 z_c$			4.3

Figure 6-14. Flight Director Algorithms, System G.

FLIGHT DIRECTOR SIGNALS	(FD) _{max}	Indif. Threshold
<u>HOVER</u>		
$FD_x = -.2078 x + 569.8 \theta - 5.652 V_x + 558.3 q$	11.2	2.8
$\dot{FD}_x = 5.517 x - 1052 \theta + 20.16 V_x - 767.1 q - 5.517 x_c$		1.4
$FD_z = -4.380 z - 23.78 V_z$	22.	5.5
$\dot{FD}_z = 2.697 z + 8.580 V_z - 2.697 z_c$		2.8
<u>APPROACH</u>		
$FD_x = .7899 x - 30.10 \theta + 3.719 V_x + 494.4 q$	21.	5.5
$\dot{FD}_x = 4.894 x - 2490 \theta + 33.46 V_x - 1458 q - 4.984 x_c$		2.8
$FD_z = -1.058 z - 15.42 V_z$	28.	7.0
$\dot{FD}_z = 1.338 z + 8.970 V_z - 1.498 z_c$		3.5

Figure 6-15. Flight Director Algorithms, System H.

The inputs to the program include the vehicle description (system dynamics, input disturbances and displayed variables), task description (cost functional weightings), human description (subjective weightings, neuromotor time constants, time delay, motor noise and observation noise), and the available capacity for control and/or monitoring tasks. The outputs include the state, output and control variances; the optimal allocation of pilot attention to the prescribed displays; control and monitoring performance metrics; pilot describing function and remnant spectra; and the state, output and control power spectra.

Figure 6-16 summarizes the important parameters of program PIREP for this analysis. The seven control systems, four displays, two flight conditions and varying control attention levels required over 200 runs of program PIREP. The following two subsections present selected results obtained with program PIREP for the control and monitoring models.

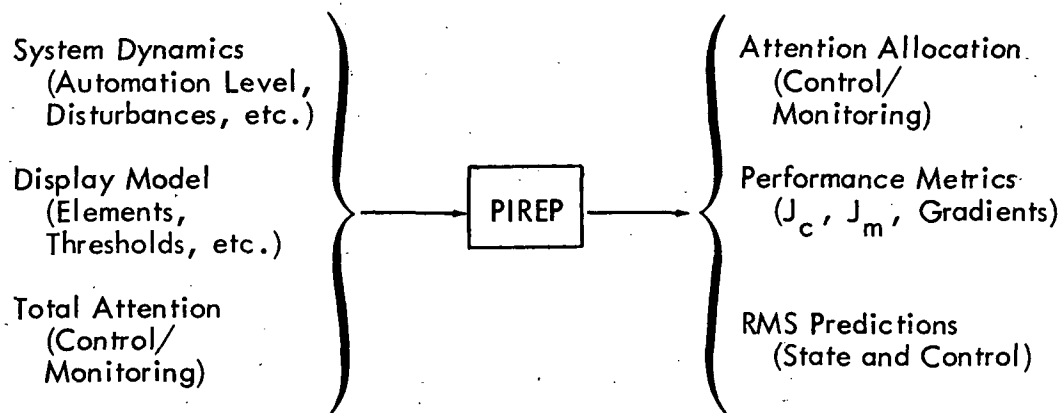


Figure 6-16. Principal Inputs and Outputs of Program PIREP.

6.4 CONTROL MODEL RESULTS

This subsection contains comprehensive results obtained using program PIREP to analyze the control performance of the aforementioned control/display configurations selected for the CH-47. For the reader's convenience, it is suggested that Table 6-2 on page 6-2 be marked for convenient reference during the ensuing

discussion. The pilot's total allowable attention to the longitudinal task was assumed to be 0.6, leaving at least 40 percent of his time for control/monitoring of the lateral axes and for miscellaneous duties (communications, etc.).

6.4.1 ATTENTION ALLOCATION VS WORKLOAD

Figure 6-17 depicts the relative attention (in percent of total control attention f_c) paid by the pilot to the display elements for the unaugmented helicopter (System A) with only situation information. At both flight conditions, most of his attention is on the pitch attitude indicator. From hover to approach, some of his attention is shifted from attitude to the position displays. For this simple control/display configuration, his relative allocation of attention remains essentially constant. For comparison, Figure 6-18 shows the relative attention allocation for System A with a full flight director. Now the forward flight director is the most important instrument, followed by the pitch indicator; the vertical flight director is significant only during hover. For this configuration, the pilot spends a lower percentage of his time on the x flight director, and more on the attitude indicator, as his total available control increases. Figure 6-19 shows the predicted rms system performance for the unaugmented system without a flight director. In general, the performance improves as the pilot spends more time on the longitudinal control task. The hover errors are consistently lower than those during approach, reflecting the cost weightings of Table 6-4.

Figures 6-20 through 6-31 compare the fractional control attention allocations for the other six automation levels with no flight director and with full flight director. In general, as the control system automation increases, the pilot is able to direct more attention to the vertical information and thereby improve the total performance cost (e.g. Figures 6-28 through 6-31). Also, as his total control attention increases, he tends to spend slightly less time on the flight director signals and more on the raw data.

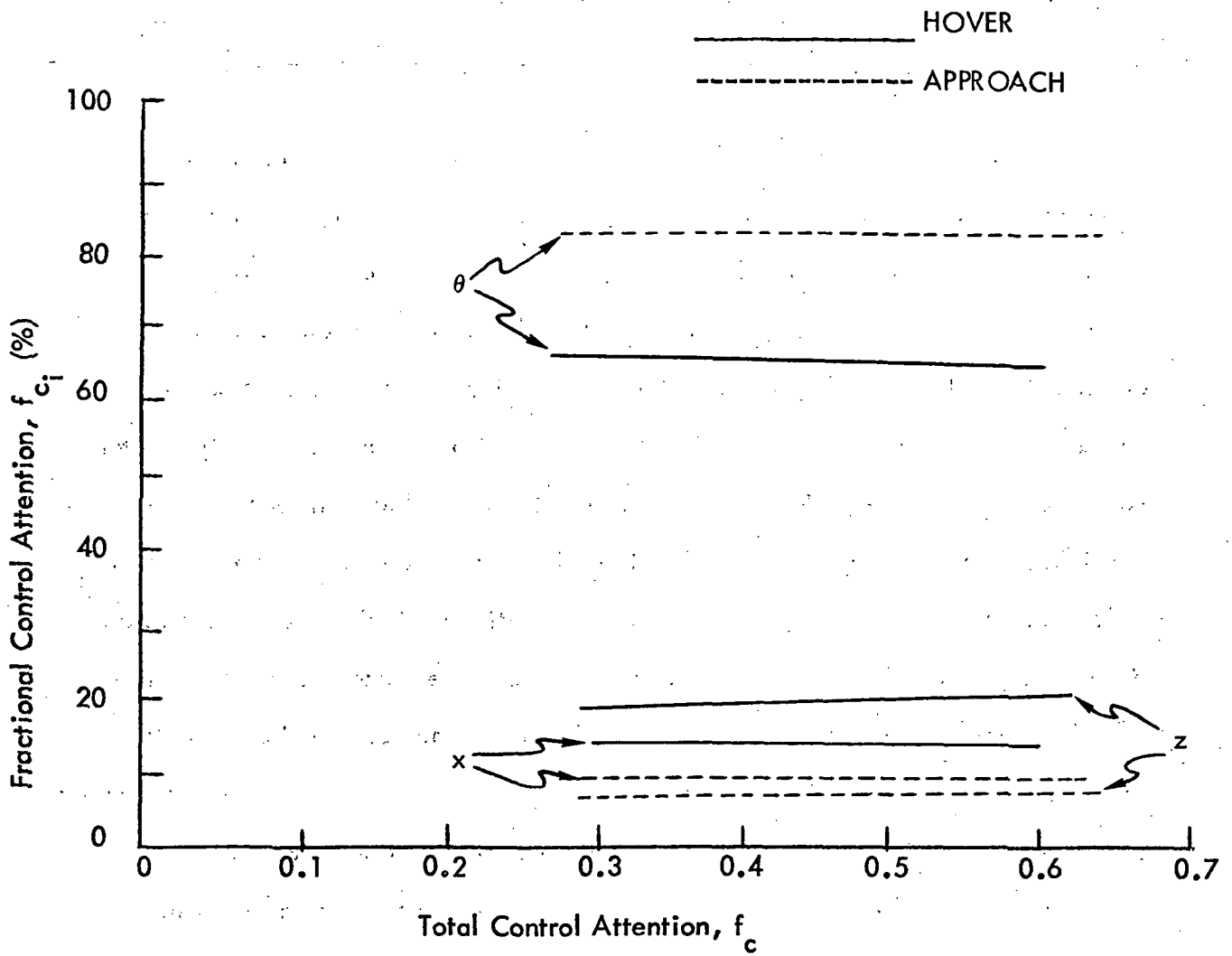


Figure 6-17. Attention Allocation vs Total Control Attention (System A - No Flight Director).

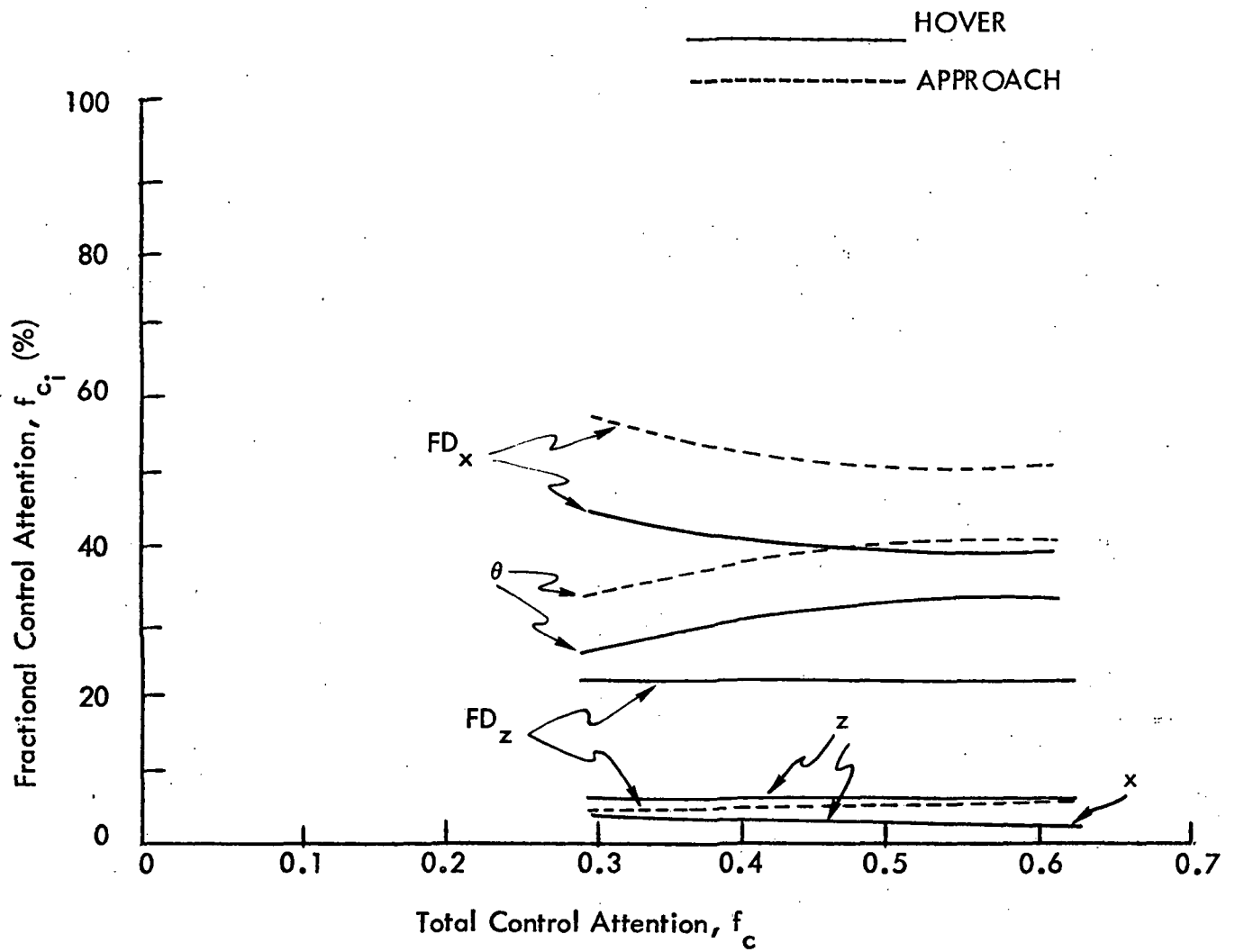


Figure 6-18. Attention Allocation vs Total Control Attention (System A - Full Flight Director).

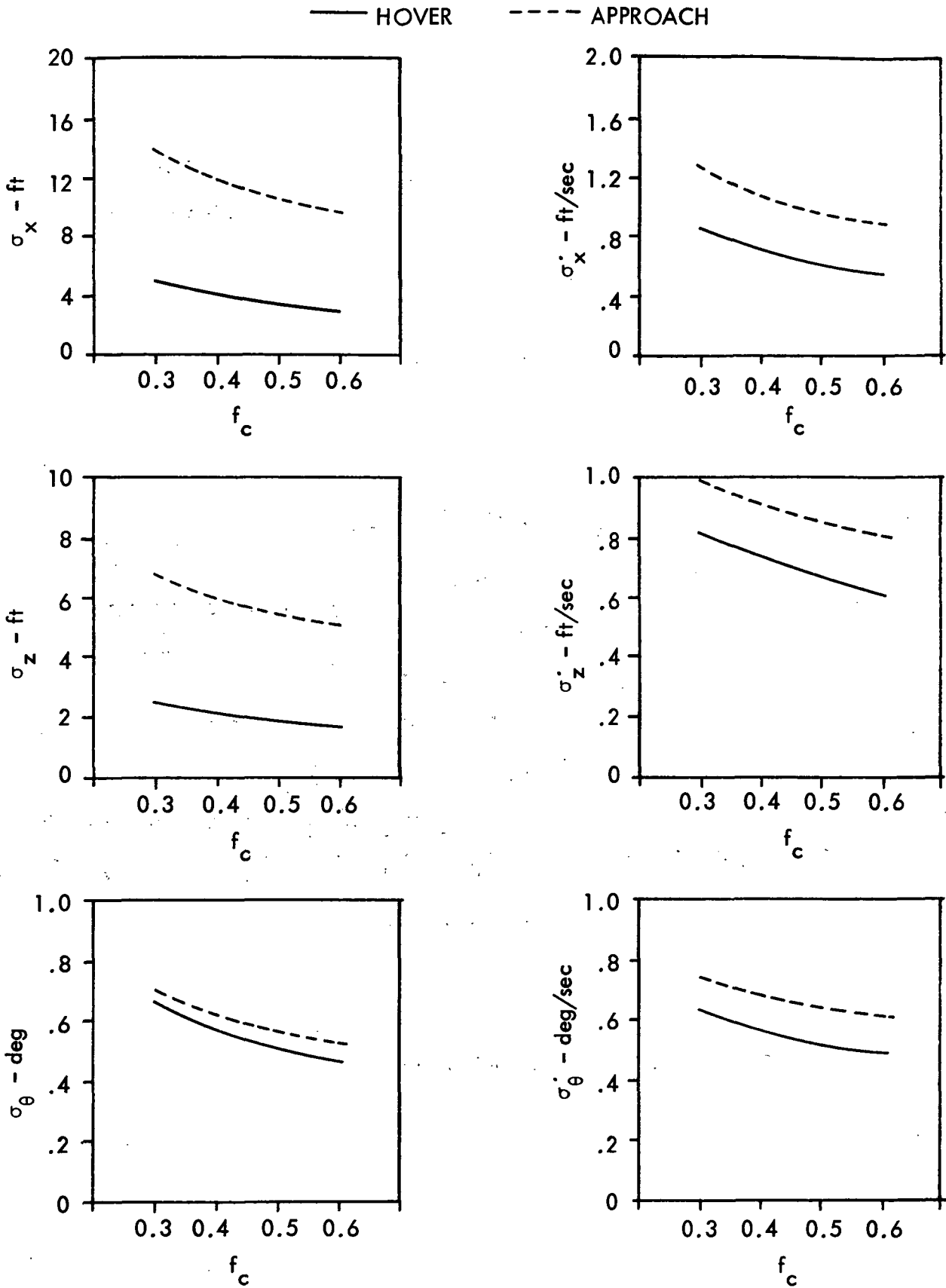


Figure 6-19. RMS Performance vs Total Control Attention (System A - No Flight Director).

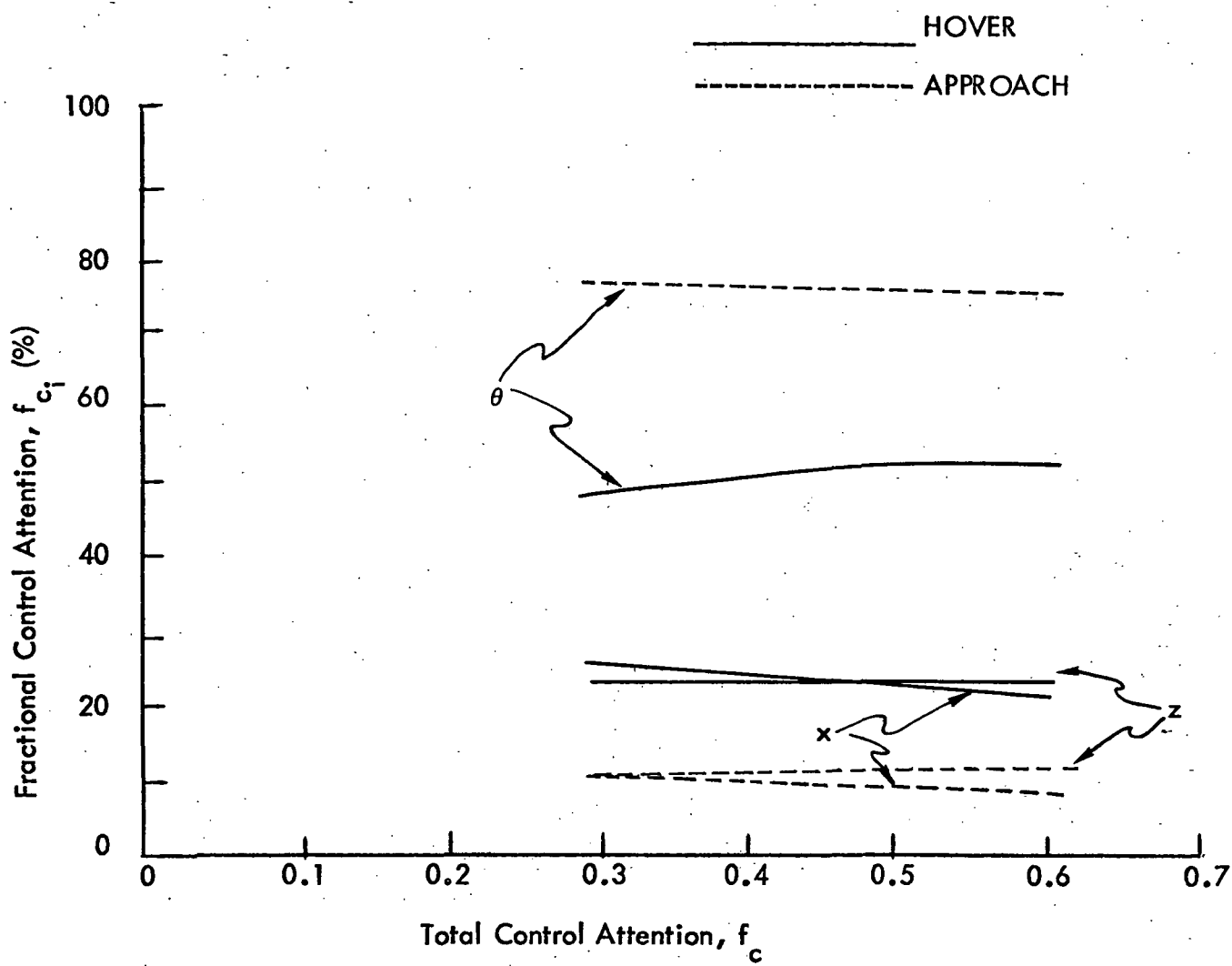


Figure 6-20. Attention Allocation vs Total Control Attention (System B - No Flight Director).

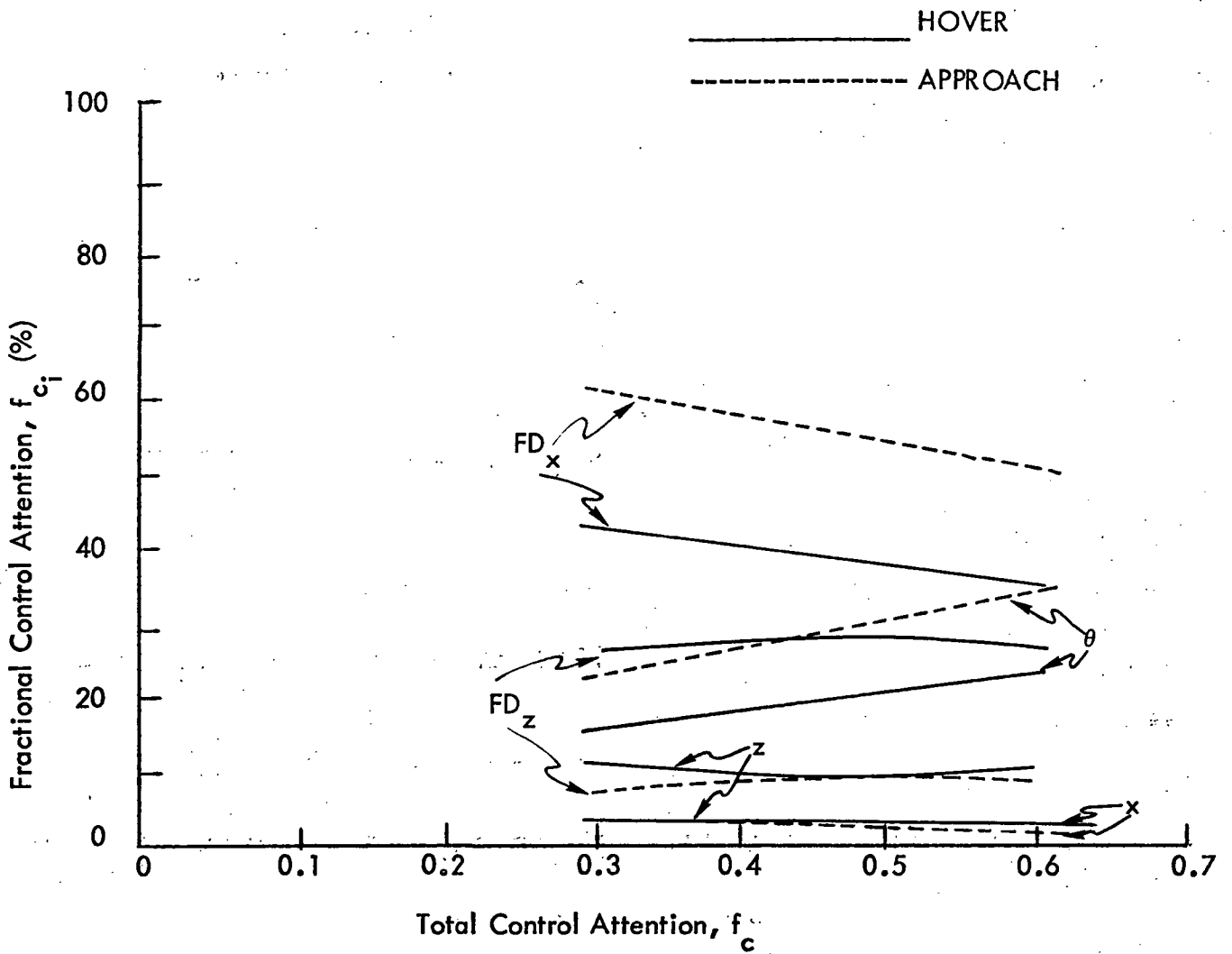


Figure 6-21. Attention Allocation vs Total Control Attention (System B - Full Flight Director).

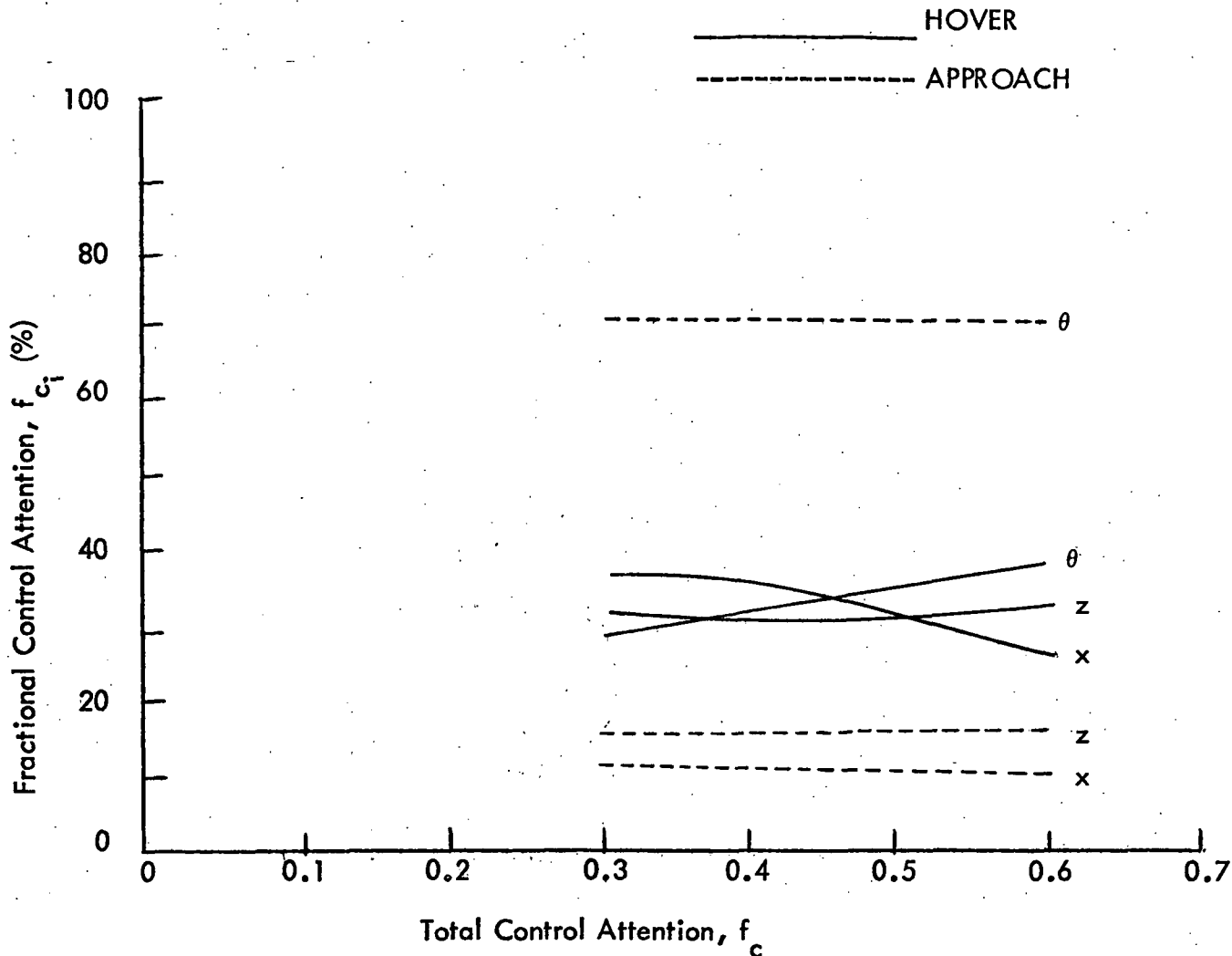


Figure 6-22. Attention Allocation vs Total Control Attention (System C - No Flight Director).

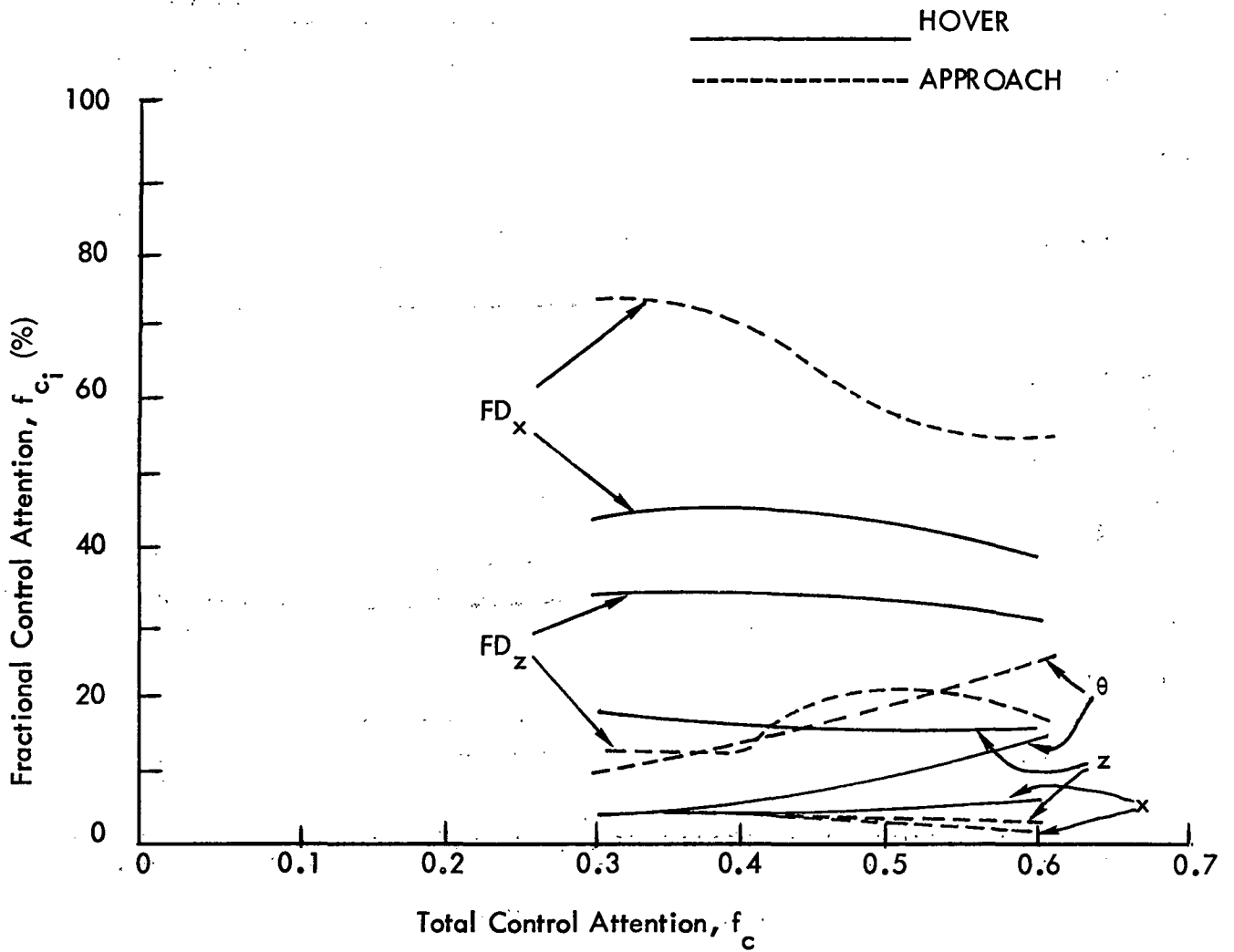


Figure 6-23. Attention Allocation vs Total Control Attention (System C - Full Flight Director).

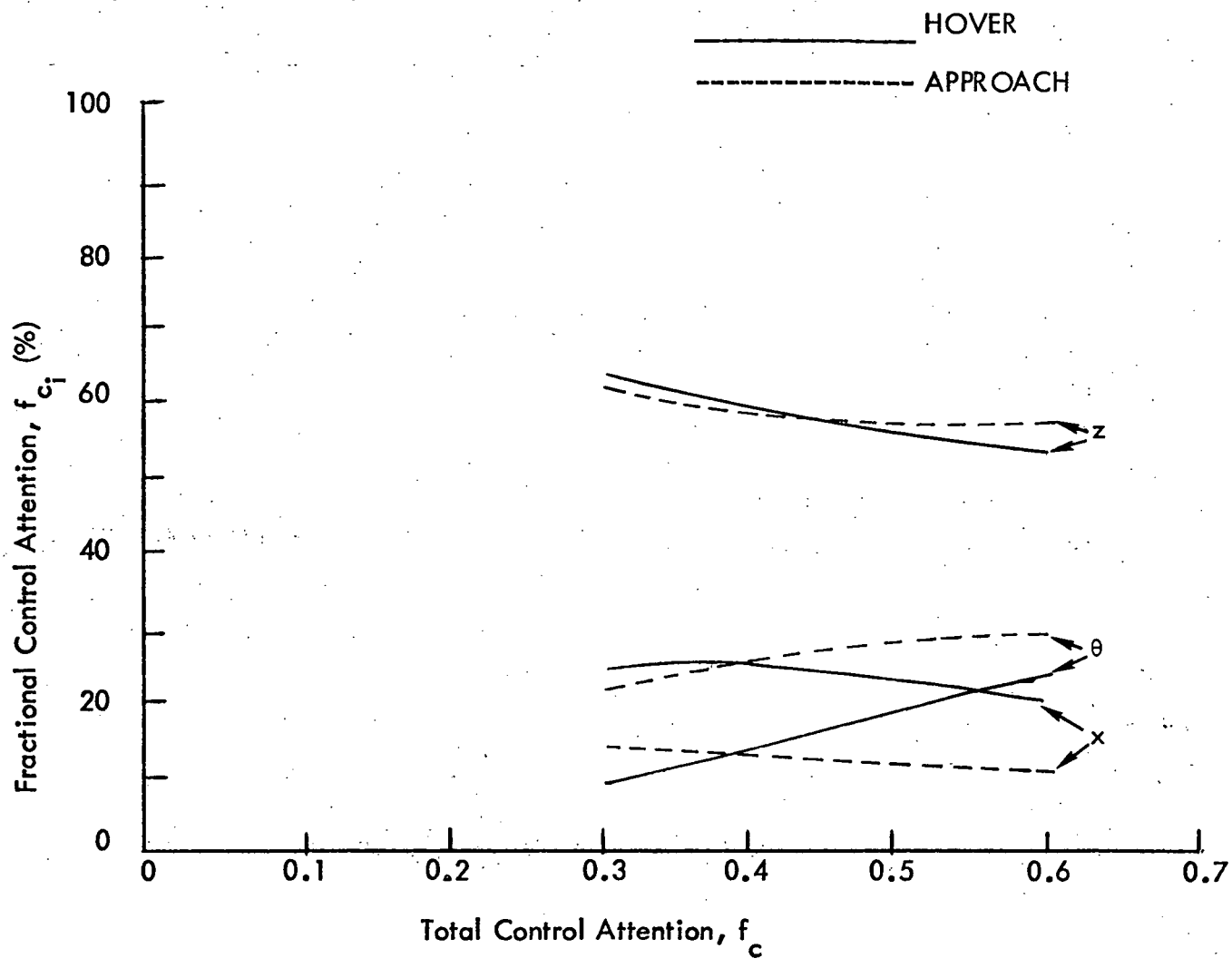


Figure 6-24. Attention Allocation vs Total Control Attention (Systems D, E - No Flight Director).

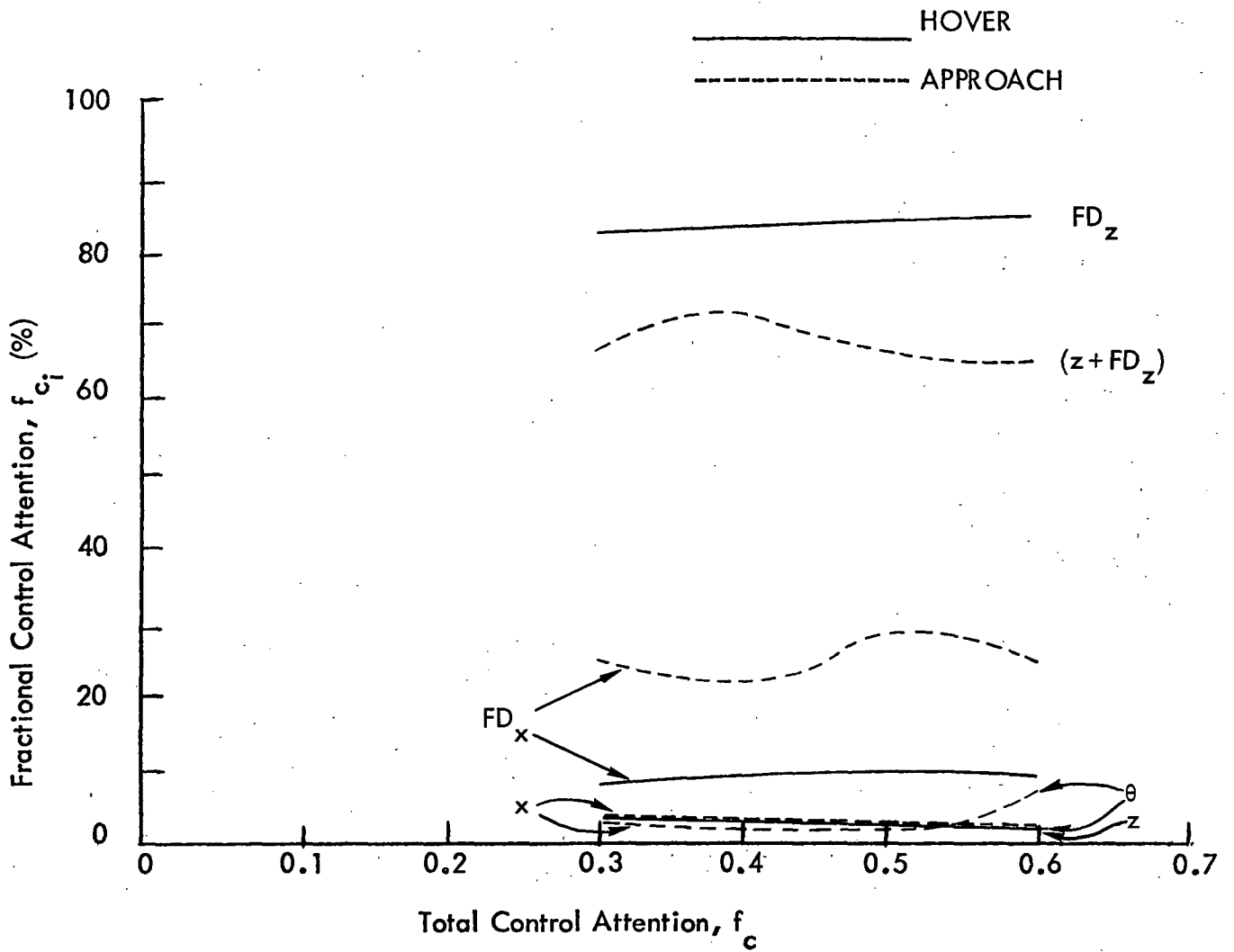


Figure 6-25. Attention Allocation vs Total Control Attention (Systems D, E - Full Flight Director).

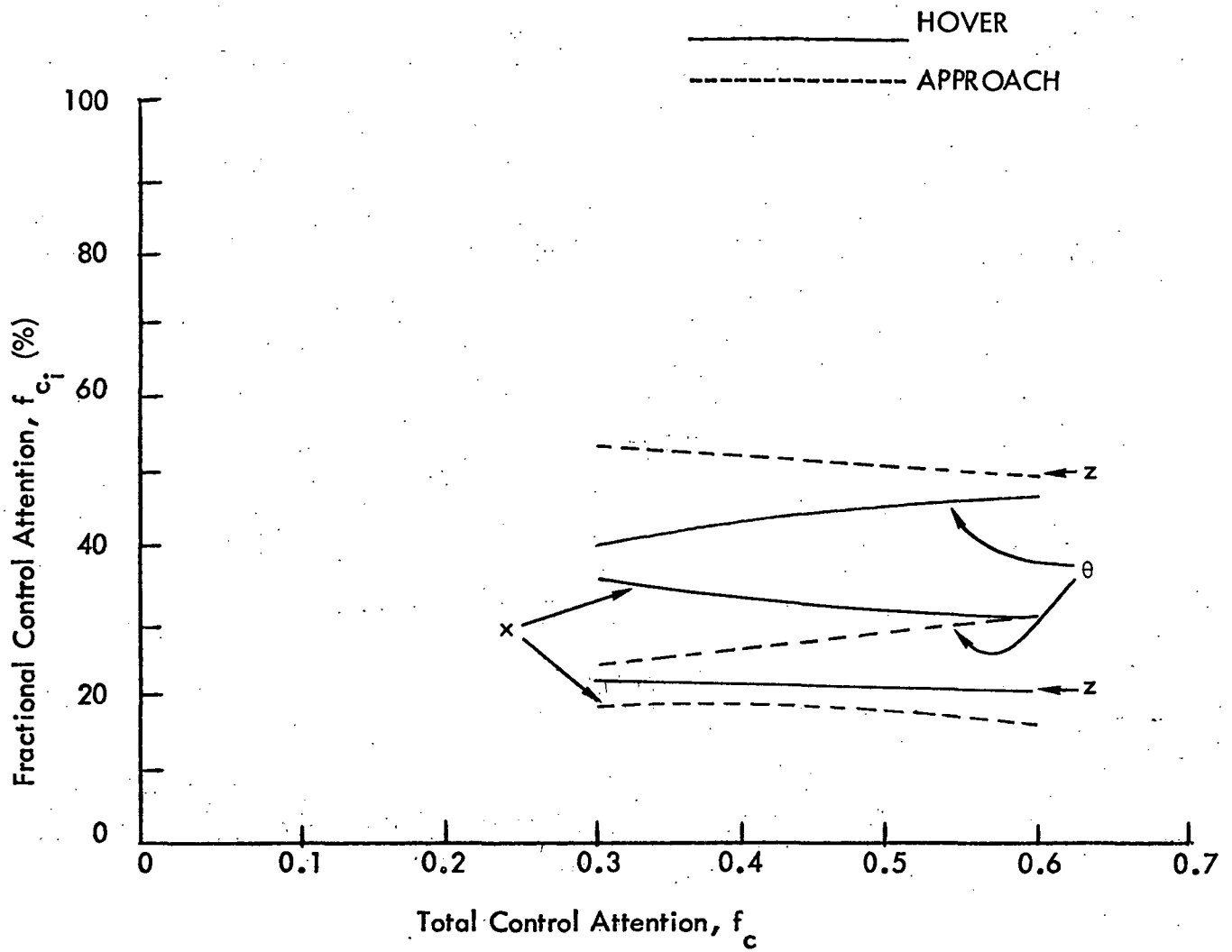


Figure 6-26. Attention Allocation vs Total Control Attention (System F - No Flight Director).

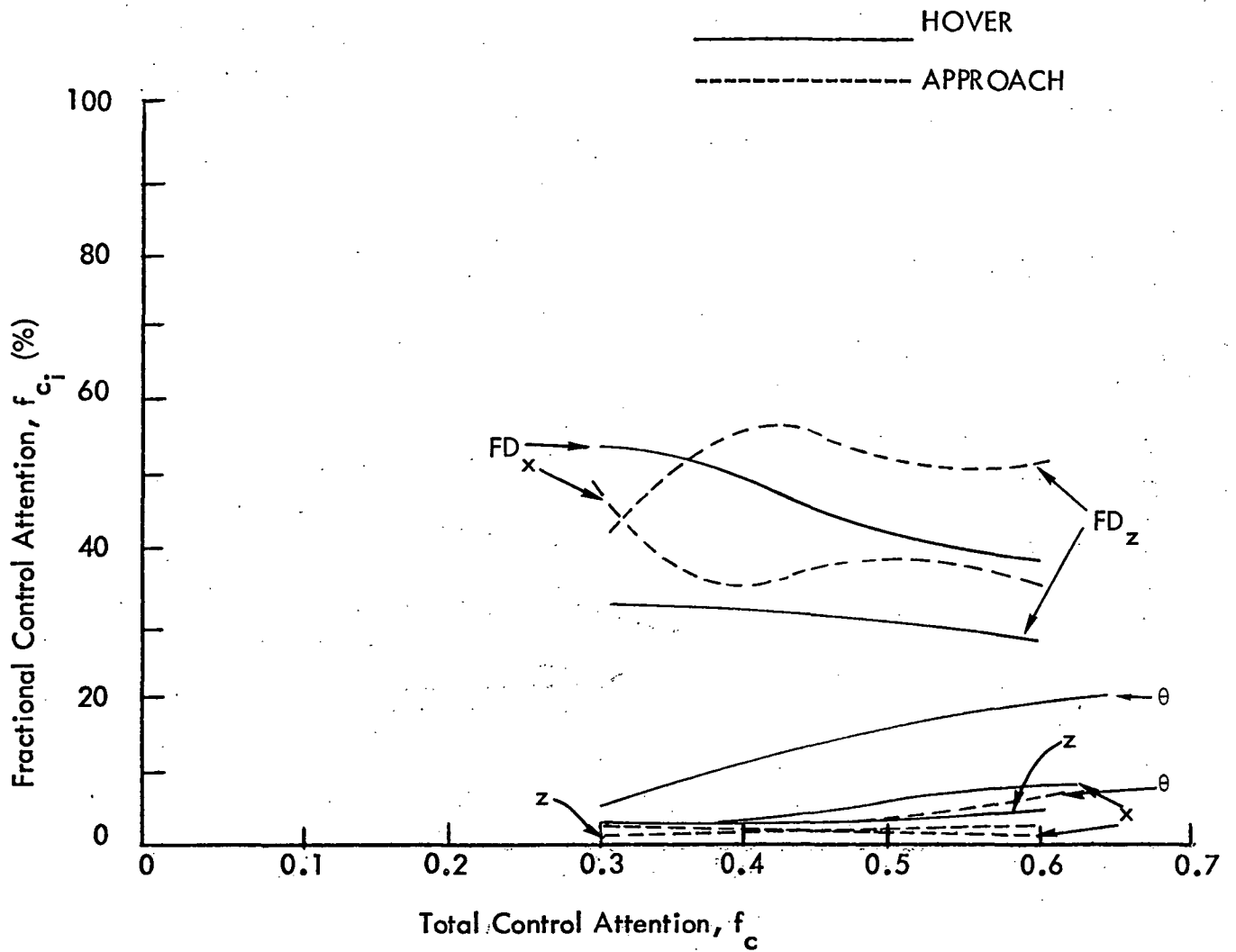


Figure 6-27. Attention Allocation vs. Total Control Attention (System F - Full Flight Director).

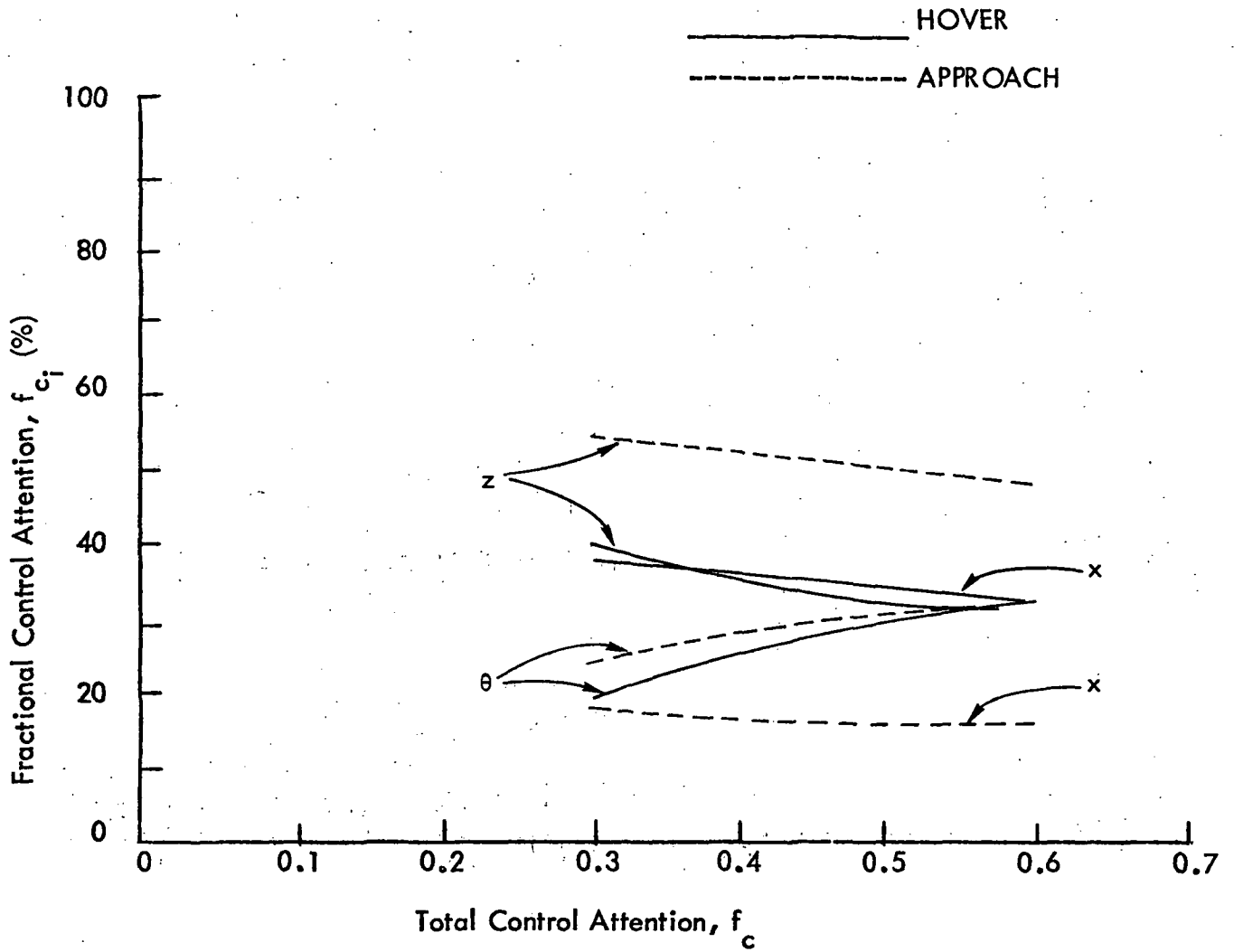


Figure 6-28. Attention Allocation vs Total Control Attention (System G - No Flight Director).

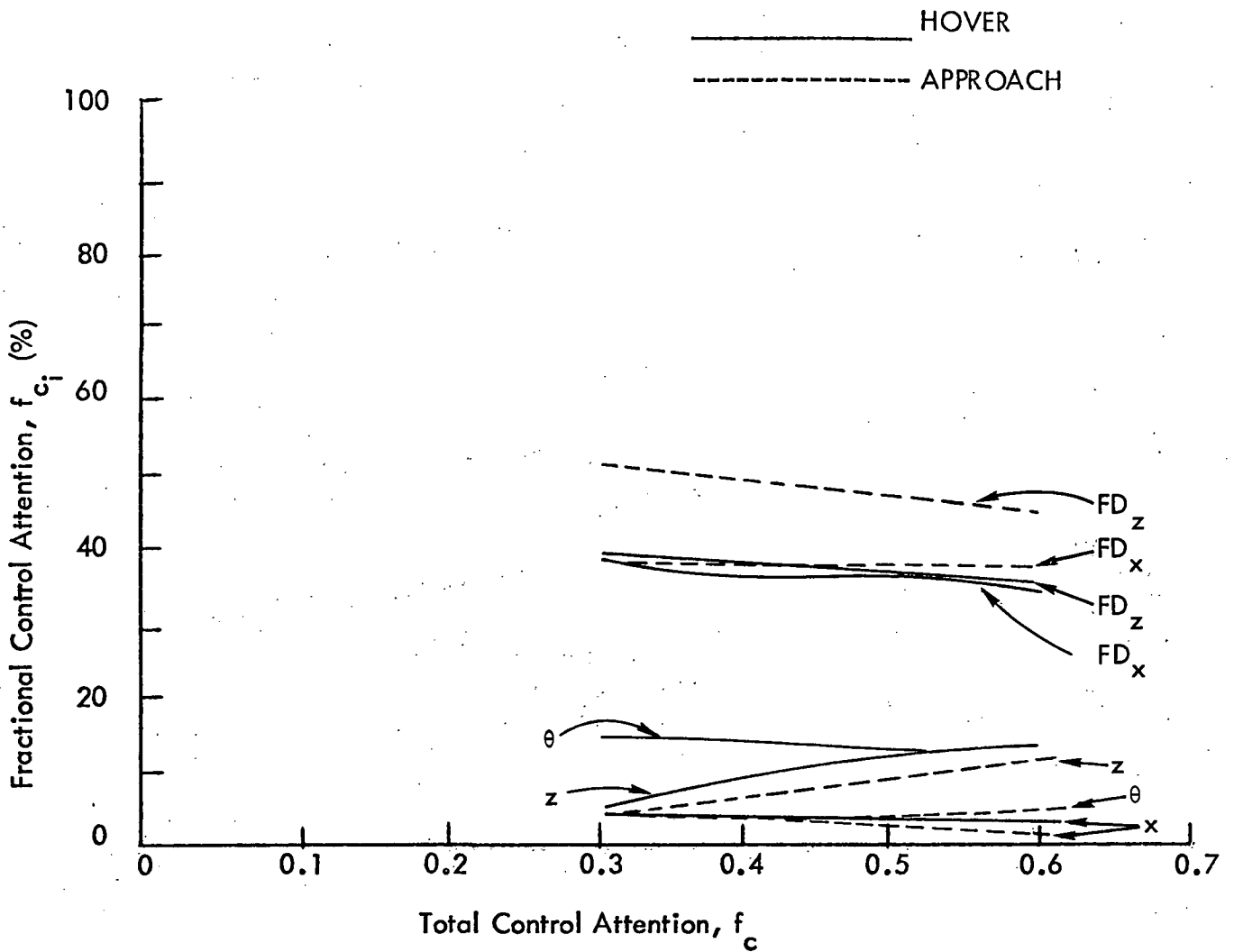


Figure 6-29. Attention Allocation vs Total Control Attention (System G - Full Flight Director).

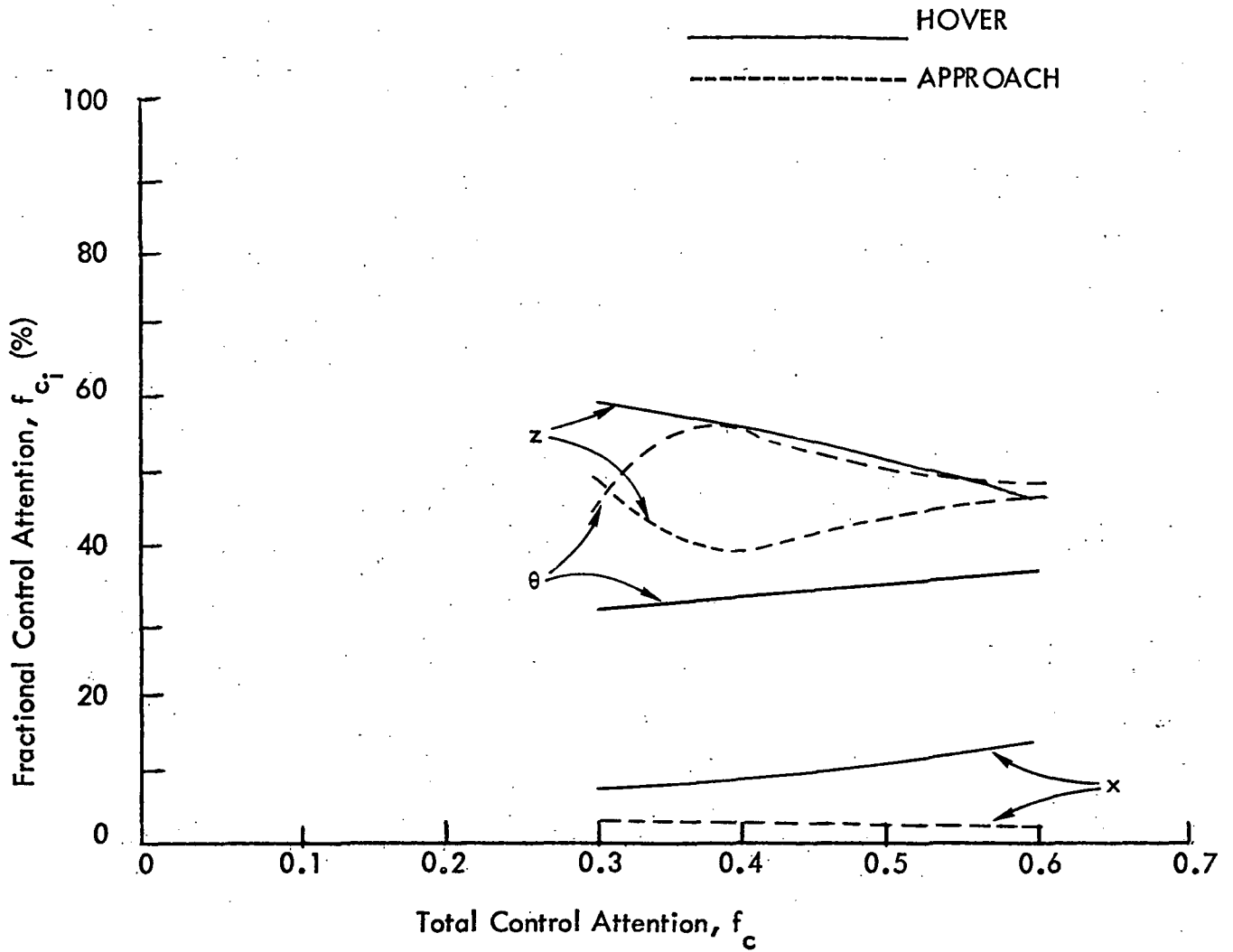


Figure 6-30. Attention Allocation vs Total Control Attention (System H - No Flight Director).

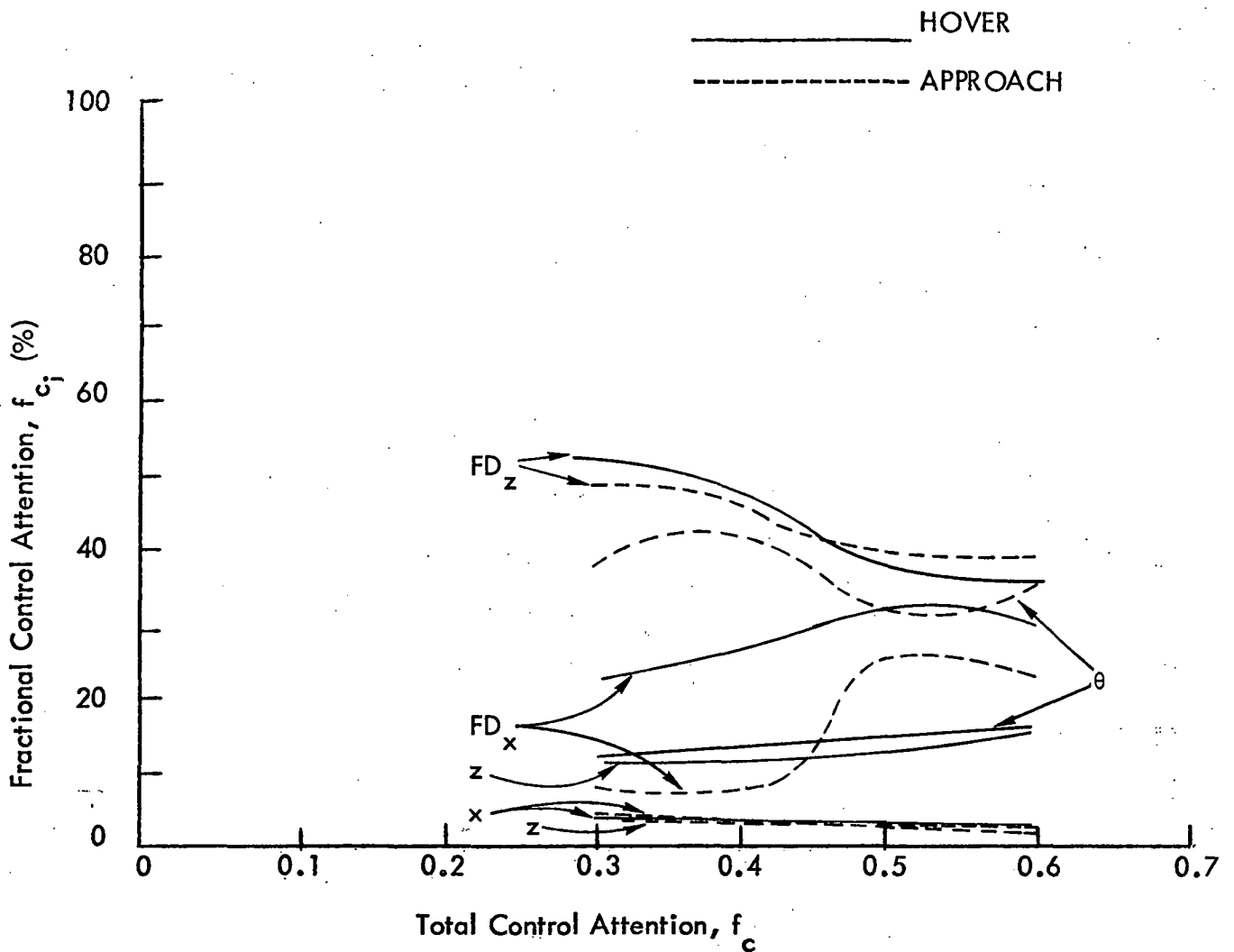


Figure 6-31. Attention Allocation vs Total Control Attention (System H - Full Flight Director).

6.4.2 SYSTEM PERFORMANCE VS WORKLOAD

Figures 6-32 through 6-35 present the overall performance cost variation with workload (e.g. control attention) at hover for each control/display configuration. Increased automation improves performance for a given workload, regardless of the display provided. Comparison of these figures shows that the vertical flight director alone helps only system G's performance, while the forward flight director improves all systems' performance. However, the full flight director gives only a marginal improvement over the x flight director by itself.

Similar results are obtained during the approach, as shown in Figures 6-36 through 6-39. In nearly all configurations the overall performance is better during the approach than at hover. However, the performance of System H (full position feedback) is approximately the same for both flight conditions. Moreover System H shows very little sensitivity either to the flight director level or to the total control attention at both flight conditions. This result is as expected, since System H is essentially a pure automatic system. In general, the more automated systems become considerably less sensitive to workload variations.†

6.4.3 PREDICTED RMS PERFORMANCE

Figures 6-40 and 6-41 show the rms position and attitude error contributions to the overall system performance, at a "comfortable" workload of 0.4. The position errors are considerably lower at hover than during approach, while the attitude errors are nearly the same; this reflects the higher penalties on x, z in the performance metric at hover (Table 6-2). In general (except System D), the errors tend to decrease with system automation and the flight director also reduces the errors.

† An exception of these generalizations is System D, whose predicted performance is extremely good during approach and very poor at hover. The erratic results are not yet fully understood, but it appears that numerical difficulties with this system are producing two local minima in the optimization algorithm.

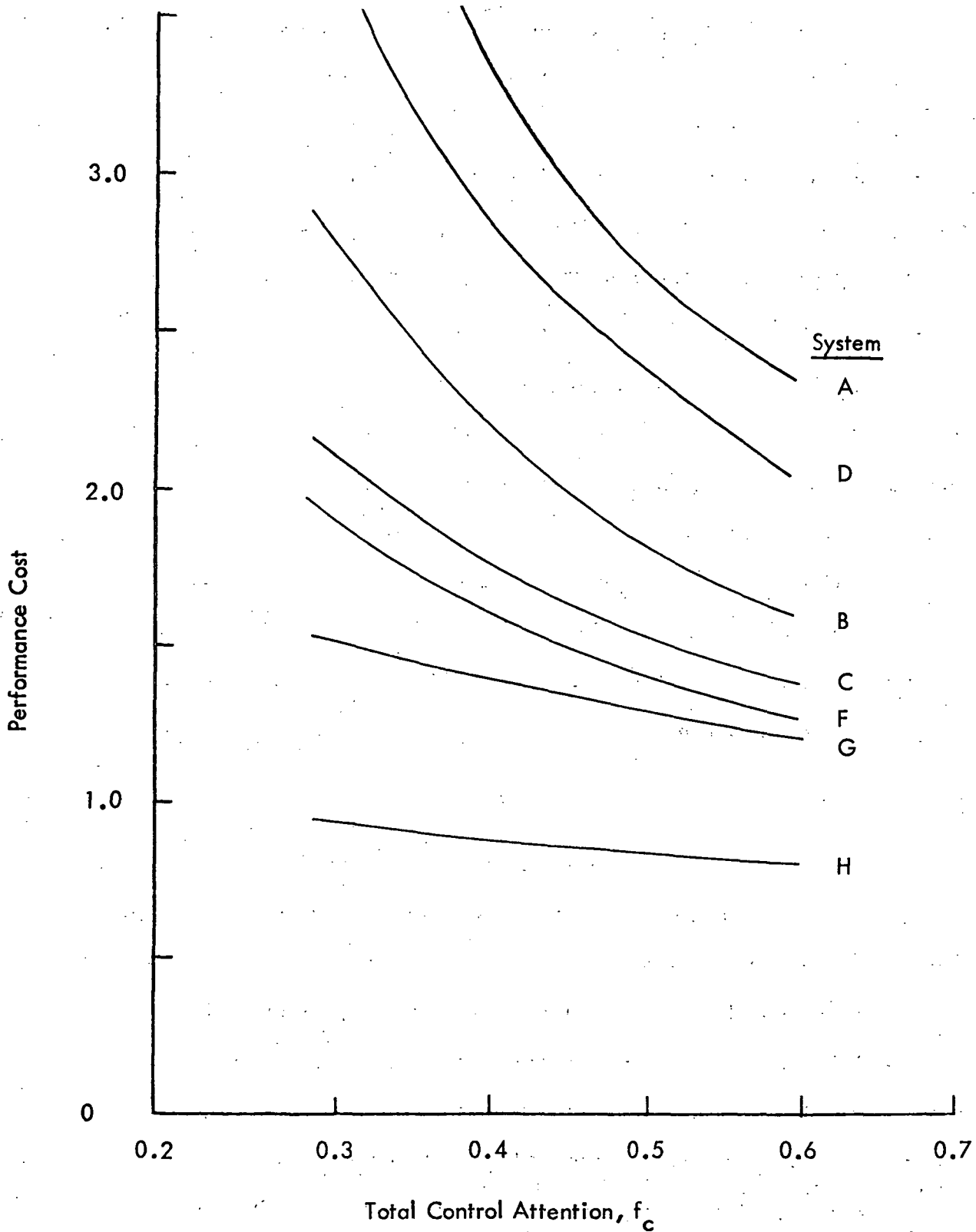


Figure 6-32. Control Performance Cost vs Total Control Attention (Hover - No Flight Director).

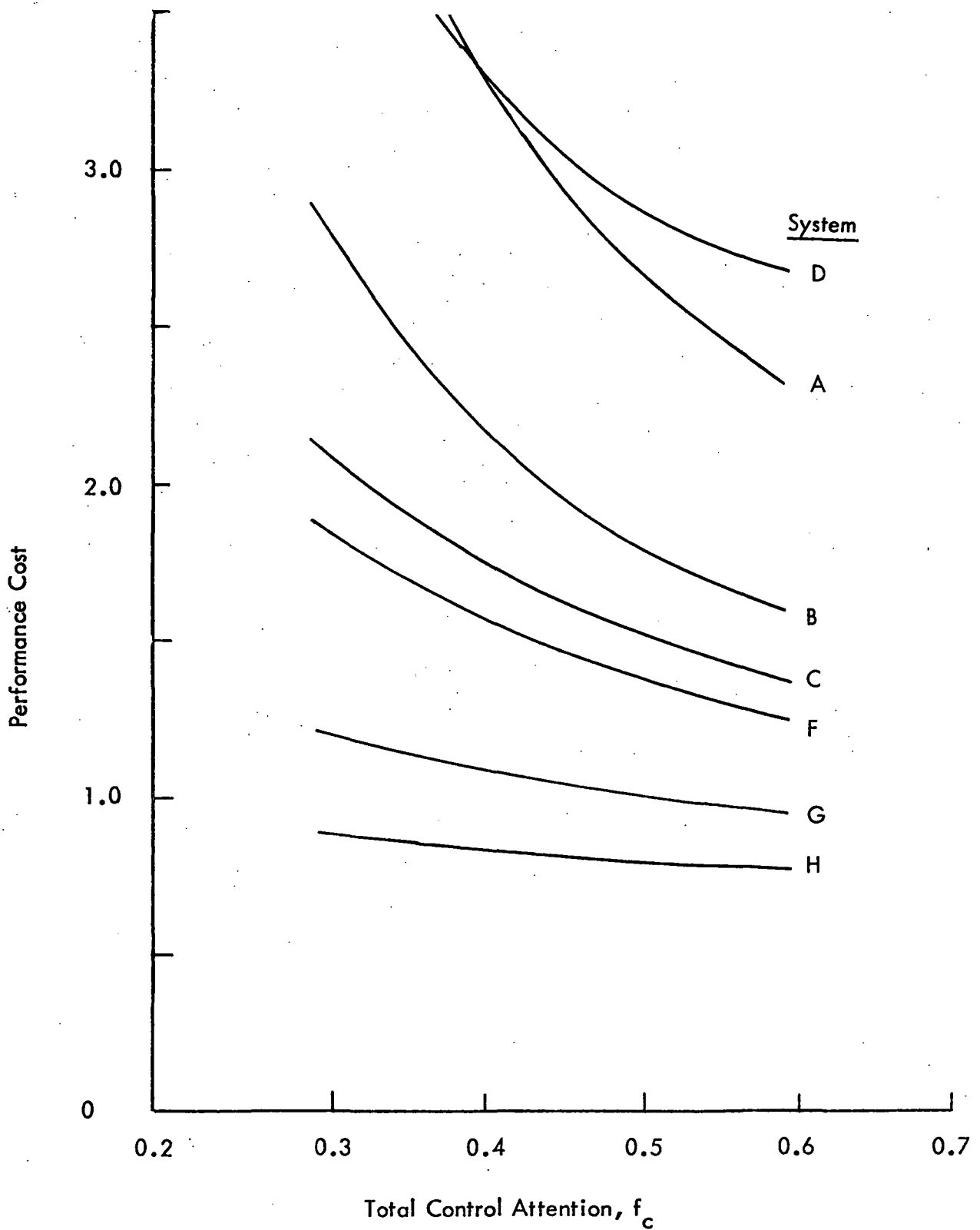


Figure 6-33. Control Performance Cost vs. Total Control Attention (Hover - z Flight Director).

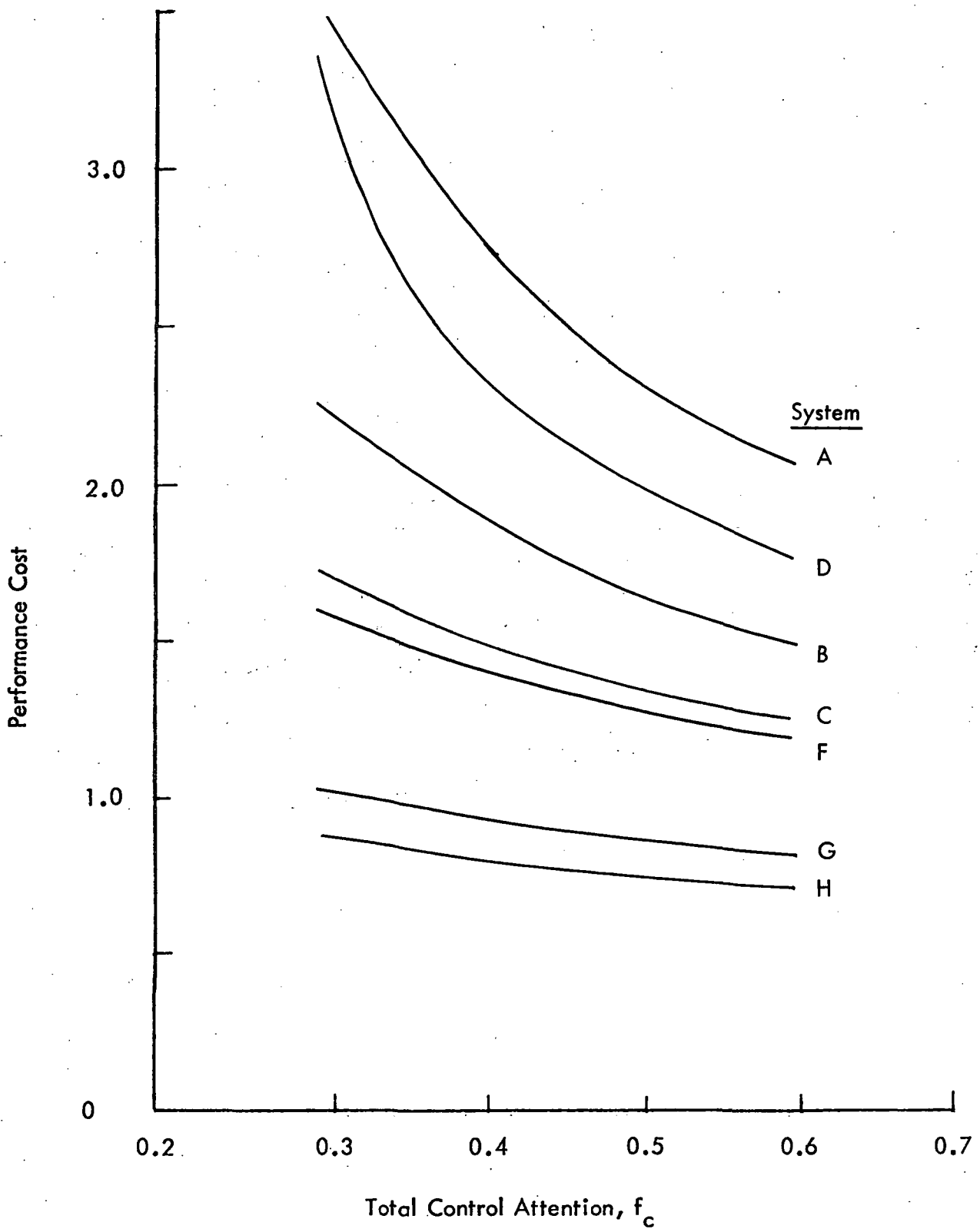


Figure 6-34. Control Performance Cost vs Total Control Attention (Hover - x Flight Director).

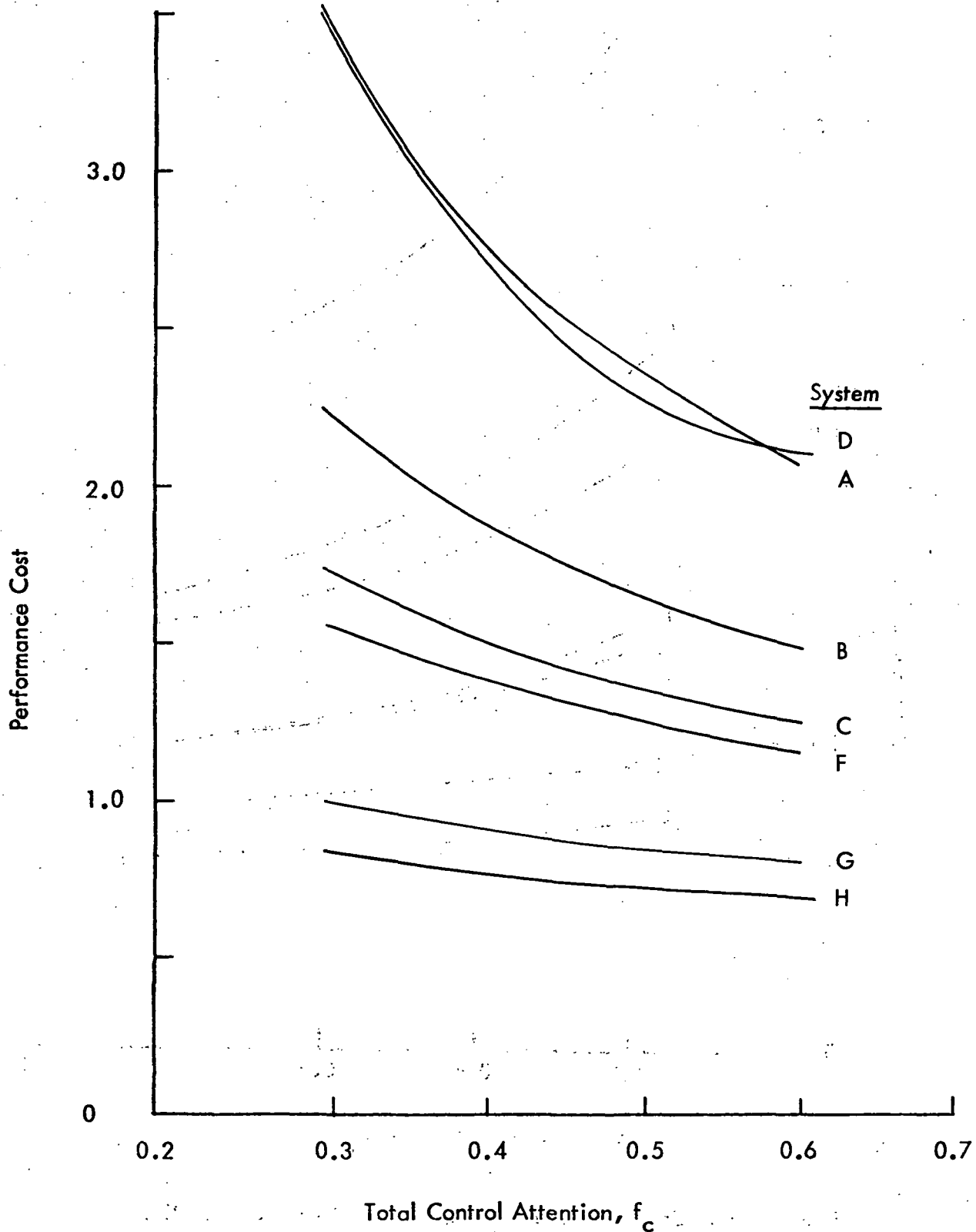


Figure 6-35. Control Performance Cost vs Total Control Attention (Hover - Full Flight Director).

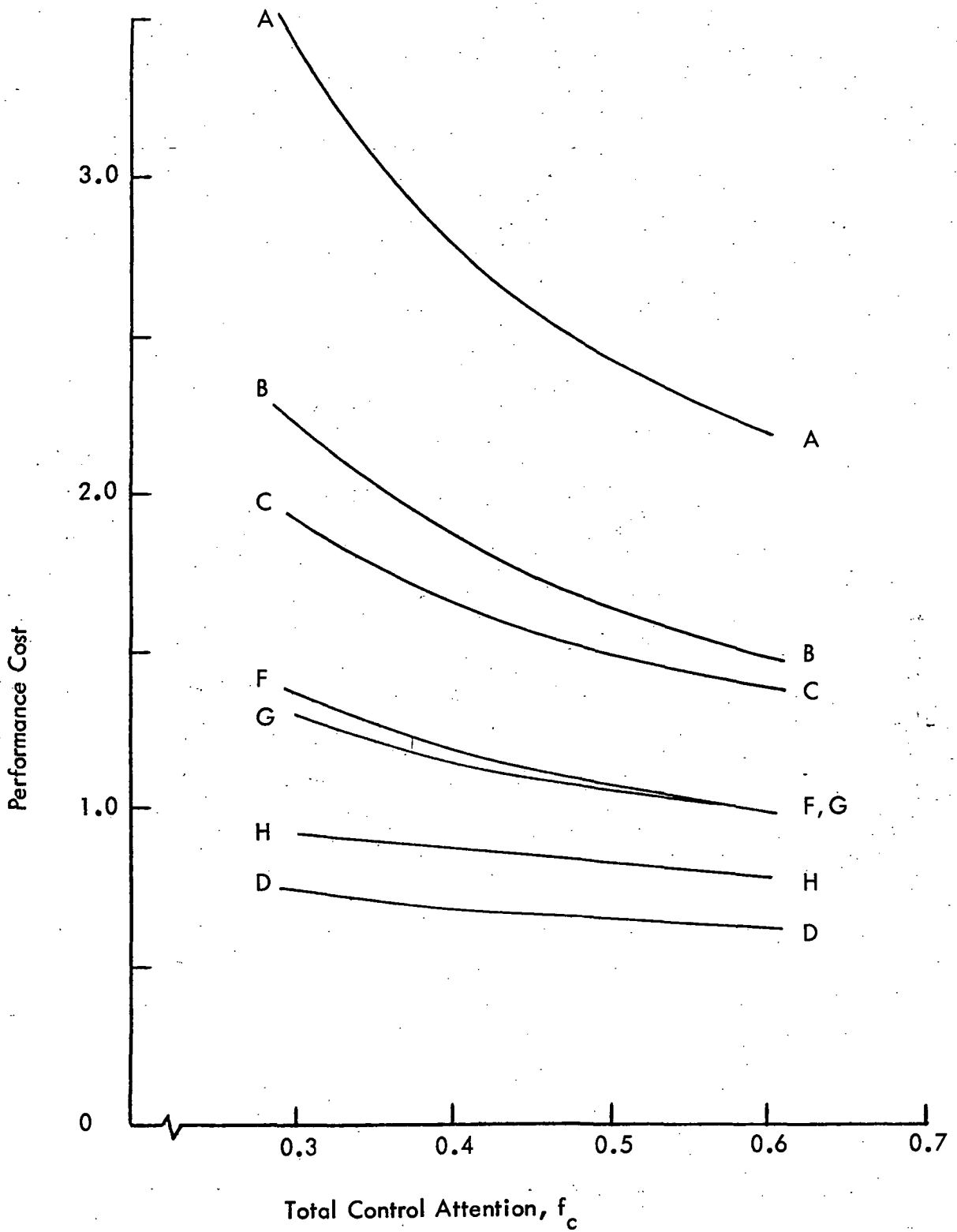


Figure 6-36. Control Performance Cost vs Total Control Attention (Approach - No Flight Director).

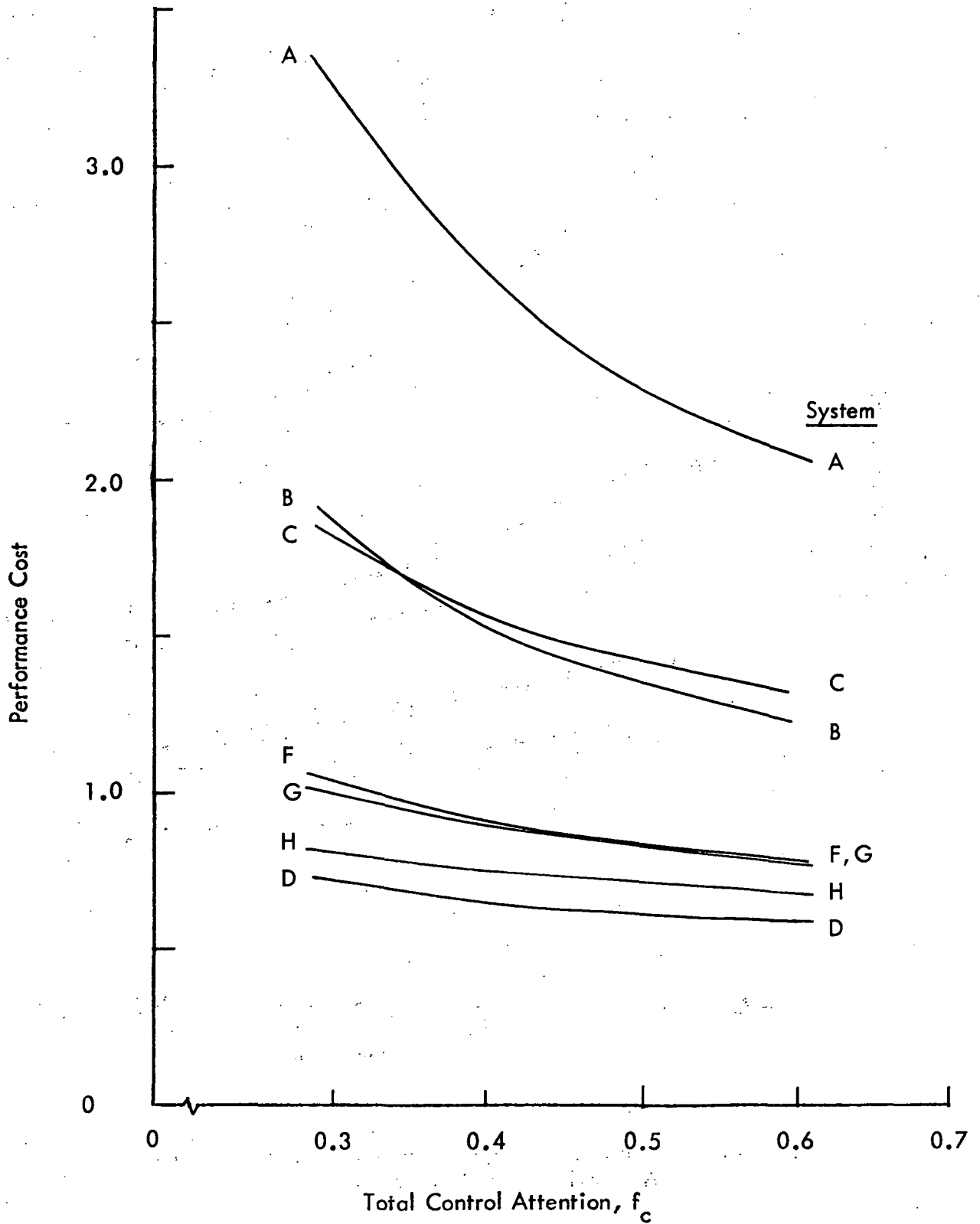


Figure 6-37. Control Performance Cost vs Total Control Attention (Approach - z Flight Director).

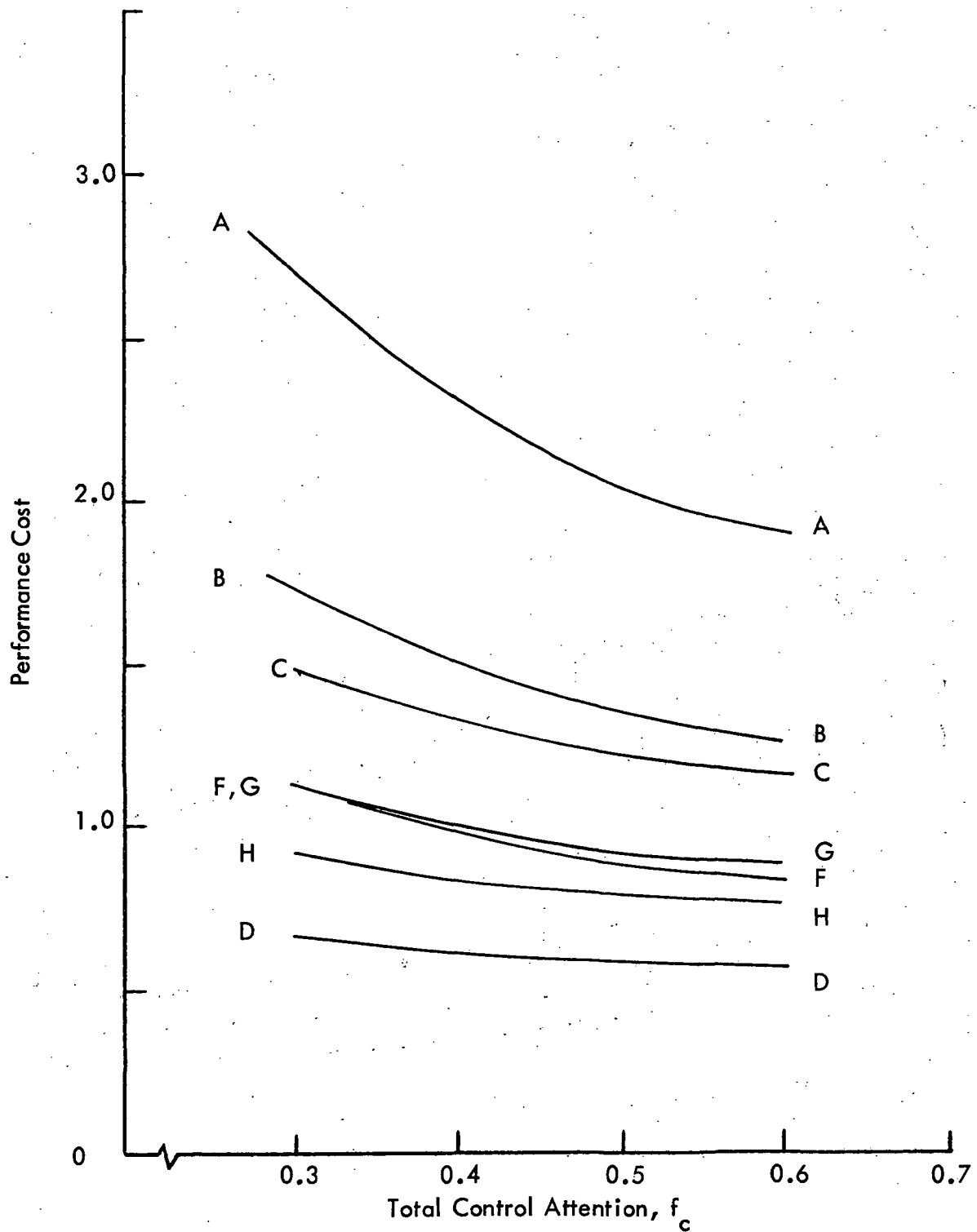


Figure 6-38. Control Performance Cost vs Total Control Attention (Approach - x Flight Director).

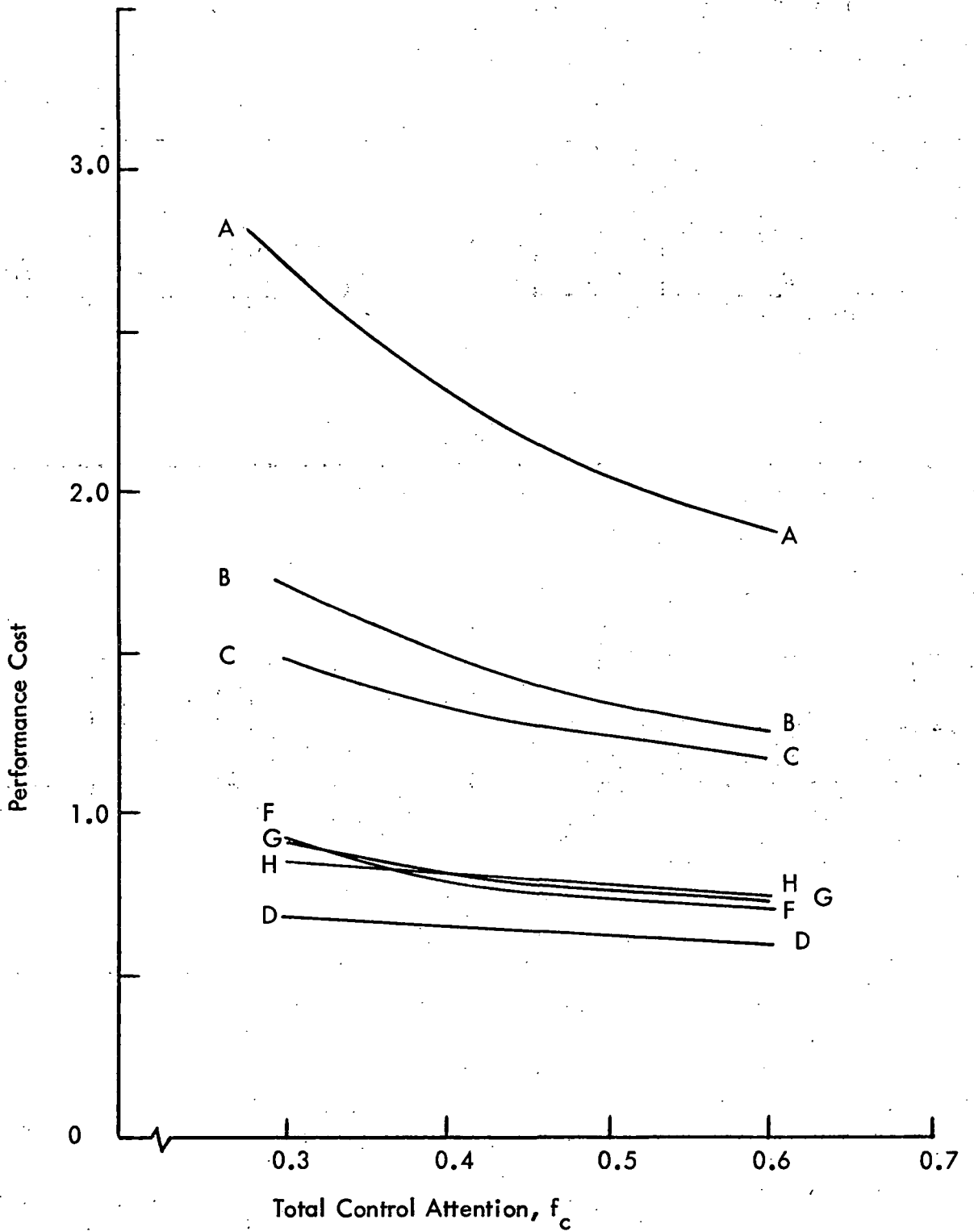


Figure 6-39. Control Performance Cost vs Total Control Attention (Approach - Full Flight Director).

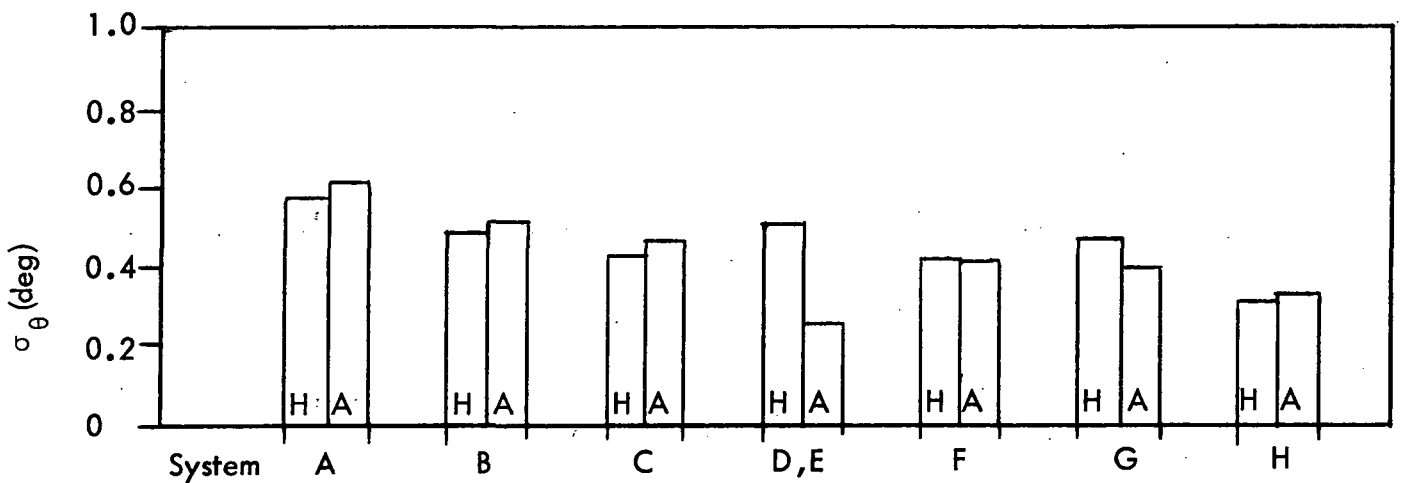
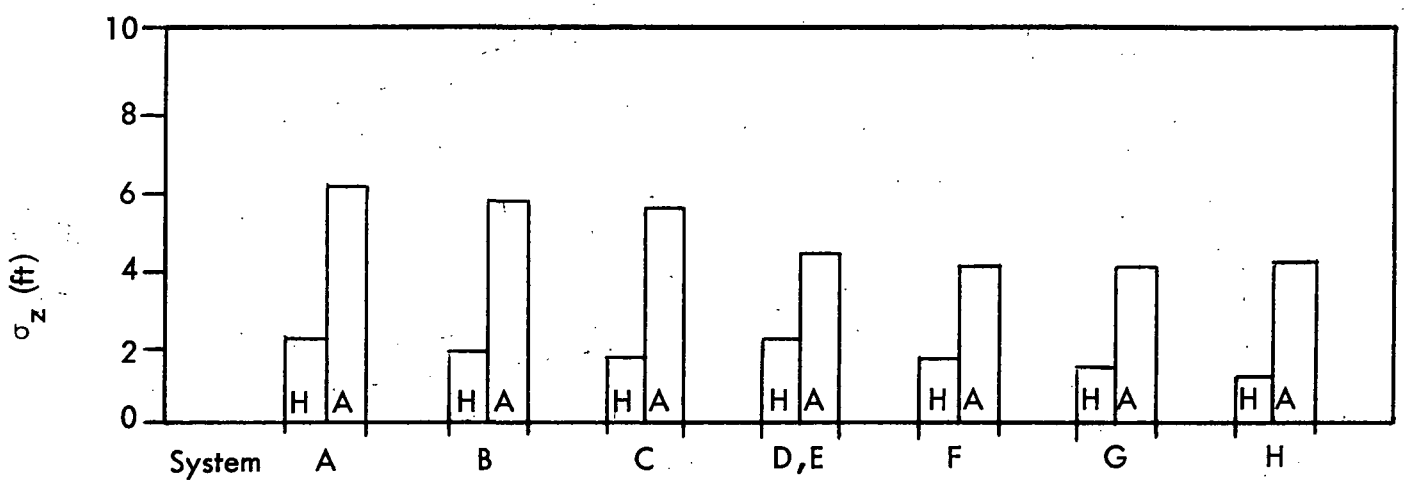
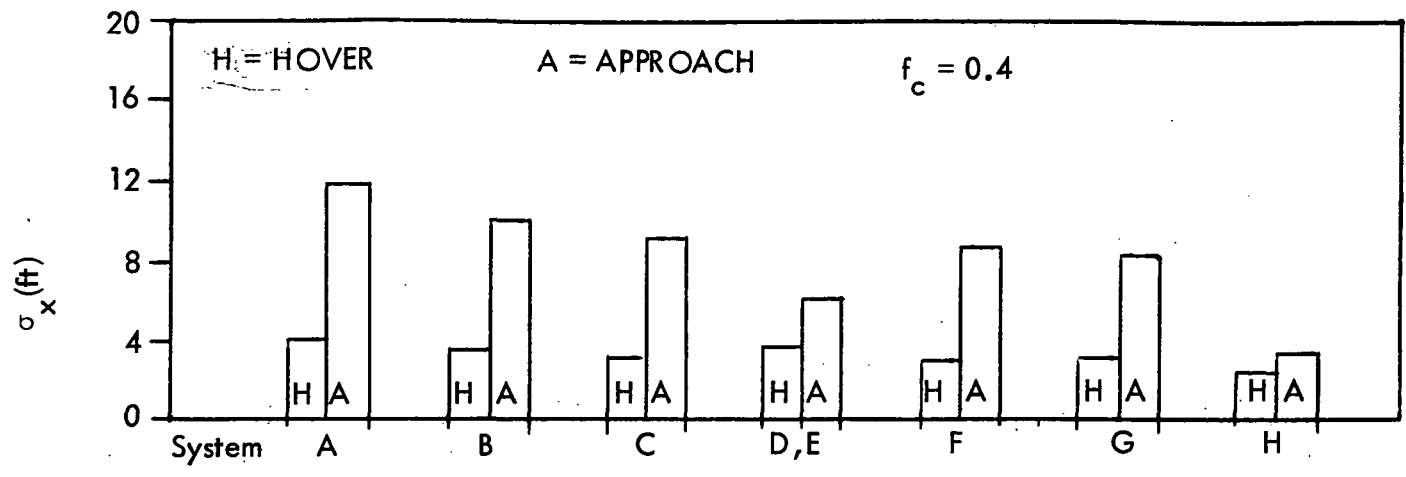


Figure 6-40. RMS Performance vs System Automation (No Flight Director).

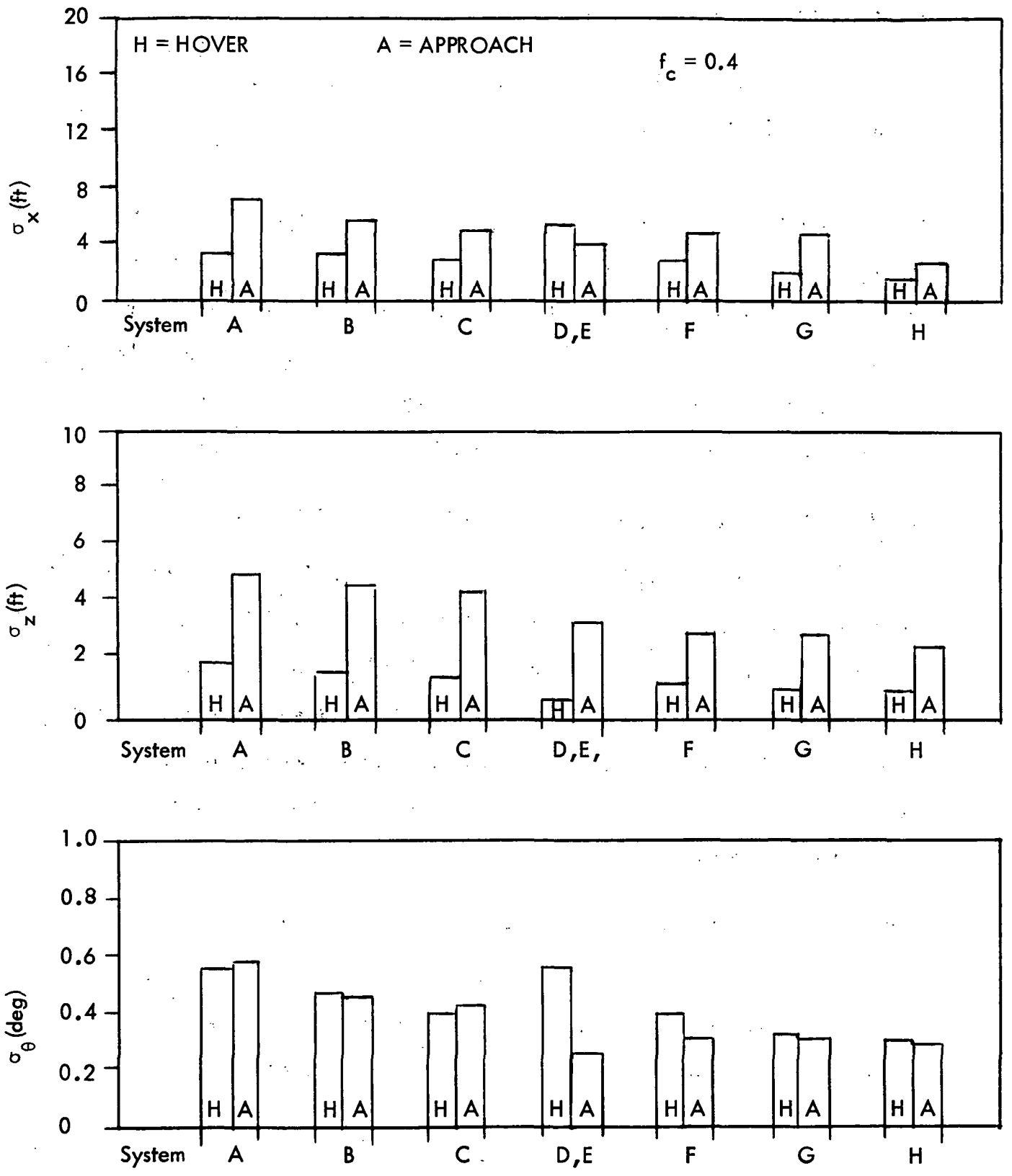


Figure 6-41. RMS Performance vs System Automation (Full Flight Director).

6.4.4 ATTENTION ALLOCATION VS CONTROL AUTOMATION

Figures 6-42 and 6-43 compare the fractional control attention for the various levels of control automation, with no flight directors and with full flight directors respectively, and at a "comfortable" pilot workload ($f_c = 0.4$). These charts indicate the comparative importance of the instruments as the flight conditions change and/or as the system automation changes. For example, in Figure 6-43 the raw position instruments are used infrequently in all systems, particularly during the approach. As another example, adding pitch rate feedback (System B) and pitch attitude feedback (System C) allows the pilot to shift some attention from the attitude indicator to the vertical instruments (z and FD_z), thereby improving his overall performance.

6.4.5 ATTENTION ALLOCATION VS DISPLAY SOPHISTICATION

Figures 6-44 through 6-50 show the change in fractional control attention with display sophistication for each system at $f_c = 0.4$. They illustrate the importance of the available instruments at a fixed workload for each level of control automation. The information level results demonstrate the importance of the rate information from each instrument. It is interesting that although the pilot spends a large fraction of his available attention to the z flight director (when provided), this does not achieve a significant improvement in performance.

6.4.6 CONTROL/DISPLAY CONFIGURATION EVALUATION

To evaluate the various control/display configurations, the workload for each can be normalized to a specified minimum acceptable performance. The performance cost for longitudinal control of any system is defined as

$$J_p = \sum_1^6 [\sigma_{x_i} / (x_i)_{\max}]^2 \quad (6-7)$$

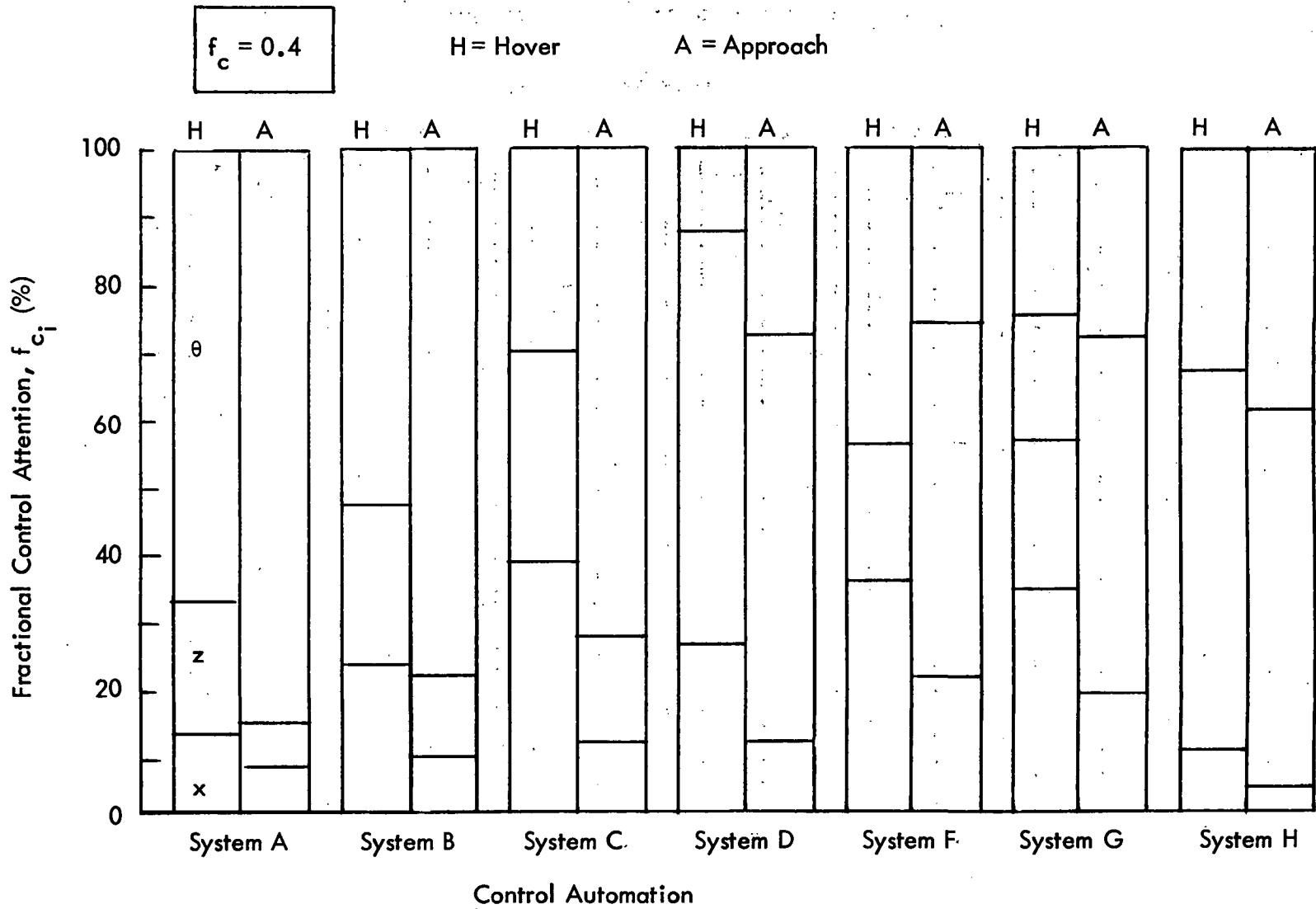


Figure 6-42. Control Attention Allocation vs System Automation (No Flight Director).

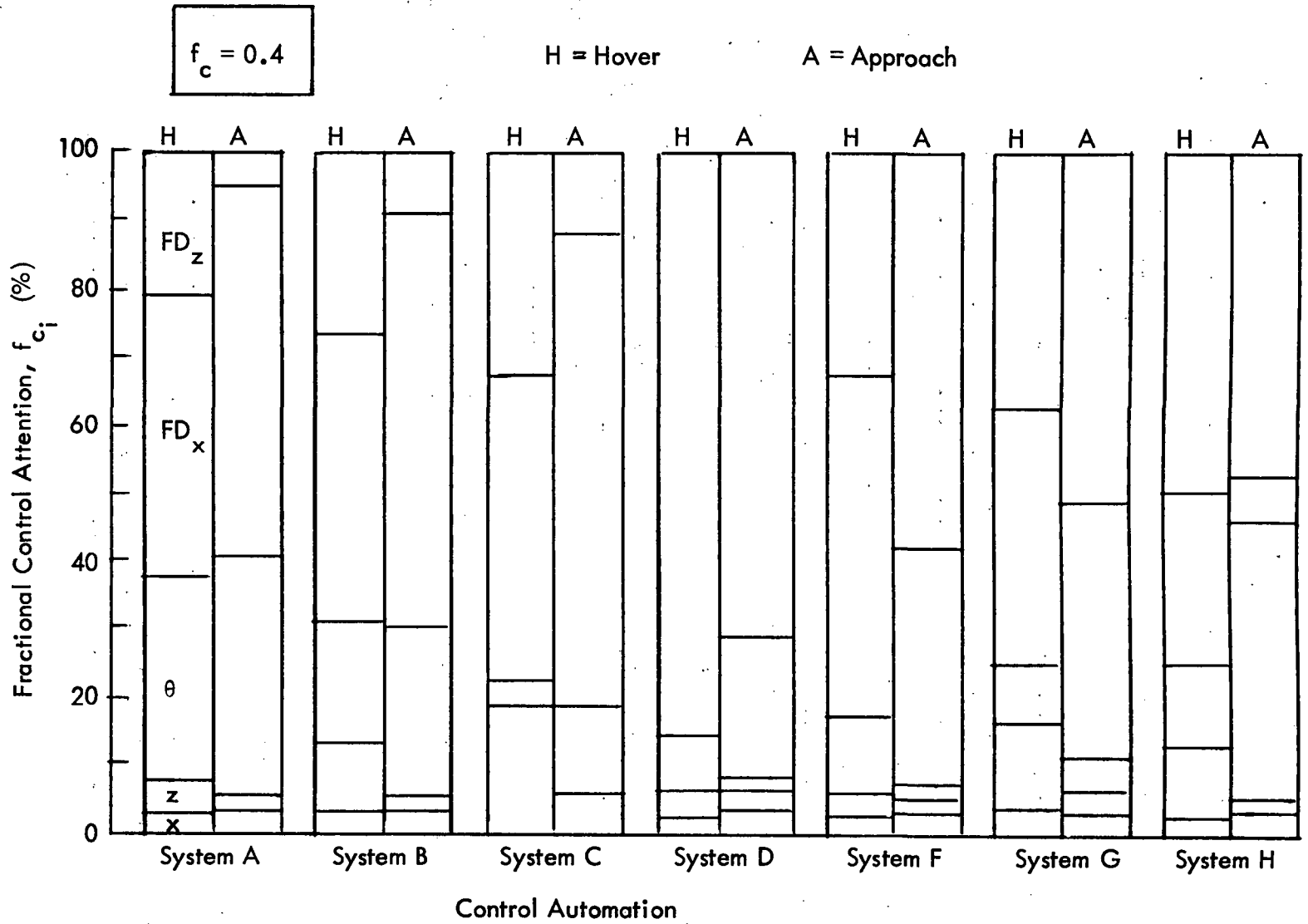


Figure 6-43. Control Attention Allocation vs System Automation (Full Flight Director).

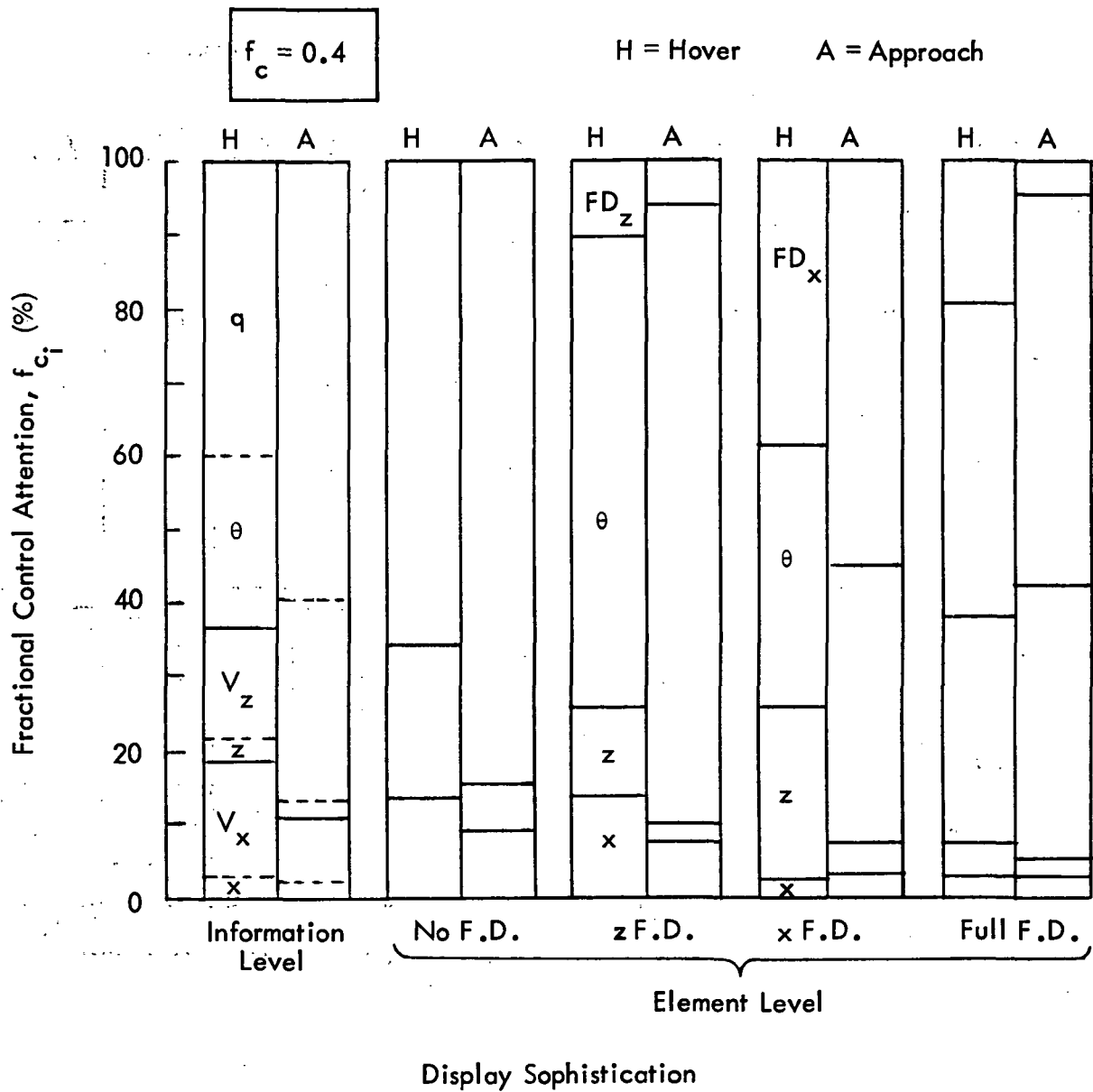


Figure 6-44. Control Attention Allocation vs Display Sophistication (System A).

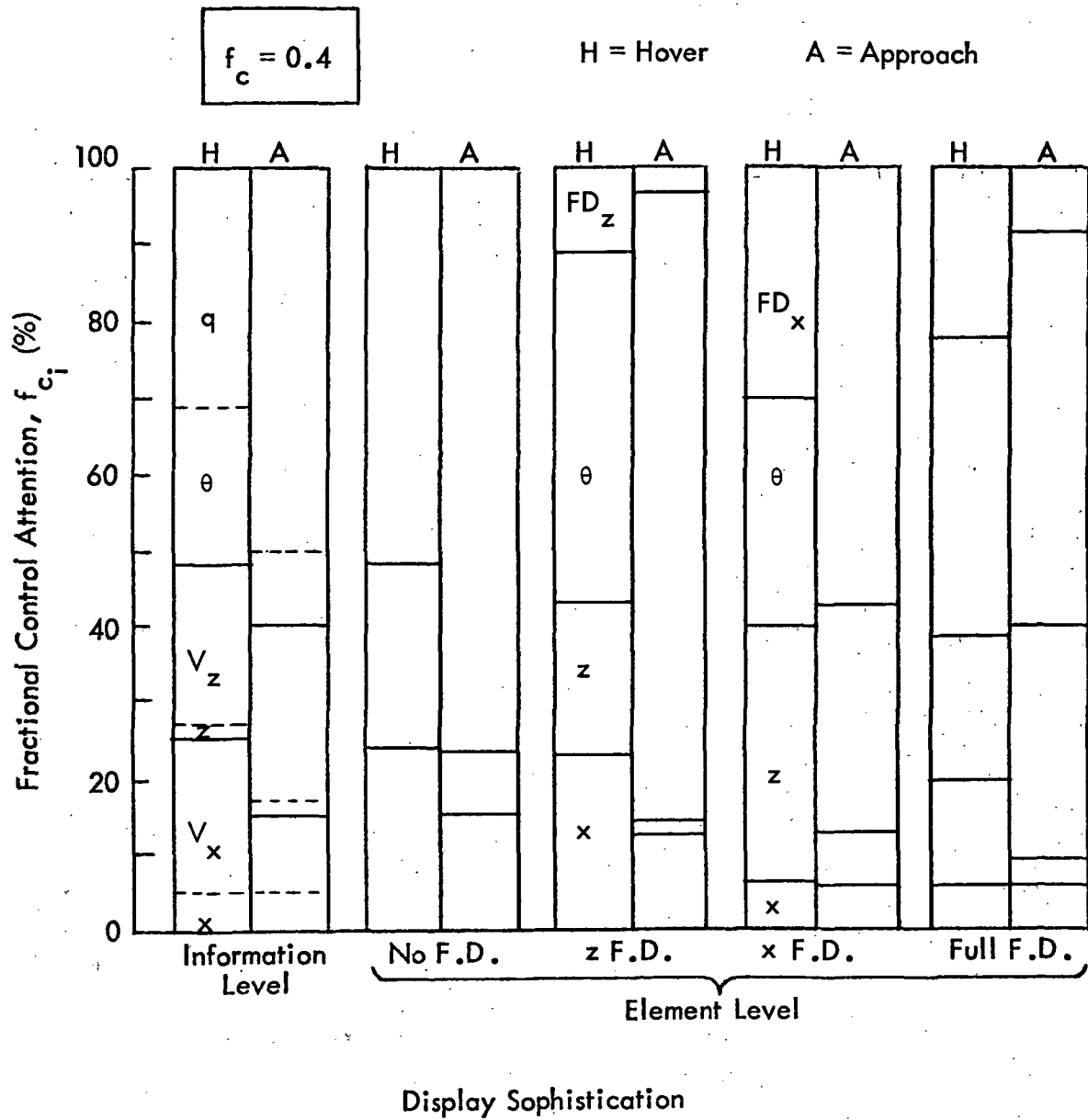


Figure 6-45. Control Attention Allocation vs Display Sophistication (System B).

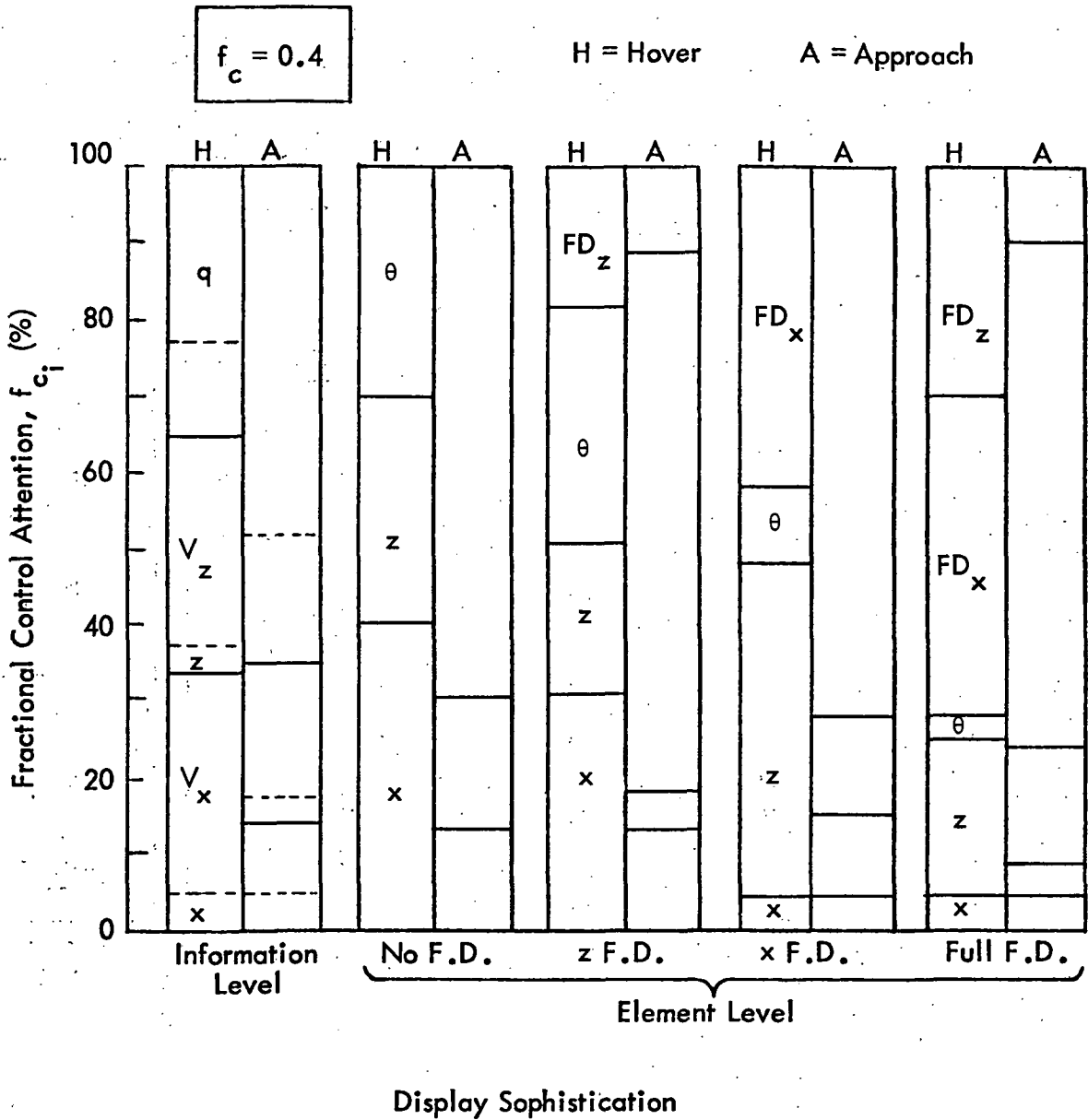


Figure 6-46. Control Attention Allocation vs Display Sophistication (System C).

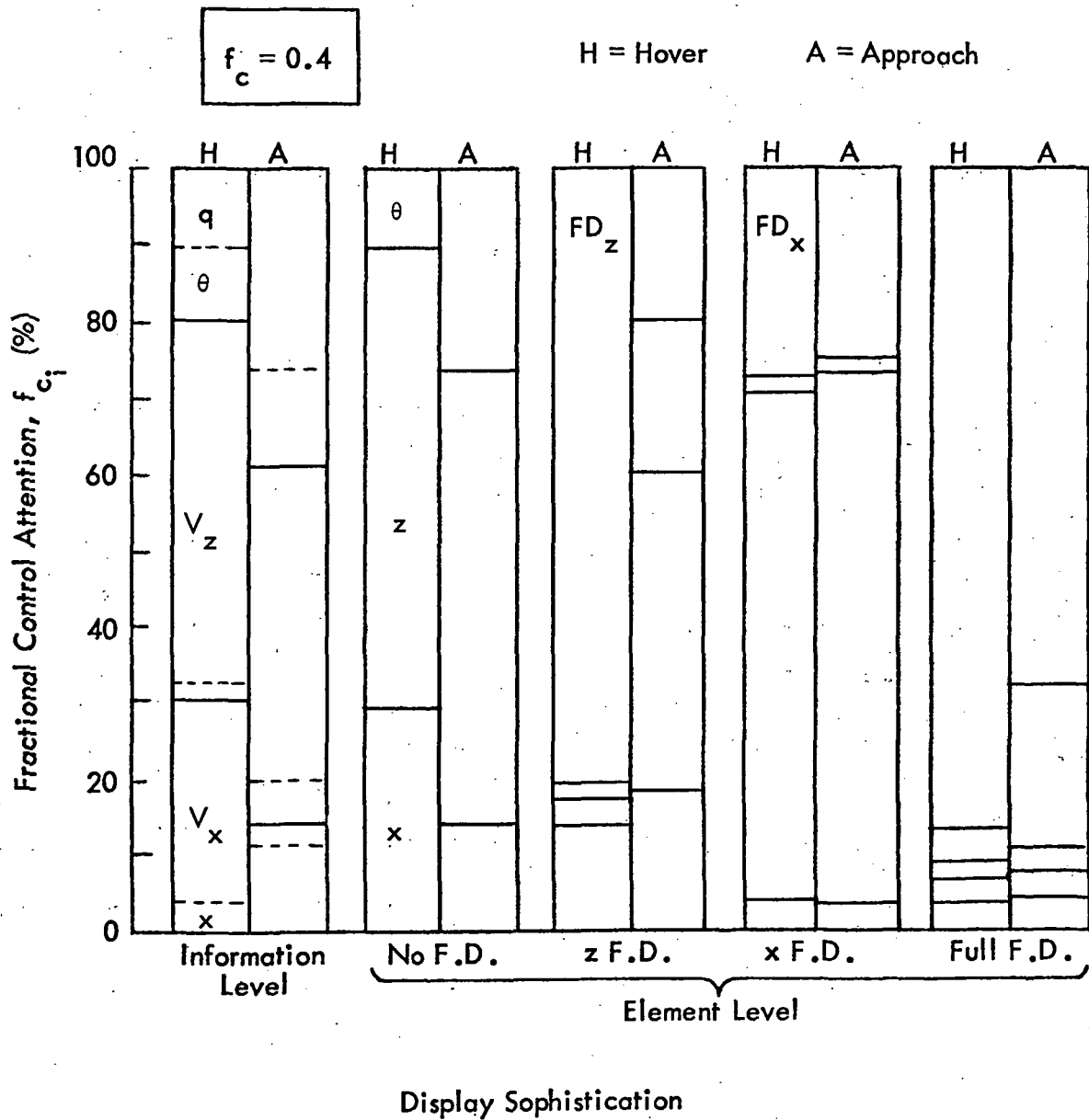


Figure 6-47. Control Attention Allocation vs Display Sophistication (System D).

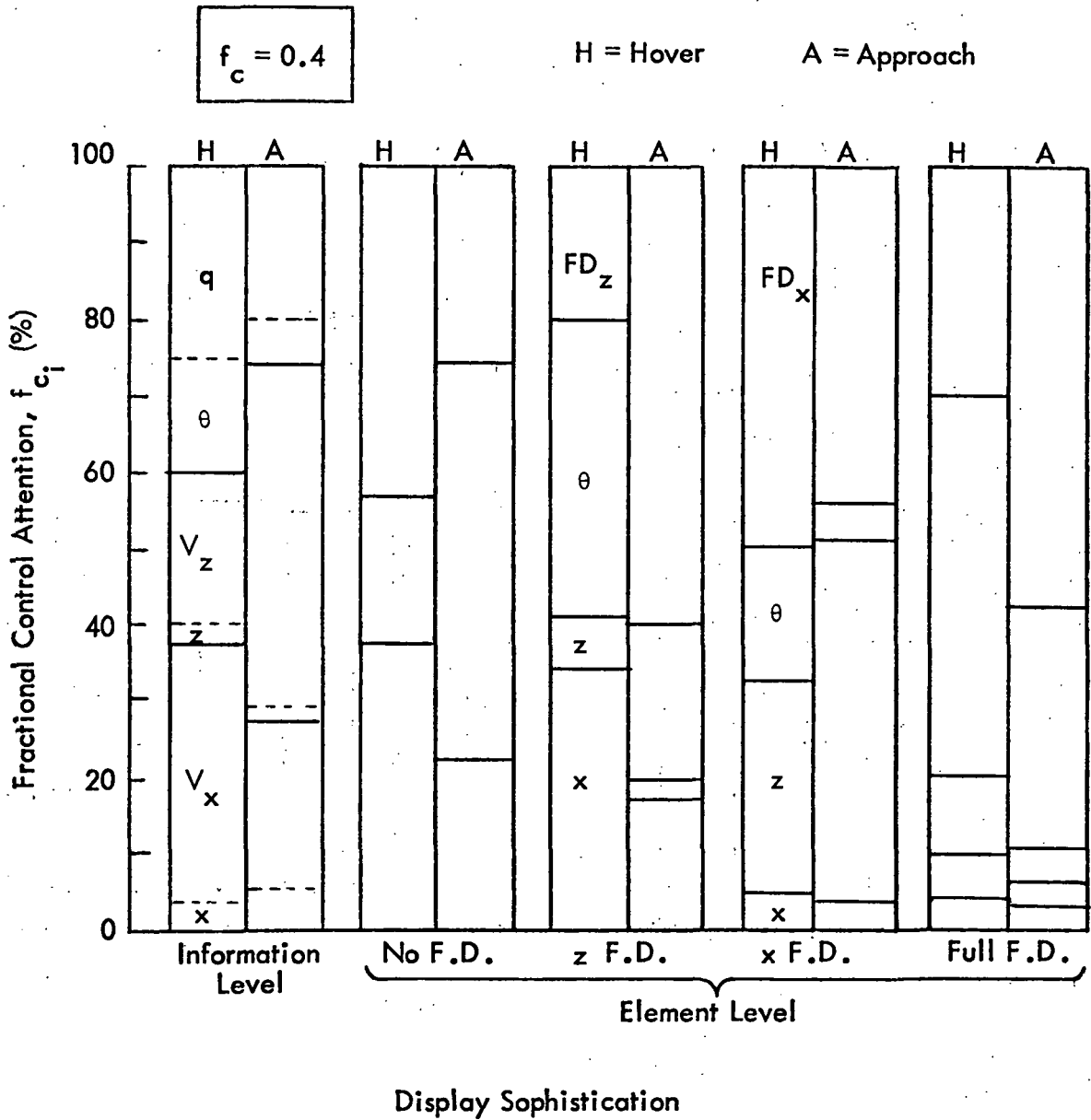


Figure 6-48. Control Attention Allocation vs Display Sophistication (System F).

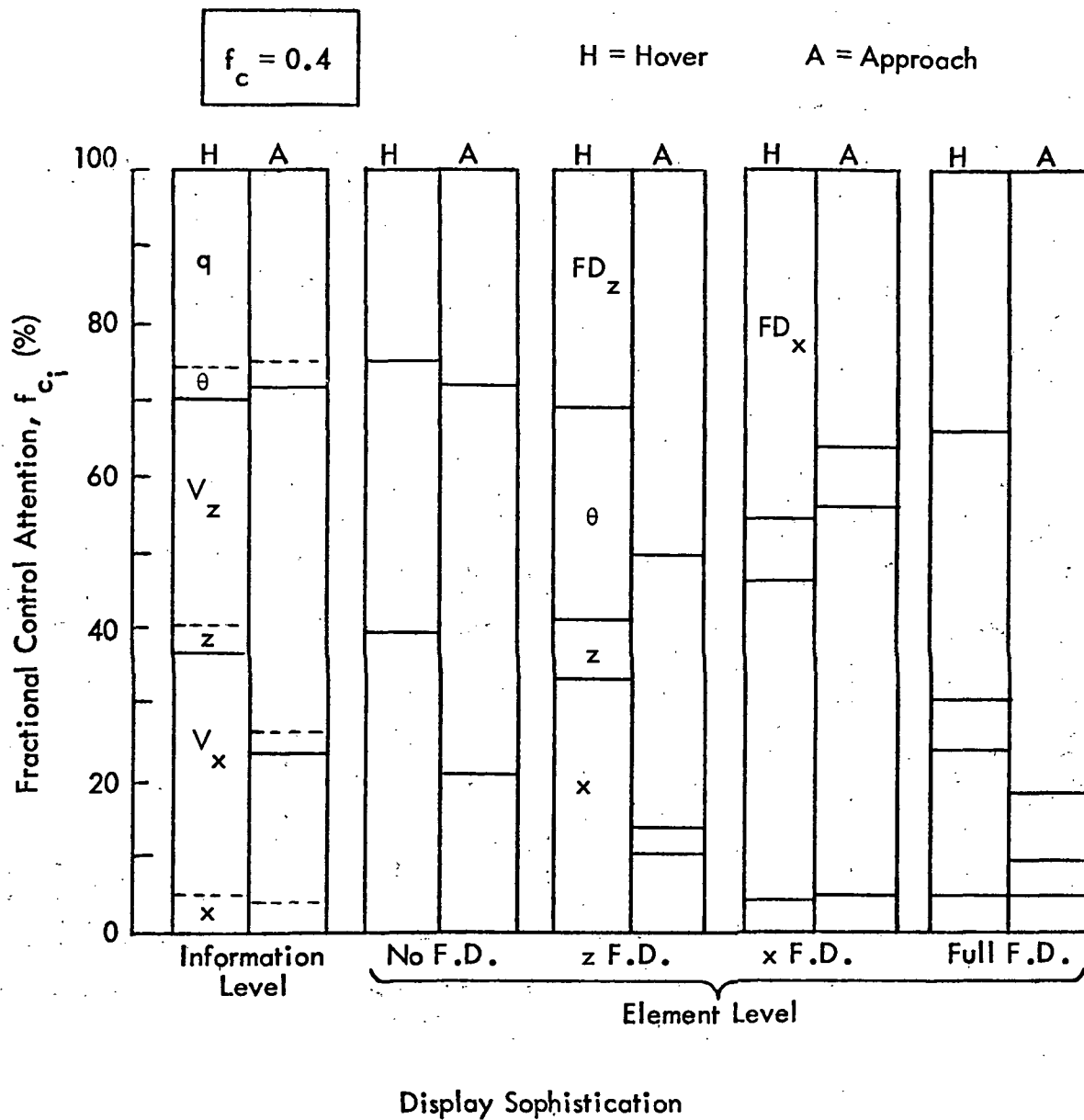


Figure 6-49. Control Attention Allocation vs Display Sophistication (System G).

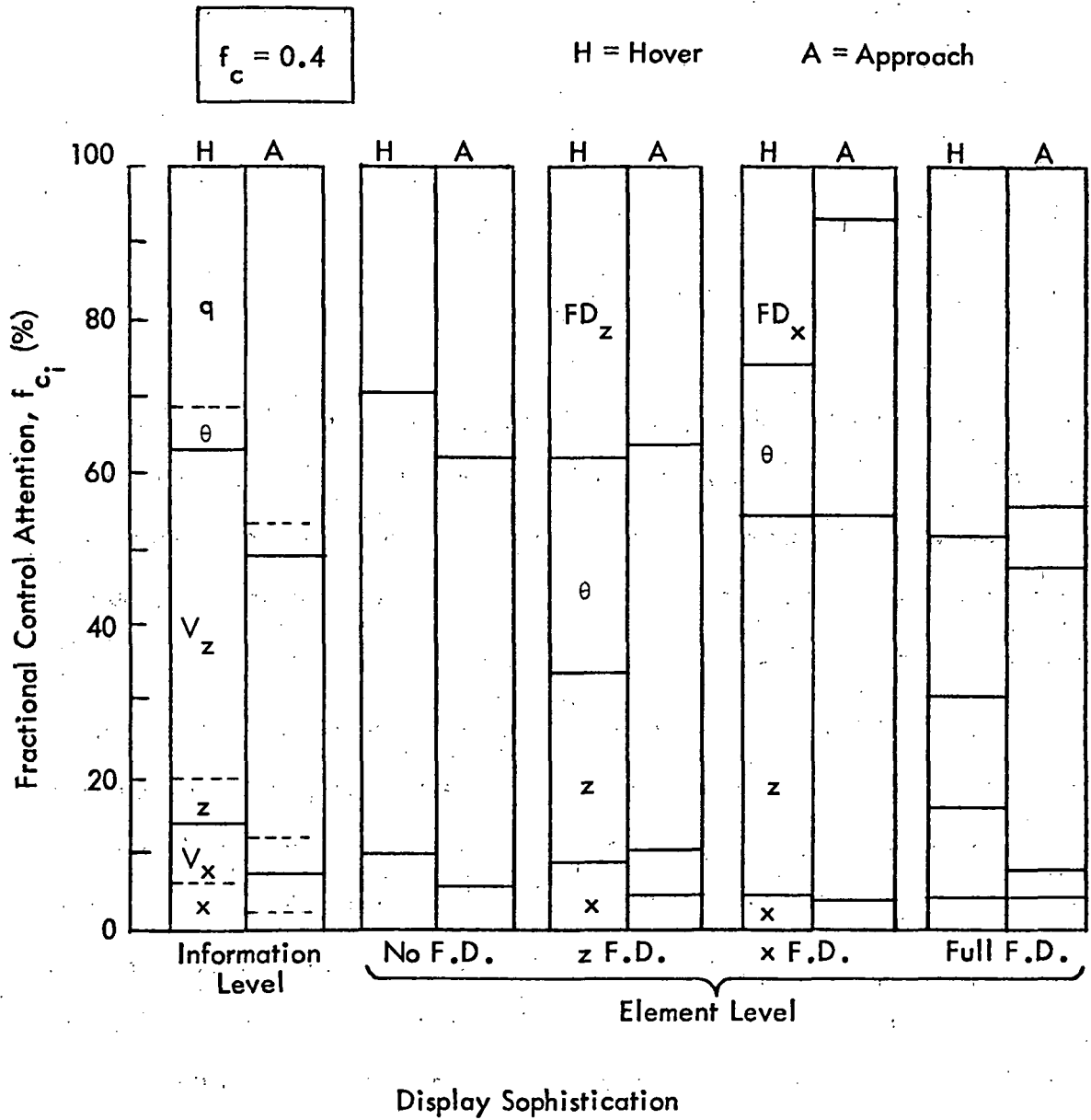


Figure 6-50. Control Attention Allocation vs Display Sophistication (System H).

where σ_{x_i} are the predicted rms state errors (x, y, θ , etc.) and $(x_i)_{\max}$ are the corresponding cost functional weightings given in Table 6-2, which correspond to 2σ values. If we specify the minimum acceptable performance as 1σ errors in all states, i.e.

$$\sigma_{x_i} = (x_i)_{\max}/2 \quad (6-8)$$

the maximum allowable value in Equation (6-7) is:

$$(J_p)_{\max} = 6(1/2)^2 = 1.5 \quad (6-9)$$

For the longitudinal control task, the maximum capability for both control and monitoring is about 0.6, and a "comfortable" value for control is $f_c \sim 0.4$. By defining an acceptable workload to be ± 0.1 from the comfortable level, the control/display configurations can all be classified into three categories (unacceptable, acceptable, excellent) as shown in Figure 6-51.

Applying this normalization technique to the candidate control/display systems for the CH-47, we obtain the performance evaluation shown in Figure 6-52 for hover and approach. Besides quantifying the well-known conceptual plots of control automation vs display sophistication[†], Figure 6-53 provides a great deal of information on the various configurations. For example, System C is acceptable in both flight conditions if at least an x flight director is provided. However, if the flight director should fail, the performance would be unacceptable in the hover condition.

[†] If the System D results are neglected, it is possible to sketch contours of constant workload as functions of control automation and display sophistication in Figure 6-52.

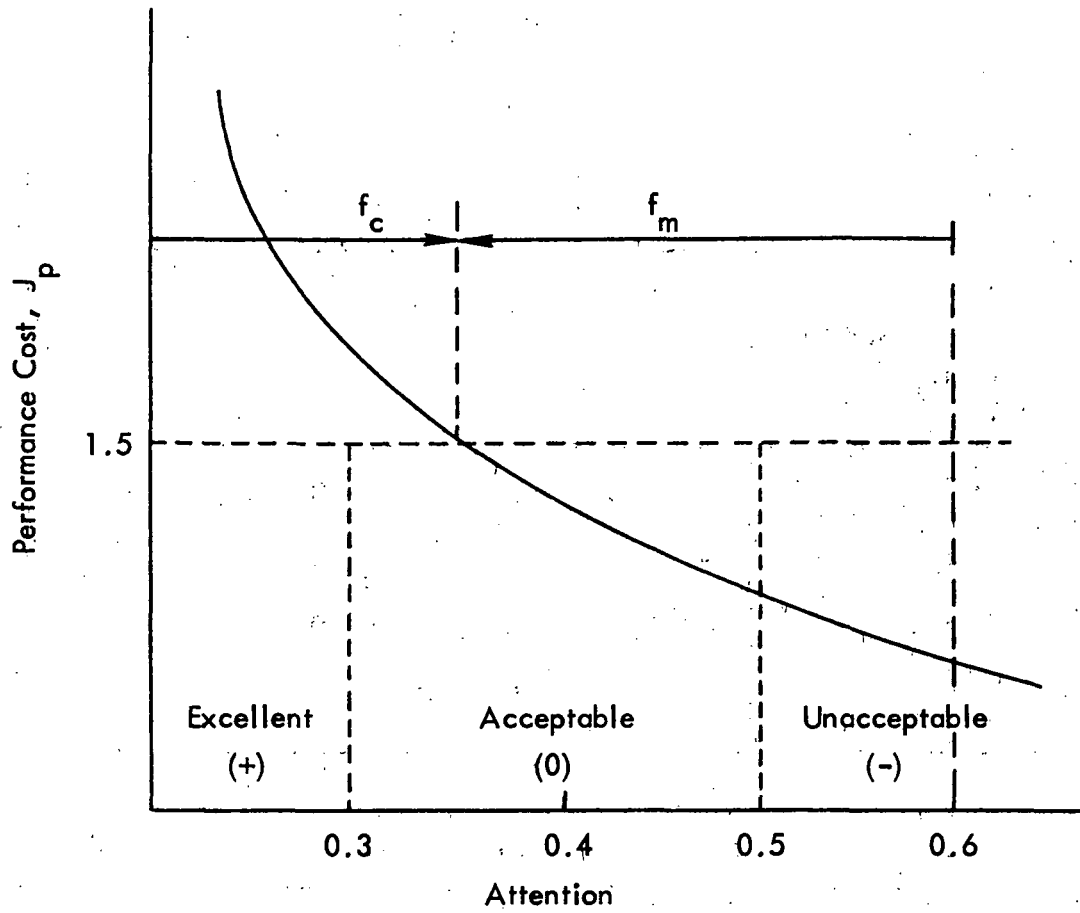


Figure 6-51. Normalization of Performance and Workload Metrics.

+ Excellent
 0 Acceptable
 - Unacceptable

HOVER

Control System \ Display System	A	B	C	D	F	G	H
No F.D.	-	-	-	-	0	0	+
z F.D.	-	-	-	-	0	+	+
x F.D.	-	-	0	-	0	+	+
Full F.D.	-	-	0	-	0	+	+

APPROACH

Control System \ Display System	A	B	C	D	F	G	H
No F.D.	-	-	0	+	+	+	+
z F.D.	-	0	0	+	+	+	+
x F.D.	-	0	0	+	+	+	+
Full F.D.	-	0	+	+	+	+	+

Figure 6-52. Normalized Control Display Configuration Evaluation for CH-47.

AVERAGE GAIN FLIGHT DIRECTORS

FLIGHT DIRECTOR SIGNALS		(FD) _{max}	Indif. Threshold
<u>SYSTEM C</u>			
$FD_x =$	$.00388 x - 2.09 \theta + .0376 V_x - 3.72 q$	0.14	0.035
$FD_x =$	$8.94 \theta + .00305 V_x + 6.60 q - 5.49 \theta_c$		0.018
$FD_z =$	$.0458 z + .262 V_z$	1.2	0.30
$FD_z =$	$-.0454 V_z - 2.25 \delta_c$		0.15
<u>SYSTEM G</u>			
$FD_x =$	$-.277 x + 121 \theta - 1.37 V_x + 184 q$	9.2	2.3
$FD_x =$	$-503 \theta + 4.97 V_x - 344 q - 5.22 V_{x_c}$		1.1
$FD_z =$	$-2.84 z - 20.7 V_z$	72.	18.
$FD_z =$	$1.85 z + 8.94 V_z - 2.07 z_c$		9.

Figure 6-53. Average Gain Flight Director Algorithms.

6.4.7 FIXED-GAIN FLIGHT DIRECTOR

The flight director algorithms presented in Subsection 6.2 were designed specifically for the given flight conditions. This implies the flight director computer would have to vary all the gains as the flight conditions change. As an alternative, a preliminary analysis of a fixed-gain flight director was conducted. The technique used was simply to average the "optimum" flight director algorithms for hover and approach. The control cost weightings and indifference thresholds are based on the maximum permissible position and attitude errors, which are the approach values. The resulting flight director signals are shown in Figure 6-53 for Systems C and G.

Figures 6-54 and 6-55 compare the respective system's performance at hover and approach. For comparison, the corresponding performance with no flight director and with the optimum (variable-gain) flight director is shown. Obviously, the optimum flight director is significantly better than the fixed-gain flight director for both systems. For System G, the fixed-gain flight director performance is about midway between the optimum flight director and that with no flight director. However, in System C, the fixed-gain flight director is no better than having no flight director at all.

Obviously, it is impossible to draw general conclusions from this brief examination, but it does appear that some form of flight director gain adjustment or sensitivity switching may be required to meet the desired system performance throughout the flight regime.

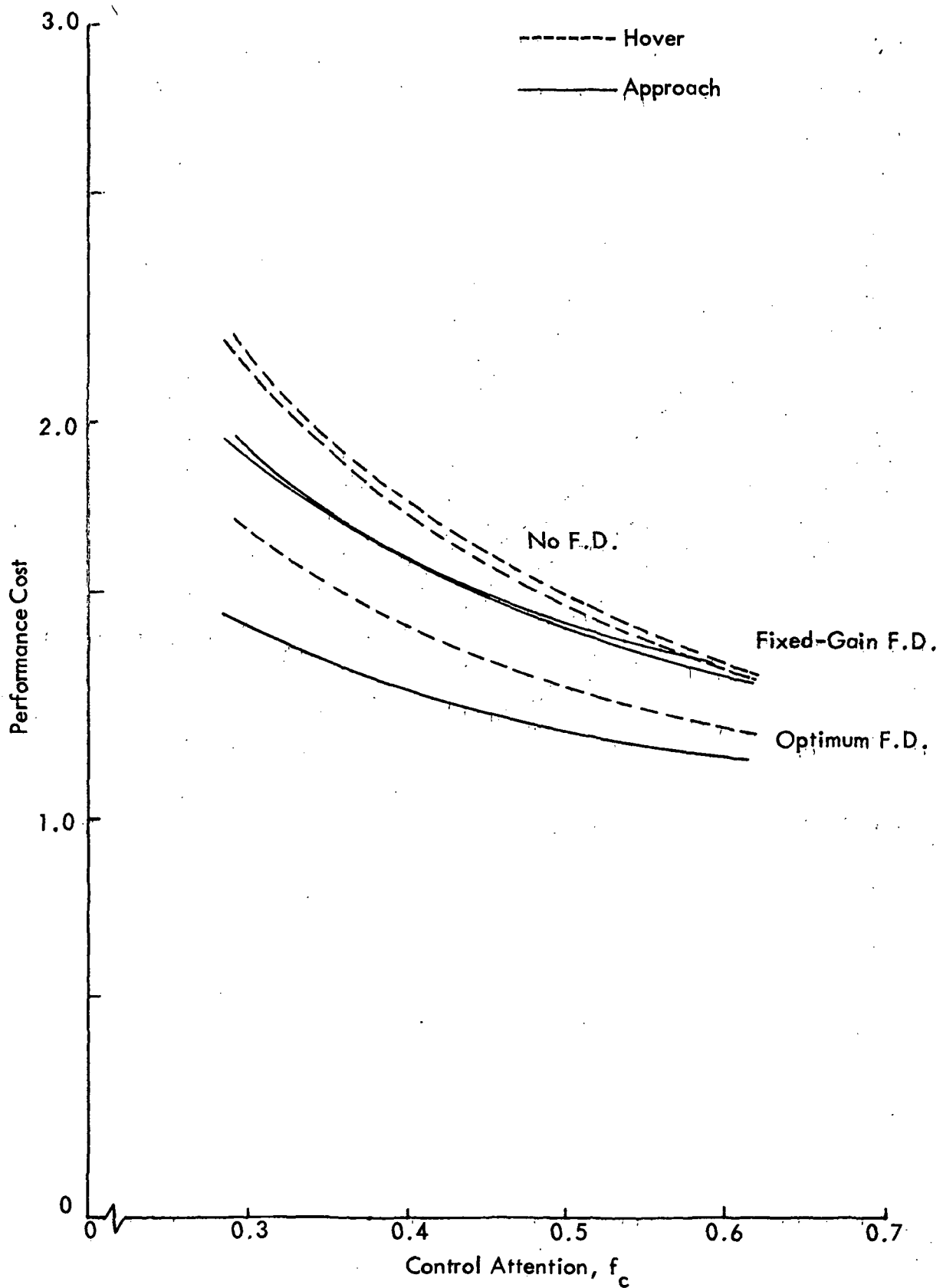


Figure 6-54. Fixed-Gain Flight Director Performance (System C).

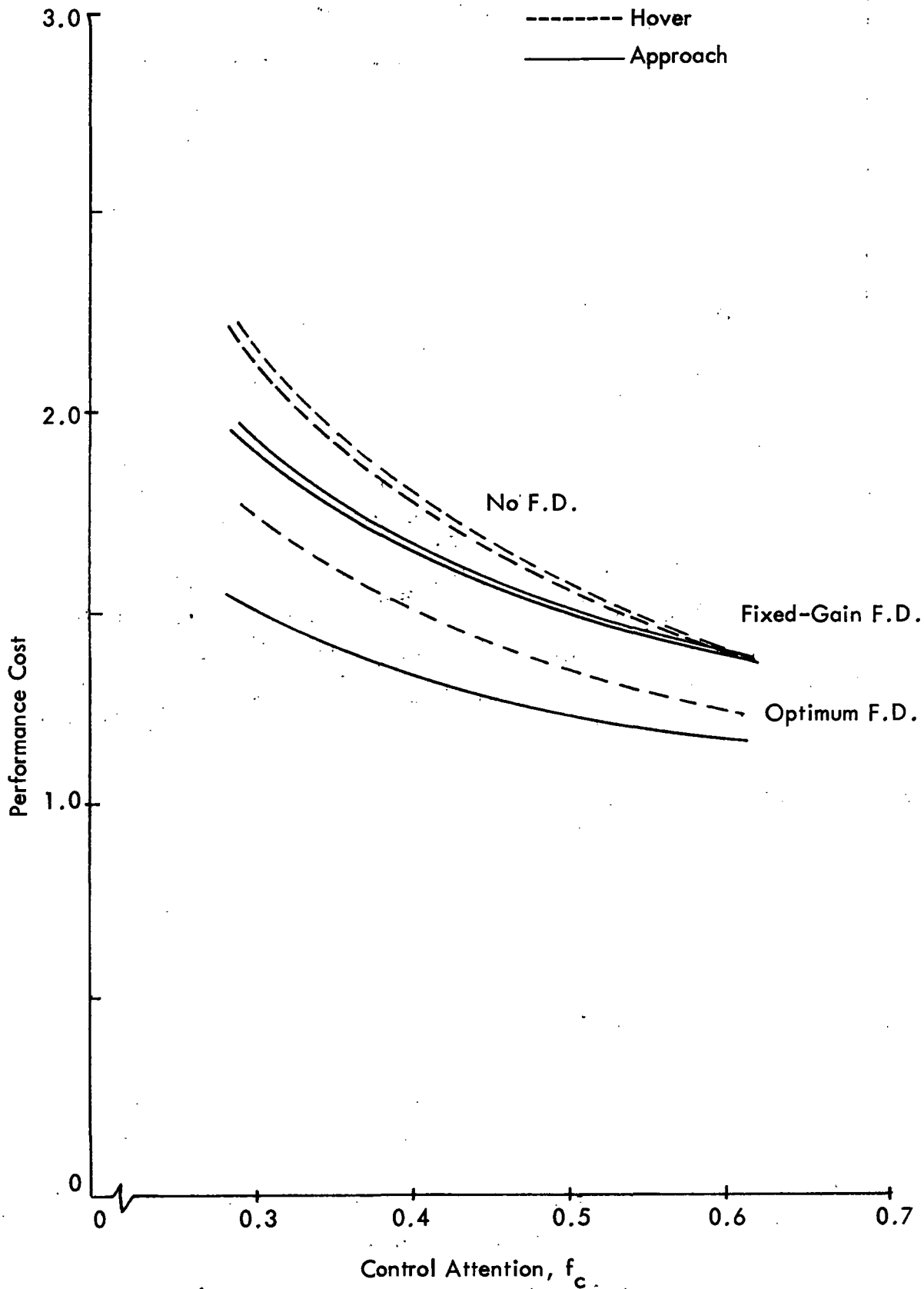
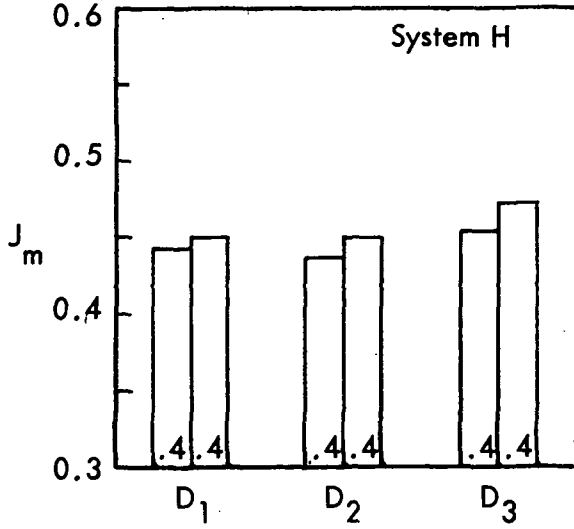
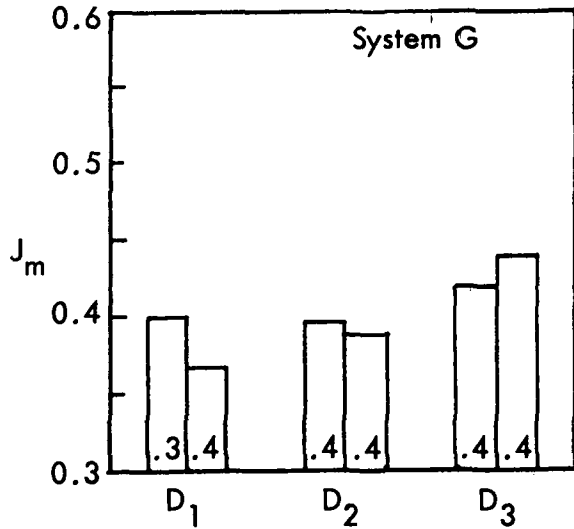
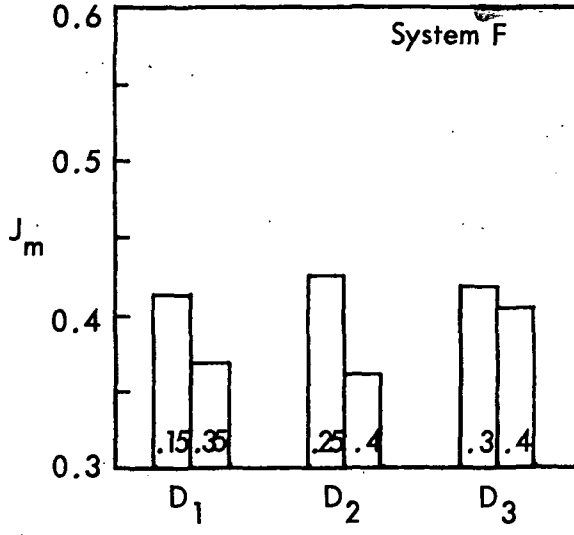
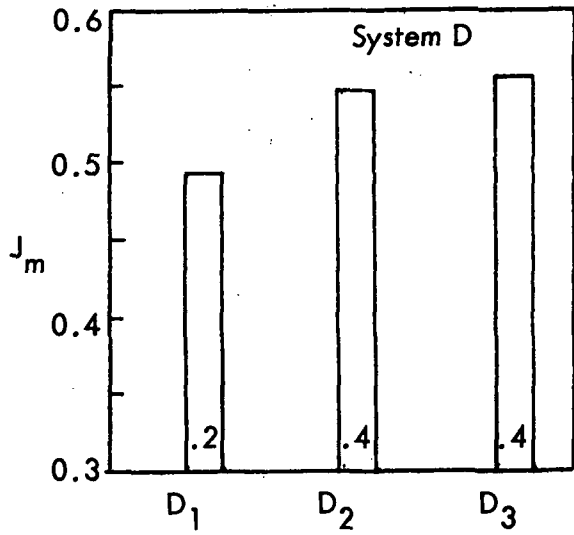
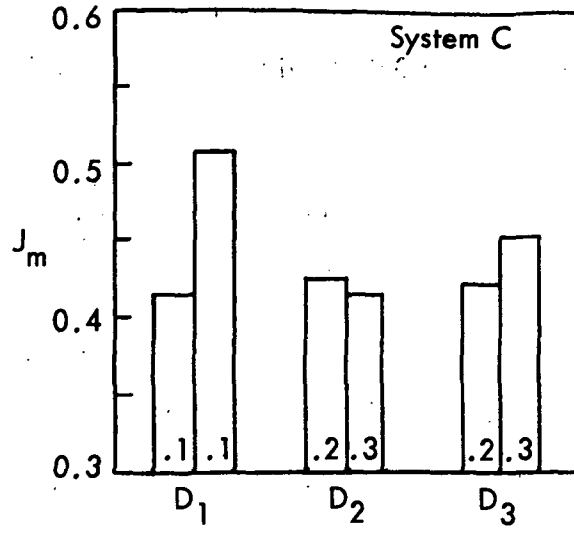
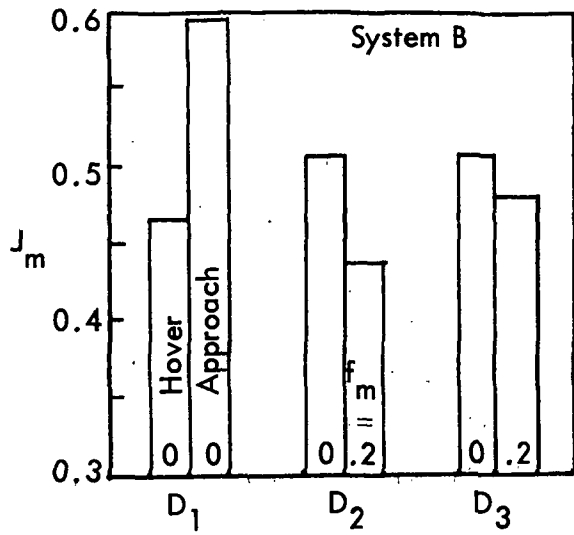


Figure 6-55. Fixed-Gain Flight Director Performance (System G).

6.5 MONITORING MODEL RESULTS

Having established the necessary control workload and corresponding performance, we can turn to the pilot's monitoring capability. Referring to Figure 6-51 the minimum control workload is determined by $J_p = 1.5$. If this is less than $f_c = 0.6$, the difference between 0.6 and f_c is available for monitoring the status instruments, as described in Section 2. Applying the monitoring model described in Section 4 to each acceptable system, we obtain the monitoring performance shown in Figure 6-56. It is interesting to note that monitoring performance does not always improve with increased automation. However, looking at the combined control and monitoring performance, Figure 6-57, we see that increased automation generally does improve total performance.



D_1 = No Flight Director $f_c + f_m = 0.6$
 D_2 = x Flight Director
 D_3 = x & z Flight Directors

Figure 6-56. Monitoring Performance Cost Summary.

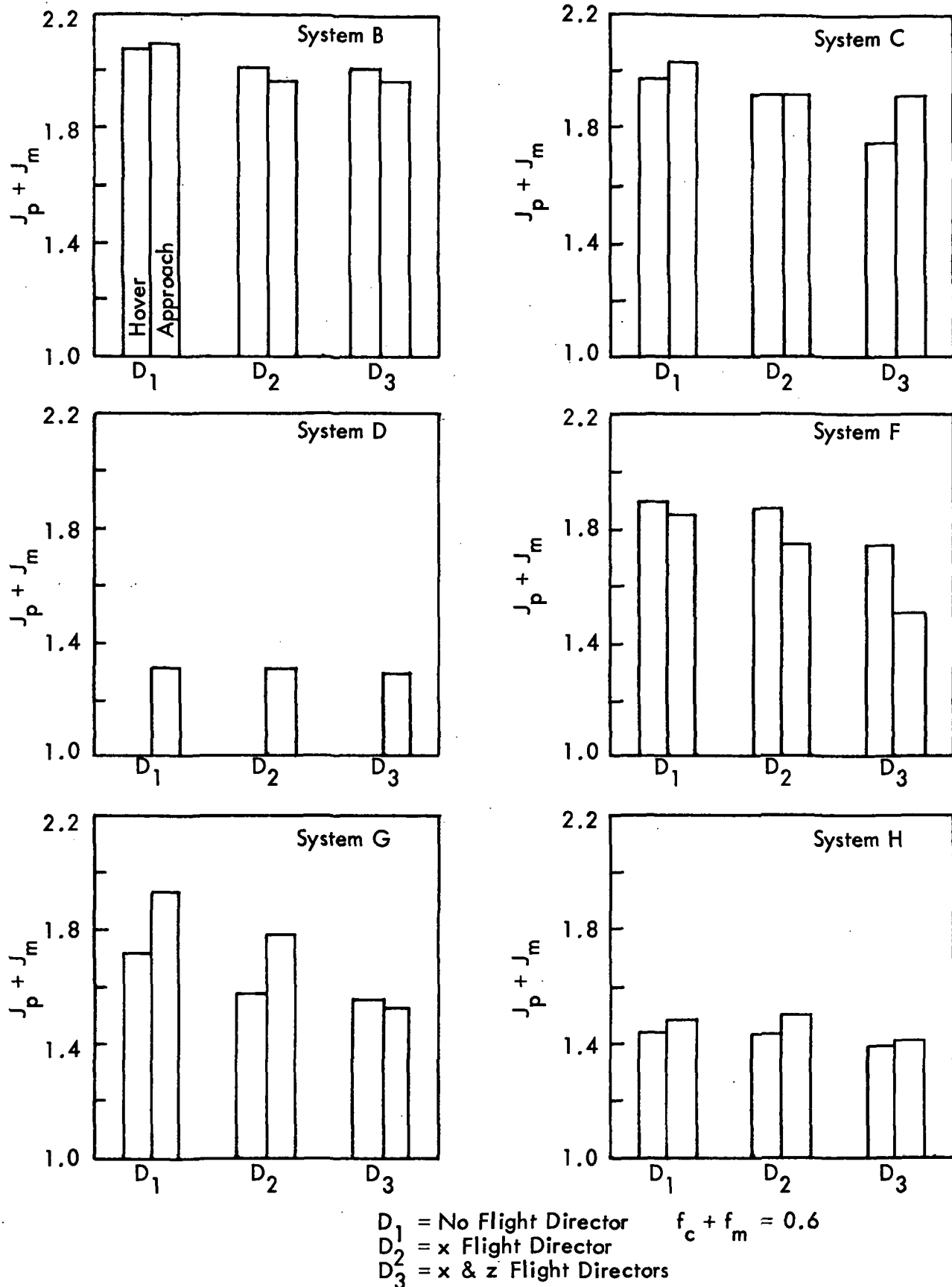


Figure 6-57. Total Performance Cost Summary.

SECTION 7

DISPLAY CONCEPT AND FORMAT

Although no unique transformation from analytically determined information requirements to display layout is available, there are nonetheless a number of important design principles which must be taken into account. This is of particular importance when dealing with integrated displays and with the problem of VTOL control. Some of these principles, outlined in Reference 20 and reiterated below, are generally useful in the design of flight control displays. They are not in any sense fundamental rules, and individual display situations may call for variations in their application. These principles are supplementary to the generally accepted conventional display criteria relating to instrument design, including location, size, contrast, quantization, and display-control compatibility.

- Operator Centered and Oriented Display - This is an extension of the inside-out display principle for integrated displays and favors a presentation with the aircraft position and orientation fixed in the display and the other pictorial information (horizon, glide-slope, hover point, velocity impact point, altitude reference, etc.) moving with respect to this reference.
- Geometric Real World Compatibility for Pictorial Displays - Although the integrated display is not in general a contact analog (and typically includes command and/or situation information not present in the VFR view), such pictorial information as is present should be compatible with a view of the real world situation. The integrated display is at its best when the information contained in it is perceived by the pilot as a single complex picture giving all the attitude and position information required, rather than as a densely packed code through which he can successively determine the aircraft flight path.
- "Status at a Glance" for Situation Displays - In keeping with geometric real world compatibility, the essential elements of the display must be clearly delineated by size, shape, or color and coordinated with respect to one another so that the status of the aircraft, especially in unusual attitudes, is immediately obvious and does not require element decoding.

- Predictive Capacity - In addition to indicating the current state of the aircraft, the integrated display must readily show the dynamic situation so that the future state can be easily surmised. This kind of information is necessary for lead generation in fast loops such as attitude control and for planning maneuvers in guidance or collision avoidance. Display quickening, explicit rate symbols, display prediction, and historical trail markers may all be used to this end, and should follow the practice of derivative information "leading" the variable on the display.
- Geometric Sensitivity and Scaling - The symbols and elements in an integrated display must move far enough and fast enough so that the pilot will be able to notice the motion and estimate its magnitude in performing the appropriate control response. Maximum range and desired pilot gain in each loop must be considered in scaling the integrated display elements for various phases of flight.
- Use of Digital Information Where Required - An exception to the pictorial compatible principle is in the display of information which is slowly varying and which must be read accurately over a large range. In this case, the judicious use of some digital presentations on the integrated display is appropriate. As a simple example, altitude may be displayed digitally; although altitude deviation from a glideslope is best handled by analog motion of lines in the display. The amount of digital information should be kept as small as possible, displayed only when necessary (perhaps on pilot demand), be legible, and contain as few digits as absolutely required.

These design principles were adhered to in the development of straw-man display format concepts for the implementation of Systems C and G designed and analyzed in the previous sections.

7.1 STRAW-MAN DISPLAY CONCEPT - PANEL LAYOUT

The general layout of the display panel is illustrated in Figure 7-1. Details of the ADI and HSI differ between Systems C and G. However, since both systems assume dependence upon a flight director, they are treated as integrated command displays rather than situation indicators. Although a full complement of flight instruments is anticipated, in this discussion we will concentrate only on the instruments essential for the flight control functions considered in the study and will therefore limit the consideration to the quantities displayed on the ADI, HSI and altimeter. The assumption is made that the pilot derives vertical rate information from the altimeter rather than from an IVSI in both Systems C and G.

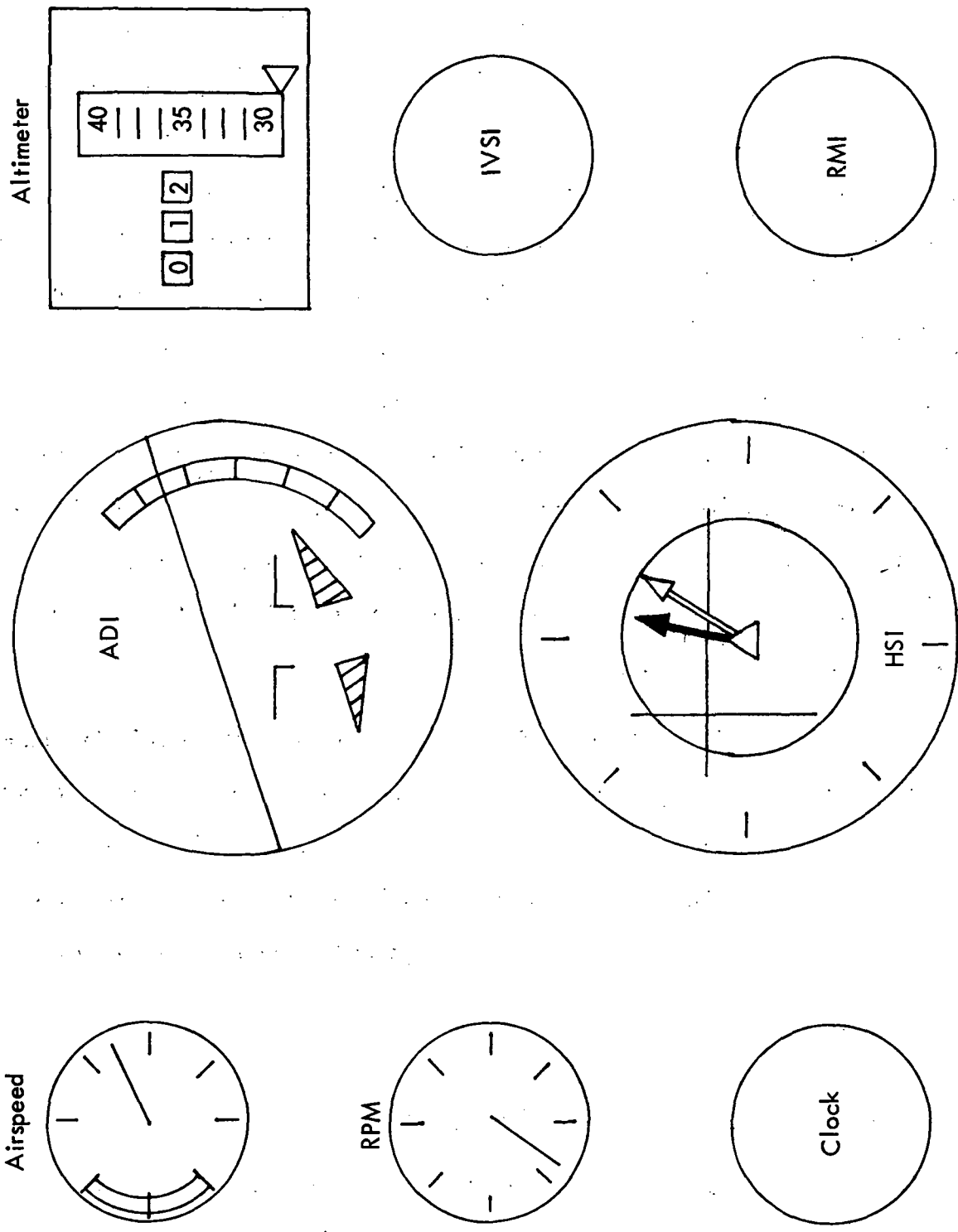


Figure 7-1. Straw-Man Display Concept - Panel Layout.

7.2 ATTITUDE DIRECTOR INDICATOR (ADI)

In System C the pilot's control task consists of primarily following the flight director commands for aircraft attitude and collective pitch. The ADI format shown in Figure 7-2 is based on the well accepted moving aircraft symbol flight director and artificial horizon ball with modifications for VTOL applications. Indicated and commanded roll angle are scaled one to one. Pitch angle is scaled to permit display of $\pm 5^\circ$ of pitch on the attitude ball permitting the pilot to resolve changes in pitch angle of less than 0.25 degrees. The turn rate indicator at the bottom of the ADI has the capability of including a commanded turn rate independent of the commanded roll angle if so desired. It also indicates lateral acceleration in the conventional manner. The additional indicators on the right side of the ADI are for use in the commanded collective for independent control of altitude. Consistent with the other elements of the flight director system is a pursuit display with commanded and actual collective stick indicated on either side of a fixed scale.

The principal difference in the ADI format for System G is the attitude information displayed on the right side of the instrument. The ADI as used in System G becomes strictly a secondary monitoring instrument for attitude and turn rate. The flight director symbols are normally not displayed, and as envisioned in System G, not utilized. The collective indicator on the right side of the ADI in System C is not required for System G.

7.3 HORIZONTAL SITUATION INDICATOR (HSI)

The HSI is discussed first for System G where it is used as one of the two principal command instruments for the pilot's direction. In System C the HSI is used

7 - 5

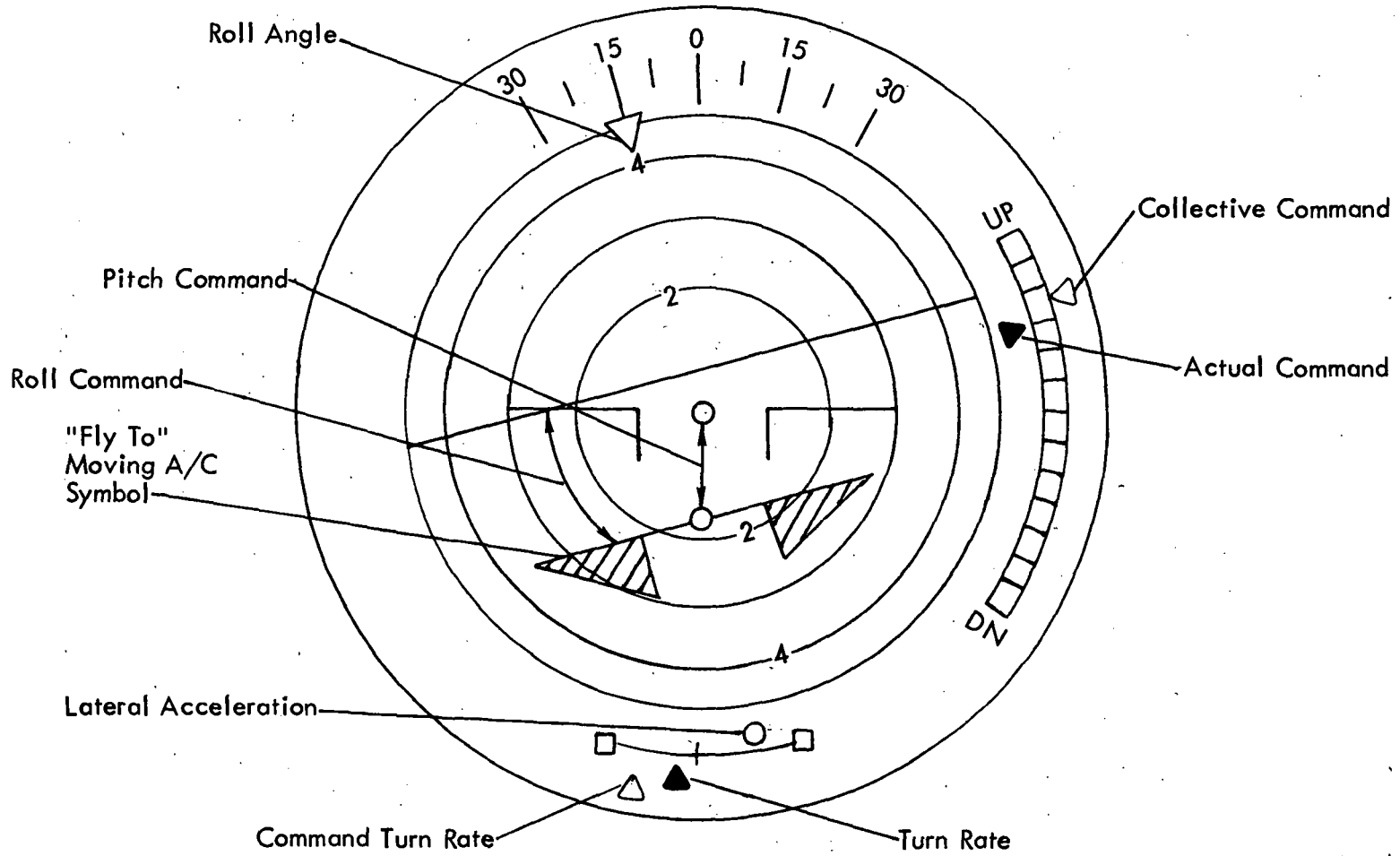


Figure 7-2. Straw-Man Display Concept - ADI Layout for System C.

as a secondary situation indicator only while the pilot flies the vehicle using attitude commands from the ADI. Consequently the HSI for System C will be simpler.

The HSI format shown in Figure 7-3 is a heading-up moving-map display with command information on required x and y velocity. The aircraft symbol in the center of the display is surrounded by range rings of a variable scale which may be set manually to a pre-selected sensitivity indicated by the number of feet for the first ring, or in an automatic mode. The automatic mode selects the scale sensitivity which is the highest possible one that does not place the landing pad off the screen. The landing pad indicator which is used principally in the final phases of descent does not move entirely off scale when a range sensitivity too great to permit it to be displayed is selected. Instead it is moved to the edge of the display and indicated with a semi-circle rather than a full circle, to indicate the relative direction to the pad. The compass rose fixed to the moving map indicates heading in the conventional manner for System G. A command heading bug is also available as a supplementary flight director output.

The pilot uses the HSI in System G principally as a horizontal velocity command display. The command velocity is shown as an open arrow with origin at the aircraft symbol, indicating both magnitude and direction of the commanded horizontal velocity. Full scale on the command velocity vector is taken as 100 kt. The actual velocity vector indicated by the solid arrow with origin at the aircraft symbol is the quantity directly controlled by the pilot's control stick in System G. To follow the flight director commands the pilot must line up the tip of the actual velocity vector with the command velocity vector. In this pursuit display the accuracy with which the alignment can be resolved is of the order of 2 percent of full scale or approximately 3 ft/sec which is greater than the assumed indifference thresholds for velocity. Small errors in

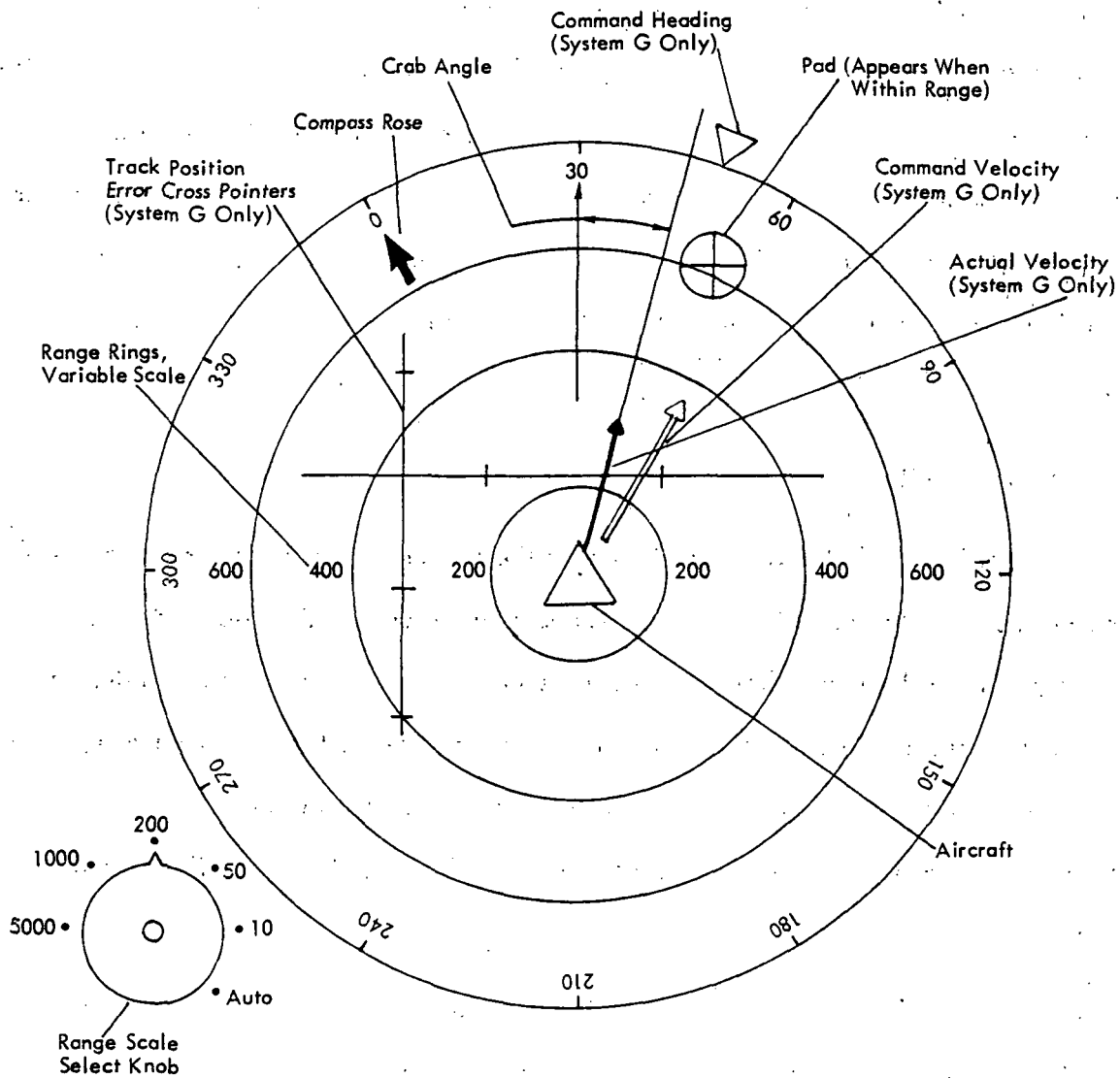


Figure 7-3. Straw-Man Display Concept - HSI Layout.

velocity matching, however, are detected by the rate of change of the track position error crosspointers.

When the aircraft is within 50 ft of the commanded position for hover or descent the crosspointers indicate cross-track and along-track position errors. Each ticmark is a nominal error of 25 ft. The crosspointers are not on the same scale as the moving map range rings and are used for a fine error adjustment on velocity control. They are consistent with the other flight director information in being a "fly-to" display in which the aircraft symbol is flown towards the intersection of the crosspointers in order to null the error. Drift of the crosspointers is the most sensitive indication of a lack of perfect alignment of the command velocity with the actual velocity.

7.4 ALTIMETER

In System G the altimeter is one of the principal flight director instruments enabling the pilot to use the vertical command to achieve the altitude hold or altitude track required by the flight director. At the same time, however, the altimeter must serve as an accurate situation indicator to indicate actual altitude for monitoring purposes in both Systems C and G. The solution to these conflicting demands of range and precision is a type of combined digital and moving tape display as illustrated in Figure 7-4.

The first three numerals are a digital display giving altitude in hundreds of feet. To the right is a moving tape giving altitude to the nearest foot. The portion of this tape centered within the viewing window is the actual altitude at the mid-point with a visible range of ± 10 ft. This accuracy of altitude information is available from the radar altimeter in the hover case. To eliminate difficulty of reading the moving tape, the information will be filtered at a corner frequency of about 1 Hz prior to being

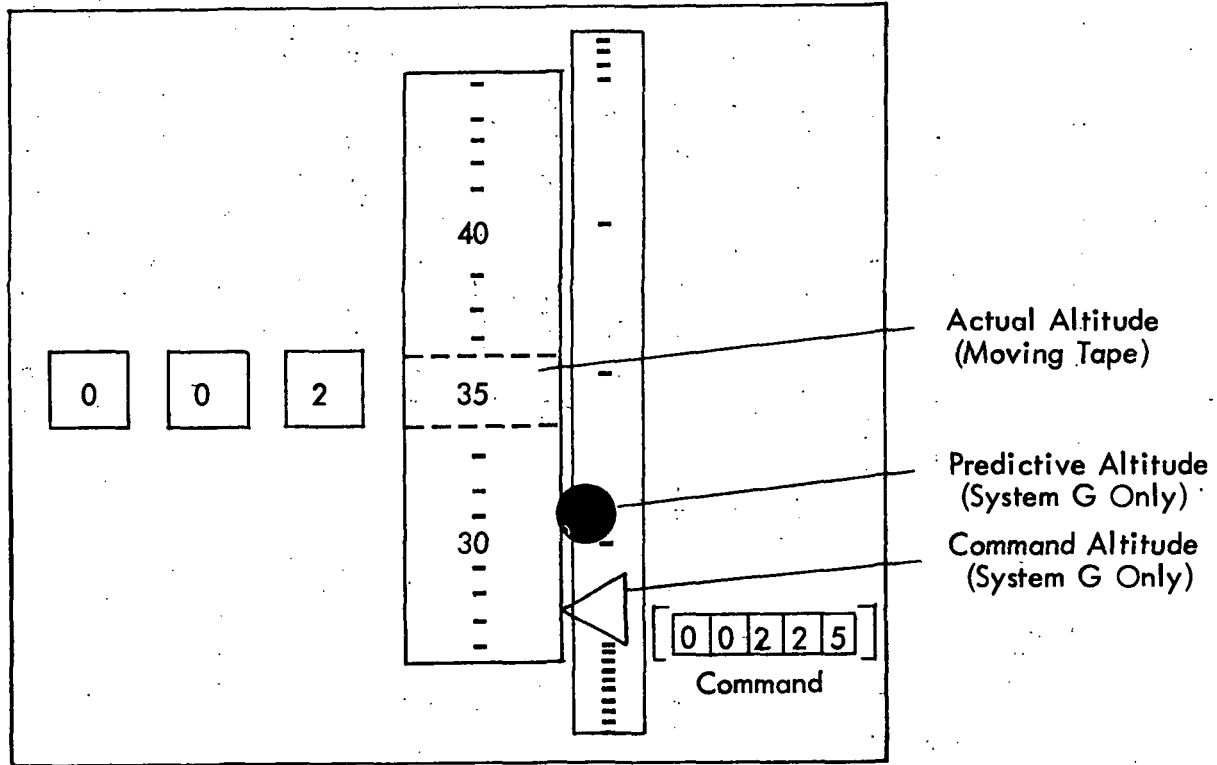


Figure 7-4. Straw-Man Display Concept - Altimeter Layout.

displayed. Altitude rate is not assumed to be displayed explicitly on an IVSI in these systems, but rather is assumed to be determined by the pilot implicitly from the altimeter. This is particularly easy for low altitude rates using the moving tape which moves upward or downward at a speed proportional to altitude rate. (Transfer of a numeral through the moving tape window in one second indicates a 20 ft/sec ascent or descent rate. Drift of less than 0.25 ft/sec will be observable).

The commanded altitude is indicated in System G in two ways: by a numerical six-digit command which is set either manually for an altitude hold or by the flight director system for control descent, and by a command altitude bug which moves up and down to the right of the altitude moving tape. The command bug is at the same scale as the moving tape altimeter when the commanded altitude is within ± 10 ft of the actual altitude; however, the command altitude bug moves over a vastly reduced scale (approximately 100 ft per division) when the commanded altitude is more than 10 ft above or below the actual altitude. The predictive altitude symbol shown by a solid circle is controlled directly by the vertical control stick in System G. The pilot's task is to place the predictive altitude indicator at the same point as the command altitude bug. In the situation indicated in Figure 7-4, for example, the pilot would press down on the vertical control stick to move the predictive altitude indicator down to the level of the command altitude bug which is indicating a commanded altitude of 00225 ft. The predictive altitude and command altitude indicators would both move up until they are aligned with 00225 in the center of the tape window.

The altimeter layout is the same for System C with the exception that the predictive altitude indicator, command altitude bug and command altitude numeric display are not present.

SECTION 8

SUMMARY AND CONCLUSIONS

This section presents a summary of the principal accomplishments achieved during this effort and a review of the most significant results. The next section will contain some suggestions for additional research and experimental investigations based on the study results.

The primary accomplishment of this investigation has been the development of a systematic design methodology for pilot displays in advanced VTOL aircraft for commercial operations. This design approach accounts for various levels of control automation and display sophistication. It is based on the optimal control model for the human operator, but includes several significant extensions in the state-of-the-art of pilot modeling. An explicit attention allocation procedure has been established which determines the optimal division of the pilot's total attention between monitoring and control tasks, and among the various displays available to him for each task.

The design methodology separates the model into three levels of detail. At the "information level," all of the state variables are assumed to be perfectly displayed to the pilot. Thus, the pilot has perfect knowledge of each state variable and his allocation of attention among these indicates their relevant importance in the ideal situation. At the display element level the effects of pilot indifference thresholds are introduced, and the pilot's ability to detect both position and rate from a given display element is included. At this level the relative importance of each display element is determined, and a more realistic estimate of the overall system performance is obtained. Finally, at the "display format level" realistic performance estimates due to display thresholds, maximum deflections, instrument noise, scan frequency, etc. are determined for an actual display format which has been designed from the display element results.

The design methodology includes a model for simultaneous monitoring and control, which is based on the premise that the pilot first attempts to control the aircraft to a given level of performance, and then uses any additional capability for monitoring status information and/or automatic system performance. The model uses as a metric for control performance a quadratic function of the state errors. The control workload metric is the pilot's total control attention to all the displayed elements that is required to achieve a desired level of system performance. The model optimizes the control performance metric by allocating his total control attention among the available displayed elements. Then his available attention for monitoring is determined as the difference between his total capacity and that required for control to the given performance level. The model next determines the optimum allocation of monitoring attention among the available status displays and the overall monitoring performance metric which is a quadratic index similar to the control performance metric.

In summary, the VTOL display/control design methodology is:

- Determine $(x_i)_{\max}$ and $(J_c)_{\max}$ from mission requirements.
- Select candidate control systems.
- Calculate J_c vs f_c at the information level for each control system (include director/steering commands).
- Choose display elements.
- Calculate J_c vs f_c at the display element.
- Determine $f_m = f_{TOT} - f_c$ and J_m from monitoring model.
- Select display/control system.
- Select display format candidates.
- Determine J_c, J_m vs f_c for each format.
- Select display format.

A computer program entitled PIREP has been developed to implement the extended optimal control/monitoring model for the pilot. It can be used at the informa-

tion level, at the display element level, or at the display format level, to determine the optimal allocation of pilot's attention for either monitoring or control, as well as the associated system performance. The principal inputs of PIREP are the system dynamics (automation level, external disturbances, etc.), the display model (display elements, threshold, etc.), and the total attention (control/monitoring). The primary outputs of PIREP are the optimum attention allocation (control/monitoring), the system performance metrics (J_c , J_m , cost gradients), and the rms predictions (state, display, control).

The extended optimal control model for the pilot was validated by attempting to reproduce flight results obtained by NASA/LaRC with the CH-46 tandem rotor helicopter. Descriptions of the CH-46 model-following control system, evaluation display panel, and the flight director algorithms were obtained from NASA publications. The optimal control model was exercised at the display format level for a hover flight condition and the results were compared with limited flight data. Both the analytical and experimental results show that the pilot could not adequately hover without the flight director, but that he had very little difficulty with the flight director.

A flight director design technique using quadratic synthesis was developed as a straightforward means of generating flight director algorithms. These algorithms were designed to relate to the pilot task objectives, to minimize his workload and/or improve his control performance, and to satisfy the pilot's desired goal of behaving approximately as a gain and time delay. The flight director signals are obtained as linear functions of the system states as a direct fallout from the optimal control model. When applied to the CH-46 helicopter, the flight director design technique produced nearly identical time constants to those of the empirically determined flight director algorithms used by NASA/LaRC.

A similar approach using quadratic synthesis was applied to determine flight control automation levels for the helicopter. By appropriately specifying the control

and state weights in a quadratic performance index, various levels of automatic feedback control systems can be systematically designed. These range from a totally manual basic vehicle with no feedback to the fully automatic system with complete position feedback.

The display/control design methodology was then applied to predict the performance of the LaRC CH-47 helicopter which will be used as the VALT research aircraft. Two flight conditions were investigated, hover at sea level and an approaching condition at 60 knots and 1,000 ft/min. descent. Seven levels of control automation were considered:

- Basic system without any feedback
- Pitch-rate feedback
- Pitch-attitude feedback
- Pitch-attitude and vertical speed feedback
- Pitch-attitude and vertical position feedback
- Forward-speed and vertical position feedback
- Full position feedback.

Five display system levels were also considered:

- Information Level
- Element level with no flight director
- Element level with vertical flight director
- Element level with horizontal flight director
- Element level with vertical and horizontal flight director.

Cost weighting functions and indifference thresholds for the CH-47 were selected based on the desired performance requirements for an advanced VTOL commercial helicopter.

In general, the numerical results indicated that the flight director does improve system performance. Although this is a fairly obvious and expected result, the model does

provide quantitative indications of the performance improvement with the flight director. The results also showed that the vertical flight director provides marginal performance improvement; most of the performance gain is produced by the forward flight director. The CH-47 results also showed that control automation generally improves performance. Again, this is an obvious and expected conclusion, but the model provides quantitative measures of the performance improvement for various automation systems. Moreover, in order to achieve the desired system performance, some level of automation will be required for most advanced VTOL missions. The numerical results showed that at hover and approach the CH-47 helicopter without control automation cannot be flown to an acceptable performance level. They also indicated that the hover condition is considerably more difficult than the approach. However, increasing system automation tends to reduce the difference in difficulty between the two flight conditions. Also, the more automatic systems tend to be less sensitive to pilot workload variations; as automation increases, the slope of the performance curve versus workload is lower. This means that other temporary demands on the pilot's attention will cause less deterioration in system performance as automation increases.

A fixed-gain flight director was used to examine the effects of changing flight conditions on system performance. This flight director used the average of the hover and approach gains and was examined at both flight conditions for two automation levels. At the lower automation level, the fixed-gain flight director was no better (perhaps slightly worse) than no flight director at all; whereas in the other case, the fixed-gain flight director performance lay about mid-way between the optimum flight director and no flight director. From this limited examination, it appears that in general the flight director gains will probably have to be adjustable to handle a wide range of flight conditions.

The relative importance of the individual display elements was clearly demonstrated for all display sophistication and control automation levels. The model provides a quantitative measure of the relative importance of each display element by means of the optimum attention allocation. For example, at a given level of control automation and control attention, the information level results show that the pilot is far more interested in forward and vertical velocities and pitch rate than he is in the position and attitude elements. As the display sophistication increases -- that is as vertical, forward, and full-flight director signals are provided -- he spends less attention on the situation displays and more on the flight director signals. Similarly, as system automation increases for a given display configuration, the pilot adjusts his attention accordingly. For example, as pitch-rate feedback and pitch-attitude feedback are included, he spends less time on the pitch display and more time on the position display.

The monitoring model confirms the a priori conjecture that more monitoring generally improves system performance, since more monitoring time implies less control workload. However, it is interesting to note that monitoring performance itself does not necessarily improve either with increased system automation or with display sophistication. Several questions still remain regarding the interpreting of the monitoring model and merging the monitoring results with the control results.

The actual design of a display format is still far more of an art than a science. However, there are several design principles that should be used to simplify the translation of display element analytical results to the instrument format:

- Operator Centered and Oriented Displays
- Geometric Real-World Compatibility for Pictorial Displays
- "Status at a Glance" for Situation Displays
- Predictive Capacity

- Geometric Sensitivity and Scaling
- Digital Information Where Required

Using these principles, a straw-man display concept was designed in an attempt to satisfy the results of the optimal control/monitor model for the CH-47 with two levels of control automation. These control systems were pitch-attitude feedback with no vertical feedback and velocity command with altitude hold. The three primary instruments of interest for both cases are: the attitude director indicator (ADI), the horizontal situation indicator (HSI), and the altimeter. For the pitch-attitude feedback system, the ADI provides all four flight director commands in addition to pitch and roll attitude information, while the HSI and the altimeter provide accurate situation information. For the velocity command system, however, the ADI is primarily a monitoring instrument and provides no flight director commands, while the HSI and the altimeter provide the principal flight director commands as well as situation information.

SECTION 9

RECOMMENDATIONS

During the course of the study, several areas have been identified in which additional research is needed to define, test and validate the use of the pilot in an automated VTOL aircraft operated as a short-haul commercial aircraft. These subject areas are outlined below.

9.1 COMBINED LATERAL AND LONGITUDINAL ANALYSIS

The pilot/vehicle/control system models, computer programs and design procedures developed in the study should be utilized to conduct a combined lateral and longitudinal analysis of pilot/automatic system task allocation for the VALT Project CH-47 helicopter. Such an analysis will extend the results obtained in the present study and will investigate a number of flight conditions including hover, straight-in approach, turning approach and cruise phases of flight. Effects of wind gusts and wind shears should be included in the analysis. Different levels of control automation ranging from fully automatic to fully manual should be investigated. Consideration should be given to use of an advanced stability augmentation system such as that designed for the VALT Project CH-47 helicopter. The work effort under this task would culminate in a recommended display/control system concept for the CH-47.

9.2 MONITORING MODEL INVESTIGATION

The investigation of the monitoring model developed in the study for varying levels of automation should be extended. This effort would utilize the model to determine the monitoring attention allocation to each of the primary instruments, and to the longitudinal and lateral axes. Analysis and interpretation of the monitoring model results obtained should then be conducted to determine 1) the effects of different monitoring strategies (i.e., current status or future status) on attention allocation and 2) the extent to which attention used for control (f_c) can also be used for monitoring.

9.3 EFFECTS OF SYSTEM FAILURES ON THE PILOTING TASK

The effects of system failures on the piloting task should be investigated. Representative failure modes should be defined (i.e., actuator failure, sensor failure, etc.) consistent with the generic augmentation systems. The optimal control model developed in the study should then be utilized to examine the pilot control workload and performance under the assumed failure mode conditions. For example, results could be obtained that indicate whether a flight director designed for a velocity command system can be used when that augmentation system fails. Consideration should be given to investigation of transient conditions to determine the time required by the pilot to recover from different assumed failures.

9.4 FIXED-BASE SIMULATION EXPERIMENTS

A series of fixed-base pilot-in-the-loop simulation experiments should be planned and conducted to 1) validate the extensions in the pilot model accomplished during the initial phase of the study and 2) evaluate and verify the display/control system concept for the CH-47. The experiments should be conducted initially on a relatively simple and inexpensive interactive display facility such as a PDP-11/10 and on the NASA VALT fixed-base display research facility with a good cross section of subject pilots. Consideration should be given to experiments for measuring the performance differences and subjective differences between integrated displays and separate displays. Based on the results of the experiments, methods for representing appropriate changes in the analytical model should be made. Experiments to measure monitoring strategies in the simulation should be included to determine whether the pilot actually uses a normative strategy (i.e., how he should do it) as represented in the present model.

9.5 PILOT INTERACTION WITH AUTOMATIC SYSTEMS

The pilot's interaction with an automatic system has been only briefly addressed by control theory models. Studies of this interaction should be conducted to include factors such as pilot acceptance of the system; the "harmony" of the system (does it respond the way the pilot thinks he would?); does the pilot interact with the system by monitoring a closed-loop system or by "controlling" the open-loop system? Actuator movement information can be presented to the pilot by dedicated displays, or by control stick motion. In one case only visual information is presented (actuator monitoring is done through the visual channel); and in the other case the monitoring is done through the kinesthetic channel (thus allowing more time to visually monitor other displays). The model should be examined to see whether differences in failure detection times using these two methods can be accurately represented by the model.

REFERENCES

1. Hoffman, W. C.; Hollister, W. M.; and Howell, J. D.: Navigation and Guidance Requirements for Commercial VTOL Operations. Aerospace Systems, Inc. Interim Technical Report, ASI-TR-74-17, NASA CR 132423, January 1974.
2. Hoffman, W. C.; and Hollister, W. M.: Navigation and Guidance Requirements for Commercial VTOL Operations - Navigation System Sensitivity Analysis. Aerospace Systems, Inc. Interim Technical Report, ASI-TR-75-25, May 1975.
3. Hoffman, W.C.; and Hollister, W. M.: A Spiral Guidance Approach Concept for Commercial VTOL Operations. Aerospace Systems, Inc. Technical Report, ASI-TR-75-21, March 1975.
4. Curry, R. E.; Kleinman, D. L.; and Hoffman, W. C.: A Model for Simultaneous Monitoring and Control. Paper presented at Eleventh Annual Conference on Manual Control, NASA Ames Research Center, May 1975.
5. Kleinman, D. L.; Baron, S.; and Levison, W. H.: An Optimal Control Model of Human Response, Part I: Theory and Validation. Automatica, 1970, Vol. 6, pp. 357-369.
6. Kleinman, D. L.; Baron, S.; and Levison, W. H.: A Control Theoretic Approach to Manned-Vehicle Systems Analysis. IEEE Trans. Auto. Control. Vol. AC-16, No. 6, December 1971, pp. 824-832.
7. Levison, W. H.: A Model for Task Interference. Proceedings of the Sixth Annual Conference on Manual Control, April 1970, pp. 585-616.
8. Weir, D.H.; Klein, R. H.; and McRuer, D. T.: Principles for the Design of Advanced Flight Director Systems Based on the Theory of Manual Control Displays. NASA Cr-1748, March 1971.
9. Baron, S.; and Levison, W. H.: A Manual Control Theory Analysis of Vertical Situation Displays for STDL Aircraft. Bolt Beranek and Newman, Inc. Report No. 2484, April, 1973.
10. Chen,; Lebacqz,; and Aiken: A Preliminary Look at Flight Director Design Philosophies for Application to a VTOL Landing Approach Flight Experiment. Proceedings of the Tenth Annual Conference on Manual Control, April 9-11, 1974.
11. Kleinman, D. L.; and Baron, S.: Manned-Vehicle Systems Analysis by Means of Modern Control Theory. NASA CR-1753, June 1971.
12. Garren, J. F., Jr.; Kelly, J. R.; Sommer, R. W.; and DiCarlo, D. J.: Flight Investigation of VTOL Control and Display Concept for Performing Decelerating Approaches to an Instrument Hover. NASA TN D-6108, February 1971.
13. Senders, J. W.: The Human Operator as a Monitor and Controller of Multi-Degree of Freedom Systems. IEEE Trans. on Human Factors in Electronics, HFE-5, No. 1, September 1964.

14. Senders, J. W.; Ward, J. L.; and Carbonell, J. R.: Human Visual Sampling Processes: A Simulation Validation Study. NASA-CR-1258, January 1969.
15. Senders, J. W.; Elkind, J. I.; Grignetti, M. C.; and Smallwood, R.: An Investigation of the Visual Sampling Behavior of Human Observers. NASA Report No. CR-434, April 1966.
16. Gai, E.: Psychophysical Models of Signal Detection with Time Varying Stimuli. Ph. D. Thesis, Dept. of Aeronautics and Astronautics, M.I.T., 1974.
17. Kelly, J. R.; Niessen, F. R.; and Sommer, R. W.: Evaluation of a VTOL Flight-Director Concept During Constant-Speed Instrument Approaches. NASA TN D-5860, June 1970.
18. Kelly, J. R.; Niessen, F. R.; Thibodeaux, J. J.; Yenni, K. R.; and Garren, J. F., Jr.: Flight Investigation of Manual and Automatic VTOL Decelerating Instrument Approaches and Landings. NASA TN D-7524, July 1974.
19. Kleinman, D. L.; and Killingsworth, W.: A Predictive Pilot Model for STOL Aircraft Landing. NASA CR-2374, March 1974.
20. Young, L. R.: Integrated Display Principles and Some Applications to V/STOL Aircraft. AGARD Conference Proceedings No. 96 on Guidance and Control Displays, Oct. 1971.
21. Kleinman, D. L.: Optimal Control of Linear Systems with Time Delay and Observation Noise. IEEE Trans. Autom. Control, Vol. AC-14, No. 5, October 1969.
22. Kleinman, D. L.: Suboptimal Design of Linear Regulator Systems. MIT-ESL-R-297, February 1967.
23. Bartels, R. H.; and Stewart, G. W.: Solution of the Matrix Equation $AX + XB = C$. Comm. of ACM, Vol. 15, No. 9, September 1972.
24. Press, H.; Meadows, M. J.; and Hodlack, I.: A Reevaluation of Data on Atmospheric Turbulence and Airplane Gusts Loads for Application in Spectral Calculations. NACA Report 1272, 1956.
25. Schlundt, R. W., et al.: STOL Traffic, Environment and Operational Procedures. R-717, C. S. Draper Laboratory, March 1972.

BIBLIOGRAPHY

1. Adams, G. D.: V/STOL Approach System Flight Tests: Final Report. FAA Report No. RD-66-95, December 1966.
2. Allen, R. W.; Clement, W. F.; and Jex, H. R.: Research on Display Scanning, Sampling, and Reconstruction Using Separate Main and Secondary Tracking Tasks. NASA Report CR-1569, Washington, D. C., July 1970.
3. Anon.: Space Vehicle Displays Design Criteria. NASA Space Vehicle Design Criteria (Guidance and Control), NASA SP-8086, March 1972.
4. Anon.: Theoretische und experimentelle Untersuchungen von Verfahren ein Kombiniertes Navigations- und Allwetter-Landesystem (KNL) für V/STOL Flugzeuge. Teldix Luftfahrt-Ausrüstungs-GmbH, Heidelberg, Germany, June 1967.
5. Anon.: V/STOL Displays for Approach and Landing. AGARD Report 594, 1972.
6. Ashkenas, I. L.; and McRuer, D. T.: A Theory of Handling Qualities Derived from Pilot-Vehicle System Considerations. Aerospace Eng., 1962, Vol. 21, No. 2, pp. 60, 61, 83-102.
7. Baron, S.: Analysis of Response to Wind-Shears Using the Optimal Control Model of the Human Operator. Proceedings of 9th Annual Conference on Manual Control, May 1973, pp. 419-428.
8. Baron, S., et al.: Application of Optimal Control Theory to the Prediction of Human Performance in a Complex Task. AFFDL TR-69-81, March 1970.
9. Baron, S.; and Kleinman, D. L.: The Human as an Optimal Controller and Information Processor. IEEE Trans. Man-Machine Sys., Vol. MMS-10, March 1969, pp. 9-17.
10. Baron, S.; and Levison, W. H.: A Display Evaluation Methodology Applied to Vertical Situation Displays. Proceedings of 9th Annual Conference on Manual Control, May 1973, pp. 121-132.
11. Bergstrom, B.: Interpretability Studies of Electronic Flight Instruments. Saab Aktiebolag, Linkoping, Sweden. Saab TN 61, January 1967.
12. Bondurant, R. A., III; and Kearns, J. H., III: V/STOL Vertical Situation Display. Paper presented at the SAE National Aeronautics and Space Engineering Meetings, Los Angeles, CA, Society of Automotive Engineers. Paper No. 690694, October 1969.
13. Clement, W. F.; Hofman, L. G.; and Graham, D.: A Direct Procedure for Partitioning Scanning Workload in Control Display System Design. Proceedings of 9th Annual Conference on Manual Control, May 1973, pp. 389-400.

14. Clement, W. F.; and Hofman, L. G.: A Systems Analysis of Manual Control Techniques and Display Arrangements for Instrument Landing Approaches in Helicopters, Vol. 1: Speed and Height Regulation. JANAIR Report 690718, Systems Technology, Inc. Tech. Report 183-1, July 1969.
15. Clement, W. F.; McRuer, D. T.; and Klein, R. H.: Systematic Manual Control Display Design. AGARD Conference Proceedings No. 96 on Guidance and Control Displays, October 1971.
16. Dunham, R. E.; and Sommer, R. W.: Evaluation of a Moving-Graph Instrument Display for Landing Approaches With a Helicopter. NASA TN D-6025, October 1970.
17. Elkind, J. I.: Characteristics of Simple Manual Control Systems. MIT Lincoln Laboratory, Tech. Report III, April 1956.
18. Etkin, B.: Dynamics of Flight: Chapter 10, Flight in Turbulent Air. Wiley & Sons, New York, 1962.
19. Garren, J. F., Jr.; and Kelly, J. R.: Description of an Analog Computer Approach to V/STOL Simulation Employing a Variable-Stability Helicopter. NASA TN D-1970, January 1964.
20. Garren, J. F.: VTOL Flight Investigation to Develop a Decelerating Instrument Approach Capability. SAE Paper 690693, October 1969.
21. Garren, J. F., et al.: Flight Investigation of VTOL Control and Display Concept for Performing Decelerating Approaches to an Instrument Hover. National Aeronautics and Space Administration, NASA Technical Note TN D-6108, February 1971.
22. Gracey, W., et al.: Evaluation of Cross-Pointer-Type Instrument Display in Landing Approaches With a Helicopter. NASA TN D-3677, November 1966.
23. Gracey, W.; Sommer, R. W.; and Tibbs, D. F.: Evaluation of a Moving-Map Instrument Display in Landing Approaches With a Helicopter. NASA TN D-3986, May 1967.
24. Gracey, W.; Sommer, R. W.; and Tibbs, D. F.: Evaluation of a Closed-Circuit Television Display in Landing Operations With a Helicopter. NASA TN D-4313, February 1968.
25. Gracey, W.: Comparison of Information Display Concepts for Landing of VTOL Aircraft. NASA Technical Note TN D-4861, November 1968.
26. Hoffman, W. C.; Zvara, J.; and Bryson, A. E.: Automatic Guidance Concept for VTOL Aircraft. J. Aircraft, Vol. 8, No. 8, August 1971, pp. 637-642.
27. Hofman, L. G.; Clement, W. F.; and Blodgett, R. E.: Further Examination of Pilot Instrument Scanning Data and Development of a New Link Value Estimator. Proceedings of 9th Annual Conference on Manual Control, May 1973, pp. 379-388.

28. Hollister, W. M., et al.: Effect of the City Center Environment on VTOL Terminal Operations. American Helicopter Society Preprint No. SW-70-48, Presented at the Joint Symposium on Environmental Effects on VTOL Designs, Arlington, Texas, November 1970.
29. Illingworth, J. K. B.; and Shazler, J. E.: Blink Flying of V/STOL Aircraft, With Particular Reference to Takeoff and Landing. AGARD Report, June 1960.
30. Kelly, J. R.; Garren, J. F., Jr.; and Deal, P. L.: Flight Investigation of V/STOL Height-Control Requirements for Hovering and Low-Speed Flight Under Visual Conditions. NASA TN D-3977, May 1967.
31. Ketchel, J. M.; and Jenny, L. L.: Electronic and Optically Generated Aircraft Displays: A Study of Standardization Requirements. JANAIR Report No. 680505, May 1968.
32. Kleinman, D. L.: Optimal Control of Linear Systems With Time-Delay and Observation Noise. IEEE Trans. Auto. Control, Vol. AC-14, October 1969, pp. 524-527.
33. Kleinman, D. L.; and Baron, S.: Manned Vehicle Systems Analysis by Means of Modern Control Theory. Bolt, Beranek and Newman, Inc., BBN Report 1967, June 1970.
34. Kornstadt, H. J.; and Pfennigstorf, J.: Evaluation of an Integrated Flight Display for the Manual IFR Landing of VTOL Aircraft. AGARD Conference Proceedings No. 96 on Guidance and Control Displays, October 1971.
35. Levison, W. H.; Baron, S.; and Kleinman, D. K.: A Model for Human Controller Remnant. IEEE Trans. Man-Mach. Syst., 1969, MMS-10, pp. 101-108.
36. Levison, W. H.: The Effects of Display Gain and Signal Bandwidth on Human Controller Remnant. Report No. AMRL-TR-70-93, Aerospace Medical Research Laboratory, Wright-Patterson Air Force Base, Dayton, Ohio, March 1971.
37. Levison, W. H.; Elkind, J. I.; and Ward, J. L.: Studies of Multivariable Manual Control Systems: A Model for Task Interference. NASA Report CR-1746, Washington, DC, May 1971.
38. Levison, W. H.; and Tanner, R. B.: A Control-Theory Model for Human Decision-Making. NASA CR-1953, December 1971.
39. McRuer, D. T.; and Jex, H. R.: A Review of Quasi-Linear Pilot Models. IEEE Trans. Human Factors Electronics, 1967, HFE-8, pp. 231-249.
40. McRuer, D.; and Weir, D. H.: Theory of Manual Vehicular Control. IEEE Trans. Man-Mach. Syst., 1969, MMS-10, Vol. 4, pp. 257-291.

41. Murphy, M. R., et al.: Simulator Evaluation of Three Situation and Guidance Displays for V/STOL Zero-Zero Landings. Presented at 10th Annual Conference on Manual Control (Wright-Patterson Air Force Base), April 1974.
42. NASA Langley Research Center: VTOL & STOL Technology in Review. *Astronautics & Aeronautics*, Vol. 6, No. 9, September 1968, pp. 56-67.
43. Reeder, J. P.: The Impact of V/STOL Aircraft on Instrument Weather Operations. NASA TN D-2702, February 1965.
44. Reeder, J. P.: The Changing World of the Pilot in the Next Decade - V/STOL Aircraft Operations. Paper presented at the Human Factors Society National Symposium, San Francisco, CA, October 1970.
45. Ringland, R. F.; Stapleford, R. L.; and Magdaleno, R. E.: Motion Effects on an IFR Hovering Task - Analytical Predictions and Experimental Results. *Systems Technology, Inc. Tech. Report 188-1*, October 1970.
46. Russel, L.: Characteristics of the Human as a Linear Servo Element. M.D. Thesis, MIT Dept. Elec. Eng., May 1951.
47. Seckel, E., et al.: A Note on the Effect of Helicopter Dynamics on Steep Instrument Approaches. Report No. 600, Department of Aeronautical Engineering, Princeton University, February 1962.
48. Simpson, R. W.; and Miller, R. H.: V/STOL in the Northeast Corridor. *Astronautics & Aeronautics*, September 1968.
49. Simpson, R. W.: The Outlook for Future Commercial VTOL Transportation. AIAA Paper No. 69-198, AIAA/AHS VTOL Research, Design, and Operations Meetings, Georgia Institute of Technology, Atlanta, Georgia, February 17-19, 1969.
50. Sommer, R. W.; and Dunham, R. E.: Evaluation of a Contact-Analog Display in Landing Approaches With a Helicopter. NASA TN D-5241, June 1969.
51. Stepniewski, W. Z.; and Schmitz, F. H.: Possibilities and Problems of Achieving Community Noise Acceptance of VTOL. Presented at the Eighth Congress of the ICAS, Amsterdam, September 1972.
52. Sweeney, J. S.; and Runner, G.: A Comparison of Quickened and Unquickened Displays for the Monitoring of Vehicle Performance Under Full Automatic Control. Proceedings of the IEEE International Congress on Human Factors in Electronics, Long Beach, May 1962.
53. Trant, J. P.; and Algranti, J. S.: Investigation of VTOL Approach Methods by Use of Ground-Controlled-Approach Procedures. NASA TN D-1489, October 1962.
54. Van Houtte, N. A. J.: Display Instrumentation for V/STOL Aircraft in Landing. Ph.D. Thesis, MIT Dept. of Aeronautics and Astronautics, June 1970.

55. Vreuls, D., et al.: All-Weather Landing Flight Director and Fault Warning Display Simulator Studies. Proceedings of Fifth Annual Symposium: Human Factors in Aviation, 1968 (Los Angeles), June 1968.
56. Walters, D. J.; and Bayer, R.: V/STOL Displays for Approach and Landing. AGARD Conference Proceedings No. 96 on Guidance and Control Displays, October 1971.
57. Weir, D. H.; and Johnson, W. A.: Pilot Dynamic Response to Sudden Flight Control System Failures and Implications for Design. NASA Report CR-1087, Washington, DC, 1968.
58. Winn, A. L.; and Lewis, R. B., II: Pilot Workload During Instrument Flight. American Helicopter Society, Preprint No. 820, May 1974.
59. Winter, F. J., Jr.: Controls and Displays for Helicopter IFR Operation - Pilot Factor Considerations. American Helicopter Society, Preprint No. 825, May 1974.
60. Wolf, J. D.; and Barrett, M. F.: IFR Steep-Angle Approach: Effects of System Noise and Aircraft Control-Augmentation Variables. JANAIR Report No. 700810, April 1971 (AD 724 336).
61. Wolf, J. D.: Display and Related System Requirements for IFR Steep Approach. Honeywell, Inc. (St. Paul), AD-736 247, January 1972.
62. Wolkovitch, J.; LaMont, C. W.; and Lochtie, D. W.: Fundamental Limitations on V/STOL Terminal Guidance Due to Aircraft Characteristics. NASA CR-1901, National Aeronautics and Space Administration, Washington, DC, December 1971.
63. Youens, F. P.: Approach and Landing Problems in Jet VTOL Aircraft. AGARD Report 489, October 1964.
64. Young, L. R., et al.: The Adaptive Dynamic Response Characteristics of the Human Operator in Simple Manual Control. NASA TN D-2255, April 1964.

APPENDIX A

EQUATIONS FOR THE OPTIMAL CONTROL MODEL FOR THE HUMAN OPERATOR

A.1 BACKGROUND

The human operator's basic task is to control, in some prescribed way, a dynamical system that is subject to external random disturbances. It is assumed that the system dynamics, which may include actuator, sensor, and noise dynamics, are described by the linear, time invariant equations of motion.

$$\dot{x}(t) = Ax(t) + Bu(t) + w(t) \quad (A-1)$$

where the n -vector $x(t)$ represents the vehicle state, $u(t)$ is the human's control input to the system, and where $w(t)$ represents random external disturbances, $w(t)$ is assumed to be a vector of independent zero-mean, Gaussian white noises with autocovariance

$$E \{w(t)w'(\sigma)\} = W \delta(t - \sigma). \quad (A-2)$$

In controlling the vehicle, the human perceives a delayed, noisy replica of the m displayed outputs $y = Cx(t) + Du(t)$. Thus,

$$y_p(t) = Cx(t - \tau) + Du(t - \tau) + v_y(t - \tau). \quad (A-3)$$

It is assumed that the control task is adequately reflected in the human's choice of a feedback control $u(\cdot)$ which, in the steady-state, minimizes the general quadratic cost functional

$$J(u) = E \left\{ \lim_{T \rightarrow \infty} \frac{1}{T} \int_0^T y'(t) Q_y y(t) + \dot{u}(t) Q_r \dot{u}(t) dt \right\} \quad (A-4)$$

It has been shown that the control which minimizes $J(u)$, conditioned on the observations $y_p(\cdot)$, is generated by the linear feedback law

$$T_N \dot{u}(t) + u(t) = -L \hat{x}(t) = u_c(t) \quad (A-5)$$

where $\hat{x}(t)$ is the best estimate of the system state $x(t)$ based on the observed data $y_p(\sigma), \sigma \leq t$. The matrices T_N and L are obtained as

$$\begin{aligned} T_N &= P_{22}^{-1} Q_r \\ L &= P_{22}^{-1} P'_{12} \end{aligned} \quad (A-6)$$

where

$$P = \begin{bmatrix} P_{11} & P_{12} \\ P'_{12} & P_{22} \end{bmatrix}$$

satisfies the Riccati equation

$$0 = P A_o + A_o' P + \tilde{Q} - P B_o Q_r^{-1} B_o' P \quad (A-7)$$

where

$$A_o = \begin{bmatrix} A & B \\ 0 & 0 \end{bmatrix} \quad B_o = \begin{bmatrix} 0 \\ 1 \end{bmatrix} \quad \tilde{Q} = \tilde{C}' Q_y \tilde{C}$$

and $\tilde{C} = [C : D]$

Note that the Control Equation (A-5) can also be written as

$$\dot{u} = -L_1 \begin{bmatrix} \hat{x} \\ u \end{bmatrix}$$

where

$$L_1 = Q_r^{-1} B_o' P = \begin{bmatrix} Q_r^{-1} P_{12} & Q_r^{-1} P_{22} \end{bmatrix} = \begin{bmatrix} T_N^{-1} L & T_N^{-1} \end{bmatrix}$$

The human operator injects noise into the generation of the control input.

In the model, a Gaussian white noise $v_m(t)$ is added directly to the "commanded control" $u_c(t)$ in Equation (A-5) with covariance

$$E \{v_m(t) v_m'(\sigma)\} = V_m \delta(t - \sigma) \quad (A-8)$$

Thus the human's control input is assumed to be generated by

$$T_N \dot{u}(t) + u(t) = u_c(t) + v_m(t) \quad (A-9)$$

with

$$u_c(t) = -L \hat{x}(t)$$

The estimate $\hat{x}(t)$ is obtained from the cascade combination of a Kalman filter and predictor. Define the augmented state vector $x(t) = \begin{bmatrix} x(t) \\ u(t) \end{bmatrix}$ where the new $x(t)$ satisfies

$$\dot{x}(t) = \tilde{A}x(t) + \tilde{B} u_c(t) + \tilde{w}(t) \quad (A-10)$$

where

$$\tilde{A} = \begin{bmatrix} A & B \\ 0 & -T_N^{-1} \end{bmatrix} \quad \tilde{B} = \begin{bmatrix} 0 \\ T_N^{-1} \end{bmatrix} \quad \tilde{w}(t) = \begin{bmatrix} w(t) \\ T_N^{-1} v_m(t) \end{bmatrix}$$

The Kalman filter generates $\hat{x}(t - \tau)$, the least-mean-square estimate of the delayed state from

$$\frac{d}{dt} \hat{x}(t - \tau) = \tilde{A} \hat{x}(t - \tau) + \Sigma \tilde{C}' V_y^{-1} [y_p(t) - \tilde{C} \hat{x}(t - \tau)] + \tilde{B} u_c(t - \tau) \quad (A-11)$$

where V_y is the covariance of the observation noise $v_y(t)$, and Σ satisfies

$$0 = \tilde{A} \Sigma + \Sigma \tilde{A}' + \tilde{W} - \Sigma \tilde{C}' V_y^{-1} \tilde{C} \Sigma \quad (A-12)$$

with

$$\tilde{W} = \begin{bmatrix} W & & 0 \\ 0 & T_N^{-1} V_m & T_N^{-1} \end{bmatrix}$$

The predictor generates the best estimate $\hat{x}(t)$ from the estimator output $\hat{x}(t - \tau)$ according to the equation

$$\hat{x}(t) = e^{\tilde{A} \tau} \hat{x}(t - \tau) + \int_{t-\tau}^t e^{\tilde{A}(t-\sigma)} \tilde{B} u_c(\sigma) d\sigma \quad (A-13)$$

A differential equation for $\hat{x}(t)$ can be derived from Equation (A-13),

$$\begin{aligned} \frac{d}{dt} \hat{x}(t) &= A \hat{x}(t) + e^{\tilde{A} \tau} \Sigma \tilde{C}' V_y^{-1} [y_p(t) - \tilde{C} \hat{x}(t - \tau)] \\ &\quad + \tilde{B} u_c(t - \tau) \end{aligned} \quad (A-14)$$

A.2 STATISTICAL CHARACTERISTICS

A closed form expression for the covariance of $x(t)$ may be derived

(Reference 21) as

$$\begin{aligned}
X = E \{x(t)x'(t)\} &= e^{\tilde{A}\tau} \Sigma e^{\tilde{A}'\tau} + \int_0^{\tau} e^{\tilde{A}\sigma} \tilde{W} e^{\tilde{A}'\sigma} d\sigma \\
&+ \int_0^{\infty} e^{\bar{A}\sigma} e^{\tilde{A}\tau} \tilde{C}' V_y^{-1} \tilde{C} \Sigma e^{A'\tau} e^{\bar{A}'\sigma} d\sigma \quad (A-15)
\end{aligned}$$

where $\bar{A} = \tilde{A} - BL = A_o - \tilde{B}_o L_1$ is the closed-loop system matrix.

There are three terms in X ; they arise from writing

$$X(t) = E_f(t) + E_p(t) + \hat{X}(t)$$

where $E_f(t)$ = filtering error, $E_p(t)$ = prediction error and $\hat{X}(t)$ = "pilots" state estimate. The covariance matrices for these terms are all affected by the time delay with

$$E_f = e^{\tilde{A}\tau} \Sigma e^{\tilde{A}'\tau} ; \quad E_p = \int_0^{\tau} e^{\tilde{A}\sigma} \tilde{W} e^{\tilde{A}'\sigma} d\sigma \quad (A-16)$$

and $\hat{X} = E \{ \hat{x}(t) \hat{x}'(t) \}$ is given by the last integral term in Equation (A-15). Note that \hat{X} satisfies

$$\bar{A} \hat{X} + \hat{X} \bar{A}' + e^{\tilde{A}\tau} \Sigma \tilde{C}' V_y^{-1} \tilde{C} \Sigma e^{\tilde{A}'\tau} = 0 \quad (A-17)$$

APPENDIX B

ATTENTIONAL ALLOCATION USING THE OPTIMAL CONTROL MODEL

The basic approach that we follow in applying the optimal control pilot model to predict attention allocation among a set of display indicators is to optimize a quadratic cost functional with respect to pilot attentional constraints. In order for the entire scheme to be computationally attractive, the following must be accomplished:

- Relate attentional model parameters (f_i) to pilot model parameters.
- Obtain an expression for $J^* = \text{minimum } J$ that shows explicitly how the f_i affect the various cost functional terms.
- Obtain an expression for the gradient terms $\frac{\partial J^*}{\partial f_i}$ that will be needed in subsequent optimization algorithms.
- Develop an algorithm to minimize J^* with respect to the f_i , subject to total workload constraints on f_i .

In this appendix we discuss these items. The discussion is pertinent to a pilot control task, although the concepts can be applied to a pilot monitoring situation as well.

B.1 INCLUDING ATTENTIONAL CONSTRAINTS

In the optimal control model, a fractional allocation of attention f_i to the informational variable y_i modifies the "observation" noise $V_{y_i}(t)$ associated with that variable (Reference 7). Thus, the noise covariance associated with y_i is

$$V_{y_i} = \frac{\rho_i^0}{f_i} \hat{\sigma}_i^2 \quad (\text{B-1})$$

where $\hat{\sigma}_i = \sigma_i / N(\sigma_i)$ (B-2)

$\sigma_i = \text{RMS value of } y_i$

$N(\sigma_i) = \text{describing function gain of threshold } a_i$

$$= \text{erfc} \left(\frac{a_i}{\sigma_i \sqrt{2}} \right) \quad (\text{B-3})$$

The noise/signal ratio ρ_i^0 is the "full attention" noise ratio, which typically is 0.01 or -20dB. Note that Equation (B-1) represents an implicit relationship for the actual noise variance V_{y_i} since $\hat{\sigma}_i^2$ is itself a function of V_{y_i} . For a given ρ_i^0/f_i , the requisite V_{y_i} is solved for via an iterative procedure. The quantity $\rho_i^0/f_i = \rho_i$ is called the modified noise/signal ratio.

The method that is used to determine how a pilot allocates attention among the various y_i is to minimize the optimal control cost with respect to f_i subject to constraints. This step will require an iterative process to arrive at the optimal f_i , where successive iterates f_i^n result in lower values for the cost functional. The cost functional that is used to determine the f_i is

$$J^* = \min_u J(u) \quad (B-4)$$

where $J(u)$ is the basic cost functional in the optimal control pilot model.

B.2 EXPRESSION FOR OPTIMUM QUADRATIC COST, J^*

In lieu of attempting to minimize the entire expression for J^* numerically with respect to f_i , it is more efficient to isolate those terms in J^* that are affected by f_i . Since changes in f_i are reflected as changes in observation noise V_{y_i} , we first obtain an expression for J^* that shows the V_{y_i} dependence.

The cost functional $J(u)$, in the steady-state is given by

$$J(u) = E\{x' \tilde{Q} x + \dot{u}' Q_r \dot{u}\} \quad (B-5)$$

where Q is defined in Equation (A-7) and x is the augmented vector $x = \text{col}[x, u]$.

Equation (B-5) may be rewritten as

$$J(u) = \text{tr}[\tilde{Q} X + Q_r E\{\dot{u} \dot{u}'\}] \quad (B-6)$$

where $X = E\{x(t)x'(t)\}$. Assuming optimal pilot control, X is given by Equation (A-15).

The control rate, \dot{u} , may be approximated by the pilot's own estimate of \dot{u} (as the actual \dot{u} is modeled to contain a white motor noise). Thus

$$\begin{aligned}\dot{u} \sim \hat{\dot{u}} &= -T_N^{-1} L \hat{x} - T_N^{-1} u \\ &= -T_N^{-1} \hat{u} - T_N^{-1} L \hat{x} - T_N^{-1} u_e \\ &= -L_1 \hat{x} - T_N^{-1} u_e\end{aligned}\tag{B-7}$$

where u_e is the error ($u - \hat{u}$). Thus, since \hat{x} and u_e are uncorrelated for optimal linear estimation

$$E\{\dot{u}\dot{u}'\} = L_1 \hat{X} L_1' + \begin{bmatrix} 0 & \\ & T_N^{-1} \end{bmatrix} (E_f + E_p) \begin{bmatrix} 0 \\ \hline T_N^{-1} \end{bmatrix}\tag{B-8}$$

where E_f , E_p and \hat{X} are the filtering error, prediction error and (augmented) state estimate covariance matrices respectively. They are given by Equations (A-16) and (A-17).

Substituting Equations (B-8) and (A-16) into Equation (B-6) yields with optimal control,

$$\begin{aligned}J^* &= \text{tr} \left\{ \tilde{Q}_1 e^{\tilde{A} \tau} \tilde{\Sigma} e^{\tilde{A}' \tau} \right\} + \text{tr} \left\{ \tilde{Q}_1 \int_0^T e^{\tilde{A} \sigma} \tilde{W} e^{\tilde{A}' \sigma} d\sigma \right\} \\ &\quad + \text{tr} \left\{ (\tilde{Q} + L_1' Q_r L_1) \hat{X} \right\}\end{aligned}\tag{B-9}$$

where

$$\tilde{Q}_1 = \tilde{Q} + \begin{bmatrix} 0 & & 0 \\ \hline & & \\ 0 & & (T_N Q_r^{-1} T_N')^{-1} \end{bmatrix}\tag{B-10}$$

The observation noise V_y affects only the error covariance matrix Σ which appears in the first and third terms J_1 and J_3 in J^* . To show this dependence more clearly, we rearrange J_3 . Substituting for \hat{X} and using the cyclic property of the trace gives

$$J_3 = \text{tr} \int_0^{\infty} e^{\tilde{A}'\sigma} (\tilde{Q} + L_1' Q_r L_1) e^{\tilde{A}\sigma} d\sigma \cdot e^{\tilde{A}'\tau} \tilde{\Sigma} \tilde{C}' V_y^{-1} \tilde{C} \Sigma e^{\tilde{A}\tau} \quad (\text{B-10})$$

But the integral term is identified as P, the solution of the Riccati Equation (A-7), thus using Equation (A-12),

$$J_3 = \text{tr} \left[e^{\tilde{A}'\tau} P e^{\tilde{A}\tau} (\Sigma \tilde{A}' + \tilde{A} \Sigma + \tilde{W}) \right] \quad (\text{B-11})$$

which may be combined with J_1 and rewritten as

$$J_1 + J_3 = \text{tr} [e^{\tilde{A}'\tau} P e^{\tilde{A}\tau} W] + \text{tr} [e^{\tilde{A}'\tau} (\tilde{Q}_1 + P\tilde{A} + \tilde{A}'P) e^{\tilde{A}\tau} \Sigma] \quad (\text{B-12})$$

The first term in the above expression is independent of V_y and may be combined with J_2 which is also independent of V_y . Thus, the only term of interest that remains is called the "scanning cost":

$$\begin{aligned} J_0 &= \text{part of } J^* \text{ dependent on } V_y \\ &= \text{tr} [e^{\tilde{A}'\tau} (\tilde{Q}_1 + P\tilde{A} + \tilde{A}'P) e^{\tilde{A}\tau} \Sigma] \end{aligned} \quad (\text{B-13})$$

This expression can be simplified by noting that

$$\tilde{Q}_1 + P\tilde{A} + \tilde{A}'P = \left[\begin{array}{cc|cc} P_{12} Q_r^{-1} P_{12}' & & 0 & 0 \\ \hline & & -P_{22} Q_r^{-1} P_{22}' & (T_N Q_r^{-1} T_N')^{-1} \\ \hline 0 & & & \end{array} \right]$$

but $Q_r^{-1} P_{12}' = T_N^{-1} L$ and $T_N = P_{22}^{-1} Q_r$ so that

$$J_0 = \text{tr} \{ L_e \Sigma L_e' \} \quad (\text{B-14})$$

where $L_e =$ "Equivalent" gains

$$= Q_r^{1/2} \begin{bmatrix} T_N^{-1} L \\ \vdots \\ 0 \end{bmatrix} e^{\tilde{A}\tau} \quad (\text{B-15})$$

and Σ satisfies the variance equation

$$0 = \tilde{A}\Sigma + \Sigma\tilde{A}' + \tilde{W} - \Sigma\tilde{C}'V_y^{-1}\tilde{C}\Sigma \quad (\text{B-16})$$

B.3 GRADIENT EXPRESSIONS

Minimizing J_0 (and hence J^*) with respect to f_i represents a difficult nonlinear optimization problem. The difficulty is two-fold. First, f_i affects V_y in an implicit manner; second, V_y affects J_0 through the Riccati solution Σ . As it is unlikely that a closed-form solution for the optimum f_i can be found, the optimization process will be carried out numerically via some form of gradient algorithm.

In order that the numerical process be reasonably efficient, it is desired to obtain closed-form expressions for the gradients $\frac{\partial J_0}{\partial f_i}$ or $\frac{\partial J_0}{\partial V_y}$. Thus, the time-consuming process of numerically evaluating these derivatives can be avoided.

We wish to obtain the gradient vector

$$g_f = \frac{\partial}{\partial f} J_0 \quad (\text{B-17})$$

Where the i^{th} element is $\frac{\partial J_0}{\partial f_i}$. Consider a small change in f_i . This will result primarily in a change in V_{y_i} (since $V_{y_i} = \frac{\rho_0}{f_i} \hat{\sigma}_i^2$) but will also cause changes in the other noise variances V_{y_j} , $j \neq i$ since σ_i will be modified. Thus,

$$\begin{aligned} \frac{\partial J_0}{\partial f_i} &= \frac{\partial J_0}{\partial V_1} \cdot \frac{\partial V_1}{\partial f_i} + \frac{\partial J_0}{\partial V_2} \cdot \frac{\partial V_2}{\partial f_i} + \dots \\ &= \left\langle \frac{\partial J_0}{\partial V_y}, \frac{\partial V_y}{\partial f_i} \right\rangle = \left(\frac{\partial V_y}{\partial f_i} \right)' \frac{\partial J_0}{\partial V_y} \end{aligned} \quad (\text{B-18})$$

and so the gradient vector becomes

$$g_f = \frac{\partial J_0}{\partial f} = \Gamma' \frac{\partial J_0}{\partial V_y} \quad (\text{B-19})$$

where $\frac{\partial J_0}{\partial V_y}$ is the gradient vector of J_0 with respect to V_{y_i} , $i = 1, 2, \dots, m$, and Γ is a "transformation" matrix where

$$(\Gamma)_{ij} = \frac{\partial V_{y_i}}{\partial f_j} \quad (B-20)$$

The gradient vector $\frac{\partial J_0}{\partial V_y}$ can be evaluated using a technique of Kleinman (Reference 22) for derivatives of trace functionals. From Equation (B-16), the change in Σ due to a change in V_y to $V_y + \delta V$ is given by

$$\delta \Sigma \hat{A}' + \hat{A} \delta \Sigma + \Sigma \tilde{C}' V_y^{-1} (\delta V) V_y^{-1} \tilde{C} \Sigma = 0 \quad (B-21)$$

where we note $(V_y + \delta V)^{-1} \cong V_y^{-1} \left[1 - \delta V \cdot V_y^{-1} + (\delta V \cdot V_y^{-1})^2 \dots \right]$. The matrix $\hat{A} = \tilde{A} - \Sigma \tilde{C}' V_y^{-1} \tilde{C}$ is the closed-loop system matrix for the Kalman filter and has eigenvalues with negative real parts. The term $G = \Sigma \tilde{C}' V_y^{-1}$ is the Kalman filter optimal gain matrix.

The solution to Equation (B-21) is given by

$$\delta \Sigma = \int_0^{\infty} e^{\hat{A}\sigma} G \delta V G' e^{\hat{A}'\sigma} d\sigma \quad (B-22)$$

Substituting into $\delta J_0 = \text{tr} (L_e' \delta \Sigma L_e)$ gives

$$\frac{\partial J_0}{\partial V} = \text{diag} (G' M G) \quad (B-23)$$

where

$$M = \int_0^{\infty} e^{\hat{A}\sigma} L_e' L_e e^{\hat{A}'\sigma} d\sigma \quad (B-24)$$

and is easily computed by solving the linear (Lyapunov) equation

$$\hat{A}' M + M \hat{A} + L_e' L_e = 0 \quad (B-25)$$

The elements of the matrix Γ must be computed. Since $V_{y_i} = \frac{\rho_i \hat{\sigma}_i^2}{f_i}$, we obtain

$$\frac{\partial V_{y_i}}{\partial f_i} = \frac{V_{y_i}}{f_i} \left[S_{f_i}^{\hat{\sigma}_i^2} - \delta_{ij} \right] = \Gamma_{ij} = \frac{V_{y_i}}{f_i} S_{f_i}^V \quad (B-26)$$

where S_y^x is the used sensitivity coefficient, defined as

$$S_y^x = \frac{\partial x/x}{\partial y/y} \quad (B-27)$$

If the terms $S_{f_i}^{\hat{\sigma}_i^2}$ happen to be $\ll 1$, then Γ is approximately a diagonal matrix

$$\Gamma \cong \Gamma_{ii} = - \frac{V_{y_i}}{f_i} = - \frac{\rho_i \hat{\sigma}_i^2}{f_i} \quad (B-28)$$

To determine more precisely the matrix Γ , rewrite Equation (B-26) as

$$S_{f_i}^V y_i = S_{f_i}^{\hat{\sigma}_i^2} - \delta_{ij} \quad i, j = 1, \dots, m \quad (B-29)$$

so that if we can obtain $S_{f_i}^V y_i$, the matrix Γ is readily obtained. Since a change in f_i induces a change in all of the V_{y_i} , we can write

$$S_{f_i}^{\hat{\sigma}_i^2} = \sum_{k=1}^m S_{V_k}^{\hat{\sigma}_i^2} \cdot S_{f_i}^V \quad (B-30)$$

using the chain rule for sensitivity coefficients. Defining the $m \times m$ matrices

$$Q = S_{f_i}^V y_i = q_{ij} \quad (B-31)$$

and

$$R = S_V \frac{\hat{\sigma}_i^2}{y_i} = r_{ij} \quad (B-32)$$

we obtain, substituting Equation (B-30) into Equation (B-29),

$$Q = RQ - I$$

or

$$Q = -(I - R)^{-1} \quad (B-33)$$

The matrix R is next obtained since the terms r_{ij} involve changes in the additive observation noises and not in the multiplicative ratios.

B.4 COMPUTING THE SENSITIVITY MATRIX, $S_V \frac{\hat{\sigma}_i^2}{y_i}$

The main computations required above are in obtaining the matrix R. Below, the method used to obtain R is described. We first consider the case of zero observational thresholds for simplicity. (This case is pertinent to informational level studies or laboratory situations with high resolution displays.) Modifications for the case when visual thresholds $a_i > 0$, e.g., when considering attentional allocation with realistic displays, are then presented.

The augmented state covariance matrix is given by

$$\begin{aligned} X = & e^{\tilde{A}\tau} \Sigma e^{\tilde{A}'\tau} + \int_0^\tau e^{\tilde{A}\sigma} \tilde{W} e^{\tilde{A}'\sigma} d\sigma \\ & + \int_0^\infty e^{\bar{A}\sigma} e^{\tilde{A}\tau} (\Sigma \tilde{A}' + \tilde{A}\Sigma + \tilde{W}) e^{\tilde{A}'\tau} e^{\bar{A}'\sigma} d\sigma \end{aligned} \quad (B-34)$$

and the covariance of the outputs is

$$Y = E \{ y(t) y'(t) \} = \tilde{C} X \tilde{C}'$$

Consequently, the variance σ_i^2 is given by

$$\sigma_i^2 = c_i' X c_i = \text{tr} \{ X c_i c_i' \} \quad (\text{B-35})$$

where c_i' is the i -th row of the \tilde{C} matrix. Substituting Equation (B-34) into Equation (B-35) yields, after some manipulation,

$$\sigma_i^2 = \text{tr} \left\{ \left[c_i c_i' + \tilde{A}' Z_i + Z_i \tilde{A} \right] e^{\tilde{A}' \tau} \Sigma e^{\tilde{A} \tau} \right\} + \text{terms independent of } V_y \quad (\text{B-36})$$

where

$$Z_i = \int_0^{\infty} e^{\tilde{A}' \sigma} c_i c_i' e^{\tilde{A} \sigma} d\sigma \quad (\text{B-37})$$

and satisfies the linear equation

$$\tilde{A}' Z_i + Z_i \tilde{A} + c_i c_i' = 0 \quad (\text{B-38})$$

Since $\tilde{A} = \hat{A} - BL$, the bracketed term in Equation (B-36) may be rewritten as

$$H_i = Z_i BL + L' B' Z_i \quad (\text{B-39})$$

Finally, since

$$\delta \Sigma = \int_0^{\infty} e^{\hat{A} \sigma} G \delta V G' e^{\hat{A}' \sigma} d\sigma$$

we obtain

$$\frac{\partial \sigma_i^2}{\partial V_{y_j}} = \left(G' \int_0^{\infty} e^{\hat{A}' \sigma} e^{\tilde{A}' \tau} H_i e^{\tilde{A} \tau} e^{\hat{A} \sigma} d\sigma \cdot G \right)_{ij} \quad (\text{B-40})$$

so that

$$r_{ij} = \frac{V_{y_j}}{\sigma_i^2} \cdot \frac{\partial \sigma_i^2}{\partial V_{y_j}} = S_{V_{y_j}}^{\sigma_i^2}$$

The above equations form the basis for the following algorithm to compute R, one row at a time.

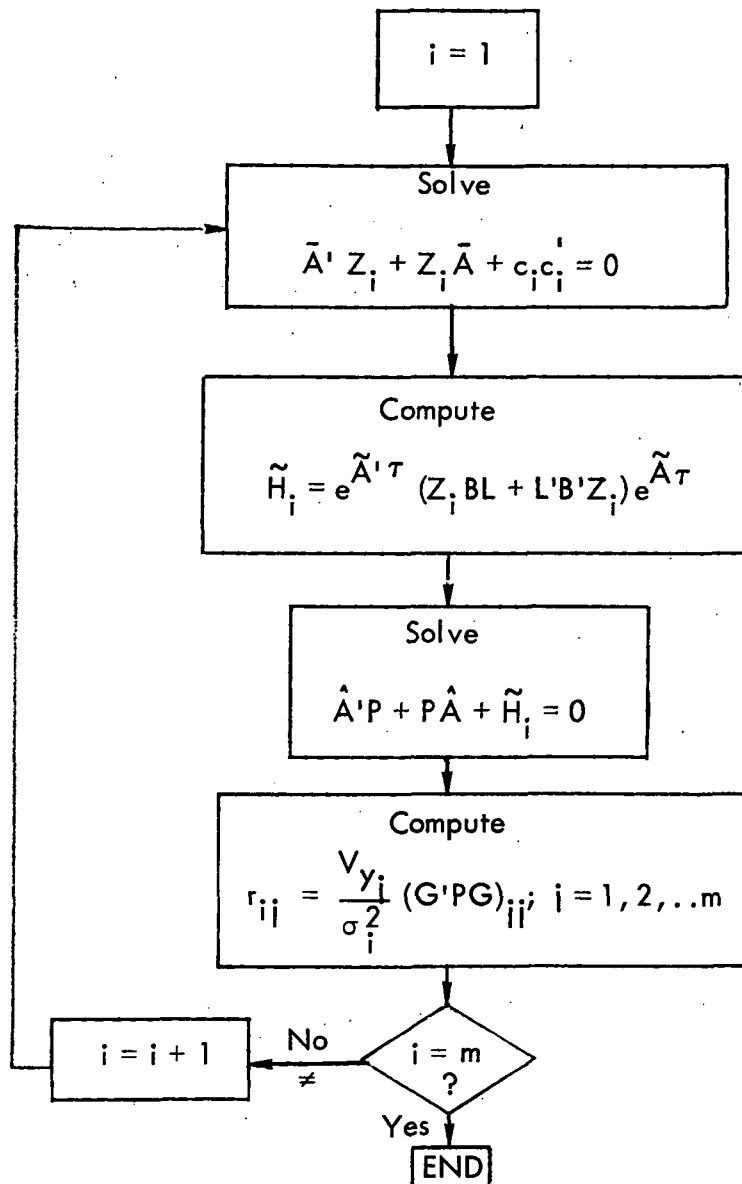


Figure B-1. Algorithm for Computing R.

To reduce the computational requirements in computing R, the $n \times r$ matrices (r = number of control inputs)

$$e^{\tilde{A}^T \tau} Z_i B \quad i = 1, \dots, m$$

are precomputed and stored. Note that these are dependent only on the optimal feedback gains, and not on any noise statistics. Further reductions in computation are possible by using the linear equation algorithm of Bartels and Stewart (Reference 23) that permits efficient multiple solutions of

$$XA + A'X = -Q$$

with different right hand sides. However, even without this algorithm, the computational requirements for R are less than those needed for one Riccati equation solution, and must be termed slight.

The above developments assumed $a_i = 0$, i.e., no visual and/or indifference thresholds, so that the noise covariance associated with output y_i is

$$V_{y_i} = \frac{\rho_i^0}{f_i} \sigma_i^2 \quad (B-41)$$

When $a_i > 0$, the effective noise covariance is determined from

$$V_{y_i} = \frac{\rho_i^0}{f_i} \hat{\sigma}_i^2 \quad (B-42)$$

where

$$\hat{\sigma} = \sigma / \operatorname{erfc} \left(\frac{a}{\sigma\sqrt{2}} \right) = \sigma \left[\frac{2}{\sqrt{\pi}} \int_b^{\infty} e^{-x^2} dx \right]^{-1}$$

and $b = a/\sigma\sqrt{2}$.

In the non-zero threshold case, the matrix R in Equation (B-32) is given by

$$(R)_{ij} = S_{V_{y_i}}^{\hat{\sigma}_i^2} = \frac{V_{y_i}}{\hat{\sigma}_i^2} \frac{\partial \hat{\sigma}_i^2}{\partial V_{y_i}} \quad (B-43)$$

To relate this to the results of Equation (B-40), we write (since $\hat{\sigma}_i$ does not depend on σ_i)

$$\frac{\partial \hat{\sigma}_i^2}{\partial V_{y_i}} = \frac{\partial \hat{\sigma}_i^2}{\partial \sigma_i^2} \cdot \frac{\partial \sigma_i^2}{\partial V_{y_i}} = \frac{\hat{\sigma}_i}{\sigma_i} \cdot \frac{\partial \hat{\sigma}_i}{\partial \sigma_i} \cdot \frac{\partial \sigma_i^2}{\partial V_{y_i}}$$

or

$$(R)_{ij} = S_{\sigma_i}^{\hat{\sigma}_i} \cdot S_{V_{y_i}}^{\sigma_i^2} \quad (B-44)$$

So that it is only necessary to obtain the m scalar quantities $\partial \hat{\sigma}_i / \partial \sigma_i$ to include the threshold effects, since the sensitivities of σ_i^2 have been determined from the zero threshold Equation (B-40). From Equation (B-42)

$$\frac{\partial \hat{\sigma}_i}{\partial \sigma_i} = \left[1 - \frac{2 b_i e^{-b_i^2}}{\sqrt{\pi} \operatorname{erfc}(b_i)} \right] \left[\operatorname{erfc}(b_i) \right]^{-1}$$

or

$$S_{\sigma_i}^{\hat{\sigma}_i} = 1 - \frac{2 b_i e^{-b_i^2}}{\sqrt{\pi} \operatorname{erfc}(b_i)} \quad (B-45)$$

where $b_i = \frac{a_i}{\sigma_i \sqrt{2}}$. Thus, multiplying the i-th row of the zero-threshold R by Equation (B-45) gives the required sensitivity matrix for the situation $a_i > 0$.

The above development assumed multiplicative observation noises. While this is true in general for manned vehicle systems, there are situations in which one might consider purely additive noises $V_{y_i}(t)$ with covariances $V_{y_i}^o$. Both additive and multiplicative cases can fit within the above framework as follows.

The effective observation noise in the pilot model is

$$V_i = \frac{\rho_i^o}{f_i} \hat{\sigma}_i^2 \quad (B-46)$$

where $\rho_i^o = \text{noise/signal ratio}$ if noises are multiplicative or $\rho_i^o = V_i^o$ additive noise variance if observation noises are purely additive. In addition,

$$\hat{\sigma}_i = x/\text{erfc}(b_i); \quad b_i = \frac{a_i}{\sigma_i \sqrt{2}} \quad (B-47)$$

where $x = \sigma_i$ if noises are multiplicative and $x = 1$ if they are additive. To obtain the gradient of J with respect to f , it was shown necessary to compute the matrix R :

$$R_{ij} = S_{\sigma_i}^{\hat{\sigma}_i} \cdot S_{V_{y_i}}^{\sigma_i^2} \quad (B-48)$$

The computation of $S_{V_{y_i}}^{\sigma_i^2}$ is identical for either additive or multiplicative noises. However, the matrix $S_{\sigma_i}^{\hat{\sigma}_i}$ will be different for these two cases. For the multiplicative case,

$$S_{\sigma_i}^{\hat{\sigma}_i} = 1 - \frac{2b_i e^{-b_i^2}}{\sqrt{\pi} \text{erfc}(b_i)} \quad (B-49)$$

while for the additive case ($x = 1$ in Equation (B-47))

$$S_{\sigma_i}^{\hat{\sigma}_i} = - \frac{2b_i e^{-b_i^2}}{\sqrt{\pi} \text{erfc}(b_i)} \quad (B-50)$$

Thus, it becomes relatively simple to compute $\partial J/\partial f$ for either type of noise case by selecting the proper form of either Equation (B-49) or Equation (B-50). Note that if $\alpha_i = 0$, then

$$\hat{\sigma}_i = \begin{cases} 0, & \text{additive case} \\ 1, & \text{multiplicative case} \end{cases}$$

B.5 GRADIENT PROJECTIONS AND OPTIMIZATION

The above algorithm is used to obtain $g_f = \frac{\partial J_0}{\partial f}$ which is the unconstrained gradient vector. However, the attentional allocations f_i are not free but are constrained by

$$\sum_{i=1}^m f_i = f^* = \text{total attention} \quad \text{and} \quad f_i \geq 0 \quad (\text{B-51})$$

The constraint, Equation (B-51), describes a portion of a hyperplane,

$$\langle c, f \rangle = f^* \quad (\text{B-52})$$

with $c = \text{col} [1, 1, \dots, 1]$. Thus, in order to determine the feasible direction for cost reduction, it is necessary to find the projection of g_f on the hyperplane, Equation (B-52). This is given by

$$g_f^p = g_f - \frac{\langle g_f, c \rangle}{\langle c, c \rangle} c \quad (\text{B-53})$$

or,

$$g_f^p = g_f - \left(\frac{1}{m} \sum_{i=1}^m g_{f_i} \right) c \quad (\text{B-54})$$

In other words, g_f^p is obtained by subtracting the average of the g_{f_i} from each element of the vector. The angle between g_f and g_f^p is

$$\cos \theta = \frac{\langle g_f, g_f^p \rangle}{\|g_f\| \cdot \|g_f^p\|} \quad (\text{B-55})$$

The gradient projection, Equation (B-54) is appropriate at the informational level, i.e., where no distinction is made that two "outputs" come from one display indicator. In the display format studies, the fact that a pilot obtains both position and velocity observations from a single display indicator provides yet another constraint on the f_i . Assuming outputs are ordered in position-rate pairs,

$$f_1 = f_2, f_3 = f_4, \dots \quad (\text{B-56})$$

(assuming $y_2 = \dot{y}_1$, etc.). For this case, secondary projections of g_f^p are necessary on the planes $f_1 - f_2 = 0$, $f_3 - f_4 = 0$, etc. This is easily done by replacing $g_{f_1}^p$ and $g_{f_2}^p$ with $(g_{f_1}^p + g_{f_2}^p)/2$, etc. Thus, the various constraints imposed by information and/or display level studies are easily treated insofar as gradient projections are involved.

In order to develop a reduced (projected) gradient optimization scheme, assume we are at iteration n , with attention vector f^n . A small change Δf^n such that $f_i^n + \Delta f^n$ still satisfies the constraints of Equation (B-51) will cause a corresponding small change in J_0^n . Thus, at iteration n ,

$$J_0^{n+1} \sim J_0^n + \langle g_f^p, \Delta f^n \rangle \quad (\text{B-57})$$

If Δf^n is selected as

$$\Delta f^n = -\epsilon J_0^n g_f^p / \|g_f^p\|^2 \quad \epsilon < 1 \quad (\text{B-58})$$

then,

$$J_0^{n+1} \sim (1 - \epsilon) J_0^n \quad (\text{B-59})$$

Thus, each successive iteration will result in a lower cost (to first order terms only) of 100ε%.

Equation (B-59) serves as the basis for a gradient optimization scheme. We set

$$\epsilon = \beta \cos \theta \quad (B-60)$$

and pick $\beta < 1/2$ and sufficiently small such that $f^{n+1} = f^n + \Delta f^n$ satisfies $f_i^{n+1} > 0$ and also $J_0^{n+1} < J_0^n$. Convergence occurs when J_0^{n+1} is arbitrarily close to J_0^n . If $J_0^{n+1} > J_0^n$, a smaller step is taken by reducing β . Note that since Δf^n is in the direction of g_f^p , the resulting f^{n+1} must necessarily continue to satisfy the constraints imposed on f^n .

When using the above gradient projection algorithm to optimize attentional allocation, it is necessary to modify the scheme whenever

$$g_{f_i}^p > 0 \quad \text{and} \quad \epsilon > f_i > 0 \quad (B-61)$$

In such a situation the mathematics do not want to place any attention on instrument i . Thus, one cannot move in the direction of the gradient since f_i would go negative. The modification that is obviously called for is to set

$$g_{f_i}^p = 0$$

whenever the above condition, Equation (B-61), is encountered. Thus, f_i remains fixed for the iteration and the re-projected gradient is modified to guarantee that

$$\sum_i g_{f_i}^p = 0$$

as required.

APPENDIX C

LINEARIZED ROTORCRAFT EQUATIONS OF MOTION

In developing a mathematical model for use in the analysis of an automatic approach and landing system for a tandem rotor helicopter, linearized equations not normally used in aircraft stability analysis are required.

C.1 DERIVATION OF THE NONLINEAR EQUATIONS OF MOTION

Before developing the linearized equations of motion for analysis purposes, the nonlinear equations are developed.

C.1.1 ROTARY MOTION

The equations are written in the conventional body axis system, with the origin at the helicopter's center of mass. The x-axis (roll) is directed forward, the y-axis (pitch) is directed out the starboard side, and the z-axis (yaw) is directed "downward" to complete the orthogonal set. Assume that the x-z plane is one of symmetry and define the inertia matrix as

$$I \triangleq \begin{bmatrix} I_{xx} & 0 & J_{xz} \\ 0 & I_{yy} & 0 \\ J_{xz} & 0 & I_{zz} \end{bmatrix}$$

where

$$\left. \begin{aligned} J_{xy} \triangleq - \int xy \, dm = 0 \\ J_{zy} \triangleq - \int zy \, dm = 0 \end{aligned} \right\} \text{due to x-z symmetry}$$
$$J_{xz} \triangleq - \int xz \, dm$$

The components of the angular velocity vector in the body axis system are given by

$$\omega \triangleq \begin{bmatrix} P \\ Q \\ R \end{bmatrix}$$

where P, Q, R are the components of the angular velocity resolved along the body axes x, y, and z, respectively. Similarly, let the applied torque be denoted as

$$T \triangleq \begin{bmatrix} L \\ M \\ N \end{bmatrix}$$

With the assumption that the angular momentum of any rotating machinery onboard, such as engines and, in helicopters, the rotor, is negligible, the equations in inertial space are written simply

$$T = \frac{d}{dt} (I\omega) \quad (C-1)$$

On the assumption that the Earth is inertial, then Equation (C-1) is written in the body axis system as

$$T = I \frac{d'\omega}{dt} + \omega \times I\omega \quad (C-2)$$

where the prime denotes "as seen by an observer fixed in the body axes," and therefore

$$\frac{d'\omega}{dt} \triangleq \begin{bmatrix} \dot{P} \\ \dot{Q} \\ \dot{R} \end{bmatrix}$$

where the dot denotes total time derivative. Substituting the appropriate definitions into Equation (C-2) results in the equation set

$$\begin{bmatrix} L \\ M \\ N \end{bmatrix} = \begin{bmatrix} I_{xx} \dot{P} + J_{xz} \dot{R} \\ I_{yy} \dot{Q} \\ J_{xz} \dot{P} + I_{zz} \dot{R} \end{bmatrix} + \begin{bmatrix} J_{xz} PQ + I_{zz} QR - I_{yy} QR \\ I_{xx} RP + J_{xz} (R^2 - P^2) - I_{zz} RP \\ I_{yy} PQ - I_{xx} PQ - J_{xz} RQ \end{bmatrix} \quad (C-3)$$

These equations define the rotary motion of the helicopter.

C.1.2 TRANSLATORY MOTION

Assume that the mass of the helicopter is constant and denoted m . Let the force vector be denoted.

$$F \triangleq \begin{bmatrix} X \\ Y \\ Z \end{bmatrix}$$

where X , Y , and Z lie along the body axes. Note that in the conventional body axis system the total velocity

$$V_T \triangleq \begin{bmatrix} U \\ V \\ W \end{bmatrix}$$

is resolved along the body axes. The equation in inertial space may then be written

$$F = \frac{d}{dt} (m V_T). \quad (C-4)$$

On the assumption that the Earth is inertial, then Equation (C-4) is written in the body axis system as

$$F = m \frac{d^i V_T}{dt} + \omega \times m V_T . \quad (C-5)$$

Making appropriate substitutions into Equation (C-5) gives the equation set

$$\begin{bmatrix} X \\ Y \\ Z \end{bmatrix} = \begin{bmatrix} m\dot{U} \\ m\dot{V} \\ m\dot{W} \end{bmatrix} + \begin{bmatrix} mQW - mRV \\ mRU - mPW \\ mPV - mQU \end{bmatrix} . \quad (C-6)$$

These equations define the translatory motion of the aircraft.

C.1.3 EULER ANGLE TRANSFORMATIONS

For an aircraft in the conventional body axis system, the attitude can be described with respect to a set of axes fixed in the Earth. To do this we define an Euler angle set denoted ψ , θ , ϕ . These three angles are the azimuth change, elevation change, and roll required to arrive at the aircraft attitude from the inertial axes. They must be taken in the given order. If a vector is denoted in the inertial coordinates as C_i and viewed from a coordinate system which has been slewed through ψ , we get

$$C_1 = T_z(\psi)C_i \quad (C-7)$$

where

$$T_z(\psi) \triangleq \begin{bmatrix} \cos \psi & \sin \psi & 0 \\ -\sin \psi & \cos \psi & 0 \\ 0 & 0 & 1 \end{bmatrix}$$

If the observer is then elevated through θ , he sees

$$C_2 = T_y(\theta)C_1 = T_y(\theta)T_z(\psi)C_i \quad (C-8)$$

where

$$T_y(\theta) \triangleq \begin{bmatrix} \cos \theta & 0 & -\sin \theta \\ 0 & 1 & 0 \\ \sin \theta & 0 & \cos \theta \end{bmatrix}$$

Finally, if the observer is rolled through ϕ , he sees from aircraft body axes

$$C_b = T_x(\phi)C_2 = T_x(\phi)T_y(\theta)T_z(\psi)C_i \quad (C-9)$$

where

$$T_x(\phi) \triangleq \begin{bmatrix} 1 & 0 & 0 \\ 0 & \cos \phi & \sin \phi \\ 0 & -\sin \phi & \cos \phi \end{bmatrix}$$

C.1.4 GRAVITY FORCES

With Equation (C-9) the gravity force may be written in body axes as

$$W_b = T_x(\phi)T_y(\theta)T_z(\psi) \begin{bmatrix} 0 \\ 0 \\ mg \end{bmatrix} = mg \begin{bmatrix} -\sin \theta \\ \sin \phi \cos \theta \\ \cos \phi \cos \theta \end{bmatrix} \quad (C-10)$$

C.1.5 EULER ANGLE RATE EQUATIONS

The body axis rates may be written as functions of the Euler angle rates:

$$\begin{aligned}
\begin{bmatrix} P \\ Q \\ R \end{bmatrix} &= T_x(\phi) \begin{bmatrix} \dot{\phi} \\ 0 \\ 0 \end{bmatrix} + T_y(\theta) \begin{bmatrix} 0 \\ \dot{\theta} \\ 0 \end{bmatrix} + T_z(\psi) \begin{bmatrix} 0 \\ 0 \\ \dot{\psi} \end{bmatrix} \\
&= \begin{bmatrix} 1 & 0 & -\sin \theta \\ 0 & \cos \theta & \sin \phi \cos \theta \\ 0 & -\sin \theta & \cos \phi \cos \theta \end{bmatrix} \begin{bmatrix} \dot{\phi} \\ \dot{\theta} \\ \dot{\psi} \end{bmatrix}
\end{aligned} \tag{C-11}$$

C.1.6 INERTIAL VELOCITY EQUATIONS

If the velocity in inertial coordinates is denoted

$$V_{T_i} \triangleq \begin{bmatrix} V_x \\ V_y \\ V_z \end{bmatrix}$$

then we may write the body axis velocities as functions of the inertial velocities

$$\begin{aligned}
\begin{bmatrix} U \\ V \\ W \end{bmatrix} &= T_x(\phi) T_y(\theta) T_z(\psi) \begin{bmatrix} V_x \\ V_y \\ V_z \end{bmatrix} \\
&= \begin{bmatrix} V_x \cos \theta \cos \psi + V_y \cos \theta \sin \psi - V_z \sin \theta \\ V_x (\sin \phi \sin \theta \cos \psi - \cos \phi \sin \psi) \\ V_x (\cos \phi \sin \theta \cos \psi + \sin \phi \sin \psi) \end{bmatrix} \\
&\quad + \begin{bmatrix} 0 \\ V_y (\sin \phi \sin \theta \sin \psi + \cos \phi \cos \psi) + V_z \sin \phi \cos \theta \\ V_y (\cos \phi \sin \theta \sin \psi - \sin \phi \cos \psi) + V_z \cos \theta \cos \phi \end{bmatrix}
\end{aligned} \tag{C-12}$$

C.2 LINEARIZING OF EQUATIONS USING DELTA PERTURBATIONS

The purpose of this linear model is to analyze an automatic approach and landing system. As such, the system is tied to the Approach Navigation Frame (ANF). This is an Earth-fixed coordinate system with the origin at the desired touchdown point, the X axis along the runway, and the Z axis down along the local vertical. The system is considered inertial. The variables to be commanded will be in the ANF such as V_x , V_y , and V_z and ψ , θ , ϕ . The control system will therefore be feeding back these quantities from an inertial platform. The linearized equations are then desired in terms of these variables. The derivation of these equations follows.

C.2.1 BODY TRANSLATORY EQUATIONS

Rewrite Equation (C-6) with the forces being divided into aerodynamic forces and the gravity forces of Equation (C-10)

$$\begin{aligned}\dot{U} &= RV - QW + \frac{X_A}{m} - g \sin \theta \\ \dot{V} &= PW - RU + \frac{Y_A}{m} + g \sin \phi \cos \theta \\ \dot{W} &= QU - PV + \frac{Z_A}{m} + g \cos \phi \cos \theta\end{aligned}\tag{C-13}$$

Assume the following perturbations

$$\left. \begin{aligned}U &= U_0 + u & P &= p & \theta &= \theta_0 + \theta \\ V &= v & Q &= q & \phi &= \phi \\ W &= W_0 + w & R &= r & \psi &= \psi\end{aligned}\right\}\tag{C-14}$$

Note that the perturbations are simply added to the Euler angles. If steady flight is assumed, the steady flight equations are obtained from Equation (C-13)

$$0 = \frac{X_{A0}}{m} - g \sin \theta_0$$

$$0 = \frac{Y_{A0}}{m} \tag{C-15}$$

$$0 = \frac{Z_{A0}}{m} + g \cos \theta_0$$

Next note that for small θ

$$\left. \begin{aligned} \sin(\theta_0 + \theta) &= \sin \theta_0 + (\cos \theta_0) \theta \\ \cos(\theta_0 + \theta) &= \cos \theta_0 - (\sin \theta_0) \theta \end{aligned} \right\} \tag{C-16}$$

Substituting the definitions of Equation (C-14) into Equation (C-13), using Equation (C-16) and subtracting off steady flight, Equation (C-15), yields the following perturbation equations

$$\dot{u} = -W_0 q - (g \cos \theta_0) \theta + \frac{\Delta X_A}{m}$$

$$\dot{v} = W_0 p - U_0 r + (g \cos \theta_0) \theta + \frac{\Delta Y_A}{m} \tag{C-17}$$

$$\dot{w} = U_0 q - (g \sin \theta_0) \theta + \frac{\Delta Z_A}{m}$$

C.2.2 BODY RATE EQUATIONS

Substituting the perturbation definitions of Equation (C-14) into Equation (C-3) and dropping second-order terms gives

$$\begin{aligned}\dot{p} &= -\frac{J_{xz}}{I_{xx}} \dot{r} + \frac{\Delta L}{I_{xx}} \\ \dot{q} &= \frac{\Delta M}{I_{yy}} \\ \dot{r} &= -\frac{J_{xz}}{I_{zz}} \dot{p} + \frac{\Delta N}{I_{zz}}\end{aligned}\tag{C-18}$$

C.2.3 EULER ANGLE EQUATIONS

The relation between Euler angle perturbed rates and body perturbed rates is desired. This is obtained by inverting Equation (C-11) and applying the perturbation definitions to give

$$\begin{aligned}\dot{\theta} &= q \\ \dot{\phi} &= p + (\tan \theta_0) r \\ \dot{\psi} &= \frac{r}{\cos \theta_0}\end{aligned}\tag{C-19}$$

C.2.4 EQUATION SET WITH AERODYNAMIC PARTIAL DERIVATIVES

The motion of the aircraft is described by Equations (C-17), (C-18), and (C-19). The force and moment perturbations are, in general, functions of the motion and can be written to first order as a linear function of the motion variables. Motions in the longitudinal plane are assumed to separate from the lateral-directional to give the total equation set which follows.

$$\begin{aligned}
\dot{u} &= -W_0 q - (g \cos \theta_0) \theta + \frac{X_u}{m} u + \frac{X_w}{m} w + \frac{X_q}{m} q + \frac{X_{\delta_e}}{m} \Delta \delta_e + \frac{X_{\delta_c}}{m} \Delta \delta_c \\
\dot{v} &= W_0 p - U_0 r + (g \cos \theta_0) \phi + \frac{Y_v}{m} v + \frac{Y_p}{m} p + \frac{Y_r}{m} r + \frac{Y_{\delta_a}}{m} \Delta \delta_a + \frac{Y_{\delta_r}}{m} \Delta \delta_r \\
\dot{w} &= U_0 q - (g \sin \theta_0) \theta + \frac{Z_u}{m} u + \frac{Z_w}{m} w + \frac{Z_q}{m} q + \frac{Z_{\delta_e}}{m} \Delta \delta_e + \frac{Z_{\delta_c}}{m} \Delta \delta_c \\
\dot{p} &= \frac{J_{xz}}{I_{xx}} \dot{r} + \frac{L_v}{I_{xx}} v + \frac{L_p}{I_{xx}} p + \frac{L_r}{I_{xx}} r + \frac{L_{\delta_a}}{I_{xx}} \Delta \delta_a + \frac{L_{\delta_r}}{I_{xx}} \Delta \delta_r \\
\dot{q} &= \frac{M_u}{I_{yy}} u + \frac{M_w}{I_{yy}} w + \frac{M_q}{I_{yy}} q + \frac{M_{\delta_e}}{I_{yy}} \Delta \delta_e + \frac{M_{\delta_c}}{I_{yy}} \Delta \delta_c \\
\dot{r} &= \frac{J_{xz}}{I_{zz}} \dot{p} + \frac{N_v}{I_{zz}} v + \frac{N_p}{I_{zz}} p + \frac{N_r}{I_{zz}} r + \frac{N_{\delta_a}}{I_{zz}} \Delta \delta_a + \frac{N_{\delta_r}}{I_{zz}} \Delta \delta_r \\
\dot{\theta} &= q \\
\dot{\phi} &= p + (\tan \theta_0) r \\
\dot{\psi} &= \frac{r}{\cos \theta_0}
\end{aligned}
\tag{C-20}$$

In the above expressions δ_e , δ_c , δ_a , δ_r are the four control displacements corresponding to differential collective, gang collective, roll cyclic and yaw cyclic, respectively.

C.2.5 EQUATION SET WITH BODY RATES ELIMINATED

Equation (C-20) may be reduced in variables by eliminating the body rates with the last three equations. The result is

$$\begin{aligned}
 \dot{u} &= \frac{X_u}{m} u + \frac{X_w}{m} w - \left(W_0 - \frac{X_q}{m} \right) \dot{\theta} - (g \cos \theta_0) \theta + \frac{X_\delta}{m} \Delta \delta \\
 \dot{v} &= \frac{Y_v}{m} v + \left(W_0 + \frac{Y_p}{m} \right) \dot{\phi} + (g \cos \theta_0) \phi - \left(\sin \theta_0 \left(W_0 + \frac{Y_p}{m} \right) + \cos \theta_0 \left(U_0 - \frac{Y_r}{m} \right) \right) \dot{\psi} \\
 &\quad + \frac{Y_\delta}{m} \Delta \delta \\
 \dot{w} &= \frac{Z_u}{m} u + \frac{Z_w}{m} w + \left(U_0 + \frac{Z_q}{m} \right) \dot{\theta} - (g \sin \theta_0) \theta + \frac{Z_\delta}{m} \Delta \delta \\
 \ddot{\phi} &= \frac{L_v}{I_{xx}} v + \frac{L_p}{I_{xx}} \phi - \left(\frac{J_{xz}}{I_{xx}} \cos \theta_0 - \sin \theta_0 \right) \ddot{\psi} - \left(\frac{L_p}{I_{xx}} \sin \theta_0 - \frac{L_r}{I_{xx}} \cos \theta_0 \right) \dot{\psi} + \frac{L_\delta}{I_{xx}} \Delta \delta \\
 \ddot{\theta} &= \frac{M_u}{I_{yy}} u + \frac{M_w}{I_{yy}} w + \frac{M_q}{I_{yy}} \dot{\theta} + \frac{M_\delta}{I_{yy}} \Delta \delta \\
 \ddot{\psi} &= \frac{1}{I_{zz} \cos \theta_0 + J_{xz} \sin \theta_0} \left(N_v v + J_{xz} \ddot{\phi} + N_p \dot{\phi} - (N_p \sin \theta_0 - N_r \cos \theta_0) \dot{\psi} + N_\delta \Delta \delta \right)
 \end{aligned} \tag{C-21}$$

where $()_\delta \Delta \delta$ indicates the summation of partial derivatives and actuator deflections.

C.2.6 REDUCED EQUATION SET IN VECTOR-MATRIX NOTATION

Putting Equation (C-21) in vector-matrix notation results in the following longitudinal equations:

$$\begin{bmatrix}
 S - \frac{X_u}{m} & -\frac{X_w}{m} & \left(W_0 - \frac{X_q}{m}\right)S + g \cos \theta_0 \\
 -\frac{Z_u}{m} & S - \frac{Z_w}{m} & -\left(U_0 + \frac{Z_q}{m}\right)S + g \sin \theta_0 \\
 -\frac{M_u}{I_{yy}} & -\frac{M_w}{I_{yy}} & \left(S - \frac{M_q}{I_{yy}}\right)S
 \end{bmatrix}
 \begin{Bmatrix}
 u \\
 w \\
 \theta
 \end{Bmatrix}
 =
 \begin{Bmatrix}
 \frac{X_\delta}{m} \\
 \frac{Z_\delta}{m} \\
 \frac{M_\delta}{I_{yy}}
 \end{Bmatrix}
 \delta
 \quad (C-22)$$

The lateral-directional equations are:

$$\begin{bmatrix}
 \left(S - \frac{Y_v}{m}\right) & -\left(W_0 + \frac{Y_p}{m}\right)S - g \cos \theta_0 & \left(\left(W_0 + \frac{Y_p}{m}\right) \sin \theta_0 + \left(U_0 - \frac{Y_r}{m}\right) \cos \theta_0\right)S \\
 \left(-\frac{L_v}{I_{xx}}\right) & \left(S - \frac{L_p}{I_{xx}}\right)S & -\left(\left(\frac{J_{xz}}{I_{xx}} \cos \theta_0 + \sin \theta_0\right)S - \frac{L_p}{I_{xx}} \sin \theta_0 + \frac{L_r}{I_{xx}} \cos \theta_0\right)S \\
 \left(-\frac{N_v}{B}\right) & -\left(\frac{J_{xz}}{B} \cdot S + \frac{N_p}{B}\right)S & \left(S + \left(\frac{L_p}{I_{xx}} \sin \theta_0 - \frac{L_r}{I_{xx}} \cos \theta_0\right)\right)S
 \end{bmatrix}
 \begin{Bmatrix}
 v \\
 \phi \\
 \psi
 \end{Bmatrix}
 =
 \begin{Bmatrix}
 \frac{Y_\delta}{m} \\
 \frac{L_\delta}{I_{xx}} \\
 \frac{N_\delta}{B}
 \end{Bmatrix}
 \delta
 \quad (C-23)$$

where $B \triangleq I_{zz} \cos \theta_0 + J_{xz} \sin \theta_0$ and $S \triangleq \frac{d}{dt}$ the Laplace differential operator.

C.2.7 INERTIAL VELOCITY EQUATIONS

If Equation (C-12) is linearized, the result is given

$$\left.
 \begin{aligned}
 u &= \Delta V_x \cos \theta_0 - \Delta V_z \sin \theta_0 - W_0 \theta \\
 v &= \Delta V_y + W_0 \phi - (U_0 \cos \theta_0 + W_0 \sin \theta_0) \psi \\
 w &= \Delta V_x \sin \theta_0 + \Delta V_z \cos \theta_0 + U_0 \theta
 \end{aligned}
 \right\}
 \quad (C-24)$$

With these equations, the body axis velocities can be eliminated from Equation (C-21) and the result is given

$$\Delta \dot{V}_x = \left(\frac{X_u}{m} + \frac{X_w}{m} \tan \theta_0 \right) \Delta V_x + (\tan \theta_0) \Delta \dot{V}_z - \left(\frac{X_u}{m} \tan \theta_0 - \frac{X_w}{m} \right) \Delta V_z$$

$$+ \frac{1}{\cos \theta_0} \left(\frac{X_q}{m} \dot{\theta} - \left(\frac{X_u}{m} W_0 - \frac{X_w}{m} U_0 + g \cos \theta_0 \right) \theta + \frac{X_\delta}{m} \delta \right)$$

$$\Delta \dot{V}_y = \frac{Y_v}{m} \Delta V_y + \frac{Y_p}{m} \Delta \dot{\phi} + \left(\frac{Y_v}{m} W_0 + g \cos \theta_0 \right) \phi - \left(\frac{Y_p}{m} \sin \theta_0 \right.$$

$$\left. - \frac{Y_r}{m} \cos \theta_0 \right) \dot{\psi} - \frac{Y_v}{m} \left(U_0 \cos \theta_0 + W_0 \sin \theta_0 \right) \psi + \frac{Y_\delta}{m} \delta$$

$$\Delta \dot{V}_z = -(\tan \theta_0) \Delta \dot{V}_x + \left(\frac{Z_u}{m} + \frac{Z_w}{m} \tan \theta_0 \right) \Delta V_x - \left(\frac{Z_u}{m} \tan \theta_0 - \frac{Z_w}{m} \right) \Delta V_z$$

$$+ \frac{1}{\cos \theta_0} \left(\frac{Z_q}{m} \dot{\theta} - \left(\frac{Z_u}{m} W_0 - \frac{Z_w}{m} U_0 + g \sin \theta_0 \right) \theta + \frac{Z_\delta}{m} \delta \right)$$

(C-25)

$$\ddot{\theta} = \left(\frac{M_u}{I_{yy}} \cos \theta_0 + \frac{M_w}{I_{yy}} \sin \theta_0 \right) \Delta V_x - \left(\frac{M_u}{I_{yy}} \sin \theta_0 - \frac{M_w}{I_{yy}} \cos \theta_0 \right) \Delta V_z$$

$$+ \frac{M_q}{I_{yy}} \dot{\theta} - \left(\frac{M_u}{I_{yy}} W_0 - \frac{M_w}{I_{yy}} U_0 \right) \theta + \frac{M_\delta}{I_{yy}} \delta$$

$$\ddot{\phi} = \frac{L_v}{I_{xx}} \Delta V_y + \frac{L_p}{I_{xx}} \dot{\phi} + \frac{L_v}{I_{xx}} W_0 \phi + \left(\frac{J_{xz}}{I_{xx}} \cos \theta_0 + \sin \theta_0 \right) \ddot{\psi} - \left(\frac{L_p}{I_{xx}} \sin \theta_0 - \frac{L_r}{I_{xx}} \cos \theta_0 \right) \dot{\psi}$$

$$- \frac{L_v}{I_{xx}} \left(U_0 \cos \theta_0 + W_0 \sin \theta_0 \right) \psi + \frac{L_\delta}{I_{xx}} \delta$$

$$\ddot{\psi} = \frac{1}{B} [N_v \Delta V_y + J_{xz} \ddot{\phi} + N_p \dot{\phi} + N_v W_0 \phi - (N_p \sin \theta_0 - N_r \cos \theta_0) \dot{\psi}$$

$$- N_v (U_0 \cos \theta_0 + W_0 \sin \theta_0) \psi + N_\delta \delta]$$

where again $B \triangleq I_{zz} \cos \theta_0 + J_{xz} \sin \theta_0$.

C.2.8 INERTIAL VELOCITY EQUATIONS IN VECTOR-MATRIX NOTATION

Equation (C-25) may be put into vector-matrix notation giving the following longitudinal equations:

$$\begin{bmatrix} (\cos \theta_0)S - \left(\frac{X_U}{m} \cos \theta_0 + \frac{X_W}{m} \sin \theta_0 \right) & (-\sin \theta_0)S + \left(\frac{X_U}{m} \sin \theta_0 - \frac{X_W}{m} \cos \theta_0 \right) & \left(-\frac{X_Q}{m} S + \frac{X_U}{m} W_0 - \frac{X_W}{m} U_0 + g \cos \theta_0 \right) \\ (\sin \theta_0)S - \left(\frac{Z_U}{m} \cos \theta_0 + \frac{Z_W}{m} \sin \theta_0 \right) & (\cos \theta_0)S + \left(\frac{Z_U}{m} \sin \theta_0 - \frac{Z_W}{m} \cos \theta_0 \right) & \left(-\frac{Z_Q}{m} S + \frac{Z_U}{m} W_0 - \frac{Z_W}{m} U_0 + g \sin \theta_0 \right) \\ -\frac{M_U}{I_{yy}} \cos \theta_0 - \frac{M_W}{I_{yy}} \sin \theta_0 & \frac{M_U}{I_{yy}} \sin \theta_0 - \frac{M_W}{I_{yy}} \cos \theta_0 & S^2 - \frac{M_Q}{I_{yy}} S + \frac{M_U}{I_{yy}} W_0 - \frac{M_W}{I_{yy}} U_0 \end{bmatrix} \begin{Bmatrix} \Delta V_x \\ \Delta V_z \\ \theta \end{Bmatrix} = \begin{Bmatrix} \frac{X_\delta}{m} \\ \frac{Z_\delta}{m} \\ \frac{M_\delta}{I_{yy}} \end{Bmatrix} \delta \quad (C-26)$$

and the following lateral equations:

$$\begin{bmatrix} \left(S - \frac{Y_v}{m} \right) & \left(-\frac{Y_p}{m} S \right) - \left(g \cos \theta_0 + \frac{Y_w}{m} W_0 \right) & \left(\frac{Y_p}{m} \sin \theta_0 - \frac{Y_r}{m} \cos \theta_0 \right) S + \frac{Y_v}{m} V_{x_0} \\ \left(-\frac{L_v}{I_{xx}} \right) & \left(S^2 - \frac{L_p}{I_{xx}} S - \frac{L_w}{I_{xx}} W_0 \right) & -\left(\frac{J_{xz}}{I_{xx}} \cos \theta_0 + \sin \theta_0 \right) S^2 + \left(\frac{L_p}{I_{xx}} \sin \theta_0 - \frac{L_r}{I_{xx}} \cos \theta_0 \right) S + \frac{L_v}{I_{xx}} V_{x_0} \\ \left(-\frac{N_v}{B} \right) & \left(-\frac{J_{xz}}{B} S^2 - \frac{N_p}{B} S - \frac{N_w}{B} W_0 \right) & S^2 + \left(\frac{N_p}{B} \sin \theta_0 - \frac{N_r}{B} \cos \theta_0 \right) S + \frac{N_v}{B} V_{x_0} \end{bmatrix} \begin{Bmatrix} \Delta V_y \\ \phi \\ \psi \end{Bmatrix} = \begin{Bmatrix} \frac{Y_\delta}{m} \\ \frac{L_\delta}{I_{xx}} \\ \frac{N_\delta}{B} \end{Bmatrix} \delta \quad (C-27)$$

where $V_{x_0} \triangleq U_0 \cos \theta_0 + W_0 \sin \theta_0$, $B \triangleq I_{zz} \cos \theta_0 + J_{xz} \sin \theta_0$ and $S \triangleq \frac{d}{dt}$ the Laplace differential operator.

C.2.9 STATE-VECTOR EQUATIONS

The equations above are not in a form suitable for the state-vector formulation because the equations containing ΔV_x , ΔV_z and $\ddot{\psi}$, $\ddot{\phi}$ are each simultaneous sets of equations. To solve for $\Delta \dot{V}_x$ and $\Delta \dot{V}_z$, we note that these two equations in Equation (C-27) can be written

$$\begin{pmatrix} \cos \theta_0 & -\sin \theta_0 \\ -\sin \theta_0 & \cos \theta_0 \end{pmatrix} \begin{pmatrix} \Delta \dot{V}_x \\ \Delta \dot{V}_z \end{pmatrix} = \begin{pmatrix} f_1(\Delta V_x, \Delta V_z, \theta, \dot{\theta}, \Delta \delta) \\ f_2(\Delta V_x, \Delta V_z, \theta, \dot{\theta}, \Delta \delta) \end{pmatrix} \quad (\text{C-28})$$

where $\Delta \delta$ are the actuator deviations from trim settings.

Inverting these equations leads to

$$\begin{pmatrix} \Delta \dot{V}_x \\ \Delta \dot{V}_z \end{pmatrix} = D \begin{pmatrix} \Delta V_y \\ \Delta V_z \\ \theta \\ \dot{\theta} \\ \Delta \delta \end{pmatrix} \quad (\text{C-29})$$

where the matrix D is given by

$$\begin{aligned} D &= \begin{pmatrix} D_{11} & D_{12} & D_{13} & D_{14} & D_{15} \\ D_{21} & D_{22} & D_{23} & D_{24} & D_{25} \end{pmatrix} \\ &= \begin{pmatrix} \cos \theta_0 & +\sin \theta_0 \\ -\sin \theta_0 & \cos \theta_0 \end{pmatrix} \tilde{D} \end{aligned} \quad (\text{C-30})$$

$$D = \begin{bmatrix} \left(\frac{X_u}{m} \cos \theta_0 + \frac{X_w}{m} \sin \theta_0 \right) & - \left(\frac{X_u}{m} \sin \theta_0 - \frac{X_w}{m} \cos \theta_0 \right) & - \left(\frac{X_u}{m} W_0 - \frac{X_w}{m} U_0 + g \cos \theta_0 \right) & \frac{X_q}{m} & \frac{X_\delta}{m} \\ \left(\frac{Z_u}{m} \cos \theta_0 + \frac{Z_w}{m} \sin \theta_0 \right) & - \left(\frac{Z_u}{m} \sin \theta_0 - \frac{Z_w}{m} \cos \theta_0 \right) & - \left(\frac{Z_u}{m} W_0 - \frac{Z_w}{m} U_0 + g \sin \theta_0 \right) & \frac{Z_q}{m} & \frac{Z_\delta}{m} \end{bmatrix} \quad (C-31)$$

Similarly, the equations containing $\ddot{\psi}$ and $\ddot{\phi}$ can be written

$$\begin{pmatrix} 1 & \frac{-J_{xz}}{I_{xx}} \cos \theta_0 - \sin \theta_0 \\ \frac{-J_{xz}}{I_{zz}} & \cos \theta_0 + \frac{J_{xz}}{I_{zz}} \sin \theta_0 \end{pmatrix} \begin{pmatrix} \ddot{\phi} \\ \ddot{\psi} \end{pmatrix} = \begin{pmatrix} q_1(\Delta V_y, \varphi, \dot{\phi}, \psi, \dot{\psi}, \Delta \delta) \\ q_2(\Delta V_y, \varphi, \dot{\phi}, \psi, \dot{\psi}, \Delta \delta) \end{pmatrix} \quad (C-32)$$

Inverting these equations to solve for $\ddot{\phi}$ and $\ddot{\psi}$ yields

$$\begin{pmatrix} \ddot{\phi} \\ \ddot{\psi} \end{pmatrix} = \frac{1}{1 - \frac{J_{xz}^2}{I_{xx} I_{zz}}} \begin{pmatrix} 1 + \frac{J_{xz}}{I_{zz}} \tan \theta_0 & \frac{J_{xz}}{I_{xx}} + \tan \theta_0 \\ \frac{J_{xz}}{I_{zz}} & \frac{1}{\cos \theta_0} \end{pmatrix} \begin{pmatrix} q_1 \\ q_2 \end{pmatrix} \quad (C-33)$$

or

$$\begin{pmatrix} \ddot{\phi} \\ \ddot{\psi} \end{pmatrix} = E \begin{pmatrix} \Delta V_y \\ \varphi \\ \dot{\phi} \\ \psi \\ \dot{\psi} \\ \Delta \delta \end{pmatrix} \quad (C-34)$$

where the matrix E is given by

$$E = \frac{1}{1 - \frac{J_{xz}^2}{I_{xx} I_{zz}}} \begin{pmatrix} 1 + \frac{J_{xz}}{I_{zz}} \tan \theta_0 & \frac{J_{xz}}{I_{xx}} + \tan \theta_0 \\ \frac{J_{xz}}{I_{zz}} & \frac{1}{\cos \theta_0} \\ \frac{1}{\cos \theta_0} & \frac{1}{\cos \theta_0} \end{pmatrix} \tilde{E} \quad (C-35)$$

$$\tilde{E} = \begin{pmatrix} \frac{L_v}{I_{xx}} & \frac{L_v}{I_{xx}} w_0 & \frac{L_p}{I_{xx}} & -(u_0 \cos \theta_0 + w_0 \sin \theta_0) \frac{L_v}{I_{xx}} & \frac{L_v}{I_{xx}} \cos \theta_0 - \frac{L_p}{I_{xx}} \sin \theta_0 & \frac{L_\delta}{I_{xx}} \\ \frac{N_v}{I_{zz}} & \frac{N_v}{I_{zz}} w_0 & \frac{N_p}{I_{zz}} & -(u_0 \cos \theta_0 + w_0 \sin \theta_0) \frac{N_v}{I_{zz}} & \frac{N_v}{I_{zz}} \cos \theta_0 - \frac{N_p}{I_{zz}} \sin \theta_0 & \frac{N_\delta}{I_{zz}} \end{pmatrix} \quad (C-36)$$

C.3 WIND GUST DISTURBANCES

C.3.1 GUST MODEL

The wind gust model is derived from the Press-Meadows analytical representation for the power spectral density (PSD) of random turbulence (Reference 24):

$$\phi(\omega) = \sigma_g^2 \frac{L}{V_o} \left[\frac{1 + 3(L/V_o)^2 \omega^2}{1 + (L/V_o)^2 \omega^2} \right] \quad (C-37)$$

where $\phi(\omega)$ = power spectral density, $\text{ft}^2/\text{rad}/\text{sec}$

σ_g^2 = mean-square gust velocity, ft^2/sec^2

L = scale of turbulence, ft

V_o = equivalent airspeed, ft/sec

ω = frequency, rad/sec

To obtain a random wind model, w_g , which satisfies the Press-Meadows power spectral density, a wind filter can be used to shape a unity rms white noise input. Since the PSD is

$$\phi(\omega) = |w_g(i\omega)|^2 = w_g(i\omega)w_g^*(i\omega) \quad (C-38)$$

where w_g^* is the complex conjugate of w_g , spectral factorization can be used to obtain $w_g(\omega)$. Replacing $j\omega$ by the Laplace transfer function equivalent for the wind filter:

$$\frac{w_g(s)}{n} = \sigma_g \gamma \frac{(s + \alpha)}{(s + \beta)^2} \quad (C-39)$$

where

$$\gamma = \sqrt{3V_\infty/L}$$

$$\alpha = V_\infty / \sqrt{3} \cdot L$$

$$\beta = V_\infty / L$$

and n is the driving white noise.

Using partial fraction expansions, Equation (C-39) can be written as

$$\frac{w_g(s)}{n} = \sigma_g \gamma \left[\frac{\alpha - \beta}{(s + \beta)^2} + \frac{1}{(s + \beta)} \right] \quad (C-40)$$

A block diagram of the wind gust model resulting from Equation (C-40) is shown in Figure C-1. The corresponding model in the time domain is obtained by defining the two wind gust variables

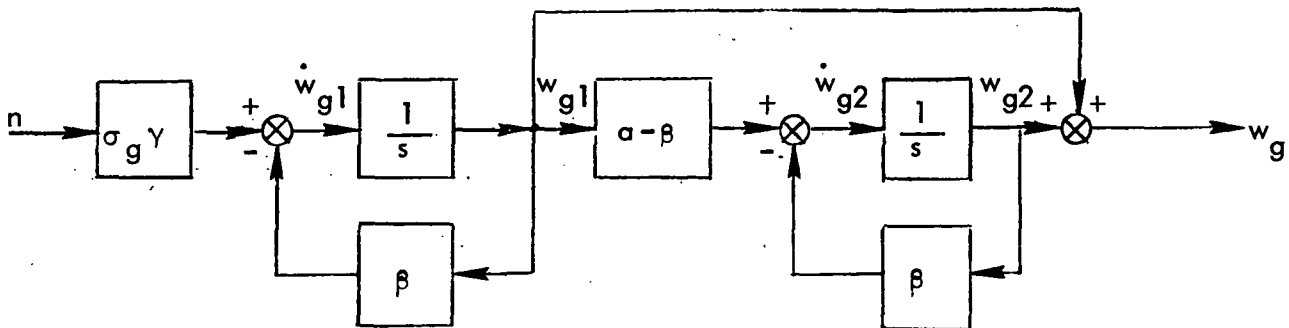


Figure C-1. Block Diagram of Press-Meadows Wind Gust Model.

$$\dot{x}_w = \begin{bmatrix} w_{g1} \\ w_{g2} \end{bmatrix} \quad (C-41)$$

The linear equations describing the wind gust model become:

$$\dot{x}_w = A_w x_w + B_w u + E_w n \quad (C-42)$$

where

$$A = \begin{bmatrix} -\beta & 0 \\ \alpha - \beta & -\beta \end{bmatrix} \quad B = \begin{bmatrix} 0 \\ 0 \end{bmatrix} \quad E = \begin{bmatrix} \sigma_g \gamma \\ 0 \end{bmatrix} \quad (C-43)$$

The total gust velocity is

$$w_g = w_{g1} + w_{g2} \quad (C-44)$$

and the wind gust rate is

$$\dot{w}_g = \dot{w}_{g1} + \dot{w}_{g2} = (\alpha - 2\beta)w_{g1} - \beta w_{g2} + \sigma_g \gamma n \quad (C-45)$$

The previous development is applicable to gusts along any of the three aircraft axes[†]. However the appropriate values must be selected for the model parameters σ_g , L and V_o . The magnitudes of the turbulent velocities are represented by their rms values σ_{gu} , σ_{gv} , and σ_{gw} (downwind, crosswind, and vertical, respectively). The rms component of σ_{gu} is approximately

$$\sigma_{gu} \approx 0.2W \quad (C-46)$$

[†]The Dryden model of atmospheric turbulence PSD is equivalent to Press-Meadows for turbulence normal to the airspeed; for turbulence parallel to the airspeed, the Dryden PSD is $2\sigma_g^2 (L/V_o) / [1 + (L/V_o)^2 \omega^2]$.

where W is the mean wind speed (Reference 25). The ratios of the rms speeds near the surface are about

$$\sigma_{gu} : \sigma_{gv} : \sigma_{gw} \cong 1.0 : 0.7 : 0.5 \quad (C-47)$$

These increase with altitude so that all components are nearly equal at 500 ft (Reference 25). The turbulence scale L is approximately equal to 1,000 ft for altitudes above 1,000 ft; below 1,000 ft, the scale for vertical turbulence is approximately equal to the altitude, while the scales for the horizontal components decrease to about 500 ft at the surface.

3.2 AERODYNAMIC FORCES DUE TO WIND GUSTS

The atmospheric turbulence provides disturbance inputs to the aircraft through the aerodynamic forces. Each of the wind gust components may induce important aircraft responses, but the vertical component w_g is primarily responsible for normal accelerations. This component is generally considered the most important disturbance, and is the only one treated explicitly in the following discussion. However, the analysis of u_g and v_g follows the same general pattern.

For most rigid-body analyses, it is sufficient to omit the small portion of the turbulence spectrum for which the gust velocity gradients are not adequately represented by equivalent rates of aircraft pitch and roll (Reference 24). The aerodynamic effect of the vertical gust is to modify the angle-of-attack and the pitch and roll rates.

$$\text{Effective angle of attack} = \alpha + \alpha_g = (w - w_g)/V_o$$

$$\text{Effective pitch rate} = q + q_g = q + \dot{w}_g/V_o$$

$$\text{Effective roll rate} = p + p_g = p - \dot{v}_g/V_o$$

These modified values are used in calculating the aerodynamic forces and moments, e.g., instead of $(X_{zw}/m)w$ in the equations of motion, there will appear the term $(X_{zw}/m)(w-w_g)$. Of course, none of the inertia terms in the equations of motion are affected.

The result of the wind input appears as additional terms on the right hand side of Equation (C-20).

$$\begin{aligned}
 \dot{u} &= \dots - \frac{X_w}{m} w_g + \frac{X_g}{m} \frac{1}{V_o} \dot{w}_g \\
 \dot{v} &= \dots - \frac{Y_p}{m} \frac{1}{V_o} \dot{w}_g \\
 \dot{w} &= \dots - \frac{Z_w}{m} w_g + \frac{Z_g}{m} \frac{1}{V_o} \dot{w}_g \\
 \dot{p} &= \dots - \frac{L_p}{m} \frac{1}{V_o} \dot{w}_g \\
 \dot{q} &= \dots - \frac{M_w}{m} w_g + \frac{M_q}{m} \frac{1}{V_o} \dot{w}_g \\
 \dot{r} &= \dots - \frac{N_p}{m} \frac{1}{V_o} w_g
 \end{aligned}
 \tag{C-48}$$

When these terms have been carried through the derivation, the end result is the addition of the following terms to the inertial frame equations:

$$\begin{aligned} \Delta \dot{V}_x &= \dots + \left[\frac{X_{wg}}{m} \cos \theta_o + \frac{Z_{wg}}{m} \sin \theta_o \right] w_g + \left[\frac{X_{\dot{w}g}}{m} \cos \theta_o \right. \\ &\quad \left. + \frac{Z_{\dot{w}g}}{m} \sin \theta_o \right] \dot{w}_g \\ \Delta \dot{V}_y &= \dots + \left[\frac{Y_{\dot{w}g}}{m} \right] \dot{w}_g \\ \Delta \dot{V}_z &= \dots + \left[-\frac{X_{wg}}{m} \sin \theta_o + \frac{Z_{wg}}{m} \cos \theta_o \right] w_g \\ &\quad + \left[-\frac{X_{\dot{w}g}}{m} \sin \theta_o + \frac{Z_{\dot{w}g}}{m} \cos \theta_o \right] \dot{w}_g \end{aligned} \quad (C-49)$$

$$\begin{aligned} \dot{p} &= \dots + J \left[\frac{L_{\dot{w}g}}{I_{xx}} - \frac{J_{xz}}{I_{xx}} \frac{N_{\dot{w}g}}{I_{zz}} \right] \dot{w}_g \\ \dot{q} &= \dots + \left[\frac{M_{wg}}{I_{yy}} \right] w_g + \left[\frac{M_{\dot{w}g}}{I_{yy}} \right] \dot{w}_g \\ \dot{r} &= \dots + J \left[-\frac{J_{xz}}{I_{zz}} \frac{L_{\dot{w}g}}{I_{xz}} + \frac{N_{\dot{w}g}}{I_{zz}} \right] \dot{w}_g \end{aligned}$$

where $J = (1 - J_{xz}^2 / I_{xx} I_{zz})^{-1}$. The gust stability derivatives have been defined as

$$\begin{aligned}
X_{wg} &= -X_w \\
\dot{X}_{wg} &= X_q/V_o \\
\dot{Y}_{wg} &= -Y_p/V_o \\
Z_{wg} &= -Z_w \\
\dot{Z}_{wg} &= Z_q/V_o \\
\dot{L}_{wg} &= -L_p/V_o \\
M_{wg} &= -M_w \\
\dot{M}_{wg} &= M_q/V_o \\
\dot{N}_{wg} &= -N_p/V_o
\end{aligned}
\tag{C-50}$$

The gust rate coefficients in Equation (C-50) are inversely proportional to the airspeed V_o , and become infinite as V_o approaches zero. To avoid this difficulty in hovering conditions, an equivalent airspeed can be used in the wind calculations. From Equations (C-46) and (C-47), the rms vertical turbulence velocity is approximately 0.1 of the mean wind; therefore, for a specified turbulence level, the equivalent airspeed can be defined as

$$V_o = 10\sigma_{gw} \tag{C-51}$$

C.3.3 LONGITUDINAL EQUATIONS WITH GUST INPUTS

The state variables for the longitudinal equations must be augmented by the wind states in Equation (C-41):

$$x = [w_{g1}, w_{g2}, \Delta x, \Delta z, \Delta \theta, \Delta V_x, \Delta V_z, q]^T \tag{C-52}$$

Using Equations (C-44), (C-45), (C-49), the wind inputs alter the vehicle equations as follows:

$$\Delta \dot{V}_x = \dots + \left[\frac{X_{wg}}{m} + \frac{X_{\dot{w}g}}{m} (\alpha - 2\beta) \right] w_{g1} + \left[\frac{X_{wg}}{m} - \frac{X_{\dot{w}g}}{m} \beta \right] w_{g2} + \left[\frac{X_{\dot{w}g}}{m} \sigma_g \gamma \right] n \quad (C-53)$$

$$\Delta \dot{V}_z = \dots + \left[\frac{Z_{wg}}{m} + \frac{Z_{\dot{w}g}}{m} (\alpha - 2\beta) \right] w_{g1} + \left[\frac{Z_{wg}}{m} - \frac{Z_{\dot{w}g}}{m} \beta \right] w_{g2} + \left[\frac{Z_{\dot{w}g}}{m} \sigma_g \gamma \right] n \quad (C-54)$$

$$\dot{q} = \dots + \left[\frac{M_{wg}}{m} + \frac{M_{\dot{w}g}}{m} (\alpha - 2\beta) \right] w_{g1} + \left[\frac{M_{wg}}{m} - \frac{M_{\dot{w}g}}{m} \beta \right] w_{g2} + \left[\frac{M_{\dot{w}g}}{m} \sigma_g \gamma \right] n \quad (C-55)$$

APPENDIX D

CH-46 DYNAMICS WITH MODEL-FOLLOWING AUGMENTATION

This appendix presents the derivation of the equations of motion for the CH-46 to be used with the optimal control model of the pilot. The basic equations of motion of the aircraft with the four actuator inputs are contained in Appendix C. The first task is to derive the equations of motion for the control stick inputs taking into account the attitude command system used on the CH-46C whose flight test data will be used to confirm the pilot model. The second task is to specify that the output equations of the controlled element are consistent with the displays implemented in the CH-46C.

D.1 ROTORCRAFT DYNAMICS WITH MODEL-FOLLOWING AUGMENTATION

A block diagram of the LaRC Model-Following Control augmentation system for the CH-46 is shown in Figure D-1. In this section we derive the effects of this type of augmentation system on the dynamics controlled by the pilot. The difficulty arises because of cross-coupling between the control actuator dedicated to provide the model response and the effect of that actuator on other state variables. For example, the differential collective may be used to satisfy the pitch response of the helicopter, but by so doing, it will have an influence in the translational equations.

The basic unaugmented vehicle equations are written in the form

$$\dot{x} = Ax + B\delta + Fw \quad (D-1)$$

or

$$\begin{bmatrix} \dot{x}_1 \\ \dot{x}_2 \end{bmatrix} = \begin{bmatrix} A_{11} & A_{12} \\ A_{21} & A_{22} \end{bmatrix} \begin{bmatrix} x_1 \\ x_2 \end{bmatrix} + \begin{bmatrix} B_1 \\ B_2 \end{bmatrix} \delta + \begin{bmatrix} F_1 \\ F_2 \end{bmatrix} w \quad (D-2)$$

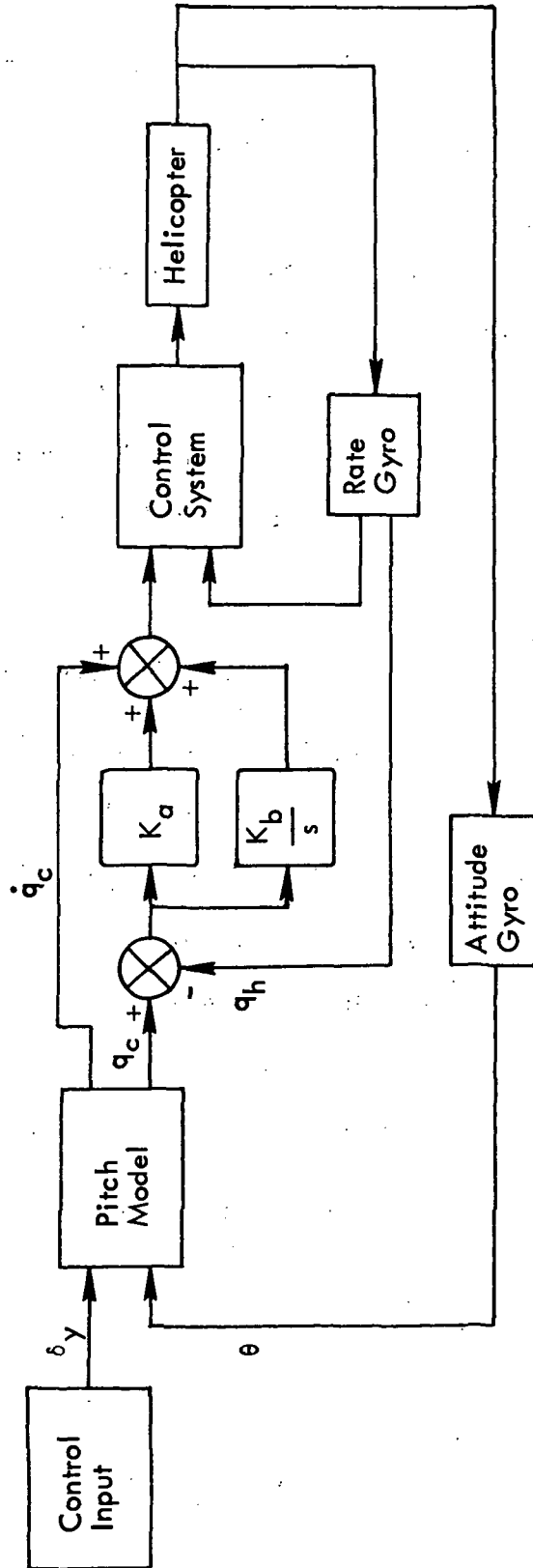


Figure D-1. CH-46 Model-Following Control Loop.

In Equation (D-2) the state vector has been partitioned such that x_2 represents that portion of the state to be controlled according to some desired model response. The inputs to this system are the actuator inputs δ which are dedicated to satisfying the model response. Disturbance inputs and other actuators affecting the equations of motion, but not being used to satisfy the model response, are included in the vector w .

Assume that it is desired to have the partition of the state vector x_2 follow a model equation given by

$$\dot{x}_2^m = A_{21}^m x_1 + A_{22}^m x_2^m + B_2^m u \quad (D-3)$$

Note that the derivative of the model response is given by linear combinations of the model state itself x_2^m , feedback of the other partition of the state vector x_1 (e.g. position), and the control stick inputs u .

If the control augmentation system is well designed, then it will force $x_2 \sim x_2^m$ and $\dot{x}_2 \sim \dot{x}_2^m$. In this case, we may subtract the second part of the state Equation (D-2) from the model Equation (D-3) and solve for the actuator activity which is dedicated to satisfy this response:

$$\delta \sim B_2^{-1} [(A_{21}^m - A_{21}) x_1 + (A_{22}^m - A_{22}) x_2 + B_2^m u - F_2 w] \quad (D-4)$$

Substituting this value of the actuator activity into Equation (D-1) provides the following form for the state equations when the system follows the model:

$$\begin{bmatrix} \dot{x}_1 \\ \dot{x}_2 \end{bmatrix} = \begin{bmatrix} A_{11}^* & A_{12}^* \\ A_{21}^* & A_{22}^* \end{bmatrix} \begin{bmatrix} x_1 \\ x_2 \end{bmatrix} + \begin{bmatrix} B_1^* \\ B_2^* \end{bmatrix} u + \begin{bmatrix} F_1^* \\ 0 \end{bmatrix} w \quad (D-5)$$

where

$$\left. \begin{aligned} A_{11}^* &= A_{11} + B_1 B_2^{-1} (A_{21}^m - A_{21}); & A_{21}^* &= A_{21}^m; & A_{22}^* &= A_{22}^m \\ A_{12}^* &= A_{12} + B_1 B_2^{-1} (A_{22}^m - A_{22}) \\ B_1^* &= B_1 B_2^{-1} B_2^m; & B_2^* &= B_2^m; & F_1^* &= F_1 - B_1 B_2^{-1} F_2 \end{aligned} \right\} (D-6)$$

Note that the partition of the state vector x_2 has the desired response of the model, but also that the dynamics of the other partition of the state vector x_1 have been altered because of the effect of the dedicated actuator δ on these equations.

D.2 LONGITUDINAL EQUATIONS OF MOTION

The equations of motion for the longitudinal axes are derived in Appendix C. We use as state variables in these equations, the Euler angles and body rates to be consistent with control augmentation schemes and guidance schemes employed. When we partition the longitudinal equations to account for the attitude command system in pitch, we have

$$\begin{Bmatrix} \Delta x \\ \Delta \dot{z} \\ \dot{\theta} \\ \Delta \dot{V}_x \\ \Delta \dot{V}_z \\ \dots \\ \dot{q} \end{Bmatrix} = \begin{bmatrix} A_{11} & | & A_{12} \\ \hline A_{21} & | & A_{22} \end{bmatrix} \begin{Bmatrix} \Delta x \\ \Delta z \\ \theta \\ \Delta V_x \\ \Delta V_z \\ \dots \\ q \end{Bmatrix} + \begin{Bmatrix} 0 \\ 0 \\ 0 \\ b_{11} \\ b_{12} \\ \dots \\ b_2 \end{Bmatrix} \delta_e \quad (D-7)$$

where

$$A_{11} = \begin{bmatrix} 0 & 0 & 0 & 1 & 0 \\ 0 & 0 & 0 & 0 & 1 \\ 0 & 0 & 0 & 0 & 0 \\ 0 & 0 & D_{11} & D_{12} & D_{13} \\ 0 & 0 & D_{21} & D_{22} & D_{23} \end{bmatrix} \quad (D-8)$$

$$A'_{12} = (0 \quad 0 \quad 1 \quad D_{14} \quad D_{24}) \quad (D-9)$$

$$A'_{21} = \begin{bmatrix} 0 \\ 0 \\ -\frac{M_u}{I_{yy}} W_o - \frac{M_w}{I_{yy}} U_o \\ \frac{M_u}{I_{yy}} \cos \theta_o + \frac{M_w}{I_{yy}} \sin \theta_o \\ \frac{M_u}{I_{yy}} \sin \theta_o - \frac{M_w}{I_{yy}} \cos \theta_o \end{bmatrix} \quad (D-10)$$

$$\left. \begin{aligned} A_{22} &= \frac{M_q}{I_{yy}} \\ b_{11} &= D_{15, \delta_e} \\ b_{12} &= D_{25, \delta_e} \\ b_2 &= \frac{M_{\delta_e}}{I_{yy}} \end{aligned} \right\} \quad (D-11)$$

The coefficients D_{ij} are given in Appendix C.

The desired pitch response system may be written, in terms of the present notation, as

$$\left. \begin{aligned} A_{21}^* &= (0, 0, -\omega_n^2, 0, 0) \\ A_{22}^* &= -2\zeta\omega_n \\ B_2^* &= K_\theta\omega_n^2 \end{aligned} \right\} \begin{aligned} \omega_n &= 2.0, 1.43 \\ \zeta &= .75 \\ K_\theta &= .15, .10 \text{ rad/in} \end{aligned} \quad (D-12)$$

Substituting these results into Equations (D-5) and (D-6) will provide the equations of motion in the longitudinal axes under the attitude command system.

D.3 LATERAL DIRECTIONAL EQUATIONS OF MOTION

In a manner similar to that for the longitudinal case, the lateral directional equations of motion can be written to account for the attitude command systems in roll and yaw. Using the formulation above, these equations become

$$\begin{Bmatrix} \Delta \dot{y} \\ \dot{\phi} \\ \dot{\psi} \\ \Delta \dot{V}_y \\ \text{---} \\ \dot{p} \\ \dot{r} \end{Bmatrix} = \begin{bmatrix} A_{11} & | & A_{12} \\ \text{---} & & \text{---} \\ A_{21} & | & A_{22} \end{bmatrix} \begin{Bmatrix} \Delta y \\ \phi \\ \psi \\ \Delta V_y \\ \text{---} \\ p \\ r \end{Bmatrix} + \begin{bmatrix} 0 & 0 \\ 0 & 0 \\ 0 & 0 \\ 0 & 0 \\ b_1 & b_2 \\ \text{---} \\ B_2 \end{bmatrix} \begin{pmatrix} \Delta \delta_a \\ \Delta \delta_r \end{pmatrix} \quad (D-13)$$

$$A_{11} = \begin{bmatrix} 0 & 0 & 0 & 1 \\ 0 & 0 & 0 & 0 \\ 0 & 0 & 0 & 0 \\ 0 & \tilde{a}_{42} & \tilde{a}_{43} & \frac{Y_v}{m} \end{bmatrix} \quad (D-14)$$

where

$$\tilde{a}_{42} = \frac{Y_v}{m} W_o + g \cos \theta_o$$

$$\tilde{a}_{43} = -(U_o \cos \theta_o + W_o \sin \theta_o) \frac{Y_v}{m}$$

$$A_{12} = \begin{bmatrix} 0 & 0 \\ 1 & \tan \theta_o \\ 0 & \frac{1}{\cos \theta_o} \\ \frac{Y_p}{m} & \frac{Y_r}{m} \end{bmatrix} \quad (D-15)$$

$$A_{21} = \begin{pmatrix} 0 & E_{11} & E_{12} & E_{13} \\ 0 & E_{21} & E_{22} & E_{23} \end{pmatrix}$$

$$A_{22} = \begin{pmatrix} E_{15} & E_{16} \\ E_{25} & E_{26} \end{pmatrix} \quad (D-16)$$

$$b_1 = Y_{\delta_a}$$

$$b_2 = Y_{\delta_r} \quad (D-17)$$

$$B_2 = \begin{pmatrix} E_{16, \delta_a} & E_{16, \delta_r} \\ E_{26, \delta_a} & E_{26, \delta_r} \end{pmatrix} \quad (D-18)$$

See Appendix C for the coefficients E_{ij} .

For simplicity, we show the model response equations in yaw assuming that the heading hold mode is employed. In this case the model response equations become

$$A_{21}^* = \begin{pmatrix} 0 & -\omega_n^2 & 0 & 0 \\ 0 & 0 & -\omega_o^2 & 0 \end{pmatrix} \quad (D-19)$$

$$A_{22}^* = \begin{pmatrix} -2\zeta\omega_n & 0 \\ 0 & -2\zeta_o\omega_o^2 \end{pmatrix} \quad (D-20)$$

where

$$\omega_n = 2, 1.43$$

$$\zeta = .75$$

$$\omega_o = 2.0$$

$$\zeta_o = .70$$

$$B_{2^* \delta} = \begin{pmatrix} \omega_n^2 K_\phi & 0 \\ 0 & \omega_o^2 K_\psi \end{pmatrix} \begin{pmatrix} \delta_y \\ \delta_z \end{pmatrix} \quad (D-21)$$

where

$$K_\phi = .15, .10 \text{ rod/in}$$

$$K_\psi = .35 \text{ rod/sec/in}$$

D.4 PHYSICAL AND AERODYNAMIC CHARACTERISTICS OF NASA/LaRC CH-46C HELICOPTER

Table D-1 summarizes the pertinent physical characteristics of the vehicle, including control displacement limits. Tables D-2 through D-7 give the trim conditions, fuel flow and stability derivatives as functions of forward speed for three rates of descent. The data in Tables D-2 through D-7 were calculated for a gross weight of 13,400 lbs, normal c.m. position and sea level flight. In Tables D-4 through D-7 (non-zero rate of descent), the data for forward speeds greater than 80 knots were extrapolated from 80 knot values by assuming constant offset from the corresponding zero rate of descent (Tables D-2 and D-3) data.

Table D-1. Physical Characteristics of LaRC YHC-1A Helicopter.

Parameter	Value	Units	English Units
Operating mass, m	6078	kg	(13,400 lbs)
Rolling moment of inertia, I_{xx}	12,474	kg-m ²	(9203 slug-ft ²)
Pitching moment of inertia, I_{yy}	102,898	kg-m ²	(75,914 slug-ft ²)
Yawing moment of inertia, I_{zz}	97,238	kg-m ²	(71,738 slug-ft ²)
Cross-product of inertia, J_{xz}	-9638	kg-m ²	(7144 slug-ft ²)
Reference area, S_r	341	m ²	(3670 ft ²)
Reference chord, c	0.4572	m	(1.5 ft)
Rotor radius, R_r	7.367	m	(24.17 ft)
Control travel limits			
Collective stick, δ_c	0-32.512	cm	(0-12.8 in.)
Longitudinal stick, δ_e	+13.97	cm	(+5.5 in.)
Lateral stick, δ_a	+9.14	cm	(+3.6 in.)
Pedal, δ_r	+5.85	cm	(+2.3 in.)

Table D-2. YHC-1A Longitudinal Stability Derivatives (Rate of Descent - 0 ft/min).

FORWARD VELOCITY	KTS	0	20	40	60	80	100	120	140
θ_o	deg	9.30627	8.19834	6.62235	4.75227	2.32294	1.43387	-2.28871	-6.63316
δ_{c_o}	in	.66523	-.06503	-.23518	.28888	.77817	-.06119	.16392	.34293
δ_{c_o}	in	5.01959	4.47346	3.73135	3.51111	3.84917	4.67777	6.04983	8.02095
f	lb/hr	921.685	854.123	763.341	732.363	755.190	827.894	869.854	1230.747
X_u/m	$\frac{ft/sec^2}{ft/sec}$	-.02540	-.00181	-.02156	-.03604	-.04642	-.05579	-.06456	-.07206
X_w/m	$\frac{ft/sec^2}{ft/sec}$.05449	.06818	.08255	.08944	.08548	.10343	.08523	.05666
X_q/m	$\frac{ft/sec^2}{rad/sec}$.60185	.74915	.87508	.84957	.73079	1.24872	.77601	.25183
X_{δ_c}/m	$\frac{ft/sec^2}{in}$.17696	.13988	.12312	.14237	.16406	-.05165	-.03776	-.01954
X_{δ_c}/m	$\frac{ft/sec^2}{in}$	1.20482	.97467	.87948	.80253	.68335	.88200	.72040	.48341
Z_u/m	$\frac{ft/sec^2}{ft/sec}$.06009	-.12594	-.08296	-.02192	.01396	-.06077	.06546	-.04980
Z_w/m	$\frac{ft/sec^2}{ft/sec}$	-.36933	-.48399	-.63639	-.80152	-.92055	-1.00063	-1.04552	-1.10516
Z_q/m	$\frac{ft/sec^2}{rad/sec}$	-.71511	-1.16872	-1.77844	-1.81400	-1.81986	-2.22039	-2.25955	-2.47935
Z_{δ_c}/m	$\frac{ft/sec^2}{in}$	-.00407	.21188	.51943	.56820	.52527	.46341	.41480	.36743
Z_{δ_c}/m	$\frac{ft/sec^2}{in}$	-7.43006	-7.23138	-7.65410	-8.52446	-9.49008	-10.26600	-11.08740	-11.71110
M_u/I_{yy}	$\frac{rad/sec^2}{ft/sec}$.00656	.00645	-.00587	-.00670	-.00582	-.00185	-.00120	-.00089
M_w/I_{yy}	$\frac{rad/sec^2}{ft/sec}$	-.00285	.00978	.01630	.01363	.01154	.00956	.00774	.00691
M_q/I_{yy}	$\frac{rad/sec^2}{rad/sec}$	-.73173	-.96002	-1.31158	-1.45996	-1.52219	-1.62003	-1.59067	-1.51570
M_{δ_c}/I_{yy}	$\frac{rad/sec^2}{in}$.35447	.35364	.40144	.45022	.48135	.51572	.53335	.54565
M_{δ_c}/I_{yy}	$\frac{rad/sec^2}{in}$	-.04765	-.04252	.04556	.06776	.06725	.04707	.03948	.03505

Table D-3. YHC-1A Lateral Stability Derivatives (Rate of Descent = 0 ft/min).

FORWARD VELOCITY	KTS	0	20	40	60	80	100	120	140
δ_{a_0}	in	.12983	.08462	.09191	.13466	.17931	.29754	.44154	.49785
δ_{r_0}	in	-.17764	-.04701	-.08508	-.33705	-.61293	-.75397	-1.04713	-1.14123
Y_V/m	$\frac{\text{ft/sec}^2}{\text{ft/sec}}$	-.02663	-.05408	-.07986	-.11823	-.16121	-.18040	-.19766	-.23442
Y_P/m	$\frac{\text{ft/sec}^2}{\text{rad/sec}}$	-.76514	-.95618	-1.15981	-1.24824	-1.23341	-1.02295	-.76619	-.29372
Y_R/m	$\frac{\text{ft/sec}^2}{\text{rad/sec}}$	-.12517	-.18179	-.20082	-.12813	-.05819	.13380	.12514	.22125
$Y\delta_a/m$	$\frac{\text{ft/sec}^2}{\text{in}}$.99794	.99700	.97673	.96426	.96955	.97123	1.01613	1.10225
$Y\delta_r/m$	$\frac{\text{ft/sec}^2}{\text{in}}$.14652	.13634	.11652	.10583	.09849	.11641	.13883	.15262
L_V/I_{xx}	$\frac{\text{rad/sec}^2}{\text{ft/sec}}$	-.00778	-.01305	-.01338	-.01720	-.02442	-.03188	-.04724	-.05080
L_P/I_{xx}	$\frac{\text{rad/sec}^2}{\text{rad/sec}}$	-.50730	-.57483	-.64045	-.65271	-.62549	-.52243	-.41134	-.23476
L_R/I_{xx}	$\frac{\text{rad/sec}^2}{\text{rad/sec}}$	-.02297	-.04571	-.05943	-.02270	.01172	.09531	.11659	.19955
$L\delta_a/I_{xx}$	$\frac{\text{rad/sec}^2}{\text{in}}$.46536	.46558	.45954	.45575	.45805	.45820	.47354	.50528
$L\delta_r/I_{xx}$	$\frac{\text{rad/sec}^2}{\text{in}}$	-.12638	-.13036	-.13422	-.13544	-.13910	-.13256	-.13248	-.14433
N_V/I_{zz}	$\frac{\text{rad/sec}^2}{\text{ft/sec}}$.00013	.00037	-.00123	-.00290	-.00415	-.00536	-.00377	-.00060
N_P/I_{zz}	$\frac{\text{rad/sec}^2}{\text{rad/sec}}$	-.01831	-.02076	-.02598	-.03947	-.05344	-.06864	-.07747	-.07471
N_R/I_{zz}	$\frac{\text{rad/sec}^2}{\text{rad/sec}}$	-.05847	-.05450	-.04597	-.05020	-.05438	-.08078	-.08642	-.12617
$N\delta_a/I_{zz}$	$\frac{\text{rad/sec}^2}{\text{in}}$.03001	.02923	.02764	.02663	.02633	.02696	.02857	.02970
$N\delta_r/I_{zz}$	$\frac{\text{rad/sec}^2}{\text{in}}$.17534	.17578	.17261	.17032	.17141	.17146	.17933	.19536

Table D-4. YHC-1A Longitudinal Stability Derivatives (Rate of Descent = 1500 ft/min).

FORWARD VELOCITY	KTS	0	20	40	60	80	100*	120*	140*
θ_o	deg	8.9881	8.13867	6.99471	5.34340	3.21352	2.32445	-1.37813	-5.74252
δ_{e_o}	in	.03060	-1.69234	-.56815	.11550	.60565	-.23371	-.00860	.17046
δ_{c_o}	in	3.89872	3.25038	1.25071	.90347	1.15881	1.98741	3.35947	5.32989
f	lb/hr	791.849	711.302	500.687	470.262	495.961	568.665	610.625	971.518
X_u/m	$\frac{ft/sec^2}{ft/sec}$.01143	.02237	-.01281	-.03179	-.04306	-.05243	-.06120	-.06870
X_w/m	$\frac{ft/sec^2}{ft/sec}$.04368	.05111	.10637	.10919	.10653	.12448	.10628	.07771
X_q/m	$\frac{ft/sec^2}{rad/sec}$	1.02536	.93903	1.55534	1.45965	1.37043	1.88836	1.41565	.89147
X_{δ_e}/m	$\frac{ft/sec^2}{in}$.16625	.12347	.08223	.12593	.14599	-.06972	-.05583	-.03761
X_{δ_c}/m	$\frac{ft/sec^2}{in}$	1.13928	.94352	.82126	.88028	.82702	1.02567	.86407	.62708
Z_u/m	$\frac{ft/sec^2}{ft/sec}$	-.13435	-.23640	-.12619	-.02151	.01777	.06458	.06927	.05361
Z_w/m	$\frac{ft/sec^2}{ft/sec}$	-.28748	-.26321	-.82254	-.90575	-.98052	-1.06060	-1.10549	-1.16513
Z_q/m	$\frac{ft/sec^2}{rad/sec}$	-.79039	.30060	-2.45731	-2.40596	-2.42975	-2.83028	-2.86944	-3.08924
Z_{δ_e}/m	$\frac{ft/sec^2}{in}$.00615	.19996	.94841	.77315	.71536	.65350	.60489	.55752
Z_{δ_c}/m	$\frac{ft/sec^2}{in}$	-7.45257	-7.38250	-6.35173	-8.00904	-9.05358	-9.82953	-10.65093	-11.27463
M_u/I_{yy}	$\frac{rad/sec^2}{ft/sec}$.01308	.01863	-.00906	-.00696	-.00635	-.00238	-.00173	-.00142
M_w/I_{yy}	$\frac{rad/sec^2}{ft/sec}$.00368	.03420	.00228	.00469	.00683	.00485	.00303	.00220
M_q/I_{yy}	$\frac{rad/sec^2}{rad/sec}$	-.58241	-.81810	-1.48310	-1.56553	-1.62309	-1.72093	-1.69157	-1.61660
M_{δ_e}/I_{yy}	$\frac{rad/sec^2}{in}$.34363	.30612	.43861	.47166	.50338	.53775	.55538	.56768
M_{δ_c}/I_{yy}	$\frac{rad/sec^2}{in}$	-.05591	-.16472	.15368	.11620	.10884	.09602	.08843	.08400

* Data extrapolated from values at 80 knots.

Table D-5. YHC-1A Lateral Stability Derivatives (Rate of Descent = 1500 ft/min).

FORWARD VELOCITY	KTS	0	20	40	60	80	100*	120*	140*
δ_{a_0}	in	.09255	.04445	.01404	.05177	.09882	.21705	.36105	.41736
δ_{r_0}	in	-.07915	.32928	.06918	-.19696	-.43185	-.57289	-.86605	-.96015
Y_v/m	$\frac{ft/sec^2}{ft/sec}$	-.08635	-.04068	-.11126	-.15170	-.18262	-.20181	-.21907	-.25583
Y_p/m	$\frac{ft/sec^2}{rad/sec}$	-1.10440	-1.30270	-1.78540	-1.86230	-1.73270	-1.52224	-1.26548	-.79301
Y_r/m	$\frac{ft/sec^2}{rad/sec}$	-.18435	-.10798	-.30137	-.22815	-.19244	-.00045	-.00911	.08700
$Y\delta_{a/m}$	$\frac{ft/sec^2}{in}$.98054	.97047	.92561	.89687	.87675	.87843	.92333	1.00945
$Y\delta_{r/m}$	$\frac{ft/sec^2}{in}$.14250	.11217	.09751	.07301	.07008	.08800	.11042	.12421
L_v/I_{xx}	$\frac{rad/sec^2}{ft/sec}$	-.00996	-.00799	-.00448	-.00371	-.00289	-.01035	-.02571	-.02927
L_p/I_{xx}	$\frac{rad/sec^2}{rad/sec}$	-.63036	-.71659	-.86876	-.87455	-.79734	-.69428	-.58319	-.40661
L_r/I_{xx}	$\frac{rad/sec^2}{rad/sec}$	-.05234	-.02797	-.10977	-.07677	-.05688	.02671	.04799	.13095
$L\delta_a/I_{xx}$	$\frac{rad/sec^2}{in}$.45903	.45705	.44170	.43230	.42630	.42645	.44179	.47353
$L\delta_r/I_{xx}$	$\frac{rad/sec^2}{in}$	-.12454	-.13516	-.13185	-.13554	-.13256	-.12602	-.12594	-.13779
N_v/I_{zz}	$\frac{rad/sec^2}{ft/sec}$.00122	-.00016	-.00236	-.00456	-.00706	-.00827	-.00668	-.00351
N_p/I_{zz}	$\frac{rad/sec^2}{rad/sec}$	-.02085	-.01101	-.02424	-.04001	-.05921	-.07441	-.08324	-.08048
N_r/I_{zz}	$\frac{rad/sec^2}{rad/sec}$	-.04986	-.02575	-.03287	-.03310	-.03704	-.06380	-.06944	-.10919
$N\delta_a/I_{zz}$	$\frac{rad/sec^2}{in}$.02925	.02744	.02580	.02385	.02313	.02376	.02537	.02650
$N\delta_r/I_{zz}$	$\frac{rad/sec^2}{in}$.17285	.17149	.16373	.15906	.15540	.15545	.16332	.17935

*Data extrapolated from values at 80 knots.

Table D-6. YHC-1A Longitudinal Stability Derivatives (Rate of Descent = -1500 ft/min).

FORWARD VELOCITY	KTS	0	20	40	60	80	100*	120*	140*
$\dot{\theta}_o$	deg	9.09615	8.24561	6.51804	4.34680	1.74707	.85800	-2.84458	-7.20897
δ_{c_o}	in	.56611	.45244	.38166	.63183	1.02115	.18179	.40690	.58596
δ_{c_o}	in	6.51301	6.30131	5.94168	5.94845	6.38886	7.21746	8.58952	10.55994
f	lb/hr	1102.055	1076.035	1023.741	1012.939	1055.591	1128.295	1170.255	1531.148
X_u/m	$\frac{ft/sec^2}{ft/sec}$	-.02649	-.01935	-.03260	-.04491	-.05277	-.06214	-.07091	-.07841
X_w/m	$\frac{ft/sec^2}{ft/sec}$.07505	.08122	.08209	.07521	.06568	.08363	.06543	.03686
X_q/m	$\frac{ft/sec^2}{rad/sec}$.15633	.20875	.26690	.17058	.09717	.61510	.14239	-.38179
X_{δ_e}/m	$\frac{ft/sec^2}{in}$.17842	.16228	.14484	.16227	.18105	-.03466	-.02077	-.00255
X_{δ_c}/m	$\frac{ft/sec^2}{in}$	1.16992	1.04008	.90570	.78861	.62563	.82428	.66268	.42569
Z_u/m	$\frac{ft/sec^2}{ft/sec}$.04316	-.02454	-.00971	.00737	.02520	.07201	.07620	.06104
Z_w/m	$\frac{ft/sec^2}{ft/sec}$	-.52217	-.60121	-.72925	-.85332	-.94171	-1.02179	-1.06668	-1.12632
Z_q/m	$\frac{ft/sec^2}{rad/sec}$	-1.07268	-1.20010	-1.25010	-1.38662	-1.47426	-1.87479	-1.91395	-2.13375
Z_{δ_e}/m	$\frac{ft/sec^2}{in}$.05444	.16010	.36218	.41296	.41472	.35286	.30425	.25688
Z_{δ_c}/m	$\frac{ft/sec^2}{in}$	-7.5865	-7.64041	-8.2477	-8.9541	-9.7090	-10.48495	-11.30635	-11.93005
M_u/I_{yy}	$\frac{rad/sec^2}{ft/sec}$.00251	.00163	.00321	-.00458	-.00467	-.00070	-.00005	.00025
M_w/I_{yy}	$\frac{rad/sec^2}{ft/sec}$	-.00148	.00327	.00726	.00765	.00730	.00532	.00350	.00267
M_q/I_{yy}	$\frac{rad/sec^2}{rad/sec}$	-.93433	-1.03020	-1.24040	-1.37428	-1.4243	-1.52214	-1.49278	-1.41781
M_{δ_e}/I_{yy}	$\frac{rad/sec^2}{in}$.37472	.37930	.40095	.43815	.46558	.49995	.51758	.52958
M_{δ_c}/I_{yy}	$\frac{rad/sec^2}{in}$	-.04570	-.03118	.01909	.03637	.04212	.02194	.01435	.00992

* Data extrapolated from values at 80 knots.

Table D-7. YHC-1A Lateral Stability Derivatives (Rate of Descent = -1500 ft/min).

FORWARD VELOCITY	KTS	0	20	40	60	80	100*	120*	140*
δ_{a_o}	in	.16567	.15081	.14181	.15535	.20065	.31888	.46288	.51919
δ_{r_o}	in	-.23383	-.21772	-.28008	-.42584	-.61869	-.75973	-1.05289	-1.14699
Y_v/m	$\frac{\text{ft/sec}^2}{\text{ft/sec}}$	-.02060	-.08482	-.10455	-.12256	-.14842	-.16761	-.18487	-.22163
Y_p/m	$\frac{\text{ft/sec}^2}{\text{rad/sec}}$	-.40249	-.48197	-.63817	-.68143	-.63180	-.42134	-.16458	.30789
Y_r/m	$\frac{\text{ft/sec}^2}{\text{rad/sec}}$	-.04204	.04052	-.06921	-.04086	.01514	.20713	.19847	.29458
Y_{δ_a}/m	$\frac{\text{ft/sec}^2}{\text{in}}$	1.03950	1.04228	1.04066	1.04266	1.06287	1.06455	1.10945	1.19557
Y_{δ_r}/m	$\frac{\text{ft/sec}^2}{\text{in}}$.14982	.14802	.12894	.11875	.12938	.14730	.16972	.18351
L_v/I_{xx}	$\frac{\text{rad/sec}^2}{\text{ft/sec}}$	-.02127	.01846	-.01978	.02294	-.02866	-.03612	-.05148	-.05504
L_p/I_{xx}	$\frac{\text{rad/sec}^2}{\text{rad/sec}}$	-.37496	-.40345	-.45470	-.46318	-.42905	-.32599	-.21490	-.03832
L_r/I_{xx}	$\frac{\text{rad/sec}^2}{\text{rad/sec}}$.02907	.06798	.02113	.03740	.07088	.15447	.17575	.25871
L_{δ_a}/I_{xx}	$\frac{\text{rad/sec}^2}{\text{in}}$.48113	.48228	.48271	.48417	.49124	.49139	.50673	.53847
L_{δ_r}/I_{xx}	$\frac{\text{rad/sec}^2}{\text{in}}$	-.13312	-.13406	-.14131	-.14556	-.14455	-.13801	-.13793	-.14978
N_v/I_{zz}	$\frac{\text{rad/sec}^2}{\text{ft/sec}}$.00108	.00098	.00044	.00052	.00041	-.00080	.00079	.00396
N_p/I_{zz}	$\frac{\text{rad/sec}^2}{\text{rad/sec}}$	-.02133	-.02122	-.02478	-.02754	-.03643	-.05163	-.06046	-.05770
N_r/I_{zz}	$\frac{\text{rad/sec}^2}{\text{rad/sec}}$	-.07653	-.06348	-.07218	-.07450	-.08262	-.10902	-.11466	-.15441
N_{δ_a}/I_{zz}	$\frac{\text{rad/sec}^2}{\text{in}}$.03076	.03053	.02424	.02856	.02918	.02981	.03142	.03255
N_{δ_r}/I_{zz}	$\frac{\text{rad/sec}^2}{\text{in}}$.18338	.18355	.18366	.18425	.18730	.18735	.19522	.21125

*Data extrapolated from values at 80 knots.

APPENDIX E

STABILITY DERIVATIVES CH-47 HELICOPTER

This appendix presents the stability derivatives provided by NASA LaRC for the CH-47 VALT research helicopter, which will be used to evaluate the advanced display concepts for commercial VTOL aircraft. The column labeled 0.00000 was derived by fitting a third order curve through -40, -20, +20 and +40 values.

LDL= -0000.00, YDUL= 0.00

XDUT	-40.00000	-20.00000	0.00000	20.00000	40.00000	60.00000	80.00000	100.00000	120.00000	140.00000	160.00000	
XU/A	1/SEC	-05118	-04400	-02862	-01680	-02032	-02594	-03059	-03473	-04149	-04742	-05539
XV/A	1/SEC	-00316	-00371	-00564	-00504	00121	-00002	-00074	-00162	-00288	-00477	-00913
XW/A	1/SEC	007545	05517	05517	04082	03871	03191	02074	00780	00789	00076	-02732
XUB/A	1/SEC	15941	14142	12943	12308	12502	13553	14923	15833	12347	08479	-04701
XUC/A	1/SEC	103701	129423	90852	72507	50871	29371	03588	24779	-29769	-48805	-110707
XUD/A	1/SEC	-00130	-00093	-00368	-00051	-00307	-00027	-00017	-00006	-00007	00003	00037
XUE/A	1/SEC	-00070	-00054	-00045	-00041	-00036	-00037	-00042	-00052	-00045	-00037	-00037
XVF/A	1/SEC	06319	06770	01851	-02621	-00925	-00064	00158	00758	00911	01015	01518
XVW/A	1/SEC	-23021	-21555	-12490	-04060	-04446	-05976	-07565	-09320	-10096	-12259	-19875
XVX/A	1/SEC	-00205	-00344	-00344	-00118	-00041	-00034	-00034	-00057	-00090	-00096	-00059
XVY/A	1/SEC	-11966	-19226	-18665	-14146	-07535	-18665	-10660	-12218	-13994	-16058	-18770
XVZ/A	1/SEC	00420	00448	00468	00500	00532	00530	00527	00536	00491	00431	00217
YUB/A	1/SEC	00255	00783	01503	02270	02942	02752	01832	00366	-02691	-07455	-15112
YUC/A	1/SEC	08859	08289	08387	08603	08687	08665	08740	08727	09656	09836	07447
YUD/A	1/SEC	119595	119100	118384	117568	116770	117240	118739	121011	123366	126841	135059
YUE/A	1/SEC	-09284	-07297	-06955	-03025	-02371	-02280	-02200	-01386	-02614	-08949	-11619
YU/A	1/SEC	-101152	-84513	-78321	-82669	-97650	-109171	-114141	-112691	-104293	-89819	-72210
YU/A	1/SEC	-06963	-04832	-01149	03498	08596	11887	12534	12738	13159	13265	13921
YU/A	1/SEC	15413	13780	03773	-05601	-05338	-03476	-02517	-02305	-00183	02673	03788
ZU/A	1/SEC	-00626	-00078	00138	00090	00156	-00109	00022	00112	-00174	00206	00555
ZU/A	1/SEC	-31004	-42984	-41575	-45665	-54146	-66165	-68038	-73471	-71791	-66132	-58574
ZUB/A	1/SEC	-18454	-07609	02530	12574	23139	30079	32456	32456	27513	16413	34962
ZUC/A	1/SEC	-904134	-861642	-95956	-871609	-923146	-996946	-107577	-1154134	-1144896	-1040171	-915237
ZUD/A	1/SEC	00083	00656	00589	00555	00528	00545	00609	00749	00812	00900	01211
ZUE/A	1/SEC	00082	00029	00010	00037	00053	00075	00117	00119	00078	00105	00273
ZU/A	1/SEC	118366	12884	11306	06937	02413	10043	10083	06560	08210	10083	14145
ZU/A	1/SEC	109826	50943	52048	55436	02603	2048	18900	-05936	20901	25632	23303
ZU/A	1/SEC	08575	04197	00325	-77589	-79252	-73035	-68374	-69348	-71694	-71756	-78478
ZU/A	1/SEC	-00357	-00063	-00055	-00036	-00020	-00008	00004	00018	00012	00026	00036
ZU/A	1/SEC	00736	00041	00030	00073	00070	00072	00171	00788	00859	00975	01190
ZU/A	1/SEC	00043	00044	00046	00046	00070	00087	00101	00113	00138	00175	00184
ZU/A	1/SEC	-03983	-03832	-03477	-02964	-02337	-02039	-02045	-02319	-03197	-04800	-07546
ZU/A	1/SEC	-01166	-01491	-01721	-01865	-01933	-01978	-02016	-02025	-01804	-01292	-01547
ZU/A	1/SEC	03513	03104	02225	04478	41662	41781	42164	42697	43141	47857	45767
ZU/A	1/SEC	-15274	-14717	-14046	-13469	-13194	-13241	-13395	-13425	-12660	-11929	-11618
ZU/A	1/SEC	049483	04596	01947	01426	05422	01782	07104	06336	05249	04679	03453
ZU/A	1/SEC	15014	14593	14176	13165	10961	09877	09740	10394	13124	17750	24050
ZU/A	1/SEC	-03513	-03104	-02967	-03047	-03480	-03759	-03817	-03692	-03457	-02936	-02151
ZU/A	1/SEC	00027	00104	00138	00095	00060	00023	00293	00236	00162	00238	00302
ZU/A	1/SEC	00220	00245	00015	00257	00176	00077	00014	00094	00179	00236	00302
ZU/A	1/SEC	-00703	-00255	00169	00600	01066	01324	01460	01571	01495	01474	01069
ZU/A	1/SEC	37256	36008	35545	35805	37046	39201	41467	43642	41832	37555	31234
ZU/A	1/SEC	03008	03104	02225	04478	41662	41781	42164	42697	43141	47857	45767
ZU/A	1/SEC	00002	00000	00024	00003	00004	00005	00008	00010	00010	00010	00007
ZU/A	1/SEC	-00162	-00138	-00124	-00115	-00107	-00107	-00121	-00145	-00152	-00162	-00215
ZU/A	1/SEC	02734	03360	00252	-03813	-03030	-01752	-00916	00600	01516	02173	02756
ZU/A	1/SEC	-15274	-14717	-14046	-13469	-13194	-13241	-13395	-13425	-12660	-11929	-11618
ZU/A	1/SEC	01017	00456	00456	00908	01362	01562	01186	00608	00152	00333	00421
ZU/A	1/SEC	00030	00052	00065	00085	00044	00031	00025	00022	00015	00004	00035
ZU/A	1/SEC	-00197	-00355	-00110	00051	00043	00021	00030	00021	00037	00047	00034
ZU/A	1/SEC	00045	00035	00035	00039	00037	00020	00032	00031	00115	00251	00444
ZU/A	1/SEC	06166	06515	06613	06460	06053	05815	05767	05942	06320	07025	08162
ZU/A	1/SEC	-00419	-00110	00191	00518	00902	01239	01474	01592	01013	00506	03196
ZU/A	1/SEC	00703	00822	00963	01078	01119	01125	01137	01137	01582	01185	03150
ZU/A	1/SEC	20917	20917	20812	20687	20556	20646	20895	21303	21747	22385	23344
ZU/A	1/SEC	03790	02569	00744	-01049	-02254	-03137	-04039	-05300	-07687	-10728	-14968
ZU/A	1/SEC	-21913	-23281	-23718	-23246	-21888	-20645	-19017	-19464	-17704	-16343	-15835
ZU/A	1/SEC	-04328	-04433	-04351	-04660	-04736	-05025	-05339	-05964	-06983	-08889	-11644
ZU/A	1/SEC	18425	16325	24597	34123	35786	18502	09439	0521	66573	91705	134546
ZU/A	1/SEC	58964	56235	58805	57606	54631	53353	54049	56751	61191	68747	82019
ZU/A	1/SEC	30373	32866	32059	30141	28408	26408	25759	26471	26471	30274	36246
ZU/A	1/SEC	64319	16355	07431	-01311	-08732	-18775	-31210	-45927	-63590	-85940	-12164
ZU/A	1/SEC	904930	798786	61948	510268	402518	258770	161870	-07356	-13030	-24068	-617521
ZU/A	1/SEC	-53690	-54449	-56340	-57188	-54015	-52384	-51909	-53071	-59492	-62282	-70325

2001 = -1500.000 YDUIT = 0.00

ADJ.	-40.00000	-20.00000	0.00000	20.00000	40.00000	60.00000	80.00000	100.00000	120.00000	140.00000	160.00000
XU/M	-0.5033	-0.4387	-0.2686	-0.1355	-0.1818	-0.2447	-0.2928	-0.3329	-0.3977	-0.4612	-0.5283
XV/M	-0.0115	-0.0711	-0.0230	0.0340	0.0060	0.0015	-0.0064	-0.0126	-0.0216	-0.0379	-0.0591
Y/M	0.7103	0.5143	0.4213	0.3923	0.3884	0.3340	0.2340	0.1158	0.0149	0.0531	0.1181
XDU/M	1.6116	1.3934	1.2584	1.1997	1.2108	1.2584	1.4978	1.5949	1.6458	1.6657	1.6407
YDU/M	1.5977	1.2697	0.9728	0.7196	0.5199	0.3253	0.2153	0.1649	0.17508	0.18266	0.18044
AD5/Y	-0.0093	-0.0068	-0.0048	-0.0034	-0.0024	-0.0018	-0.0013	-0.0007	-0.0001	-0.0004	-0.0004
AD6/Y	-0.0054	-0.0040	-0.0030	-0.0026	-0.0022	-0.0023	-0.0026	-0.0034	-0.0043	-0.0057	-0.0078
XP/A	0.6864	0.6545	0.6134	0.5659	0.5069	0.4799	0.4313	0.3792	0.3288	0.2808	0.2372
X/A	2.4200	2.5913	2.6028	2.56639	2.50696	2.47299	2.4248	2.3616	2.29970	2.24823	2.19659
A/Y	-2.2351	-2.1195	-1.1195	-0.1805	-0.2481	-0.4254	-0.5814	-0.7309	-0.8786	-0.9831	-1.0467
Y/Y	-0.0169	-0.0265	-0.0087	0.0100	0.0032	0.0024	0.0048	0.0079	0.0101	0.0087	0.0086
Y/M	-1.9873	-1.7212	-1.6982	-1.3168	-0.8753	-0.8844	-1.0083	-1.1743	-1.3536	-1.5579	-1.8139
Y/M	0.0340	0.0379	0.0493	0.0440	0.0476	0.0467	0.0457	0.0444	0.0434	0.0421	0.0411
YDU/M	0.0670	0.0230	0.0145	0.02619	0.07819	0.15787	0.27636	0.40827	0.50335	0.63328	0.7999
YDU/M	0.7619	0.7713	0.7965	0.7965	0.7819	0.7649	0.7636	0.7636	0.7636	0.7636	0.7636
YDU/M	1.18133	1.17516	1.16595	1.15528	1.1528	1.15787	1.16867	1.18731	1.20578	1.23445	1.26812
YDU/M	0.9076	0.7337	0.5071	0.3216	0.2712	0.3021	0.3384	0.3915	0.4628	0.5473	0.6315
Y/M	-1.23216	-1.04164	-0.97175	-1.02387	-1.19941	-1.32643	-1.57600	-1.95442	-2.5516	-3.49089	-4.80315
Y/M	-0.3506	-0.2204	-0.0682	0.0608	0.1291	0.2147	0.3147	0.4289	0.5562	0.7059	0.8733
Y/M	-1.3065	-1.1491	-1.0426	-0.928	-0.8256	-0.7431	-0.6851	-0.6495	-0.6298	-0.6179	-0.6133
Y/M	1.6121	1.5040	0.3464	0.1480	0.0644	0.0075	-0.2741	-0.6259	-1.0052	-1.4186	-1.8686
Z/A	-0.0716	-0.0141	0.0089	0.0059	-0.0144	-0.0031	-0.0100	-0.0172	-0.0240	-0.0326	-0.0426
Z/M	-4.8786	-4.0112	-3.8687	-3.3138	-2.5093	-2.0080	-1.6690	-1.4274	-1.2914	-1.2121	-1.1676
ZDU/M	0.2924	0.08395	0.2643	0.33573	0.25785	0.3436	0.35668	0.35174	0.3441	0.3211	0.2913
ZDU/M	-8.40506	-8.47970	-8.37162	-8.37537	-9.08549	-9.6153	-10.65535	-11.66771	-11.66779	-10.25269	-9.84852
ZDU/M	0.0566	0.0479	0.0416	0.0330	0.0340	0.0342	0.0360	0.0380	0.0413	0.0453	0.0495
Z/M	-0.0079	-0.0024	-0.0010	-0.0028	-0.0035	-0.0041	-0.0041	-0.0041	-0.0041	-0.0041	-0.0041
Z/M	1.28526	0.9370	0.5091	0.2584	0.19061	0.1239	0.0777	0.0407	0.0334	0.0322	0.0319
Z/M	51.806	52030	0.2824	0.86673	-0.87324	7.5676	-6.6760	-6.6488	-6.6472	-6.6427	-7.2414
LV/AX	-0.0053	-0.0061	-0.0049	-0.0030	-0.0017	-0.0015	-0.0011	-0.0013	-0.0016	-0.0020	-0.0025
LV/AX	0.0690	0.0701	0.0696	0.0680	0.0663	0.0669	0.0694	0.0736	0.0799	0.0864	0.0935
LV/AX	0.0050	0.0046	0.0047	0.0056	0.0080	0.0099	0.0112	0.0123	0.0161	0.0169	0.0210
LV/AX	0.3817	0.3628	0.3173	0.2528	0.1769	0.1520	0.1394	0.1317	0.12269	0.1196	0.1119
LV/AX	0.1021	0.1376	0.1616	0.1744	0.1766	0.1759	0.1773	0.1782	0.1782	0.1782	0.1782
LV/AX	4.2301	4.1950	4.1644	4.1431	4.1353	4.1431	4.1720	4.2176	4.2508	4.2809	4.3089
LV/AX	1.5044	1.4626	1.3985	1.3416	1.3174	1.3281	1.3489	1.3750	1.4068	1.4418	1.4813
LV/AX	0.6432	0.5928	0.5692	0.5688	0.6079	0.6365	0.66013	0.6800	0.6938	0.7007	0.7072
LV/AX	1.4214	1.3625	1.2938	1.1315	0.8715	0.7420	0.6401	0.5753	0.5374	0.5180	0.5010
LV/AX	0.4261	0.3797	0.3559	0.3466	0.4158	0.4487	0.4553	0.4410	0.4345	0.4270	0.4200
LV/AX	0.0082	0.0203	0.0255	0.0190	0.0036	0.0253	0.0311	0.0304	0.0208	0.0158	0.0127
LV/AX	0.0200	0.0216	0.0006	0.021	0.143	0.0058	0.0019	0.0091	0.0165	0.0204	0.0267
LV/AX	0.0826	0.0303	0.0174	0.0654	0.1184	0.1413	0.1510	0.1593	0.1739	0.1938	0.2147
LV/AX	3.6851	3.5481	3.4973	3.5351	3.6638	3.9071	4.1484	4.3722	4.615	4.8660	5.1197
LV/AX	0.3176	0.2620	0.2162	0.1820	0.1624	0.1603	0.1603	0.1603	0.1603	0.1603	0.1603
LV/AX	0.0001	0.0000	0.0001	0.0002	0.0003	0.0003	0.0003	0.0003	0.0003	0.0003	0.0003
LV/AX	0.0119	0.0101	0.0088	0.0077	0.0067	0.0066	0.0066	0.0066	0.0066	0.0066	0.0066
LV/AX	0.3643	0.4140	0.4240	0.4582	0.4770	0.4255	0.3915	0.3620	0.3400	0.3240	0.3120
LV/AX	-1.52562	-1.36512	-1.1090	-0.86209	-0.61781	-0.43613	-0.3036	-0.2159	-0.1519	-0.1015	-0.0744
LV/AX	-0.1319	-0.0270	-0.0330	-0.0125	-0.0184	-0.02036	-0.0236	-0.0267	-0.0271	-0.0271	-0.0271
LV/AX	0.0023	0.0047	0.0062	0.0061	0.0039	0.0027	0.0023	0.0021	0.0016	0.0005	0.0005
LV/AX	0.0180	0.00320	0.0094	0.0144	0.0039	0.0006	-0.0014	-0.0029	-0.0046	-0.0059	-0.0075
LV/AX	0.0042	0.0030	0.0032	0.0037	0.0036	0.0015	-0.0004	-0.0004	-0.0006	-0.0016	-0.0035
LV/AX	0.0568	0.0521	0.0508	0.0576	0.0536	0.0501	0.04924	0.0529	0.05402	0.0590	0.0719
LV/AX	0.0067	0.0146	0.0158	0.0079	0.0081	0.0163	0.0194	0.0156	0.0124	0.0086	0.0051
LV/AX	0.0703	0.0811	0.0949	0.1058	0.1081	0.1063	0.1049	0.1094	0.1133	0.1160	0.11928
LV/AX	0.2064	0.2051	0.2063	0.2081	0.2081	0.2081	0.2081	0.2081	0.2081	0.2081	0.2081
LV/AX	0.3068	0.2154	0.0344	0.1082	-0.02047	0.2704	-0.3383	0.4389	0.6407	0.8988	1.2650
LV/AX	-1.9053	-2.0835	-2.1434	-2.0859	-1.9118	-1.7488	-1.6413	-1.5939	-1.4690	-1.3211	-1.1531
LV/AX	-0.4228	-0.4328	-0.4532	-0.4511	-0.4536	-0.4581	-0.4646	-0.4739	-0.4842	-0.4959	-0.5085
LV/AX	-0.4989	-0.9073	0.25840	-4.3378	-5.0978	-3.2418	4.79996	4.84093	5.08308	5.49268	6.2151
LV/AX	5.09593	5.40061	5.48036	5.33684	4.97169	4.79996	4.84093	5.08308	5.49268	6.2151	7.45641
LV/AX	2.6770	2.9913	2.9913	2.9190	2.7169	2.5913	2.5115	2.4009	2.3112	2.2604	2.2250
LV/AX	1.8005	1.2923	0.7131	0.1383	-0.3566	-1.2515	-2.4009	-3.7341	-5.2654	-7.1934	-1.02469
LV/AX	9.28055	7.92430	6.6124	5.34968	4.14412	2.78578	1.17638	-0.53930	-2.92517	-1.90961	-5.45690
LV/AX	-4.8783	-5.1836	-5.3998	-5.3556	-4.9431	-4.6426	-4.5899	-4.5899	-4.5899	-4.5899	-4.5899

ACCT	-40.00000	-20.00000	0.00000	20.00000	40.00000	60.00000	80.00000	100.00000	120.00000	140.00000	160.00000	
XU/M	1/SEC	-04972	-04402	-02511	-01009	-01604	-02307	-02806	-03200	-03833	-04501	-05093
XU/M	1/SEC	-00001	-00001	-00149	-00175	-00326	-00411	-00537	-00618	-00718	-00833	-00976
XU/M	1/SEC	-06619	-04724	-03904	-03759	-03869	-03484	-02603	-00018	-00138	-00261	-00376
AD/M	F1/SEC2-IN	1.6333	1.3727	1.2217	1.1608	1.1705	1.3105	1.4845	1.6082	1.6431	1.4845	0.8900
AD/M	F1/SEC2-IN	1.55476	1.24691	0.95914	0.71302	0.53009	0.36094	0.14858	-0.08836	-0.5048	-0.76597	-0.9618
XU/M	F1/SEC2-IN	-00062	-00044	-00030	-00019	-00013	-00009	-00006	-00006	-00009	-00009	-00021
XU/M	F1/SEC2-IN	-00036	-00027	-00019	-00014	-00010	-00011	-00014	-00020	-00021	-00018	-00326
XU/M	F1/SEC	-07878	-06776	-02112	-01601	-00205	-00396	-00926	-00465	-00651	-00746	-01105
AD/M	F1/SEC	2.34955	2.57095	2.59638	2.53239	2.48428	2.43266	2.41469	2.45538	2.60669	2.93349	3.28150
AD/M	F1/SEC	-22192	-21234	-09958	-00983	-00098	-03151	-04247	-05503	-05724	-07393	-12226
YU/M	F1/SEC	-00139	-00208	-00060	-00090	-00024	-00013	-00039	-00071	-00094	-00084	-00371
YU/M	F1/SEC	-04938	-15574	-15610	-12340	-08054	-08301	-04629	-11328	-13143	-15165	-17610
YU/M	F1/SEC	-00324	-00324	-00348	-00391	-00434	-00412	-00391	-00395	-00463	-00338	-00396
YU/M	F1/SEC2-IN	-01600	-00370	-01329	-03014	-04281	-04004	-02892	-01435	-00388	-05315	-10396
YU/M	F1/SEC2-IN	-06701	-07144	-07384	-07355	-06990	-06667	-06490	-06780	-08390	-07431	-07618
YU/M	F1/SEC2-IN	1.07124	1.17331	1.16814	1.15778	1.14427	1.14416	1.15126	1.16540	1.17883	1.20148	1.26714
YU/M	F1/SEC2-IN	-08862	-07386	-05181	-03383	-03128	-03393	-04536	-04462	-01384	-01970	-05677
YU/M	F1/SEC	-1.45203	-1.23353	-1.15428	-1.21632	-1.42169	-1.56230	-1.61167	-1.58215	-1.46677	-1.28139	-1.07361
YU/M	F1/SEC	-00060	-00269	-00217	-00908	-01072	-04349	-12548	-21334	-30627	-49772	-69216
YU/M	F1/SEC	-15641	-13647	-12434	-12737	-15294	-16880	-17261	-16914	-16560	-15594	-15084
YU/M	F1/SEC	-16925	-16588	-03148	-09572	-07749	-04789	-03020	-02241	-00280	-03274	-02714
YU/M	F1/SEC	-00722	-00162	-00072	-00082	-00032	-00107	-00206	-00242	-00244	-00281	-00464
YU/M	F1/SEC	-46315	-37131	-35751	-40538	-49832	-58473	-65759	-71086	-74411	-64564	-47701
YU/M	F1/SEC2-IN	-23793	-09152	-02774	-14579	-29857	-37286	-49135	-38110	-25913	-22713	-38045
YU/M	F1/SEC2-IN	-8.76072	-8.34844	-8.24424	-8.44039	-8.92918	-9.65911	-10.54486	-11.36450	-11.86153	-10.13481	-8.00431
YU/M	F1/SEC2-IN	-00387	-00314	-00253	-00205	-00170	-00165	-00196	-00207	-00325	-00385	-00801
YU/M	F1/SEC2-IN	-00055	-00019	-00004	-00022	-00041	-00037	-00029	-00030	-00011	-00076	-00233
YU/M	F1/SEC	-34012	-23042	-06929	-02006	-08558	-06678	-02233	-01533	-00011	-00330	-05494
YU/M	F1/SEC	1.52823	1.52018	1.48008	1.47277	1.45790	1.52443	1.52443	1.52443	1.52443	1.52443	1.52443
YU/M	F1/SEC	-00048	-00054	-00044	-00022	-00014	-00012	-00030	-00008	-00031	-00010	-00020
YU/M	F1/SEC	-00057	-00065	-00064	-00049	-00026	-00027	-00044	-00066	-00074	-00038	-00395
YU/M	F1/SEC	-00056	-00048	-00044	-00060	-00095	-00116	-00127	-00135	-00170	-00172	-00269
YU/M	F1/SEC	-03692	-03461	-02893	-02102	-01198	-00814	-00774	-03964	-01429	-03073	-04918
YU/M	F1/SEC	-00893	-01275	-01523	-01630	-01588	-01506	-01491	-01497	-01082	-01017	-01227
YU/M	F1/SEC	41947	41992	41776	41443	41089	41112	41322	41678	41901	42347	43874
YU/M	F1/SEC	-14907	-14554	-13379	-13162	-13162	-13330	-13756	-13759	-13090	-12480	-12480
YU/M	F1/SEC	-69755	-63945	-61095	-61745	-63629	-63931	-70323	-68840	-64553	-58229	-53997
YU/M	F1/SEC	-05003	-04422	-04119	-04217	-04644	-05242	-05301	-05123	-04777	-04132	-03326
YU/M	F1/SEC	13520	13148	11838	09605	06460	04995	04770	05246	07124	12280	16163
YU/M	F1/SEC	-05003	-04422	-04119	-04217	-04644	-05242	-05301	-05123	-04777	-04132	-03326
YU/M	F1/SEC	-00175	-00175	-00001	-00104	-00104	-00037	-00024	-00083	-00144	-00175	-00247
YU/M	F1/SEC	-00079	-00067	-00055	-00044	-00035	-00033	-00039	-00054	-00063	-00073	-00144
YU/M	F1/SEC	3452	3428	34363	34790	36241	39000	41550	43835	45158	47301	48161
YU/M	F1/SEC	-03381	-00557	-02092	-03816	-08318	-13137	-15150	-17332	-19352	-13769	-09461
YU/M	F1/SEC	-00031	-00000	-00001	-00002	-00002	-00001	-00002	-00004	-00006	-00004	-00001
YU/M	F1/SEC	-00079	-00067	-00055	-00044	-00035	-00033	-00039	-00054	-00063	-00073	-00144
YU/M	F1/SEC	-04726	-05177	-00231	-05689	-04588	-02274	-01296	-00130	-00063	-00073	-00144
YU/M	F1/SEC	-1.53243	-1.33744	-1.27220	-1.33496	-1.52399	-1.64610	-1.71462	-1.75868	-1.74931	-1.4584	-1.41351
YU/M	F1/SEC	-01843	-00283	-00458	-01302	-01750	-01806	-01523	-01126	-00419	-00077	-00163
YU/M	F1/SEC	-00015	-00041	-00057	-00056	-00033	-00025	-00023	-00021	-00017	-00006	-00010
YU/M	F1/SEC	-00166	-00292	-00081	-00139	-00034	-00001	-00020	-00036	-00055	-00069	-00068
YU/M	F1/SEC	-00082	-00027	-00029	-00034	-00025	-00001	-00011	-00026	-00047	-00183	-00310
YU/M	F1/SEC	04797	05365	05544	05332	04299	04473	04085	04119	04473	04994	06088
YU/M	F1/SEC	-00492	-00173	-00127	-00334	-00075	-01029	-01239	-01436	-01360	-00023	-01422
YU/M	F1/SEC	00706	00601	00936	01040	01045	01003	00962	00978	01184	01415	01704
YU/M	F1/SEC	20565	20613	20542	20376	20143	20136	20254	20502	20762	21185	22357
YU/M	F1/SEC	-02324	-01752	-01103	-01103	-01831	-02288	-02765	-03532	-05220	-07347	-10472
YU/M	F1/SEC	-16274	-18593	-19391	-10670	-16426	-14334	-12999	-12401	-11246	-10165	-10566
YU/M	F1/SEC	-04141	-04249	-04345	-04383	-04318	-04306	-04377	-04566	-04974	-05676	-06986
YU/M	F1/SEC	11903	00195	-26730	-54684	-47876	-47876	-44407	-19205	-64430	-49280	-49280
YU/M	F1/SEC	49785	49785	510272	4933.3	4.94221	6.27929	4.49493	6.88498	5.56785	6.74024	6.74024
YU/M	F1/SEC	-23401	-26147	-27159	-26337	-24373	-22403	-20728	-19475	-20091	-22942	-28157
YU/M	F1/SEC	11189	09206	06837	04340	01995	06639	07239	09414	12749	15910	18563
YU/M	F1/SEC	7.86562	6.61257	5.39523	4.25924	2.96332	1.82339	1.45286	1.55312	1.45286	1.45286	1.45286
YU/M	F1/SEC	-43595	-48766	-51126	-49798	-43906	-40330	-39769	-41458	-45802	-52990	-62193

ZUOT=-50J.OJ. VUOT= 0.00 -40.00000 -20.00000 0.00000 20.00000 40.00000 60.00000 80.00000 100.00000 120.00000 140.00000 160.00000

ZUOT	0.00	20.00000	40.00000	60.00000	80.00000	100.00000	120.00000	140.00000	160.00000
XU/N	1/SEC	-0.0431	-0.2325	-0.1307	-0.2174	-0.2695	-0.3084	-0.3374	-0.4364
XU/M	1/SEC	-0.0046	-0.0097	-0.0008	-0.0001	-0.0006	-0.0027	-0.0062	-0.0137
XU/Y	1/SEC	-0.0284	-0.3504	-0.3884	-0.3625	-0.2864	-0.1910	-0.0253	-0.0421
XU/Z	1/SEC	-0.1350	-0.1655	-0.1123	-0.1831	-0.14825	-0.1281	-0.1496	-0.0254
XU/AA	1/SEC	-0.0025	-0.0013	-0.0007	-0.0002	-0.0004	-0.0003	-0.0005	-0.0008
XU/AB	1/SEC	-0.0021	-0.0013	-0.0005	-0.0002	-0.0004	-0.0007	-0.0008	-0.0012
XU/AC	1/SEC	-0.0475	-0.07629	-0.04178	-0.0570	-0.0410	-0.0332	-0.0476	-0.0960
XU/AD	1/SEC	-0.2649	-0.2172	-0.2090	-0.3990	-0.3665	-0.3979	-0.4027	-0.5155
XU/AE	1/SEC	-0.0115	-0.0038	-0.0087	-0.0000	-0.0032	-0.0066	-0.0082	-0.0101
XU/AF	1/SEC	-0.0288	-0.1426	-0.14525	-0.1822	-0.19235	-0.1782	-0.12806	-0.17168
XU/AG	1/SEC	-0.0288	-0.0272	-0.0412	-0.0366	-0.0328	-0.0328	-0.0374	-0.0426
XU/AH	1/SEC	-0.0811	-0.1042	-0.1244	-0.0601	-0.0324	-0.0169	-0.0117	-0.07617
XU/AI	1/SEC	-0.0815	-0.0676	-0.0672	-0.0672	-0.0514	-0.0716	-0.06128	-0.08542
XU/AJ	1/SEC	-0.1691	-0.16274	-0.13461	-0.13154	-0.13474	-0.14425	-0.14934	-0.12750
XU/AL	1/SEC	-0.0652	-0.05248	-0.03515	-0.04552	-0.05689	-0.0622	-0.03415	-0.0552
XU/AM	1/SEC	-0.167033	-0.132917	-0.160184	-0.179907	-0.184855	-0.180984	-0.167724	-0.145290
XU/AN	1/SEC	-0.03860	-0.02677	-0.02457	-0.02338	-0.11371	-0.20437	-0.27705	-0.43075
XU/AO	1/SEC	-0.18165	-0.14545	-0.15189	-0.15618	-0.19909	-0.19360	-0.18595	-0.15551
XU/AP	1/SEC	-0.1783	-0.18204	-0.1816	-0.05637	-0.03356	-0.02250	-0.0324	-0.0104
XU/AQ	1/SEC	-0.0005	-0.0104	-0.0135	-0.0240	-0.00319	-0.00316	-0.00384	-0.00318
XU/AR	1/SEC	-0.3594	-0.34017	-0.37819	-0.50806	-0.64615	-0.70814	-0.74979	-0.70849
XU/AS	1/SEC	-0.2781	-0.09822	-0.15524	-0.14697	-0.22949	-0.12258	-0.1258	-0.2644
XU/AT	1/SEC	-0.60511	-0.22802	-0.13578	-0.53550	-0.42244	-0.112931	-0.190365	-0.107230
XU/AV	1/SEC	-0.0234	-0.00182	-0.00125	-0.0026	-0.00044	-0.0113	-0.0139	-0.00217
XU/AX	1/SEC	-0.0030	-0.0001	-0.0009	-0.0007	-0.00013	-0.00048	-0.00022	-0.00049
XU/AY	1/SEC	-0.45039	-0.31843	-0.17822	-0.0002	-0.00013	-0.00048	-0.00048	-0.00048
XU/AZ	1/SEC	-0.11531	-0.13401	-0.1169	-0.0439	-0.0002	-0.0002	-0.0002	-0.0002
XU/BA	1/SEC	-0.0044	-0.0058	-0.0037	-0.0012	-0.0008	-0.0003	-0.0008	-0.0003
XU/BB	1/SEC	-0.0781	-0.0187	-0.0612	-0.0216	-0.0187	-0.0361	-0.0718	-0.02148
XU/BC	1/SEC	-0.1730	-0.1832	-0.1643	-0.0821	-0.0454	-0.1201	-0.1313	-0.1629
XU/BD	1/SEC	-0.1475	-0.14503	-0.1309	-0.13388	-0.1371	-0.13898	-0.12778	-0.12591
XU/BE	1/SEC	-0.7428	-0.6419	-0.6455	-0.7575	-0.7621	-0.7501	-0.63821	-0.56471
XU/BF	1/SEC	-0.12968	-0.10871	-0.07991	-0.0570	-0.02434	-0.02497	-0.0291	-0.0884
XU/BG	1/SEC	-0.05736	-0.0523	-0.04691	-0.06018	-0.06082	-0.05872	-0.05499	-0.04675
XU/BH	1/SEC	-0.0172	-0.0098	-0.0043	-0.00344	-0.00367	-0.00333	-0.00251	-0.0113
XU/BI	1/SEC	-0.0143	-0.0121	-0.0088	-0.0019	-0.0027	-0.0075	-0.0131	-0.0160
XU/BJ	1/SEC	-0.1196	-0.0447	-0.0203	-0.01635	-0.01623	-0.01641	-0.01647	-0.01715
XU/BK	1/SEC	-0.3676	-0.34340	-0.3695	-0.39006	-0.41676	-0.43986	-0.45786	-0.49580
XU/BL	1/SEC	-0.0350	-0.0187	-0.0209	-0.0821	-0.16471	-0.17736	-0.1935	-0.18049
XU/BM	1/SEC	-0.0030	-0.0000	-0.0000	-0.0002	-0.0001	-0.0002	-0.0002	-0.0002
XU/BN	1/SEC	-0.0047	-0.0037	-0.0026	-0.0006	-0.0011	-0.0022	-0.0024	-0.00107
XU/BO	1/SEC	-0.6038	-0.6421	-0.6289	-0.6126	-0.53879	-0.40409	-0.30392	-0.21315
XU/BS	1/SEC	-1.54982	-1.31840	-1.24188	-1.61293	-1.72433	-1.76349	-1.80237	-1.56573
XU/BT	1/SEC	-0.0260	-0.00735	-0.0208	-0.0915	-0.0751	-0.0622	-0.00487	-0.00176
XU/BU	1/SEC	-0.0007	-0.0033	-0.0050	-0.0026	-0.0026	-0.0023	-0.0019	-0.0010
XU/BV	1/SEC	-0.0154	-0.0271	-0.0070	-0.0004	-0.00026	-0.0004	-0.00064	-0.00079
XU/BW	1/SEC	-0.0049	-0.0026	-0.0028	-0.0012	-0.0032	-0.0039	-0.0037	-0.0017
XU/BX	1/SEC	-0.0154	-0.0849	-0.0407	-0.0354	-0.0345	-0.0308	-0.0308	-0.05191
XU/AY	1/SEC	-0.0454	-0.0194	-0.0094	-0.0829	-0.1003	-0.1225	-0.1297	-0.0455
XU/BA	1/SEC	-0.0711	-0.0791	-0.0924	-0.0944	-0.0862	-0.0862	-0.1036	-0.1478
XU/BB	1/SEC	-0.2030	-0.2048	-0.2026	-0.1909	-0.1956	-0.2019	-0.2084	-0.2164
XU/BC	1/SEC	-0.1552	-0.1341	-0.1072	-0.1901	-0.2199	-0.2739	-0.4104	-0.5623
XU/BD	1/SEC	-0.1653	-0.1760	-0.1680	-0.1156	-0.09560	-0.0867	-0.0774	-0.0692
XU/BE	1/SEC	-0.0457	-0.0419	-0.0423	-0.0406	-0.0421	-0.0454	-0.0509	-0.06183
XU/BF	1/SEC	-0.3328	-0.2223	-0.2921	-0.6428	-0.27053	-0.8356	-0.5056	-0.2420
XU/BG	1/SEC	-0.14841	-0.1718	-0.14968	-0.4510	-0.37229	-0.28691	-0.9344	-0.05306
XU/BH	1/SEC	-0.2028	-0.2411	-0.2611	-0.19658	-0.17837	-0.1654	-0.14840	-0.24210
XU/BI	1/SEC	-0.03700	-0.05063	-0.05667	-0.0240	-0.10942	-0.2212	-0.47632	-0.70471
XU/BJ	1/SEC	-0.46607	-0.61169	-0.77448	-0.0240	-0.10942	-0.2212	-0.47632	-0.70471
XU/BK	1/SEC	-0.81254	-0.53887	-0.36914	-0.13531	-0.65473	-0.423	-0.2157	-0.03887
XU/BL	1/SEC	-0.38226	-0.45397	-0.48161	-0.34133	-0.33547	-0.40420	-0.48192	-0.58188

ADUT -50.00000 -20.00000 0.00000 20.00000 40.00000 60.00000 80.00000 100.00000 120.00000 140.00000 160.00000

AW/M	1/SEC	0.4980	-0.4449	-0.2114	-0.0259	-0.1164	-0.2046	-0.2592	-0.2981	-0.3632	-0.4267	-0.4737
AV/M	1/SEC	0.0032	-0.0075	-0.0085	-0.0046	-0.0004	0.0014	0.0024	0.0021	0.0013	-0.0023	-0.0267
AW/P	1/SEC	0.5470	-0.3811	0.3259	0.3412	0.3870	0.3764	0.3412	0.2663	0.3014	0.2613	0.3075
AW/P	1/SEC2-IN	1.7130	1.3202	1.1608	1.0849	1.0866	1.2688	1.6174	1.6383	1.6612	1.3468	1.0794
AW/P	1/SEC2-IN	1.4643	1.21170	0.9367	0.6983	0.5475	0.4260	0.26174	0.1682	0.0000	0.0002	-0.1284
AW/P	1/SEC2-IN	0.0017	-0.0007	-0.0004	0.0004	0.0004	0.0003	0.0004	0.0000	0.0000	-0.0002	-0.0032
AW/P	1/SEC2-IN	0.0012	-0.0006	-0.0001	0.0002	0.0002	0.0003	0.0002	0.0000	0.0000	-0.0002	-0.0016
AW/P	1/SEC	1.1867	0.5290	0.2051	0.0784	0.0120	0.0380	0.0015	0.0506	0.0446	0.0555	0.0747
AW/P	1/SEC	2.17267	2.51458	2.58521	2.51853	2.44855	2.35790	2.30588	2.31099	2.45022	2.58151	2.91199
AW/P	1/SEC	1.1717	-0.12437	-0.10552	-0.09582	-0.07589	-0.04676	-0.03138	-0.02810	-0.02961	-0.03792	-0.0701
AW/P	1/SEC	0.0093	-0.00149	-0.0019	0.0095	-0.0006	0.0017	0.0026	0.0063	0.0074	0.0108	0.0098
AW/P	1/SEC	0.8680	-0.13255	-0.13712	-0.11155	-0.06893	-0.07404	-0.08899	-0.10671	-0.12526	-0.14524	-0.18913
AW/P	1/SEC	0.0282	0.00238	0.0265	0.0334	0.0418	0.0330	0.0267	0.0260	0.0308	0.0476	0.0409
AW/P	1/SEC2-IN	0.4111	-0.16824	0.1175	0.0476	0.0673	0.5185	0.4378	0.309	0.3476	0.2895	-0.0397
AW/P	1/SEC2-IN	0.4978	0.5992	0.6353	0.6166	0.5535	0.4654	0.4187	0.4208	0.5709	0.8842	0.8941
AW/P	1/SEC2-IN	1.15225	1.16217	1.15902	1.14599	1.12623	1.11989	1.11395	1.12371	1.12706	1.13824	1.18927
AW/P	1/SEC2-IN	0.8654	-0.07540	-0.5395	-0.3632	-0.3866	-0.5258	-0.6842	-0.7593	-0.9459	-1.3095	-0.0433
AW/P	1/SEC	1.08643	-1.60055	-1.49303	-1.57519	-1.83531	-2.03591	-2.08734	-2.03928	-1.88459	-1.65634	-1.47095
AW/P	1/SEC	0.8534	0.5194	0.0414	0.6279	-0.7332	0.0340	0.10630	0.2036	0.2702	0.40930	0.5181
AW/P	1/SEC	-0.2039	-0.17280	-0.16450	-0.17614	-0.20480	-0.22199	-0.22455	-0.21743	-0.20654	-0.18446	-0.16326
AW/P	1/SEC	1.9109	1.9817	0.2884	1.4099	-1.1142	-0.6631	-0.3744	-0.2283	0.00337	0.0361	0.2053
AW/P	1/SEC	0.0364	0.0100	0.0374	0.0524	0.0592	0.0487	0.0425	0.0381	0.0437	0.0302	0.0355
AW/P	1/SEC	-0.4074	-0.30703	-0.29557	-0.36885	-0.44538	-0.55118	-0.63488	-0.6967	-0.7653	-0.8281	-0.70389
AW/P	1/SEC2-IN	0.31253	-0.10291	0.3031	0.1269	0.36980	0.46734	0.7107	0.44616	0.4968	0.6504	0.72689
AW/P	1/SEC2-IN	0.43145	-0.12808	-0.66188	-0.21477	-0.56870	-0.35989	-10.28788	-11.19359	-11.89379	-11.22671	-11.36673
AW/P	1/SEC2-IN	0.0107	0.00519	0.0028	0.0040	0.0030	0.0044	0.0032	0.0016	0.0007	0.0054	0.0033
AW/P	1/SEC2-IN	0.0027	0.0014	0.0011	0.0012	0.0014	0.0008	0.0034	0.0000	0.0003	0.0008	0.0001
AW/P	1/SEC	-0.1531	-0.19244	0.4190	1.1709	3.1348	2.1681	1.2453	0.6661	0.8962	0.3030	0.6456
AW/P	1/SEC	2.15197	0.9186	0.43507	0.21703	-1.14324	-1.17918	-0.87636	-0.52818	-0.1613	0.78476	1.9533
AW/P	1/SEC	0.1138	0.47219	0.3222	0.39339	0.48508	0.2835	0.08312	0.09338	0.18839	-0.26671	-0.5531
AW/P	1/SEC	0.0040	0.0059	0.0028	0.0004	0.0014	0.0024	0.0014	0.0002	0.0016	0.0004	0.0009
AW/P	1/SEC	0.0568	0.0601	-0.0608	-0.0591	-0.0555	-0.0548	-0.0564	-0.0595	-0.0646	-0.0725	-0.0853
AW/P	1/SEC	0.0072	0.0050	0.0068	0.0077	0.0151	0.0166	0.0166	0.0167	0.0179	0.0241	0.0214
AW/P	1/SEC	0.3269	-0.3269	0.2410	0.1247	0.0000	0.0376	0.0369	0.0188	0.0077	0.01278	0.02629
AW/P	1/SEC	0.0683	-0.11116	-0.1403	-0.1453	-0.1174	-0.0864	-0.0804	-0.0807	-0.0528	0.0225	-0.0075
AW/P	1/SEC2-IN	4.1715	4.1582	4.153	4.0660	4.0554	4.0554	4.0590	4.0740	4.0935	4.0935	4.2129
AW/P	1/SEC2-IN	1.6031	1.4475	-1.3896	-1.3309	-1.3156	-1.3452	-1.3834	-1.4076	-1.3570	-1.3089	-1.2961
AW/P	1/SEC	0.79828	0.72706	0.69495	0.70862	0.77476	0.81835	0.82866	0.81192	0.76384	0.69295	0.59746
AW/P	1/SEC	0.2624	0.1283	0.10020	0.06396	0.1569	0.0117	0.0203	0.0221	0.0089	0.0211	0.0761
AW/P	1/SEC	0.6426	-0.05530	-0.5220	0.5466	-0.6241	0.6732	0.6815	0.6596	0.6182	0.5353	0.4309
AW/P	1/SEC	0.0181	0.0727	0.0025	0.0679	0.30104	0.0420	0.00405	0.0351	0.0280	0.0389	0.0147
AW/P	1/SEC	0.0108	0.0054	0.0017	0.0006	0.0020	0.0006	0.0006	0.0067	0.0112	0.0135	0.0193
AW/P	1/SEC	-0.1465	-0.00562	0.0234	0.0992	0.1778	0.1764	0.1684	0.1666	0.1624	0.1950	0.1556
AW/P	1/SEC2-IN	3.5758	3.3528	3.2921	3.3528	3.5584	3.9113	4.1870	4.4180	4.6426	4.7114	4.1639
AW/P	1/SEC2-IN	-0.4062	0.2013	0.1905	0.2107	0.9114	1.5286	1.7320	1.8202	1.8825	2.1272	1.6717
AW/P	1/SEC2-IN	0.0000	0.0000	0.0000	0.0000	0.0002	0.0000	0.0000	0.0000	0.0000	0.0000	0.0004
AW/P	1/SEC2-IN	0.0024	-0.0012	-0.0000	0.0009	0.0011	0.0011	0.0009	0.0003	0.0001	0.0000	-0.0063
AW/P	1/SEC	0.710	0.5658	0.4267	0.3618	0.3792	0.2270	0.1306	0.0808	0.1083	0.0945	0.1158
AW/P	1/SEC	-1.57909	-1.31503	-1.22925	-1.31598	-1.56947	-1.68183	-1.73681	-1.76988	-1.80477	-1.57954	-1.54494
AW/P	1/SEC	0.3206	-0.1058	-0.0433	-0.0294	0.0397	0.0267	0.0052	0.0041	0.0022	0.0244	0.0032
AW/P	1/SEC	0.0002	0.0023	0.0040	0.0042	0.0025	0.0030	0.0030	0.0027	0.0022	0.0014	0.0009
AW/P	1/SEC	0.0144	-0.0254	-0.0362	0.0132	0.0026	0.0009	-0.0033	0.0051	0.0072	0.0087	0.0069
AW/P	1/SEC	0.0064	0.0026	0.0022	0.0021	-0.0012	-0.0036	-0.0042	-0.0043	-0.0058	-0.0107	-0.0177
AW/P	1/SEC2-IN	0.3939	0.4375	0.4655	0.4371	0.3516	0.2811	0.2400	0.2294	0.2548	0.3197	0.4195
AW/P	1/SEC2-IN	0.0671	-0.0218	0.0072	0.0344	0.0543	0.0552	0.0677	0.0919	0.1102	0.1128	0.1128
AW/P	1/SEC2-IN	0.0716	0.0782	0.0914	0.1010	0.0983	0.0887	0.0789	0.0746	0.0883	0.1042	0.1252
AW/P	1/SEC2-IN	2.0236	2.0419	2.0382	2.0170	1.9822	1.9499	1.9669	1.9746	1.9823	2.0039	2.0952
AW/P	1/SEC	0.0740	0.0066	0.0080	-0.0921	-0.1442	-0.1663	-0.1772	-0.2065	-0.3098	-0.4472	-0.6599
AW/P	1/SEC	-1.0825	-1.4697	-1.6052	-1.4872	-1.1142	-0.7923	-0.6077	-0.5316	-0.4408	-0.4746	-0.5912
AW/P	1/SEC	0.4088	-0.4172	-0.6145	-0.3979	-0.3912	-0.3912	-0.3840	-0.3947	-0.4173	-0.4588	-0.5523
AW/P	1/SEC	0.6164	0.28176	-0.24250	0.87058	-1.20173	0.83457	-0.39980	0.2471	0.23855	0.4035	0.6263
AW/P	1/SEC	3.69823	4.26139	4.42437	4.19346	3.57491	3.23321	3.87052	3.33578	3.69708	4.32420	5.39970
AW/P	1/SEC	1.7213	2.0691	2.2287	1.9446	1.9622	1.7057	1.5037	1.3696	1.1745	1.0448	0.8111
AW/P	1/SEC	0.0269	0.06336	0.11834	0.15071	0.15071	0.05761	-0.05168	-0.15797	-0.25691	-0.37766	-0.51441
AW/P	1/SEC	7.76600	6.61333	5.48044	4.47560	3.32665	3.30664	1.87456	0.35227	0.0997	-0.68214	-3.75758
AW/P	1/SEC	-0.32757	-0.41888	-0.45153	-0.42156	-0.32665	-0.27858	-0.27258	-0.29476	-0.35037	-0.43798	-0.54619

ACT	-40.00000	-20.00000	0.00000	20.00000	40.00000	60.00000	80.00000	100.00000	120.00000	140.00000	160.00000
AV/M	1.75EC	-0.5360	-0.4306	-0.1524	-0.0690	-0.1807	-0.2411	-0.2813	-0.3516	-0.4138	-0.4634
AV/Y	1.75EC	-0.00109	-0.0016	-0.00252	-0.0028	-0.0028	-0.0052	-0.0079	-0.0127	-0.0179	-0.0249
AV/Y	1.75EC	-0.0460	-0.267	-0.2453	-0.2996	-0.4039	-0.3631	-0.3021	-0.3931	-0.3962	-0.1391
XAV/M	1.75EC2-IN	1.2461	1.2461	1.0282	1.0149	0.9949	1.2317	1.6717	1.5087	1.3354	1.1176
XDC/M	1.75EC2-IN	1.35572	1.21065	0.94734	0.66735	0.5274	0.49068	0.23495	0.37365	0.35756	-0.1497
XDS/M	1.75EC2-IN	0.00037	0.00018	0.00022	0.00013	0.00012	0.00008	0.00006	0.00011	0.00014	0.0003
XDS/M	1.75EC2-IN	0.00033	0.00011	0.00014	0.00019	0.00008	0.00009	0.00009	0.00011	0.00010	0.00032
AP/Y	1.75EC	-0.06448	-0.17662	-0.10085	-0.0324	-0.00396	-0.0152	-0.0285	-0.00349	-0.00129	-0.00459
AV/Y	1.75EC	1.58055	2.37567	2.54172	2.53575	2.41481	2.28959	2.20302	2.28822	2.44636	2.69415
AV/Y	1.75EC	0.7259	1.7898	-0.2965	-0.23969	-0.13796	-0.11801	-0.0070	-0.11362	-0.1998	-0.6915
AV/Y	1.75EC	-0.0022	-0.0143	-0.0017	-0.00184	-0.00112	-0.00068	-0.00067	-0.00080	-0.00086	-0.0093
AV/Y	1.75EC	-0.07469	-0.12074	-0.12961	-0.10736	-0.06003	-0.06739	-0.03394	-0.10232	-0.12126	-0.14111
AV/Y	1.75EC	0.0425	0.0236	0.00258	0.00398	0.00560	0.0281	0.0114	0.0181	0.0287	0.0332
AV/Y	1.75EC2-IN	-0.07445	-0.3944	-0.1076	0.5881	0.4727	0.3521	-0.1163	-0.0171	-0.02523	-0.0678
AV/Y	1.75EC2-IN	0.3614	0.6450	0.4684	0.4629	0.4727	0.3360	0.1793	0.1381	0.2662	0.0498
AV/Y	1.75EC2-IN	1.13839	1.15833	1.15764	1.14093	1.11281	1.09883	1.08896	1.08391	1.07727	1.11556
AV/Y	1.75EC2-IN	-0.08126	-0.07837	-0.05628	-0.3750	-0.6752	-0.9142	-1.0750	-0.9562	-0.8185	-0.6780
AV/Y	1.75EC	-2.29354	-1.92078	-1.77801	-1.88079	-2.26388	-2.50458	-2.50174	-2.49268	-2.30235	-1.74804
AV/Y	1.75EC	-2.1454	1.2312	0.0268	-0.1079	-0.1733	-0.3710	-0.10567	-0.22106	-0.28540	-0.52818
AV/Y	1.75EC	-2.5481	-2.0538	-0.19279	-0.20763	-0.24042	-0.26938	-0.27334	-0.26330	-0.21723	-0.18318
AV/Y	1.75EC	-2.3030	2.2100	0.1607	-0.18058	-0.16505	-0.09016	-0.4638	-0.26396	-0.0024	-0.03084
AV/Y	1.75EC	-0.0523	-0.1503	-0.2266	-0.2417	-0.1560	-0.0702	-0.0477	-0.03405	-0.0473	-0.0346
AV/Y	1.75EC	-3.3298	-2.2864	-0.21583	-0.27459	-0.38494	-0.51847	-0.61350	-0.68379	-0.73257	-0.7821
AV/Y	1.75EC2-IN	-4.3318	-0.9623	-0.3261	-0.16224	-0.30157	-0.59022	-0.94993	-0.51907	-0.9070	-0.38494
AV/Y	1.75EC2-IN	-7.97548	-8.07244	-8.15139	-8.16216	-8.06660	-8.92325	-9.46202	-10.96791	-11.82412	-11.51790
AV/Y	1.75EC2-IN	-0.0042	-0.0129	-0.00192	-0.00208	-0.0055	-0.0105	-0.0116	-0.0133	-0.0181	-0.0204
AV/Y	1.75EC2-IN	-0.0002	0.0012	0.0001	0.0025	0.0050	0.0028	0.0014	0.0040	0.0050	0.0066
AV/Y	1.75EC	2.86504	1.38094	3.4201	-0.62739	-1.90768	-1.70958	-1.30247	-0.90297	-0.77260	-0.59425
AV/Y	1.75EC	-6.2915	-1.65715	-2.8656	2.37644	1.78694	1.78694	1.4237	2.25314	1.7024	0.8010
AV/Y	1.75EC	-0.0029	-0.0073	0.0007	0.0065	0.0044	0.0051	0.0030	0.0014	0.0024	0.0008
AV/Y	1.75EC	-0.0497	-0.0549	-0.0559	-0.0535	-0.0489	-0.0476	-0.0487	-0.0514	-0.0561	-0.0743
AV/Y	1.75EC	-0.0105	-0.0059	-0.0063	-0.0129	-0.0267	-0.0237	-0.0215	-0.0219	-0.0211	-0.0219
AV/Y	1.75EC2-IN	-0.3380	-0.3380	-0.3380	-0.312	-0.1386	-0.1567	-0.1117	-0.0900	-0.0020	-0.1616
AV/Y	1.75EC2-IN	-0.0502	-0.1078	-0.1546	-0.1535	-0.0555	-0.0038	0.0050	0.0159	0.0079	0.0369
AV/Y	1.75EC2-IN	-4.113	4.1629	4.1526	4.1029	4.0342	4.0075	3.9917	3.9851	3.9636	3.9597
AV/Y	1.75EC2-IN	-1.14369	-1.4510	-1.3944	-1.3284	-1.3160	-1.3595	-1.4096	-1.4451	-1.4077	-1.3731
AV/Y	1.75EC	-8.9327	-8.0303	-7.6413	-7.8010	-8.7500	-9.3966	-9.9215	-8.7733	-8.7733	-11.720
AV/Y	1.75EC	1.2854	1.2229	0.8461	0.2537	0.4559	0.4961	-0.2589	-0.2756	-0.1156	0.2317
AV/Y	1.75EC	-0.7609	-0.6475	-0.6004	-0.6255	-0.7020	-0.7989	-0.8174	-0.7937	-0.7425	-0.6534
AV/Y	1.75EC	-0.0011	-0.1407	-0.1964	-0.1349	-0.0454	-0.0639	-0.0499	-0.0393	-0.0294	-0.0169
AV/Y	1.75EC	-0.0044	-0.0151	-0.0043	-0.0238	-0.0043	-0.0013	-0.0009	-0.0043	-0.0077	-0.0133
AV/Y	1.75EC	-0.2203	-0.0987	-0.0365	-0.1585	-0.2407	-0.2041	-0.1808	-0.1714	-0.1628	-0.1472
AV/Y	1.75EC2-IN	-3.553	3.1908	3.0668	3.1771	3.475	3.7278	4.2495	4.4704	4.7082	4.0816
AV/Y	1.75EC2-IN	-0.05979	0.6354	0.1559	-0.2651	0.0000	0.0000	0.0000	0.0000	0.0000	0.0000
AV/Y	1.75EC2-IN	-0.0000	0.0001	0.0000	0.0001	0.0000	0.0000	0.0002	0.0002	0.0002	0.0000
AV/Y	1.75EC2-IN	-0.0008	0.0025	0.0038	0.0042	0.0032	0.0035	0.0024	0.0026	0.0036	0.0042
AV/Y	1.75EC	-0.4415	-1.2564	-0.1612	1.0903	0.7542	0.3703	0.2190	0.1687	0.1539	0.1473
AV/Y	1.75EC	-1.66595	-1.39936	-1.32041	-1.4141	-1.65466	-1.73690	-1.76469	-1.78707	-1.81219	-1.84883
AV/Y	1.75EC	-0.2160	0.4825	0.6124	0.6574	0.5494	0.2445	0.1313	0.0992	0.0950	0.0146
AV/Y	1.75EC	-0.0011	-0.0015	-0.0005	0.0014	0.0036	0.0054	0.0048	0.0039	0.0031	0.0010
AV/Y	1.75EC	-0.0126	-0.0234	-0.0050	0.0132	0.0019	-0.0018	-0.0044	-0.0065	-0.0087	-0.0107
AV/Y	1.75EC	0.0131	0.0038	0.0013	-0.0007	-0.0008	-0.0006	-0.0006	-0.0003	-0.0005	-0.00123
AV/Y	1.75EC2-IN	0.2371	0.3581	0.4010	0.3627	0.2400	0.1239	0.0676	0.0443	0.0637	0.02149
AV/Y	1.75EC2-IN	-0.0299	-0.0336	0.0037	0.0352	0.0140	-0.00302	-0.0070	-0.0001	-0.00374	0.00310
AV/Y	1.75EC2-IN	0.0745	0.0760	0.0899	0.1002	0.0934	0.0777	0.0618	0.0513	0.0582	0.0669
AV/Y	1.75EC2-IN	0.1998	0.20349	0.2036	0.19581	0.19317	0.19124	0.19124	0.19124	0.18916	0.19012
AV/Y	1.75EC	-0.0473	0.0144	-0.0305	-0.1072	-0.1405	-0.1136	-0.1046	-0.1481	-0.22706	-0.30446
AV/Y	1.75EC	-0.5180	-1.1340	-1.1621	-0.5725	-0.1175	-0.1086	-0.1872	-0.2308	-0.3208	-0.0523
AV/Y	1.75EC	-0.3893	-0.3937	-0.4051	-0.4114	-0.4002	-0.3767	-0.3633	-0.3507	-0.3653	-0.4410
AV/Y	1.75EC	1.34937	0.79908	-0.33296	-1.45003	-1.95561	-2.24186	-2.66014	-2.23546	-2.19636	-1.8227
AV/Y	1.75EC	2.84932	3.64383	3.88318	3.57273	2.71768	2.07662	2.19636	2.54039	3.14279	4.14597
AV/Y	1.75EC	-0.11726	0.6030	1.1845	1.8466	1.6020	1.217C	0.9565	0.8054	0.9308	1.5682
AV/Y	1.75EC	-2.4915	-1.2608	-0.6225	-0.2349	-0.32129	-0.4623	-0.5576	-0.5576	-0.5777	-0.3669
AV/Y	1.75EC	6.54095	7.69638	6.62471	5.55735	4.67569	3.61291	2.27393	8.4619	6.2842	-2.95613
AV/Y	1.75EC	-2.1729	-3.5113	-3.9740	-3.3599	-2.1433	-1.5149	-1.1744	-0.24432	-0.35026	-0.47574

UNIT - 2000.00, UNIT - 0.00

UNIT	-40.00000	-20.00000	0.00000	20.00000	40.00000	60.00000	80.00000	100.00000	120.00000	140.00000	160.00000
XU/M	1/SEC	-0.06263	-0.03715	-0.04486	0.1280	-0.0562	-0.1522	-0.2053	-0.2449	-0.2710	-0.2842
XU/M	1/SEC	-0.00036	-0.00813	-0.01054	-0.00780	-0.00818	-0.00001	-0.00027	-0.00027	0.0100	0.0235
XU/M	1/SEC	-0.07681	-0.00783	-0.00046	0.02390	0.05288	0.05212	0.04813	0.0442	0.05183	0.05009
XU/M	1/SEC	0.2925	0.10894	0.07809	0.0430	0.07518	0.10865	0.13635	0.15723	0.14189	0.15454
XU/M	1/SEC	0.99547	1.30066	1.06503	0.68481	0.55376	0.50246	0.41950	0.31448	0.50991	0.64971
XU/M	1/SEC	0.00025	0.00046	0.00066	0.00031	0.00066	0.00001	0.00003	0.00003	0.00015	0.00019
XU/M	1/SEC	0.00007	0.00017	0.00020	0.00020	0.0002	0.00001	0.00004	0.00004	0.00011	0.00021
XU/M	1/SEC	0.06699	0.00127	-0.27477	-0.05422	-0.04339	-0.02999	-0.02436	-0.0466	-0.0021	-0.0011
XU/M	1/SEC	2.66429	2.01115	2.24670	2.62268	2.06379	2.11034	2.07184	2.05357	2.13303	2.31730
XU/M	1/SEC	0.10693	0.04870	0.05689	-0.37112	-0.05191	-0.0041	0.00349	-0.00577	-0.01057	-0.01730
XU/M	1/SEC	0.01173	-0.00581	-0.00019	0.00551	-0.01177	-0.0041	0.00331	0.0101	0.0118	0.0130
XU/M	1/SEC	-0.05914	-0.12163	-0.14542	-0.11564	-0.04339	-0.02399	-0.0100	-0.0436	-0.0021	-0.0011
XU/M	1/SEC	0.00112	0.00536	0.00932	0.00930	0.00158	0.00049	0.00005	-0.00011	0.00076	0.00245
XU/M	1/SEC	-0.06880	-0.07426	-0.01272	0.09234	0.08278	0.04478	0.01565	-0.00949	0.00439	0.00439
XU/M	1/SEC	0.04402	0.00385	-0.01157	0.00115	0.04540	0.04117	-0.01545	-0.02325	0.01110	0.03125
XU/M	1/SEC	1.11133	1.16572	1.17450	1.16623	1.08945	1.07086	1.05385	1.04068	1.02302	1.01103
XU/M	1/SEC	0.06637	0.08447	-0.05991	0.03686	-0.05949	-0.08998	-0.11967	-0.14250	-0.16095	-0.18191
XU/M	1/SEC	-2.85417	-2.14288	-1.87861	-2.10408	-2.86207	-3.07796	-3.00002	-2.97030	-2.74432	-2.76608
XU/M	1/SEC	0.10856	0.31771	-0.02562	0.33390	0.10081	0.34117	0.30021	0.1087	0.3702	0.4111
XU/M	1/SEC	-0.32607	-0.26477	-0.19242	-0.16205	-0.30665	-0.33044	-0.32602	-0.31047	-0.28792	-0.25047
XU/M	1/SEC	0.30299	0.21867	-0.01843	-0.21180	-0.16494	-0.06625	-0.03036	-0.01330	0.01087	0.03054
XU/M	1/SEC	0.00970	0.6327	0.10005	0.8775	0.0282	0.0013	0.0037	0.0150	0.0042	0.00442
XU/M	1/SEC	-0.56518	-0.10912	0.2341	-0.15034	-0.61310	-0.6055	-0.6979	-0.73454	-0.76462	-0.70239
XU/M	1/SEC	-0.93664	0.8927	0.6102	0.13049	0.89335	0.70970	0.64991	0.62243	0.59427	0.54317
XU/M	1/SEC	-6.27516	-8.47221	-9.21050	-8.57821	-6.66292	-8.51574	-10.64605	-11.50169	-11.98186	-11.45317
XU/M	1/SEC	-0.0033	-0.00275	-0.0043	-0.00354	-0.00666	-0.00015	-0.00025	-0.00032	-0.0199	-0.00351
XU/M	1/SEC	-0.0021	-0.0004	-0.0012	-0.00031	-0.00566	-0.00000	-0.00000	-0.00043	0.00064	0.00036
XU/M	1/SEC	0.35251	2.35551	2.46723	1.51900	0.00566	0.00000	0.00000	0.00000	0.00064	0.00036
XU/M	1/SEC	-1.88570	3.41505	1.6714	-2.96616	2.67039	0.80977	1.0206	-0.1444	0.8247	0.7518
XU/M	1/SEC	-0.66646	0.59722	0.54599	4.46180	-0.87482	1.4437	1.0206	1.5601	2.8536	1.7974
XU/M	1/SEC	-0.0032	-0.0161	0.0057	0.00221	-0.0074	-0.0046	-0.0032	-0.0021	-0.0039	-0.0017
XU/M	1/SEC	-0.0042	-0.06497	-0.0499	-0.0454	-0.0407	-0.00392	-0.00391	-0.00412	-0.00451	-0.00631
XU/M	1/SEC	0.0099	0.0124	-0.0250	0.00322	0.0185	0.02158	0.02239	0.02139	0.02239	0.02277
XU/M	1/SEC	-0.02974	-0.0452	-0.0215	0.00858	0.2288	0.1027	0.0982	0.1454	0.1547	0.0042
XU/M	1/SEC	-0.00539	-0.01686	-0.0137	-0.0242	0.190	0.1027	0.0982	0.1454	0.1547	0.0042
XU/M	1/SEC	0.40388	0.1840	0.41849	0.1161	0.39808	0.39451	0.39134	0.38887	0.38433	0.38123
XU/M	1/SEC	-1.3700	-1.4744	-1.4213	-1.3323	-1.3290	-1.3867	-1.4439	-1.4477	-1.4646	-1.4588
XU/M	1/SEC	-1.02597	-0.85822	-0.78941	-0.83989	-0.83004	-1.08668	-1.08656	-1.05662	-0.9569	-0.81362
XU/M	1/SEC	0.9367	1.5719	0.6028	0.5739	0.5614	0.6492	0.6492	0.6492	0.6492	0.6492
XU/M	1/SEC	-0.04530	-0.0611	-0.05610	-0.05232	-0.08940	-0.0796	-0.0727	-0.09317	-0.08681	-0.07634
XU/M	1/SEC	-0.00765	0.2819	0.03691	0.23344	-0.00727	-0.00494	-0.00604	-0.00354	-0.00275	-0.00168
XU/M	1/SEC	-0.00547	-0.00599	0.0131	0.00801	-0.0076	0.00801	-0.00300	-0.0013	0.0045	0.00103
XU/M	1/SEC	0.38894	0.29086	0.25784	0.28787	0.37890	0.40731	0.43216	0.45508	0.47838	0.47524
XU/M	1/SEC	-0.22218	0.18325	0.14893	-0.15312	0.25369	0.27014	0.20975	0.20787	0.19224	0.22199
XU/M	1/SEC	0.0011	0.0046	-0.00067	-0.00061	0.0016	0.00002	0.00004	0.00002	0.00003	0.00006
XU/M	1/SEC	-0.03520	-0.23178	-0.03066	0.18870	0.04683	-0.02245	0.00132	-0.01223	0.1217	0.1122
XU/M	1/SEC	-1.32541	-1.72901	-1.88762	-1.77125	-1.55299	-1.65381	-1.71455	-1.75956	-1.75867	-1.61366
XU/M	1/SEC	0.0046	0.0092	-0.0105	-0.0035	0.0075	0.0063	0.0037	0.00639	0.1297	0.00428
XU/M	1/SEC	0.00498	-0.0232	-0.00044	0.00143	0.00006	0.00030	0.00058	-0.00080	0.00103	0.00124
XU/M	1/SEC	0.0083	0.0083	0.0051	-0.0007	0.00037	-0.00066	-0.00083	-0.00090	-0.00087	-0.00086
XU/M	1/SEC	0.0047	0.0087	0.0401	0.03229	0.0522	-0.0649	-0.1036	-0.1614	-0.1501	-0.0849
XU/M	1/SEC	0.1378	-0.0807	-0.0002	0.0714	-0.1742	0.1777	0.1689	0.1486	-0.1032	-0.0237
XU/M	1/SEC	0.00798	0.00728	0.00890	0.1010	0.0820	0.0612	0.0410	0.0255	0.00250	0.00322
XU/M	1/SEC	1.5537	2.0472	2.0656	2.0172	1.9160	1.8810	1.8487	1.8236	1.7926	1.8216
XU/M	1/SEC	-0.2035	-0.0103	-0.0232	-0.1209	-0.1458	-0.00874	-0.0548	-0.00338	0.0265	0.0037
XU/M	1/SEC	-0.00332	-0.07806	-0.10614	-0.00390	-0.00766	0.04696	0.07417	0.09549	0.09449	0.0968
XU/M	1/SEC	0.03942	0.04289	-0.04631	-0.04567	-0.03701	-0.03287	-0.03191	-0.03179	-0.03253	-0.03595
XU/M	1/SEC	1.44763	1.87498	-0.43935	-2.65135	1.91609	-1.12726	-0.69331	-0.38327	-1.5835	-0.3747
XU/M	1/SEC	1.63934	3.22173	3.72930	3.15133	1.47707	0.87896	0.84423	0.84477	1.28634	1.85946
XU/M	1/SEC	0.04364	0.17990	0.17592	0.17592	0.08323	0.04185	0.02620	0.01304	0.02220	0.00558
XU/M	1/SEC	-0.33502	-0.36135	0.7879	0.49227	0.33507	0.4185	0.47369	0.52000	0.47994	0.6899
XU/M	1/SEC	8.21096	7.68382	6.7365	5.61325	4.93539	3.95243	2.81267	1.56647	1.51339	0.8982
XU/M	1/SEC	-0.06388	-0.30197	-0.08618	-0.30862	-0.05883	-0.06681	-0.1180	-0.05078	-0.13447	-0.25374